Optical Multicarrier Sources for Spectrally Efficient Optical Networks

Vidak Vujicic

B.Eng., M.Eng.

A Dissertation submitted in fulfilment of the
requirements for the award of
Doctor of Philosophy (Ph.D.)
to the

Dublin City University

Faculty of Engineering and Computing
School of Electronic Engineering

Supervisor: Prof. Liam P. Barry

External Supervisor: Prof. Andrew D. Ellis
(Aston University, United Kingdom).

December 2015

Declaration

I hereby certify that this material, which I now submit for assessment on the programme of study leading to the award of Doctor of Philosophy is entirely my own work, and that I have exercised reasonable care to ensure that the work is original, and does not to the best of my knowledge breach any law of copyright, and has not been taken from the work of others save and to the extent that such work has been cited and acknowledged within the text of my work.

Signed:

ID No.:

Date:

To my father Branko, mother Milka

and brother Nikola

Mom ocu Branku, majci Milki

i bratu Nikoli

“With ideas it is like with dizzy heights you climb: At first they cause you discomfort and you are anxious to get down, distrustful of your own powers; but soon the remoteness of the turmoil of life and the inspiring influence of the altitude calm your blood; your step gets firm and sure and you begin to look - for dizzier heights.”

Nikola Tesla

Table of Contents

Acknowledgements

Firstly, I would like to acknowledge the constant support of my parents, Branko and Milka, and my brother Nikola throughout my entire education. Without their encouragement and guidance I certainly would not be in a position today to complete a Ph.D. I would like also to mention my grandmother Milosava who passed away many years ago, but whose words and love still give me support in the most difficult of moments.

I would like to thank my supervisor Prof. Liam Barry both for the faith he showed in me by accepting me as his student and for the continual support, guidance and encouragement he provided throughout my time in DCU. I could not think of a better supervisor to have.

I would like also to thank my co-supervisor Prof. Andrew Ellis for inspiring conversations and his guidance.

Additionally, I would like to acknowledge Dr. Prince Anandarajah, Dr. Regan Watts, and Dr. Sean O'Duill for their help during my PhD studies, advices during the thesis preparation and long days/late nights spent in the lab.

I would also like to acknowledge the enormous help I received from my colleagues at DCU: Eamonn, Colm, Josue, Vincent, Rui, Desi, Tong, Tam, Aravind, Fernando, Kevin, Kai and John. These people not only helped me in times of need for my studies but also helped me to relax after work hours.

I would like to acknowledge my colleagues from Karlsruhe Institute of Technology, III-V Labs and CNRS LPN, for their collaboration on EU FP 7 Projects and relaxing time on conferences. Also, I would like to thank people from CERN Electronics Department for giving me the opportunity to work on one of the most advanced projects in the world – Large Hadron Collider.

A special thanks is dedicated to my friends from Belgrade: Milko, Rale, Luka, Stefan, Kole, Kosta, Jovan, Gajo, Dusan and Sale who helped to facilitate my research/life balance, and made so many "welcome back" and "goodbye" parties for me.

Lastly, I would like to thank Lisa for helping me to keep a perspective on things and who made life so much easier throughout my work and studies.

List of Figures

List of Tables

List of Acronyms

ADC - Analog-to-Digital Converter

ADSL - Asymmetric Digital Subscriber Loop

AMZI - Asymmetric Mach Zehnder Interferometer

AO - All-Optical

AON - Active Optical Network

APD - Avalanche Photodetector

ASE - Amplified Spontaneous Emission

ATM - Asynchronous Transfer Mode

AWG - Arrayed Waveguide Grating

B2B - Back-to-Back

BER - Bit-Error Rate

BERT - Bit-Error Rate Tester

BL - Bit Rate-Distance Product

CAPEX - Capital Expenditure

CD - Chromatic Dispersion

CMA - Constant Modulus Algorithm

CO - Central Office

Coax – Coaxial

Co-WDM - Coherent WDM

CP - Cyclic Prefix

CSR - Carrier-to-Signal Ratio

CSRZ - Carrier Suppressed Return-to-Zero

CW - Continuous Wave

CWDM - Coarse Wavelength Division Multiplexing

DAB - Digital Audio Broadcast

DAC - Digital-to-Analog Conversion

DBP - Digital Backpropagation

DCF - Dispersion Compensating Fibre

DCM - Dispersion Compensating Module

DD - Direct Detection

DD-MZM - Dual-Drive Mach Zehnder Modulator

DFB - Distributed Feedback

DFT - Discrete Fourier Transform

DI - Delay Interferometer

DPSK - Differential Phase Shift Keying

DQPSK - Differential Quadrature Phase Shift Keying

DS – Downstream

DSB - Double Sideband

DSL - Digital Subscriber Loop

DSP - Digital Signal Processing

DVB - Digital Video Broadcast

DWDM - Dense Wavelength Division Multiplexing

EAM - Electro-Absorption Modulator

ECL - External Cavity Laser

EDFA - Erbium Doped Fibre Amplifier

EML - Externally Modulated Laser

ESA - Electrical Spectrum Analyser

EVM - Error Vector Magnitude

FDM - Frequency Division Multiplexing

FEC - Forward Error Correction

FFH - Feed-Forward Heterodyne

FIR - Finite Impulse Response

FP - Fabry-Perot

FPGA - Field Programmable Gate Array

FSR - Free Spectral Range

FTTB - Fibre to the Block

FTTC - Fibre to the Curb

FTTH - Fibre to the Home

FTTN - Fibre to the Node

FTTx - Fibre to the x

FWHM - Full-Width Half Maximum

FWM - Four-Wave Mixing

GSCS - Gain-Switched Comb Source

GSMBE - Gas Source Molecular Beam Epitaxy

HFC - Hybrid Fibre-Coaxial

HNLF - Highly Non-Linear Fibre

HPC - High Performance Computing

ICI - Inter-Carrier Interference

IDFT - Inverse Discrete Fourier Transform

IFWM - Intra Four Wave Mixing

IM/DD - Intensity Modulation with Direct Detection

IP - Internet Protocol

ISI - Inter-Symbol Interference

ITU - International Telecommunication Union

IXPM - Intra Cross Phase Modulation

LCoS - Liquid Cristal on Silicon

LO - Local Oscillator

LTE - Long Term Evolution

MAN - Metropolitan (metro) Area Network

MCM - Multi-Carrier Modulation

MEMS - Micro Electro Mechanical System

MLL - Mode-Locked Laser

MMF - Multi-Mode Fibre

MPLS - Multi Protocol Label Switching

MZM - Mach-Zehnder Modulator

NF - Noise Figure

NRZ - Non-Return-to-Zero

Nyquist Tx - Nyquist Transmitter

OBPF - Optical Band Pass Filter

OCNR - Optical Carrier-to-Noise Ratio

OECD - Organisation for Economic Co-operation and Development

O-E-O - Optical-Electrical-Optical

OFCS - Optical Frequency Comb Source

OFDM - Orthogonal Frequency Division Multiplexing

OLT- Optical Line Terminal

ONU - Optical Network Unit

OOK - On-Off Keying

OSNR - Optical Signal-to-Noise Ratio

OTN - Optical Transport Network

PAM - Pulse Amplitude Modulation

PAPR - Pear-to-Average Power Ratio

PC - Polarisation Controller

PDM - Polarisation Division Multiplexing

PEN - Pan-European Network

PMD - Polarisation Mode Dispersion

PON - Passive Optical Network

PPG - Pulse Pattern Generator

PRBS - Pseudo-Random Bit Sequence

PSK - Phase Shift Keying

QAM - Quadrature Amplitude Modulation

Q-Dash - Quantum Dash

QoS - Quality of Service

QPSK - Quadrature Phase-Shift Keying

Q-Well - Quantum Well

RIN - Relative Intensity Noise

ROADM - Reconfigurable Optical Add/Drop Multiplexer

RTS - Real-Time Scope

RZ - Return-to-Zero

SDH - Synchronous Digital Hierarchy

SDM - Space Division Multiplexing

SNR - Signal-to-Noise Ratio

SOA - Semiconductor Optical Amplifier

SOH - Silicon Organic Hybrid

SONET - Synchronous Optical Networking

SPM - Self Phase Modulation

SSB - Single Sideband

SSMF - Standard Single Mode Fibre

TDM - Time Division Multiplexing

TIA - Trans-Impedance Amplifier

ToR - Top-of-the-Rack

UDWDM - Ultra Dense Wavelength Division Multiplexing

US – Upstream

VCSEL - Vertical Cavity Surface Emitting Laser

VDSL - Very-high-bit-rate Digital Subscriber Loop

VOA - Variable Optical Attenuator

VoIP - Voice over IP

VPI TM - Virtual Photonics Integrated Transmission Maker

WDM - Wavelength Division Multiplexing

WiFi - Wireless Fidelity

WiMax - Worldwide Interoperability for Microwave Access

WLAN - Wireless Local Area Networks

WS – Waveshaper

WSS - Wavelength Selective Switch

WWAN - Wireless Wide Area Networks

XPM - Cross Phase Modulation

Vidak Vujicic, “Optical Multicarrier Sources for Spectrally Efficient Optical Networks”

Abstract

During the last 30 years the capacity of commercial optical systems exceeded the network traffic requirements, mainly due to the extraordinary scalability of wavelength division multiplexing technology that has been successfully used to expand capacity in optical systems and meet increasing bandwidth requirements since the early 1990’s. Nevertheless, the rapid growth of network traffic inverted this situation and current trends show faster growing network traffic than system capacity.

To enable further and faster growth of optical communication network capacity, several breakthroughs occurred during the last decade. First, optical coherent communications, which were the subject of intensive research in the 1980’s, were revived. This triggered the employment of advanced modulation formats. Afterwards, with the introduction of orthogonal frequency division multiplexing (OFDM) and Nyquist WDM modulation techniques in optical communication systems, very efficient utilisation of the available spectral bandwidth was enabled. In such systems the spectral guard bands between neighbouring channels are minimised, at the expense of stricter requirements on the performance of optical sources, especially the frequency (or wavelength) stability. Attractive solutions to address the frequency stability issues are optical multicarrier sources which simultaneously generate multiple phase correlated optical carriers that ensure that the frequency difference between the carriers is fixed.

In this thesis, a number of optical multicarrier sources are presented and analysed, with special focus being on semiconductor mode-locked lasers and gain-switched comb sources. High capacity and spectrally efficient optical systems for short and medium reach applications (from 3 km up to 300 km), based on optical frequency combs as optical sources, advanced modulation formats (*m*-QAM) and modulation techniques (OFDM and Nyquist WDM) have been proposed and presented. Also, certain optoelectronic devices (i.e. semiconductor optical amplifier) and techniques (feed-forward heterodyne linewidth reduction scheme) have been utilised to enable the desired system performance.

Introduction

Demand for bandwidth, driven by media-rich applications, shows no sign of abating and is pushing service providers to deploy optical transport and access networks with increased capacity. Wavelength division multiplexing (WDM) technology has been successfully used to expand capacity in these optical systems and meet increasing bandwidth requirements for more than two decades. Previous WDM systems have been based on simple modulation formats which provide poor spectral efficiency. On the other hand, such modulation formats based on intensity modulation and “square law” direct detection enabled simple upgrade of existed systems by increasing number of channels and/or data rate per channel, providing sufficient throughput for service providers. However, the bandwidth limitations of optoelectronic devices, and the limited speed of commercially available electronic circuitry, has motivated researchers, vendors and service providers to use available resources more efficiently. This has caused the revival of coherent optical communications in order to enable the use of higher order modulation formats and, consequently, increase the spectral efficiency of communication links and throughput. Additionally, the recent introduction of modulation techniques such as optical orthogonal frequency division multiplexing (OFDM) and Nyquist WDM has enabled significant reduction of guard bands between adjacent optical channels, and the generation of highly spectrally efficient multicarrier systems and optical superchannels. In addition to deployment of high capacity optical networks, an exponential increase in the amount of network traffic due to cloud computing and other emerging web applications has created the need for more powerful data centres. WDM is gaining significant attention as a promising solution offering high throughput, reduced latency and power consumption for optical interconnects within and in-between data centres.

Along with the development of high capacity and spectrally efficient optical systems and interconnects, the requirement for compact optical sources with sufficiently good inherent properties, such as optical linewidth, phase noise, relative intensity noise (RIN), optical carrier-to-noise ratio (OCNR) and frequency stability, has been created. Recently proposed spectrally efficient multicarrier systems require closely frequency spaced lasers at the transmitter and receiver side. However, conventional WDM laser banks struggle to provide a constant frequency separation between channels without

additional control mechanisms. Furthermore, conventional WDM lasers sometimes struggle to provide a sufficiently narrow linewidth. Therefore, high performance integrated laser arrays are needed to enable the required performance. An attractive alternative is an optical multicarrier transmitter, sometimes referred to as an optical frequency comb, which simultaneously generates multiple phase correlated optical carriers. A number of optical multicarrier sources have been proposed, such as mode-locked lasers (MLL), fiber lasers, electro-optic based multicarrier sources, gain-switched comb sources (GSCS), Kerr microresonator combs and parametric frequency comb sources.

Optical multicarrier sources with good spectral flatness, frequency stability, low linewidth and RIN on each tone, tunable free spectral range (FSR), high power and OCNR per line are highly desirable in multicarrier transmission systems. All of the aforementioned optical multicarrier sources exhibit certain advantages and drawbacks relative to each other. Conventional multicarrier sources, such as mode-locked and fibre lasers, can generate multicarrier signals over a wide bandwidth, but they suffer from relatively large linewidth and RIN of individual comb lines and usually do not offer FSR tunability. Electro-optic based multicarrier sources provide tunable FSR and central wavelength, typically with low linewidth and RIN on each individual tone, and high power per line and OCNR. However, inherent modulator properties such as bias drift and high insertion loss make this technique less attractive for practical deployment. Externally injected gain-switched comb sources feature tuneable free spectral range and centre wavelength, good spectral flatness, good OCNR, low RIN and low optical linewidth. The GSCS has only a finite available spectral bandwidth, which limits the number of optical carriers. Kerr comb sources can provide a large number of lines, but require sophisticated pumping schemes and the line spacing is inherently tied to the free spectral range of the underlying resonator. Broadband frequency combs can also be generated by multi-stage parametric mixers. However, this approach requires strong optical pumps and large interaction lengths in delicately arranged sequences of specialised optical fibres.

Main contributions

The main contributions of this work are:

- **Investigation of the inherent properties of optical multicarrier sources and their performance in optical systems**.

The semiconductor MLL, electro-optical modulation based comb source and externally injected GSCS have been characterised in terms of RIN and OCNR which have been recognised as limiting parameters for the performance of back-to-back (B2B) intensity modulated and directly detected (IM/DD) OFDM systems. The influence of RIN and OCNR on the system performance has been investigated experimentally and by simulations.

- **The first demonstration of downstream transmission of single sideband OFDM signals (SSB OFDM) in a WDM access network where a mode-locked laser is employed as a multicarrier transmitter**.

The downstream transmission also demonstrates the use of semiconductor optical amplifiers (SOA) in spectrally-efficient, IM/DD WDM-SSB-OFDM passive optical network for the simultaneous amplification of optical multicarrier OFDM signals using a single SOA. Furthermore, a performance comparison with an Erbium doped fibre amplifier (EDFA) shows that the SOA exhibits performance similar to an EDFA at 7% forward error correction (FEC) limit. The spectral efficiency of the system is also optimised, as the upstream data is placed in the spectral gap between downstream channels.

- **Demonstration of Tb/s optical interconnect solutions based on Quantum-Dash passive mode-locked lasers (Q-Dash PMLL) and SSB-OFDM modulation**.

An experimental demonstration of high capacity WDM transmission (400 Gb/s, 1 Tb/s, 2 Tb/s and 4 Tb/s), for interconnect applications within and between data centres based on a Q-Dash PMLL is presented. Inherent characteristics of Q-Dash passively mode-locked lasers, such as RIN and OCNR, have been analysed in detail. The effect of RIN on the system performance is investigated by examining the error-vector magnitude (EVM) of OFDM subcarriers over the desired frequency range. This work represents (at the date of the publication) the highest reported transmission capacity for Q-Dash based comb sources, to the best of our knowledge. The maximum spectral efficiency achieved was 2.76 bit/s/Hz.

- **Demonstration of Tb/s superchannel architectures using gain-switched comb source in coherently detected system. Demonstration of Tb/s WDM coherently detected system using Q-Dash PMLL.**

Six different superchannel architectures with different carrier spacings and modulation formats are investigated, and their performance for transmission over different

distances is evaluated. Spectral efficiencies up to 7.8 bit/s/Hz are obtained using polarisation division multiplexed (PDM) 16 state quadrature amplitude modulation (16-QAM) format. Capacities up to 2.112 Tb/s and transmission up to 300 km of standard single-mode fibre (SSMF) have been reported. The aforementioned spectral efficiency and capacity are the highest reported for GSCS. Also, the reported spectral efficiency is among the highest for 16-QAM modulation format superchannel systems.

Furthermore, a feed-forward heterodyne (FFH) phase noise reduction scheme that enables simultaneous optical linewidth reduction of multiple comb lines derived from a Q-Dash PMLL is proposed. The scheme enables the coherent transmission experiment using Q-Dash PMLL as an optical source for the first time, even though this optical multicarrier source exhibit linewidth higher than 10 MHz. Tb/s data rates have been achieved within the limits of standard FEC.

Thesis Structure

This thesis is structured as follows:

Chapter 1 describes the evolution of optical communications networks as well as the motivation behind their continued growth in capacity today. The optical network topology is introduced with descriptions of each network layer given. The capacity scaling approaches are discussed, with particular attention on WDM systems, advanced modulation formats and coherent detection. The theory behind recently proposed modulation techniques such as OFDM and Nyquist WDM have been discussed in detail. Also, different types of OFDM and Nyquist WDM systems have been presented. Finally, key components which are used to construct optical communication systems are discussed.

Chapter 2 is focused on various optical multicarrier sources. Mode-locked lasers, electro-optic based multicarrier sources, gain-switched comb sources, Kerr microresonator combs and parametric frequency comb sources have been analysed and compared. Typical methods for the generation of these comb sources are presented, as well as inherent characteristics of each individual multicarrier source (linewidth, RIN, OCNR, complexity, power per line and etc.).

Chapter 3 includes the characterisation and implementation of three optical multicarrier sources in the intensity modulated and directly detected OFDM system. RIN and OCNR of the semiconductor MLL, electro-optical modulation based comb

source and externally injected GSCS have been measured and presented as the limiting parameters for the performance of B2B IM/DD OFDM systems. The influence of RIN and OCNR on the system performance has been investigated experimentally and by simulations.

Chapter 4 examines the use of SOAs in WDM-OFDM systems. The SOA is used for simultaneous amplification of multiple OFDM channels and the system performance is compared to the case when an EDFA is employed instead of an SOA. A detailed characterisation of the SOA employed is presented. Furthermore, the optical access network architecture where a MLL is used as an optical multicarrier source is proposed.

Chapter 5 is focused on Tb/s optical interconnect solutions based on a single laser source. The Q-Dash PMLL is used as an optical multicarrier source for high capacity WDM-OFDM optical interconnects within and between data centres. RIN and OCNR of Q-Dash passively mode-locked lasers have been analysed in detail, as well as their influence on the system performance. A potential future chip-scale terabit-per-second optical interconnect transceiver incorporating the mode-locked lasers used in this work is also presented.

Chapter 6 presents Tb/s superchannel architectures using GSCS and advanced modulation formats in coherently detected Nyquist WDM system. Six different superchannel architectures with different carrier spacings and modulation formats are investigated, and their performance for transmission over different distances is evaluated.

Additionally, a coherent Tb/s communications experiment using Q-Dash PMLL is presented in this chapter. A feed-forward heterodyne linewidth reduction scheme is used to simultaneously reduce optical linewidth of a multitude of comb lines.

Chapter 7 gives a brief summary of conclusions that can be drawn from the results presented in this thesis. The potential for future work in the areas discussed throughout the thesis is outlined also.

Chapter 1

1 Optical Networks

As part of cultural and technological evolution, communication is imperative for human kind. Overall technological development is closely related to the evolution of communication systems, especially during the last number of decades as high speed terabit/s data transmission became requisite. This chapter gives an introduction to optical communications and the fundamental concepts behind. It also presents an overview of past and current optical networks, and provides details on the key devices and techniques used in various optical networks.

1.1 Introduction

The invention of semiconductor lasers in the 1960s as well as the development of low-loss optical fibres in the 1970s [1], created the foundation for the development of optical communication systems. In the late 1970s, the first fibre-optic systems, used for telephone communication, were tested and deployed in the United States [1]. The first optical communication systems operated at low data rates, e.g. 45 Mb/s in 1980. The steady development of technology during the early years of optical communications made foundations for gradual change of the optical transmission windows from 850 nm to 1300 nm, and finally to 1550 nm, and therefore a slow increase of bit rate in the single channel systems, as shown in Figure 1.1 [1-3].

The rapid growth in the capacity of optical communication systems is related to the advent of optical amplifiers to optical communication systems in the late 1980s [1, 4, 5]. Optical amplifiers became available commercially by 1989, enabling significant growth of the bit rate-distance product (BL) as shown in Figure 1.2 [1, 3]. During that time, the Internet was commercially deployed, and those technological breakthroughs triggered significant investments in optical communication systems, which led to rapid growth in the capacity of optical networks (Figure 1.1). The Internet quickly evolved from primarily text based to a multimedia platform and has been the main driver behind rapid growth of optical communication systems.

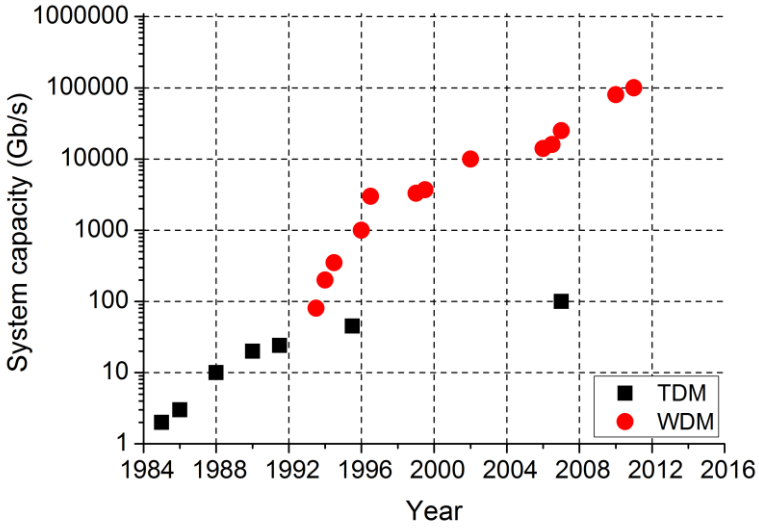

Figure 1.1. Capacities of optical lightwave systems over last 3 decades. Single channel time division multiplexed (TDM) systems (black filled squares), and WDM systems (red filled circles). After [2]

During the first three decades of development, the capacity of commercial optical systems increased more than 100 000 times (Figure 1.1). For more than two decades the capacities of installed optical systems exceeded the network traffic requirements [2].

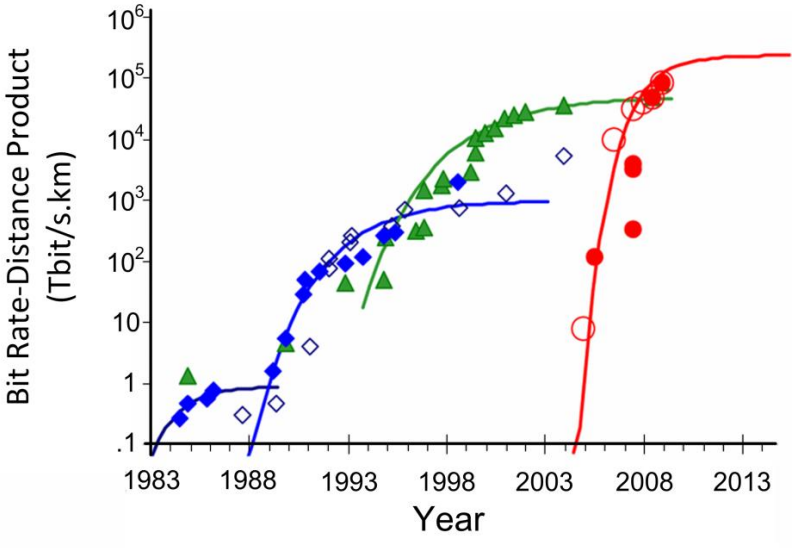

Figure 1.2. Evolution of bit rate-distance product for single wavelength (diamonds, open symbols for optical TDM), WDM (triangles), single and multi-band orthogonal frequency division multiplexing (OFDM) (filled circles) and coherent detection (open circles). The lines represent fitting between the measurement points After [3]

Nevertheless, the rapid growth of network traffic driven by media-rich applications such as on–demand HDTV, voice over IP (VoIP), video conferencing and online

gaming, inverted this situation and current trends show faster growing network traffic than system capacity [2]. Figure 1.3 illustrates global internet traffic for the period 1990-2012 estimated by Cisco Systems [6], along with the forecast for the internet traffic growth for the period between 2013 and 2018 (forecasted also by Cisco Systems [7]). The presented data indicates that from 1990 to 1994 internet traffic doubled every year. After rapid traffic increase in the period 1994-1996, growth has slowed with an annual growth rate of about 100% for the years 1997 to 2002 and 50–60% from then up to the present. Despite the decrease in annual traffic growth rate, the Cisco forecast predicts that global data traffic will reach 1.4 Zettabytes per year, or 120.6 Exabytes per month by 2017 [8]. The current trends predict that network traffic will grow 10 times faster than system capacity over the next decade [2]. The telecommunication industry will experience significant technological challenges to meet ever-increasing traffic requirements in the following decade, and development of optical solutions in order to solve such challenges is of crucial importance.

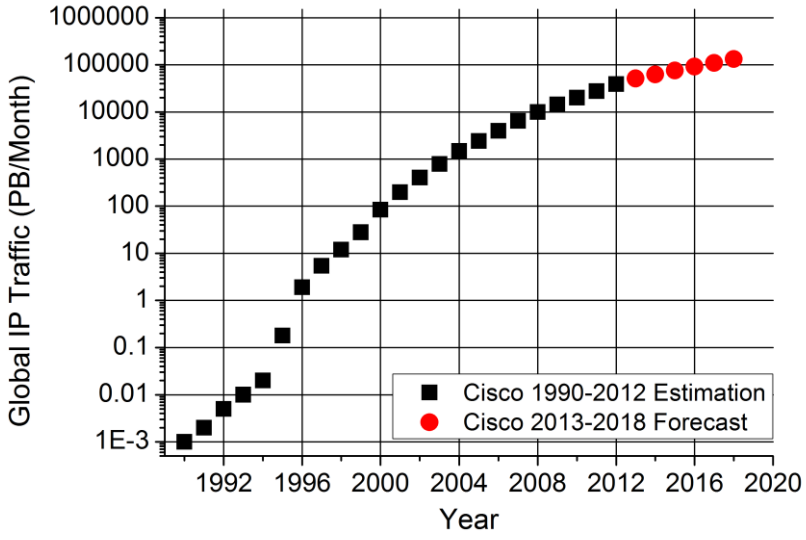

Figure 1.3. Estimated and forecasted global internet traffic growth for period 1990-2018.

1.2 Network Topology

The overall communication network is a complicated system which consists of a number of interconnected sub-networks. The mesh-like topology is typically used to provide robust communication links between major information exchange nodes.

However, geographical and functional division of such a communication system into core, metropolitan and access networks could be useful as these individual parts usually operate with different functionalities and specific requirements. The illustration of the general network topology is illustrated in Figure 1.4.

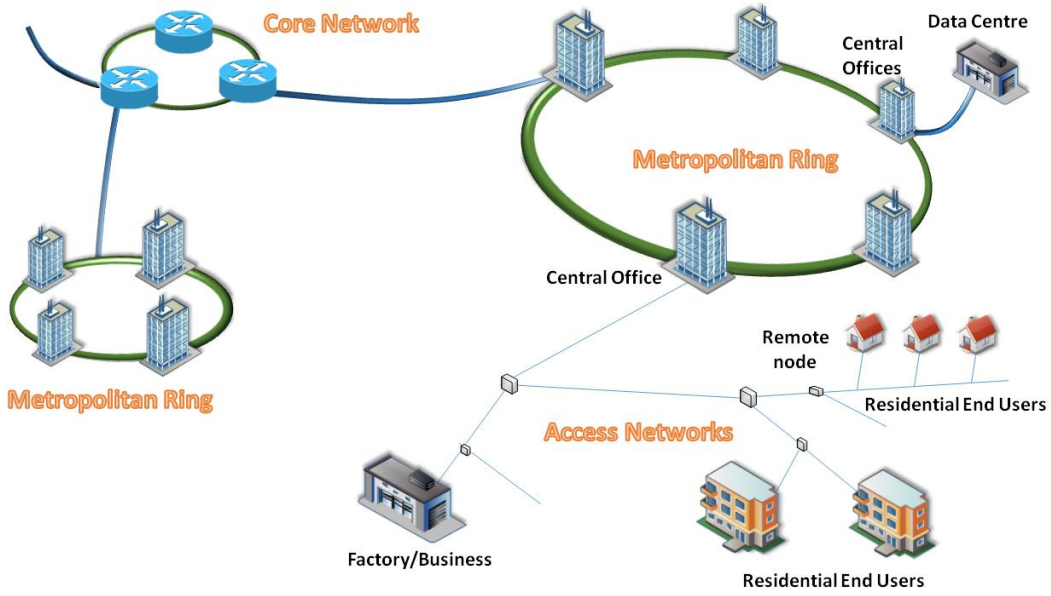

Figure 1.4. Illustration of network topology which includes core, metropolitan and access networks.

1.2.1 Core Networks

Core networks serve to connect continents and countries, and are made up of terrestrial or submarine links. While submarine systems are optically amplified point-to-point long-haul links, terrestrial networks consists of many nodes each interconnected by an amplified fibre link. These nodes serve as interconnections between core and metro networks by transferring data from the core network to the metro network or vice versa using either optical or electrical switching. Core networks are optimised to transport large amounts of aggregated data over a few hundreds to a few thousands of kilometres. The terrestrial core networks typically span up to a few thousands of kilometres, whilst ultra-long-haul submarine links cover Trans-Atlantic and Trans-Pacific distances. This has been made possible through the use of distributed optical amplification, advanced modulation formats, dispersion compensating fibre (DCF), forward error correction and recently by coherent detection

[9-12]. Figure 1.5 provides an example of terrestrial core networks in USA and Europe, and submarine links between the two continents.

Early core networks were time division multiplexed (TDM) based systems which primarily employed Synchronous Optical Networking (SONET) and Synchronous Digital Hierarchy (SDH) protocols for traffic control, with 2.5 and 10 Gb/s interface rates. Commercial deployment of WDM systems increased network capacity by allowing multiple wavelengths to be carried on the same fibre.

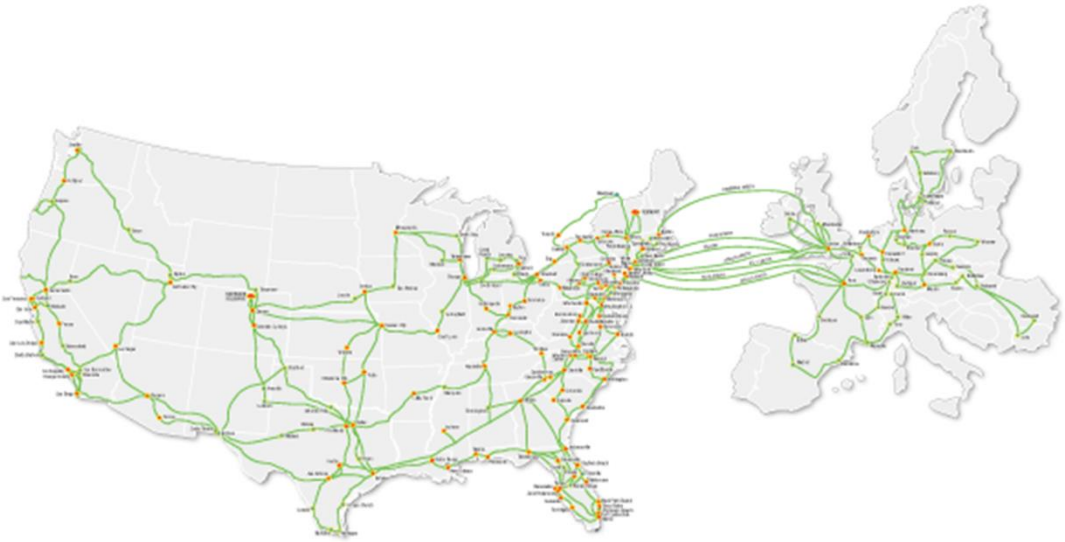

Figure 1.5. An example of core network which includes terrestrial core networks in USA and Europe, and submarine links between USA and Europe. After [13].

By the mid-1990s, operators started to use SONET/SDH networks to carry data services such as Ethernet and Asynchronous Transfer Mode (ATM), primarily to avoid the need to operate two separate networks, one dedicated to voice and another dedicated to data [14]. Legacy core networks used optical-electrical-optical (O-E-O) conversion in the exchange nodes for traffic switching and routing, which often created bottlenecks and increased latency [15]. In order keep pace with continually growing traffic demands and to support diversity of network protocols, the requirement for modernisation and transformation of optical core networks has risen. Modern core networks, designed to have capacity greater than 1 Tb/s or even 10 Tb/s [16], which are achieved by using WDM and data rates of 40 and/or 100 Gb/s per channel, employ Optical Transport Network (OTN) protocol defined in ITU G.709 [17] to multiplex services onto optical light paths. It allows service providers to converge networks through the transport of numerous types of legacy protocols, whilst

providing the flexibility required by supporting future protocols [17]. Simultaneously with advances on the traffic management plane, intensive research on physical layer technologies showed that optical signals can be routed through network nodes without conversion into an electrical domain, which significantly reduces the latency, energy consumption, size and cost of modules. A significant step towards all-optical traffic switching was the development of reconfigurable add-drop multiplexers (ROADM) which enable the traffic exchange in the optical domain without conversion to an electrical signal [18, 19].

An example of a modern submarine link is the Asian Submarine-cable Express which carries 40 Gb/s per channel and has a maximum projected aggregate capacity of 15 Tb/s [20]. Asian Submarine-cable Express extends across approximately 7,800 km to link Japan with the Philippines, Hong Kong, Malaysia, and Singapore. An example of a core terrestrial network is the pan-European network (PEN) which connects London, Paris, Lyon, Marseille, Turin, Milan, Zurich, Frankfurt, Amsterdam, Brussels and other European cities [21]. The PEN is currently about 6160 km long, with span lengths ranging from 60 km to 95 km. The amplification is performed using EDFAs only. The PEN has been upgraded from 10 to 40 Gb/s by using return-to-zero differential quadrature phase-shift keying (RZ-DQPSK) on a 50 GHz grid, and further increases in total capacity are being considered by using 100 Gb/s data channels employing polarisation division multiplexed quadrature phase-shift keying (QPSK) format on 50 GHz grid. Besides EDFA based optical amplification, which is dominantly used in the current optical core and metropolitan networks, Raman amplification can be used as well. Distributed Raman amplifiers can be deployed in conjunction with EDFAs to improve the signal-to-noise ratio (SNR) and reduce the nonlinear penalty and therefore increase BL product [9].

1.2.2 Metropolitan Networks

Metropolitan (metro) area networks (MAN) provide the connection between core networks and access networks and typically span from tens up to a few hundred kilometres (e.g. 20-300 km). As shown in Figure 1.4, metro networks typically implement a ring topology and connect several central stations which represent traffic exchange nodes. Metropolitan networks provide backwards compatibility by supporting legacy technologies. The recent growth of data centre and video based

traffic means that metro traffic will grow about two times faster than traffic going into the core networks by 2017 [22]. Therefore, metropolitan networks have to meet growing traffic requirements and integrate with current core networks standards. Metropolitan networks evolved from TDM based systems which primarily employed SONET and SDH, to WDM based optical systems which support a large range of technologies such as SONET/SDH, WDM, Internet Protocol (IP), ATM, Multiprotocol Label Switch (MPLS) and Ethernet, which is enabled by OTN technology which standardises metro network operation to support these services. Legacy SONET/SDH based metro networks required O-E-O conversion in exchange nodes, while modern MANs employ ROADMs for flexible and dynamic traffic exchange [23]. Early metro networks operated at data rates up to 2.5 Gb/s using simple on-off keying (OOK) modulation format. Current metropolitan networks support higher data rates and are evolving towards 40 and 100 Gb/s interface data rates on 50 GHz grid enabled by coherent reception. An example of a metropolitan network is Deutsche Telecom network [24, 25], which mostly consists of standard single mode fibres G.652 with DCFs periodically distributed along the routes. Span lengths are usually in the range 60-80 km, and EDFA amplification is used. Coarse WDM (CWDM) or dense WDM (DWDM) is utilised depending on the required aggregate data rate.

1.2.3 Access Networks

The access network connects the end users to the rest of the network, typically to the first node of the metro network, and therefore it is often referred to as last/first mile of the network. Access networks typically cover distances from a few hundred meters up to a few kilometres. In some cases it can span up to tens of kilometres (e.g. 20 km). However, due to the high capital expenditure (CAPEX) required for deployment of optical access infrastructure from the central stations to the end users, service providers tend to exploit the existing cooper cabling infrastructure. Therefore, optical access networks are not currently widely deployed. Figure 1.6 shows the percentage of fibre connections in total broadband subscriptions among Organisation for Economic Cooperation and Development (OECD) countries in June 2014. It can be seen that the level of fibre penetration significantly varies between countries [26].

The strong competition for broadband access services between several technologies which currently satisfy end user requirements postponed deployment of optical

infrastructure in most countries. Currently, the dominant access technologies are Digital Subscriber Loop (DSL) (ITU-T G.922), coaxial cable (ITU-T J.112/122), and wireless access technologies such as Wi-Fi (IEEE 802.11) and WiMax (IEEE 802.16) [27]. DSL uses copper twisted pairs, originally designed to carry 4 kHz voice data, by assigning certain frequency bands for voice and data transmission. Several DSL techniques exist such as Asymmetric Digital Subscriber Loop (ADSL) and Very high-bit-rate Digital Subscriber Loop (VDSL). ADSL offer speeds of up to 24 Mb/s, while VDSL can increase the data rate to above 100 Mb/s.

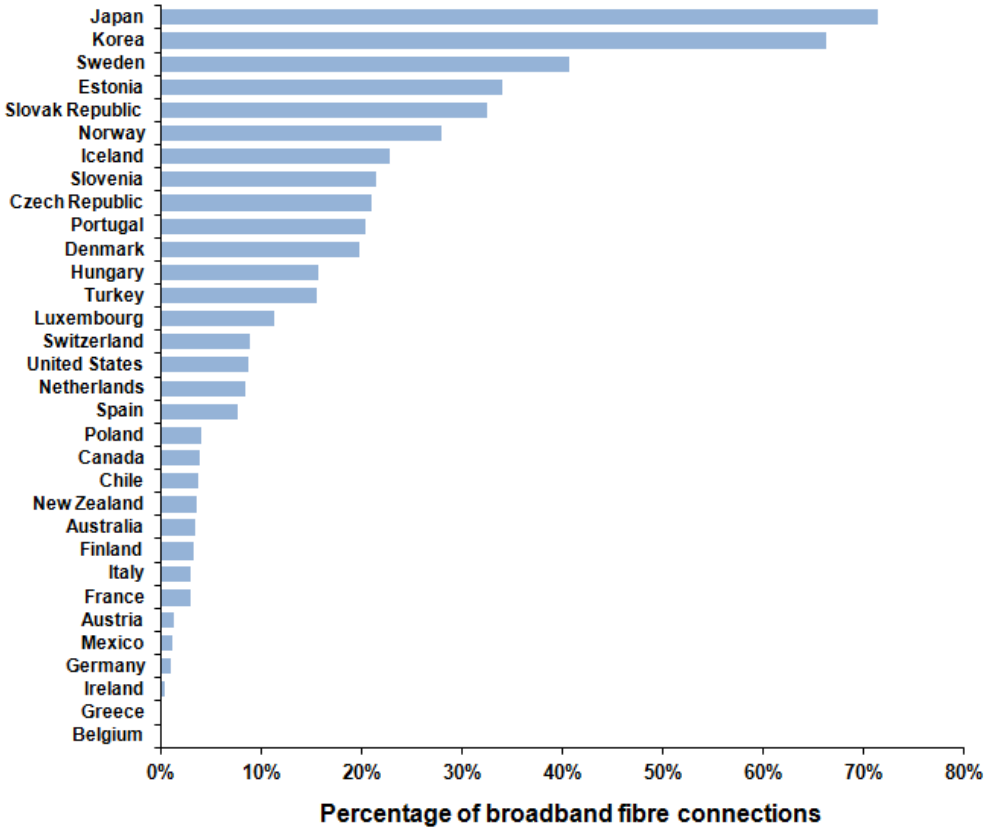

Figure 1.6. Broadband fibre connections as a percentage of all connections, OECD: June, 2014. After [26].

Another widely deployed broadband connection is coaxial (coax) copper cable, initially used for the transmission of analog TV signals. As coaxial cables typically provide higher bandwidth than twisted copper pairs, higher data rates up to 100 Mb/s and longer transmission distances can be achieved. However, transmission distances are limited due to the high loses in the coaxial cables and regeneration with electrical amplifiers is required every few hundred meters, in order to ensure sufficient received power. A solution to overcome this problem is to deploy optical fibre from the central

office (CO) to the remote node (RN), and coaxial cable from the RN to the end users (see Figure 1.4). At the RN the optical signal is converted to an electrical domain. This type of access network is known as a hybrid fibre–coaxial (HFC) network. Several forms of HFC networks have been deployed, such as Fibre–to–the–Node (FTTN), Fibre–to–the–Cabinet (FTTC) or Fibre–to–the–Basement (FTTB), and the term FTTx can be used to refer to these technologies collectively. Current FTTx access networks are capable of providing downstream speeds of up to 100 Mb/s to each user [28].

Common wireless access network designs to reach end users include Wireless Fidelity (WiFi), Worldwide Interoperability for Microwave Access (WiMAX), and Long-Term Evolution (LTE). Although wireless technologies provide flexible mobile access solution, these techniques are fundamentally limited by the unreliability of the wireless channel and also have a limited access range. Also, wireless technologies are not suitable for sending large amounts of information to many users over long distances with high quality of service (QoS) [29].

The bandwidth and/or the physical reach of copper twisted pairs, coaxial cables and wireless access technologies are limited due to the physical media constraints. The EU has set a target that all Europeans will have access to connection speeds of at least 30 Mb/s and 50%, or more, of European households should have subscriptions above 100 Mb/s by 2020. Other jurisdictions have set similar targets, for example China's national broadband strategy has set goals of reaching 12 Mbit/s in rural areas, 50 Mbit/s in urban areas and 1 Gbit/s in large cities by the end of 2020. To meet the ever-increasing bandwidth demand, service providers will need to deploy optical access networks. Industry and standards committees have been continuously working on developing and upgrading standards to meet growing bandwidth demands.

1.2.4 Optical Access Networks

Optical access networks can be realised using two common topologies: point-to-point (home run) and point-to-multipoint (star) [29]. In the point-to-point architecture, a single fibre is dedicated to each end user, which provides huge amount of bandwidth to each subscriber. However, deployment of a separate fibre from the CO to each optical network unit (ONU) requires large capital expenditure, which is the main

disadvantage of this topology. A more economical solution is point-to-multipoint architecture, where an optical fibre is deployed from the central office to the remote node which can be active or passive, and which is located near to the user premises. Point-to-multipoint access networks which use active remote node are referred as active optical networks (AON), whilst the access networks which use passive remote nodes are classified as passive optical networks (PON). AONs typically use optical amplifiers at the RN for power budget extension, which can be utilised to extend the reach or increase number of users (split ratio) [30]. In both AONs and PONs, the end users are connected with the RN using optical fibres, where a single fibre is required for each end user. Passive optical networks can employ TDM technology, WDM technology, or a hybrid TDM-WDM approach [29]. Recently, OFDM based PONs have been proposed, and hybrid WDM-OFDM architecture as well [29, 31, 32].

1.2.5 Data Centres and High Performance Computing Systems

An exponential increase in the amount of network traffic due to cloud computing and other emerging web applications has created the need for more powerful data centres [33]. The typical data centre architecture is illustrated in Figure 1.7. Data centres host a number of servers which are interconnected through the data centre network. Communication with the external networks, e.g. internet, is performed via content switches and load balance switches which are located at the front end of a data centre. Current data centres are mostly organised in a tree topology, typically consisting of two or three layers [33]. Multiple servers (located in racks) are connected to top-of-the-rack (ToR) servers using high speed electrical interconnects over maximum distances of a few meters. ToR servers are interconnected via aggregate switches using 1 or 10 Gb/s optical multimode fibre (MMF) links covering distances of tens to hundreds of meters. Finally, the aggregate switches are connected by core routers using 40 or 100 Gb/s optical links based on standard single mode fibres over maximum distances of a few kilometres. The main drawbacks of the current data centres are high power consumption of switches and routers, and mismatch in bandwidth performance between core and edge network which introduces significant latency. Integrated optical interconnects are considered as a potential solution to enable high throughput, reduce size of modules, power consumption and latency [33].

In contrast to data centres where the traffic flows in “east-west” direction, high performance computing (HPC) systems are characterised with “north-south” traffic flow due to the nature of utilised computing tasks. HPC systems perform calculation intensive tasks such as numerical modelling of various processes, which require high bandwidth interconnects, whilst the low latency is not a crucial requirement [34]. Therefore, significant research efforts have been made in development of high data rate optical interconnect HPC systems [33, 34].

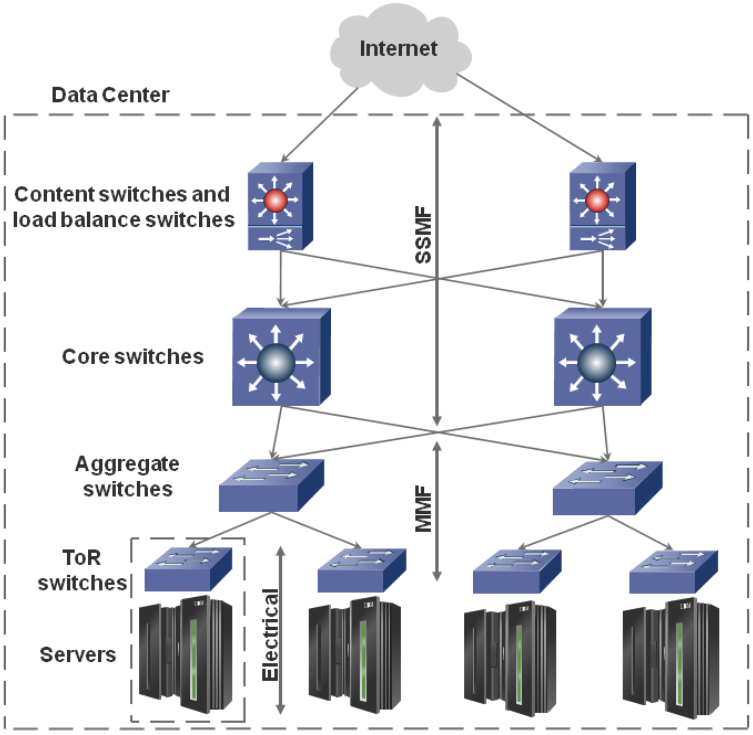

Figure 1.7. Architecture of current data centre network.

1.3 Capacity Scaling Methods

Optical signal and optical transmission media (e.g. optical fibres) possess several physical dimensions that can be used for capacity scaling. Figure 1.8 shows available physical dimensions which can be used to construct orthogonal signal spaces for modulation and/or multiplexing in optical communications [35].

- Before deployment of optical amplifiers in 1990s, optical time division multiplexing (OTDM) was used to increase capacity of optical communication systems. In OTDM, a number of lower data rate streams (tributaries) are time multiplexed to form higher speed optical signals [36]. The time dimension is used for multiplexing by allocating different time slots to different channels [35].

- The optical signal has real and imaginary parts, which are referred as the quadrature dimension. The quadrature dimension enables generation of advanced modulation formats by modulating both amplitude and phase of the optical signal. Therefore, the transmission of two or more bits per symbol is enabled.

- The wavelength multiplexing in WDM systems is enabled by the frequency dimension. Due to the importance of the WDM systems, section 1.3.1 provides much more details about previous, current and future trends in WDM systems.

- The optical signal in the optical fibre or optical waveguide exhibits two states of polarisation. Consequently, the polarisation dimension is used for independent modulation of two polarisation states, which is referred to as polarisation division multiplexing. PDM provides a twofold increase in system capacity.

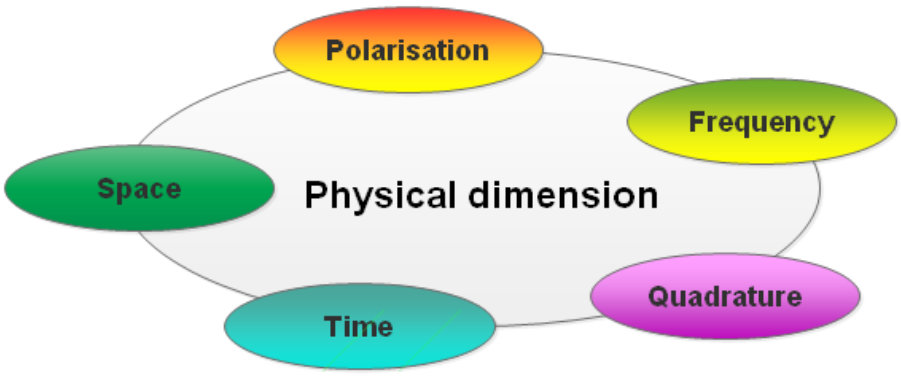

Figure 1.8. Physical dimensions available for capacity scaling.

- The space dimension has been used in its most trivial form by using parallel optical transmission links, such as a number of optical fibres connected together in standard optical cable or multi-mode ribbon cable which is often used in data centres, although multicore and multimode fibres have been introduced three decades ago [37, 38]. However, true space division multiplexing (SDM) gained significant research interest during the last few years as a promising solution to further increase system

capacity in an economical and sustainable way. Nevertheless, many issues related to the integration of the components and devices used in the SDM systems have to be solved to enable commercially available SDM technology [35]. To date, the highest reported experimentally achieved system capacities have been enabled by use of multicore or multimode SDM technology [39].

1.3.1 Wavelength Division Multiplexing

With the deployment of optical amplifiers which enabled the possibility for simultaneous amplification of multiple optical channels, WDM became the main optical multiplexing technique used to increase the system capacity. Conceptually similar to frequency division multiplexing (FDM) in radio communications, WDM uses a certain number of wavelengths to transmit data, where each wavelength represents an individual channel, with a certain frequency separation between two adjacent wavelengths. As shown in Figure 1.9, each optical carrier is modulated independently using external or direct modulation. The individual channels are then multiplexed and transmitted over the optical fibre. Insertion and removal of a desired channel is performed using optical add-drop multiplexers, which can be realised using Bragg gratings [40], micro-electro-mechanical systems (MEMS) devices [41] and liquid-crystal-on-silicon (LCoS) based filters [42].

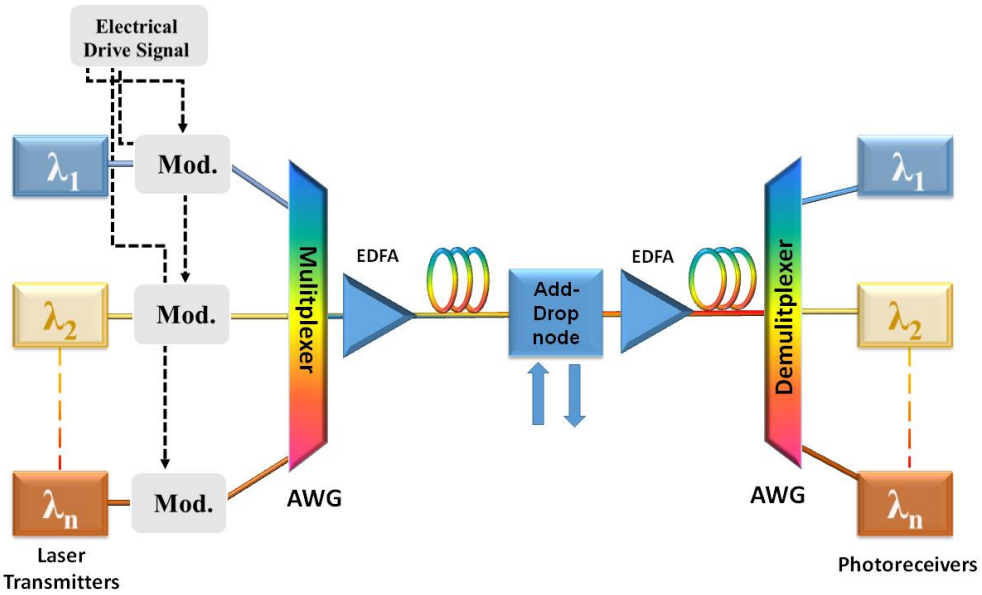

Figure 1.9. Generic WDM architecture.

At the receiver side the optical signal is demultiplexed into individual channels and distributed to the intended destination. Photodetection of optical channels can be performed using direct detection or coherent detection. In conventional directly detected WDM systems demultiplexing is carried out using an arrayed waveguide grating (AWG) which uses precise phase shifts and free space propagation to direct each WDM channel to an individual fibre [43]. WDM systems based on coherent detection do not require an optical demultiplexer as the local oscillator (LO) laser acts as a tunable filter [44].

The frequency separation between two adjacent wavelengths is known as the channel spacing. The value of the frequency separation between the adjacent channels is determined by a number of factors such as data rate per channel, modulation format used for the encoding of the data, pulse shaping and inherent characteristics of the optoelectronic components employed, e.g. bandwidth and roll-off factor of optical filters. In the early WDM systems the channel spacing was typically around 20 nm, and those systems are known as CWDM [45]. Current core and metropolitan networks employ WDM systems which operate at 100 and 50 GHz grid spacing, as standardised by International Telecommunication Union (ITU) [46]. WDM systems with 50 GHz channel spacing are known as DWDM systems and operate in the C- and L-bands [45, 46]. Requirements for further reduction of channel spacing motivated ITU to standardise WDM systems with 25 and 12.5 GHz channel spacing. Those systems are known as ultra dense WDM (UDWDM) and standardisation has been published in ITU G.694.1 [46]. Although the reduction of channel spacing implies an increase in the number of channels in WDM systems, the growth of the total capacity can also be achieved by increasing the data rate per channel and though improving the spectral efficiency. The spectral efficiency is a measure of efficient utilisation of available bandwidth to achieve a targeted data rate. It is defined as a ratio of symbol rate of the channel R_b and channel bandwidth allocation (or channel spacing) Δf. While most of the current commercial WDM systems operate at the spectral efficiency which is lower than 1 bit/s/Hz, recent research progress enabled experimental and field trial demonstrations of the optical transmission systems with very high spectral efficiencies [16, 35, 45]. The first step towards high SE systems was the revival of coherent optical communications during the previous decade, which enabled the use of higher-order modulation formats. The digital coherent receiver allows linear mapping of optical field and enables the detection of amplitude and phase components of both polarisations and, therefore, quadruples the spectral efficiency [47]. Additionally, the recent introduction of

modulation techniques which explore time and frequency domain orthogonality between neighbouring channels such as OFDM and Nyquist WDM, enabled a significant reduction of guard bands between adjacent optical channels and the generation of highly spectrally efficient multicarrier systems and optical superchannels [45, 48, 49]. It is therefore instructive to classify WDM systems based on the channel bandwidth allocation relative to the modulation symbol rate of the channel to emphasise efficient utilisation of available spectrum, as suggested by Chandrasekhar and Liu in [45]. In Table 1.1, different classes of WDM systems are thus defined [45].

As can be seen from the Table 1.1, besides CWDM, WDM and DWDM systems, the recent advances in high spectral efficiency systems has created the new regimes, identified as "quasi-Nyquist" WDM (for $1 \leq \Delta f/R_b \leq 1.2$), "Nyquist" WDM (for $\Delta f/R_b = 1$) and "super-Nyquist" WDM (for $\Delta f/R_b < 1$), respectively. Modulation techniques which enabled the creation of the new regimes, namely OFDM and Nyquist WDM are discussed in detail in the following sub-sections.

Condition $\Delta f/ R_b$	Definition	Example
> 50	Coarse WDM	10 Gb/s on 20 nm
> 5	WDM	10 Gb/s on 100 GHz
$1.2 \leq \Delta f/R_b \leq 5$	DWDM	28 GBaud PDM-QPSK on 50 GHz
$1 \leq \Delta f/R_b \leq 1.2$	Quasi-Nyquist WDM	28 GBaud PDM-QPSK on 33 GHz
$\Delta f/R_b = 1$	Nyquist WDM	28 GBaud PDM-QPSK on 28 GHz
$\Delta f/R_b < 1$	super-Nyquist WDM	28 GBaud PDM-QPSK on 25 GHz

Table 1.1. Definitions of various classes of WDM. After [45]

1.3.2 Advanced Modulation Formats

From the beginning of the previous decade it was clear that the requirements for the network capacity due to the trends in the network traffic growth could not be fulfilled with simple scaling of the existing technology, which was mainly based on 10 Gb/s non-return-to-zero (NRZ) OOK modulation format. Due to the expenses involved in deploying new fibre optic links, the main focus was to upgrade the existing network using more advanced underlying technology. Even though the possibility of the practical implementation of 40 Gb/s OOK systems was demonstrated [50], it was realised that the obtained spectral efficiency would not be sufficient for the future optical networks. Furthermore, the difficulties in managing the transmission impairments at higher data rates, such as chromatic and polarisation mode dispersion

[51], motivated researchers to revive coherent detection which was the subject of intensive research during the 1980's [44, 52].

Before the coherent systems were fully revived, higher order modulation formats such as differential phase shift keying (DPSK) and DQPSK have been considered for 40 and 100 Gb/s interface solutions [10, 53]. The field trials employing these modulation formats at 40 and 100 Gb/s data rates have been successfully demonstrated [24, 54]. At the time, DPSK and DQPSK formats were attractive solutions to increase system capacity mainly due to the direct detection based receiver which can be realised with low complexity as key components such as the optical delay-interferometer become mature. Furthermore, monolithic PDM-DQPSK receivers which allow high bit rate signal reception and automatic polarisation tracking have been proposed [55-57]. Both DPSK and DQPSK modulation formats have been deployed in carrier networks. DQPSK format at 100 Gb/s data rate is typically deployed on 100 GHz frequency grid. For transition to 50 GHz channel spacing, the data rate per channel needs to be reduced to avoid overlapping of the adjacent channels which causes significant performance degradation. In [53] the spectral efficiency of 3.4 bit/s/Hz was achieved with 84.5 Gb/s PDM-RZ-DQPSK signal on 50 GHz grid.

With the advances in speed and bandwidth of electronic circuitry and digital signal processing (DSP), the basis for development of coherent receivers and coherent reception of optical signals was founded. The digital coherent receiver allows linear mapping of the optical field and enables the detection of the real and imaginary components of the complex amplitude of both polarisations of the optical field and, therefore, quadruples the spectral efficiency. With the significant cost reduction of key components for optical coherent systems, such as high quality optical sources, optical field modulators (IQ Mach-Zehnder modulator), phase and polarisation diversity 90° optical hybrids and analog-to-digital and digital-to-analog converters (ADC/DACs), higher spectral efficiencies have been achieved with QAM formats [16] (see Figure 1.10(a)). QAM formats are often denoted as *m*-QAM, where *m* represents the number of states per symbol. With increasing of number of bits per symbol, spectral efficiency increases accordingly for a given bit rate, and the baud rate (symbol rate) reduces which allows for the use of lower cost electro-optical devices and readily available electronic circuitry. However, with the increase of the number of bits per symbol, the more stringent the requirements on the SNR of the received signal become, as shown in Figure 1.10(b). Therefore, depending on the application a specific *m*-QAM format would be used. 4-QAM, which is also known as QPSK is typically used for long reach

applications as it has the lowest SNR requirements among *m*-QAM formats [58]. Maximum spectral efficiency achievable with QPSK format per-polarisation is 2 bit/s/Hz. For the capacity oriented applications where reach is not of crucial importance, 16-QAM [59, 60], 32-QAM [61, 62] and 64-QAM [62, 63] modulation formats can be considered. The maximum achievable spectral efficiency per-polarisation for these modulation formats are 4 bit/s/Hz, 5 bit/s/Hz and 6 bit/s/Hz respectively. As shown in Figure 1.10(b), transition from QPSK to 16 QAM (which doubles the spectral efficiency and system capacity), comes at the requirement of a 3.7 dB higher SNR per bit, or 6.7 dB higher optical SNR (OSNR) [64] at fixed symbol rate [16]. A further doubling in spectral efficiency and capacity, from 16-QAM to 256-QAM, however, comes at the expense of an additional 8.8 dB in required SNR per bit (see Figure 1.10(b)), which is not feasible to accommodate without reducing system reach [16]. The implementation of 512-QAM format and transmission over 150 km has been reported in [65]. Besides SNR requirements for increasing modulation order (number of bits per symbol), the purity of optical sources, by means of phase noise and optical linewidth characteristics, becomes the limiting factor [44].

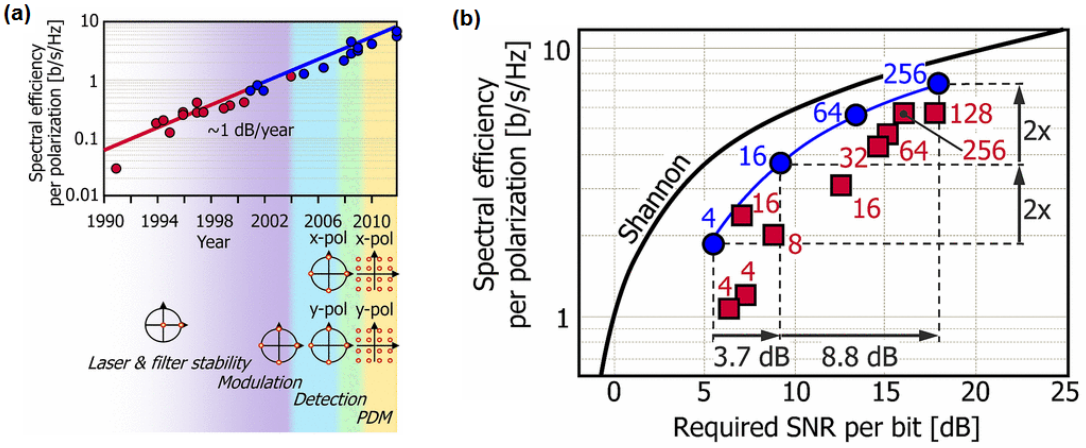

Figure 1.10. (a) Experimentally obtained *per-polarisation* spectral efficiencies in single (red) and dual-polarisation (blue) experiments. (b) Spectral efficiency versus received SNR per bit (per-polarisation). The Shannon limit for a linear, additive white Gaussian noise channel is shown together with the theoretical performance of various square QAM formats (blue circles). Red squares represent experimental results where numbers indicate QAM constellation sizes. After [16].

It has been shown that the QPSK format has the strongest bandwidth requirements, and simultaneously the lowest requirements for the resolution of DAC/ADCs [66]. With the increase of modulation order, the requirements on bandwidth relax, whilst the requirements on the DAC/ADC resolution increase [66]. The trade-off between the bandwidth of electronic circuitry and resolution of ADC/DACs has resulted in 16-QAM

being the optimum modulation format to achieve the highest per-interface data rate over longest distances [66]. Indeed, the highest interface data rate of 320 Gb/s at 80 GBaud, polarisation multiplexed to a single-carrier 640 Gb/s was achieved with 16 QAM modulation format [67]. Interface data rate of 450 Gb/s and transmission over 800 km was achieved with polarisation multiplexed 32-QAM [61].

1.3.3 Spectral and Temporal Signal Shaping

The new regimes in WDM transmission technology, such as quasi-Nyquist WDM, Nyquist WDM and super-Nyquist WDM, have been enabled by utilising spectral and temporal shaping of the pulses that carry the data. The spectral and temporal signal shaping has been used for many decades in the radio communications to mitigate transmission impairments and to enable more efficient usage of available bandwidth [68]. The initial use of the signal shaping techniques in optical communications was motivated by the requirements for the reduction of the inter-symbol interference (ISI) and improvement of the transmission performance of the signal [6, 69]. The underlying idea was to convert the NRZ signals into RZ or carrier-suppressed return-to-zero (CSRZ) signals using pulse carvers, such as Mach-Zehnder modulators (MZM) in order to obtain the desired robustness of the signal. However, the improvement in the spectral efficiency was minor as sufficient guard bands have to be provided to ensure that signal spectra would not overlap significantly. This was necessary to ensure that channel filtering in WDM systems using WDM filters would be possible without inter-carrier interference (ICI) [69].

Over the last decade, the battle to achieve higher spectral efficiencies played out on two fronts which are inextricably connected. On one front, the advances in optical coherent detection formed the basis for the employment of advanced modulation formats, which enabled the use of the quadrature dimension of the optical signal as discussed in the previous subsection. On the second front versatile pulse shaping methods were investigated, where digital signal processors, electronic filters or all-optical approaches generate the desired shape of the signal [49, 69]. The utilised signal shaping methods provide orthogonality in either spectral or temporal domain by using corresponding pulse shapes. A number of pulse shapes have been investigated but rectangular shaped, sinc-shaped, raised-cosine and root-raised-cosine shaped pulses are the dominant pulse shapes used [49, 69-71]. The orthogonality between adjacent pulses (or between any two pulses within a signal) allows transmission of

signals without ISI and ICI in an ideal linear channel [68]. In practice, the transmission channel is usually nonlinear, but the orthogonality is still well preserved. The two independent linear functions ($\phi_k, \phi_{k'}$) are orthogonal if their inner product over a specified range (*a*, *b*) normalised by weight function $\omega(t)$ is equal to Kronecker delta [69]:

$$\left\langle \phi_{k'} \middle| \phi_k \right\rangle_{\omega} = \int_a^b \phi_k(t)\phi_{k'}(t)\omega(t)dt = \delta_{kk'} \tag{1.1}$$

The recent extensive use of the orthogonal pulse shapes enabled two new transmission techniques, namely orthogonal frequency division multiplexing and Nyquist WDM (also known as orthogonal time division multiplexing), with a number of variations. OFDM employs signal orthogonality in the frequency domain, whilst Nyquist WDM uses temporal orthogonality of employed signals.

1.3.3.1 Orthogonal Frequency Division Multiplexing

The concept of OFDM was first proposed by Chang of Bell Labs in 1966 [72] for dispersive fading channels. The cognition that the employment of the discrete Fourier transform (DFT) can be used to replace the banks of sinusoidal generators and the demodulators, suggested by Weinstein and Ebert [73] in the 1970's, significantly reduces the implementation complexity of OFDM systems. Nevertheless, the lack of powerful integrated electronic circuits to support the complex computation required by OFDM postponed the commercial implementation of OFDM until the mid-1990s. In the mid–1980s, OFDM began to be considered for practical wireless applications. Cimini of Bell Labs [74] published analytical and early experimental results on the performance of OFDM modems in mobile communications channels. In 1987, Lassalle and Alard [75] proposed the use of OFDM for radio broadcasting. OFDM was standardised as the European Digital Audio Broadcast (DAB) as well as Digital Video Broadcast (DVB) scheme in mid-1990's. OFDM is now widely applied in radio systems for digital audio and video broadcasts, Wireless Local Area Networks (WLAN), Wireless Wide Area Networks (WWAN, Worldwide Interoperability for Microwave Access, or WiMax), and wire line access systems via ADSL.

The first application of OFDM to optical communications was shown by Pan and Green in 1996 [76]. They demonstrated the direct modulation of a laser diode with a

RF OFDM signal. However, the robustness of OFDM modulation to dispersion in an optical channel has been demonstrated in 2001 by Dixon *et. al.* [77]. This tolerance to dispersion in an optical channel has since been recognised as one of the key advantages of OFDM. The application of OFDM to long-haul optical communications for both coherent detection and direct detection [70, 78, 79] was introduced in 2006. After that, there are an increasing number of papers on the theoretical and practical performance of optical OFDM transmission, including 100 Gb/s [80] and 1 Tb/s channel data rate [81] transmissions. Novel optical OFDM schemes such as no-guard interval transmission [82] and all-optical OFDM [83] were also reported.

OFDM is a type of multi–carrier modulation (MCM) technique which transmits data on many subcarriers which are harmonically related. In contrast to typical MCM systems, such as WDM where sufficient frequency guard bands between the subcarriers are provided (see Figure 1.11(a)), in OFDM the subcarriers overlap as shown in Figure 1.11(b). However, in the OFDM signal the subcarrier frequencies are chosen so that the signals are mathematically orthogonal over one OFDM symbol period with the peaks of the subcarrier spectra coinciding with the nulls of the spectra from neighbouring subcarriers. The orthogonality condition can be obtained from the correlation between any two OFDM subcarriers s_k which are given by [70, 84, 85, 86]:

$$s_k(t) = \prod(t)\, e^{j2\pi f_k t}$$
$$\prod(t) = \begin{cases} 1, & (0 < t \le T_s) \\ 0, & (t \le 0, t > T_s) \end{cases} . \qquad (1.2)$$

An OFDM signal can be represented as:

$$s(t) = \sum_{i=-\infty}^{\infty} \sum_{k=0}^{N-1} c_{ik} s_k (t - iT_s) \qquad (1.3)$$

where $k = 1,2,...,N$ and N is total number of subcarriers, c_k is a complex data at k_{th} subcarrier, s_k is the waveform of the k_{th} subcarrier, f_k is the frequency of the k_{th} subcarrier, and T_s is the symbol period. In general, each temporal symbol consists of a superposition of *N* temporal sinusoids with equidistant carrier frequencies f_k inside a temporally rectangular window defining the temporal symbol length T_s. Furthermore, an OFDM signal *s*(*t*) is an infinite sequence of temporal symbols. In the frequency domain, each OFDM symbol can be represented as a set of *N* sinc-shaped functions centred at f_k, which can be observed after Fourier transforming of Eq. 1.2

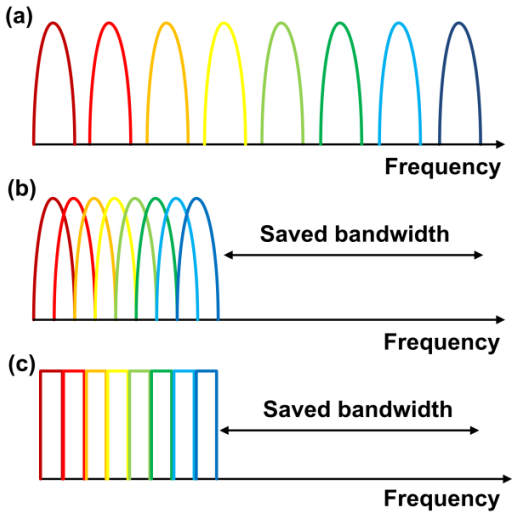

Figure 1.11 (a) Typical multi–carrier modulation with sufficient guard bands in-between the channels. (b) OFDM modulation. (c) Nyquist WDM.

and 1.3 [84]. The spectrum of the OFDM signal is then an infinite sequence of spectral symbols. Generation of OFDM signal is illustrated in Figure 1.12. For simplicity, the summation variable k is kept at 0 (i.e. only one carrier "frequency" f = 0), and Figure 1.12 illustrates the generation of an OFDM symbol for k = 0. A rectangular shaped pulse is shifted by an infinite number of equidistant time steps iTs, $i = -\infty \ldots +\infty$. These sub-pulses are modulated by complex coefficients c_{ik}. The total OFDM time signal $s(t)$ is formed after summation over variables i and k.

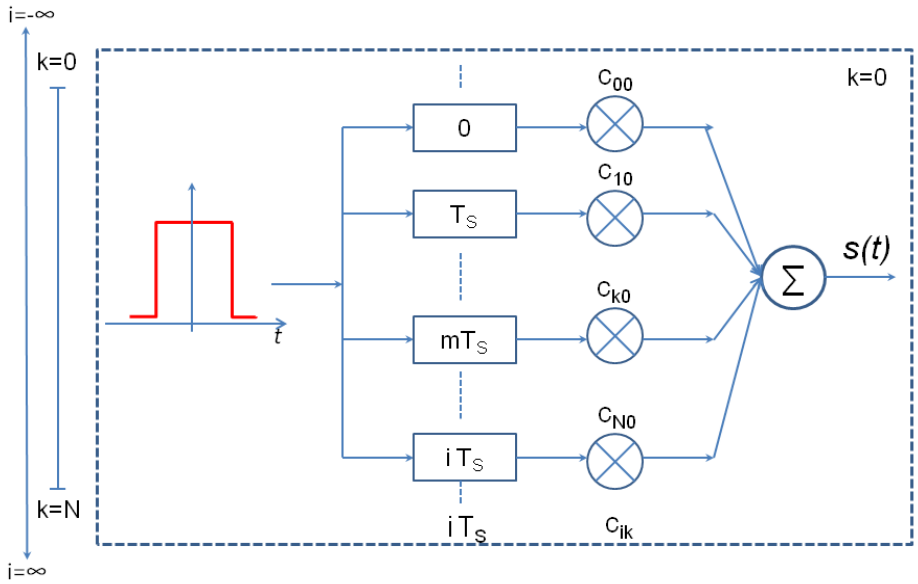

Figure 1.12. Illustration of OFDM signal generation. For simplicity, summation variable k is kept at 0. The total OFDM time signal is formed after summation over variables k and i. Infinitely many rectangular-shaped temporal pulses ($i = -\infty \ldots +\infty$) are time shifted from t = 0 by increments iTs and modulated with complex coefficients c_{ik}.

By correlating two OFDM subcarriers we have [70]:

$$\delta_{kk'} = \frac{1}{T_s}\int_0^{T_s} s_k s_{k'}^* dt = \frac{1}{T_s}\int_0^{T_s} e^{(j2\pi(f_k - f_{k'})t)} dt = e^{(j\pi(f_k - f_{k'})T_s)} \frac{\sin\left(\pi(f_k - f_{k'})T_s\right)}{\pi(f_k - f_{k'})T_s}. \quad (1.4)$$

Therefore, it can be seen that if the following condition

$$f_k - f_{k'} = m\frac{1}{T_s}, \ \ k,k' \in \{1,2...,N\} \quad (1.5)$$

is satisfied then the two subcarriers are orthogonal over OFDM symbol period T_s (m is an integer). From Eq. 1.2 and Eq. 1.3 it can be seen that the temporal OFDM signal consists of ideal rectangular pulses, whose spectrum presentation is sinc like [84].

1.3.3.2 IDFT/DFT

The practical implementation of OFDM signal, as a special class of MCM, is depicted in Figure 1.13. An OFDM signal is usually composed of a large number of subcarriers, which leads to an extremely complex architecture involving many oscillators and filters at both transmit and receive ends. However, OFDM signal generation and reception bears a close relationship to the inverse discrete Fourier transform (IDFT) and discrete Fourier transform, respectively. More precisely, the mathematical expression of an OFDM signal to be transmitted is identical to an IDFT if the OFDM signal is sampled at proper discrete times. Weinstein and Ebert first suggested the implementation of IDFT/DFT for OFDM modulation/demodulation [73].

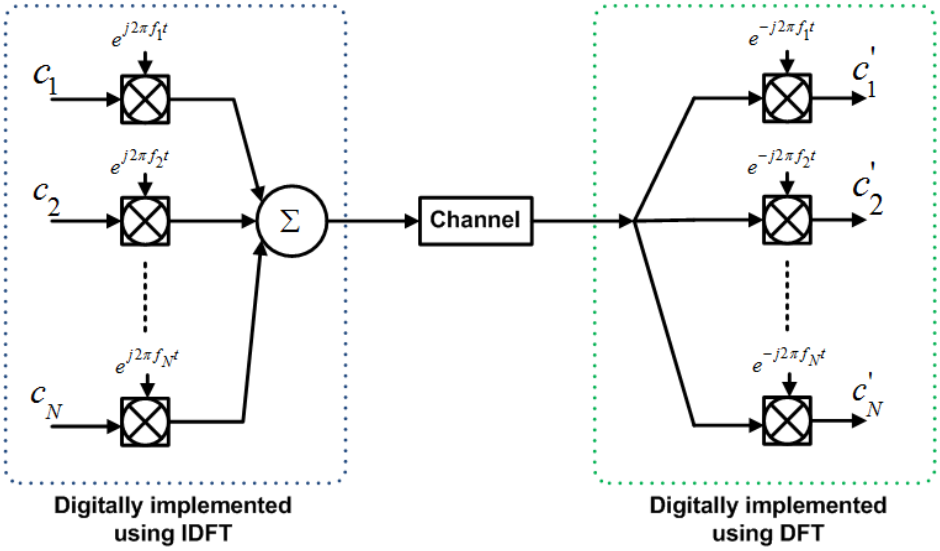

Figure 1.13. Generic architecture of an OFDM system.

Using the Eq. 1.2, Eq. 1.3 and the condition given by Eq. 1.5, i.e. $f_k = \frac{k-1}{T_s}$, and under assumption that the signal consists of one OFDM symbol and that we sample *s(t)* at every interval of T_s / N, the m_{th} sample of $s(t)$ becomes [70]:

$$s_m = \sum_{k=1}^{N} c_k e^{j2\pi \frac{(m-1)(k-1)}{N}} = F^{-1}\{c_k\}. \quad (1.6)$$

F^{-1} stands for the *N* point IDFT between the time domain discrete signal and its frequency domain representation. The complex data coefficients c_k of an OFDM signal are the spectral Fourier coefficients for an IDFT. Conversely, upon reception these complex data coefficients can be retrieved by performing the DFT on the OFDM signal. Therefore, at the receive end, we have

$$c_k^{'} = F\{r_m\}. \quad (1.7)$$

F is a DFT and r_m is received signal sampled at every T_s / N interval. Eq. 1.6 and Eq. 1.7 show that discrete value of the OFDM transmitted signal is a *N* point IDFT of the information symbol, and received information symbol value is a simple *N* point DFT of the receive sampled value. IDFT and DFT can be implemented electronically [70, 86] and optically [87].

1.3.3.3 Cyclic Prefix

One of the enabling techniques for OFDM is the insertion of a cyclic prefix (CP) to mitigate the fibre induced dispersion effects [70, 88]. The impact of transmission induced impairments, such as chromatic dispersion (CD), on a signal becomes more significant with an increase of the data rate and transmission distances. Dispersion induced time delay between OFDM subcarriers, can affect the orthogonality between subcarriers and cause ICI. Furthermore, when multiple OFDM symbols are transmitted in a series then a dispersive channel causes ISI between successive OFDM symbols. However, when a CP is used, any distortion caused by a linear dispersive channel can be corrected simply using a ‘single-tap’ equaliser [86].

As described in section 1.3.3.1, each OFDM symbol contains *N* orthogonal subcarriers. As each subcarrier is at a different frequency, the dispersion effect

manifests as a delay spread across all transmitted subcarriers. The size of the receiver FFT window is the same as the transmitted IFFT size (i.e. the size of one OFDM symbol). The operational principle of CP is illustrated in Figure 1.14. For simplicity only two subcarriers within an OFDM symbol are considered, which are aligned in time at the transmitter. Also, each OFDM symbol is preceded by a CP which is essentially an identical copy of the last portion of the data symbol appended to the front of the symbol during the guard period. Once the length of the CP is greater than the maximum delay spread caused by dispersion, t_d, then a complete copy of every subcarrier will be received and orthogonality is preserved. Therefore, the condition for ICI-free OFDM transmission is given by $t_d < \Delta G$, where ΔG is guard interval enabled by a cyclic prefix. The received subcarrier is a copy of the transmitted subcarrier with an additional phase shift caused by dispersion [70]. Each subcarrier within one OFDM symbol is delayed by a different amount of time, and therefore each received subcarrier has a different phase shift relative to the corresponding transmitted subcarrier. Accumulated phase shift can be corrected using a 'single-tap' equaliser [86].

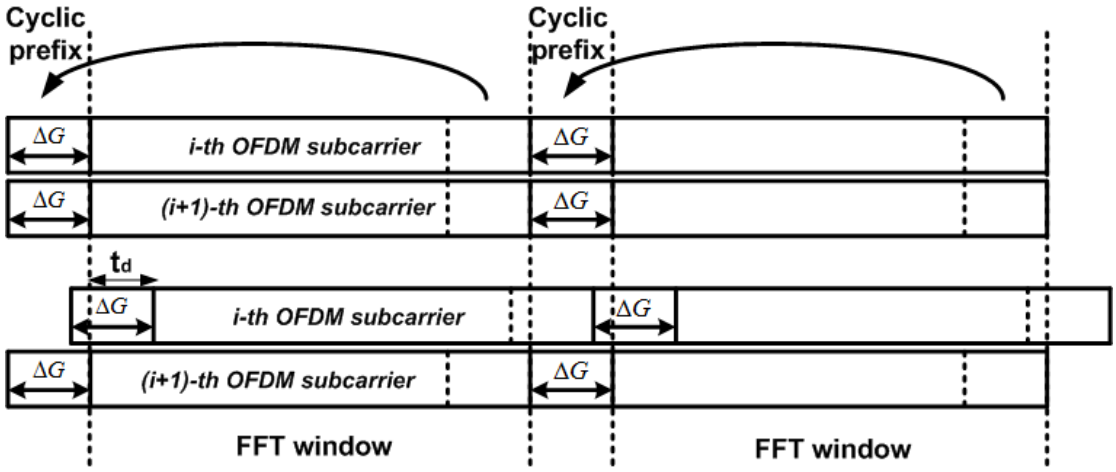

Figure 1.14. OFDM cyclic prefix implementation and ICI prevention.

1.3.3.4 Types of OFDM

Several transmitter and receiver concepts for the generation and detection of OFDM signals for optical communications applications have been proposed. OFDM signal generation, (de)multiplexing and processing can be performed in the electronic and optical domains. OFDM signal generation using digital signal processing in electronics is very popular due to its extraordinary flexibility in selecting desired

modulation formats, data rates, guard band values (cyclic prefix), up-conversion to desired frequencies and combination of lower-speed data streams into a single high-speed data signal [69]. However, bandwidth and speed limitations of the available DACs and ADCs limit OFDM signal generation using DSP and electronic circuitry to moderate aggregate data rates [70, 89, 90]. However, OFDM signal formation in the optical domain relaxes ADC/DAC requirements, which allows the generation of higher data rate channels and their combination into superchannels [69]. As OFDM signalling gained significant research and industry attention in recent years, many combinations and variations of the electronic and optical OFDM schemes have been suggested and implemented. However, the proposed OFDM concepts can be classified based on the transceiver configuration into all-optical OFDM and DSP based OFDM.

1.3.3.4.1 DSP Based Optical OFDM

Figure 1.15 shows typical schematic designs of a DSP based OFDM optical systems. Figure 1.15(a) depicts DSP based coherent optical OFDM. At the transmitter side, data is encoded using the desired modulation format and parallelised before being processed by the electronic IDFT. After the addition of the cyclic prefix and parallel-to-serial conversion, the OFDM signal is encoded onto the optical carrier using an IQ modulator (i.e. Mach-Zehnder IQ modulator) after being converted from the digital to analog domain with an appropriate DAC. At the receiver, the inverse process includes optoelectronic down-conversion, i.e. coherent detection, digitalisation of the received analog signal by an ADC, serial-to-parallel conversion, cyclic prefix removal and DFT processing. Digital signal processing is used after DFT to retrieve the transmitted data. Capacities higher than 1 Tb/s have been experimentally achieved using multi-band DSP based coherent optical OFDM [91, 92]. Also, the real-time implementation of the single channel DSP based coherent optical OFDM up to data rates of 100 Gb/s have been reported [93, 94]. The typical implementation of the coherent optical OFDM is in metro and core networks [89, 91, 93].

Figure 1.15(b) depicts DSP based electro-optical OFDM (E/O OFDM). The difference in the transmitter design compared to the coherent optical OFDM is the possibility to use an intensity electro-optical modulator instead of an IQ modulator for data encoding onto the optical carrier [90, 95]. At the receiver side, instead of using coherent detection, direct detection is used for simple E/O down-conversion. Several

possible configurations of the electro-optical OFDM systems have been proposed [70, 90]. In contrast to the coherent optical OFDM which requires two DACs and ADCs (for single polarisation detection), the E/O OFDM configuration which employs a single DAC and ADC have been reported [90]. The electro-optical OFDM (E/O OFDM) is usually implemented in optical access and metro networks due to its simple receiver configuration which does not require a coherent receiver and a high power low linewidth laser at user premises [31]. Nevertheless, experimental long-haul implementations of this system have been proposed [90, 96, 97]. The real-time implementation of the E/O OFDM at data rates up to 40 Gb/s have been reported [98-100].

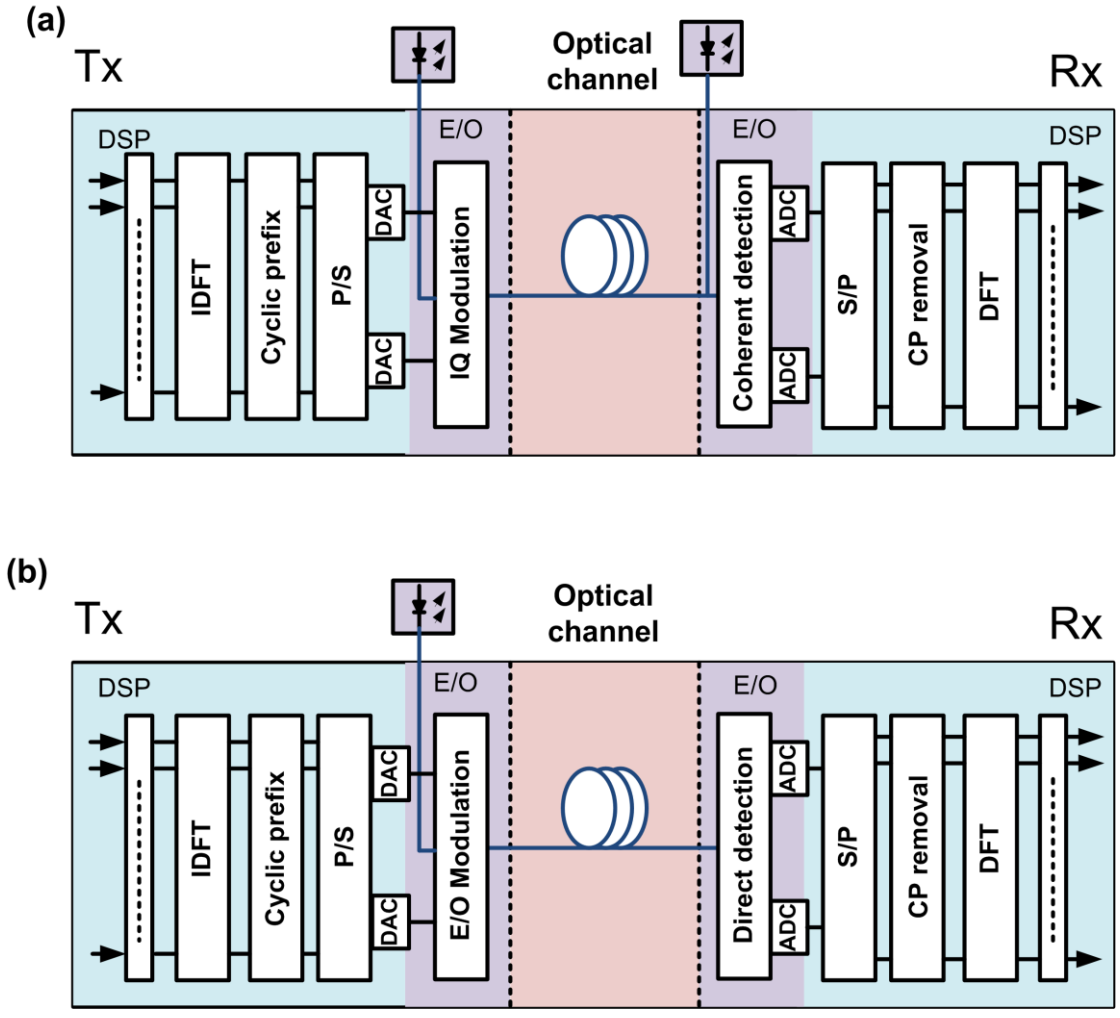

Figure 1.15. Transmitter and receiver concepts for optical OFDM. (a) DSP based coherent optical OFDM and (b) DSP based electro-optical OFDM.

In general, the maximum available capacity of the DSP based optical OFDM is limited by the bandwidth and speed of DAC and ADC [101]. The system configuration shown in Figure 1.15 illustrates the single channel systems, which can be extended to the

WDM case by simple scaling of the number of transmitters and receivers. However, that would significantly increase the total cost of the system.

1.3.3.4.2 All-Optical OFDM

All-Optical OFDM (AO-OFDM) has been proposed in order to overcome electronic circuit bandwidth limitations. Even though electronic circuits have been rapidly developed to provide higher speed and bandwidth, and lower cost implementations, they still represent a bottleneck in achieving very high data rates. Therefore, unlike DSP based OFDM which employs digital (de)multiplexing of an OFDM signal, AO-OFDM systems employ IDFT and FFT in the optical domain. Capacity scaling beyond DSP based OFDM applications was enabled using multicarrier OFDM where carriers are all-optically (de)multiplexed using optical IDFT/DFT. In practice, AO-OFDM has been implemented using several scenarios, which may differ in transmitter and receiver design but all target to benefit from orthogonality between carriers [101-107].

In the case of AO-OFDM every optical carrier represents a single OFDM subcarrier. Similar to the case when digital IDFT/DFT is used, the orthogonality condition is satisfied when carrier frequencies are spaced at multiples of the inverse of the symbol periods. Each optical carrier is modulated with the desired modulation format whose symbol rate equals the frequency separation between adjacent optical carriers in order to satisfy the orthogonality condition. Additionally, the symbols in the modulated carriers should be time-aligned [16, 104]. Carrier orthogonality can be preserved, even with arbitrary modulation formats as long as the modulation periods are equal and synchronised [101]. Furthermore, a phase correlation between all of the optical carriers is desirable in order to mitigate crosstalk between optical channels [101, 104, 106]. Therefore, multicarrier optical sources which have phase-locked optical carriers are typically used in AO-OFDM systems [92, 103, 107]. A set of free-running continuous-wave (CW) lasers can also produce AO-OFDM carriers as long as the laser frequencies are precisely tuned and locked to satisfy the orthogonality condition [101, 104]. However, in this configuration the carriers are not phase correlated. The lack of phase correlation between optical carriers might cause additional OSNR penalty as the impact of ICI may not be eliminated by digital signal processing at the receiver. The impact of ICI results in fast beat noise fluctuations due to fast phase rotations of free-running sources [101].

The modulated optical carriers are applied to an optical IDFT whose function is to multiplex optical carriers and generate the optical OFDM signal as shown in Figure 1.16. Instead of IDFT at the transmitter, a passive combiner can be used. However, it is shown that the ICI introduced by imperfect WDM multiplexers (passive combiner) can be significantly reduced by using IDFT instead [108]. A number of IDFT/DFT designs have been reported recently: cascaded delay-line interferometers (DIs) based IDFT/DFT [87], AWG based IDFT/DFT [101] and LCoS based IDFT/DFT design [109]. The optical DFT differs from its electronic counterpart by its continuous mode of operation. In an electronic implementation, the optical signal is sampled and the DFT is computed from all samples. In the optical domain, the DFT is computed continuously. However, in both cases sampling must be performed in synchronisation with the symbol over the duration of T/N [87]. Demultiplexed optical carriers are coherently detected and digital signal processing is used to retrieve the transmitted data.

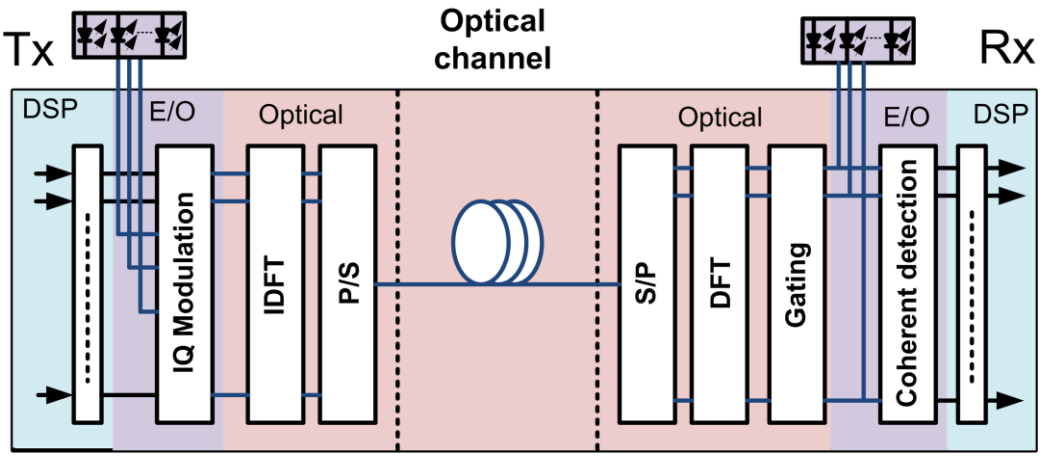

Figure 1.16. Transmitter and receiver concepts for all-optical OFDM.

1.3.3.5 Orthogonal Time Division Multiplexing (Nyquist WDM)

As already shown in the previous sections, in OFDM systems ICI and ISI can be avoided by choosing non-overlapping rectangular impulse responses with overlapping sinc-shaped channel spectra. If non-overlapping rectangular-shaped channel spectra with overlapping sinc-shaped impulse responses are chosen then orthogonality in the time domain is achieved. The corresponding MCM technique (see Figure 1.11(c)) which explores time domain orthogonality between pulses is known as orthogonal time division multiplexing, or Nyquist WDM. As shown in [84], orthogonal time division

multiplexing can be derived from the well-known OFDM technique, simply by interchanging time and frequency domain when describing the signal. The time domain representation of the Nyquist WDM symbol is given by the set of infinitely many temporal sinc-functions [84]. In contrast to OFDM, the spectrum of a Nyquist WDM signal is a finite sequence of *N* spectral symbols, where each symbol is a set of infinitely many temporal sinc-functions. Therefore, in analogy to Eq. 1.2 and Eq. 1.3 we have [84]:

$$S(f) = \sum_{i=0}^{N-1} \sum_{k=-\infty}^{+\infty} c_{ik} S_k (f - iF_s), \tag{1.8}$$

$$S_k(f) = \prod(f) e^{-j2\pi f_k t}$$
$$\prod(f) = \begin{cases} 1, & (0 < f \le F_s) \\ 0, & (f \le 0, f > F_s) \end{cases}. \tag{1.9}$$

The generation of Nyquist WDM signal in the frequency domain is illustrated in Figure 1.17. For simplicity, the summation variable *k* is kept at 0 (i.e. only one Nyquist pulse ("carrier") at *t* = 0), and Figure 1.12 illustrates the generation of Nyquist WDM symbol for *k* = 0. A rectangular shaped spectrum is shifted by a finite number of equidistant frequency steps iF_s, $i = 0 \ldots N$. These sub-spectra are modulated by complex coefficients c_{ik}. The total Nyquist WDM signal *S(f)* is formed after summation over variables *i* and *k*.

1.3.3.6 ICI-free and ISI-free Pulse Shaping

From signal theory it is known that sinc pulses can provide ICI-free and ISI-free reception of a signal [68, 110]. Non-causal sinc-shaped transmitter impulse responses lead to rectangular-shaped spectra and a characteristic temporal width of T_s between maximum and first zero as shown in Figure 1.18. The maxima of the pulses in different time frames are separated by T_s. Neighbouring Nyquist pulses strongly overlap, but at any pulse maximum all neighbouring pulses are zero. However, sinc pulses are not physically realisable, but reception without significant ICI and ISI can be achieved nonetheless [69]. Interference-free reception is possible

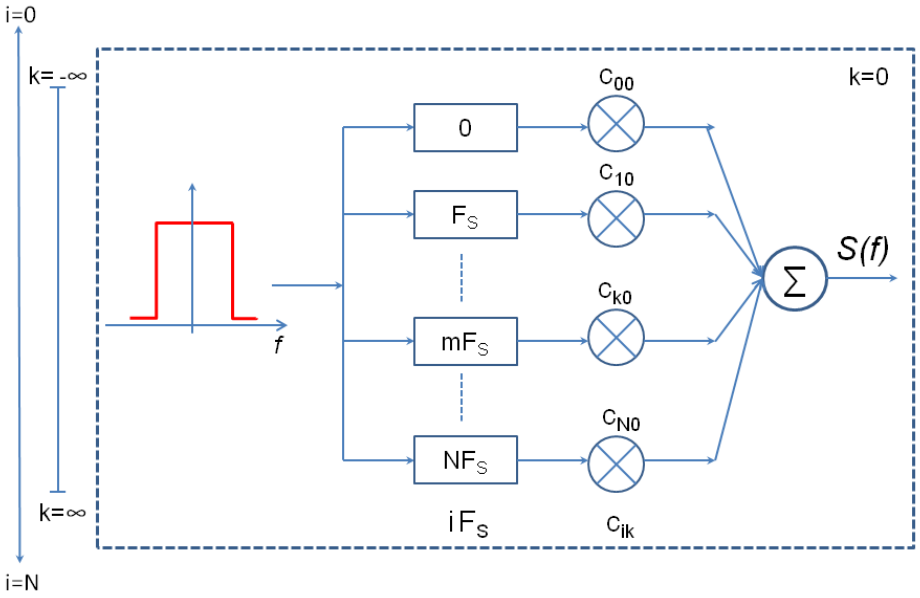

Figure 1.17. Illustration of Nyquist WDM signal generation. For simplicity, summation variable *k* is kept at 0. The total Nyquist WDM spectra is formed after summation over variables *k* and *i*. Finite number of rect-shaped sub-spectra (*i =0 ... N*) frequency shifted from *f* = 0 by increments *iFs* and modulated with complex coefficients c_{ik}.

by using a limited number of pulse shapes generated at a transmitter and detected at a receiver with optimal matched-filter reception. Besides rectangular-shaped (OFDM) and sinc-shaped pulses (Nyquist pulses), pulses with a root-raised cosine spectrum can be detected ISI-free when using a matched filter. Raised-cosine pulses are widely used in practice as they take on the shape of a sinc pulse (see Figure 1.18), as indicated by the left most term of $x(t)$ given by Eq. 1.10 [68].

$$x(t) = \frac{\sin(\pi t/T)}{\pi t/T}\frac{\cos(\pi\beta t/T)}{1-4\beta^2 t^2/T^2} \tag{1.10}$$

The precise shape of the raised cosine spectrum is determined by the parameter β (roll-off factor), where $0 \le \beta \le 1$.

1.3.3.7 Optical, Analog and Digital Nyquist Pulse Shaping

While ICI-free and ISI-free pulse shaping has been used for a long time in the domain of RF communications, it has only been applied to optical communications recently. The attempts to shift from 100 GHz to 50 GHz frequency grid using the DQPSK format during the second half of the last decade, resulted in higher spectral efficiency systems enabled by strong optical filtering of the signal spectra [53]. In 2010, the use

of optical filters for spectral shaping has been reported [112-115], which caused exponential growth of research publications in the area of pulse and spectral shaping in optical communications. Pulse shaping is performed at the transmitter using digital, analog electrical or optical filter, as shown in Figure 1.19. It is important to emphasise that only one type of filtering is used at a time.

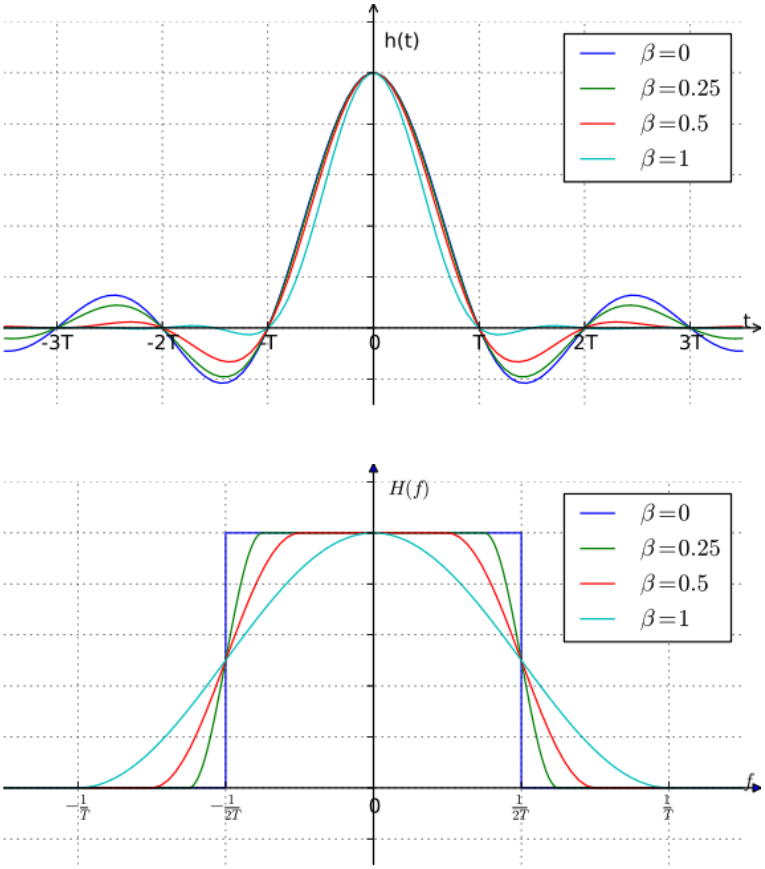

Figure 1.18. Time (upper) and frequency (lower) representation of raised cosine pulse. After [111]

Modulated optical signals can be shaped by an optical filter whose bandwidth is equal to symbol rate of the signal. Theoretically, in order to eliminate crosstalk in closely spaced multicarrier systems, the optical filter transfer function should be such that the signal spectrum at its output has a rectangular shape with a bandwidth equal to the symbol rate [114]. This shape is not physically realizable, especially at lower baud rates. However, at higher baud rates optical filters have a smaller roll-off factor and exhibit sharper transitions, and can be modelled with higher order super Gaussian (SG) transfer functions (e.g. 4th order SG) [114]. It is reasonable to assume that the state-of-the-art commercial optical filters at lower baud rates will be characterised with higher order SG transfer functions as well [116]. Nyquist optical filtering is usually performed by using wavelength selective switches (WSS) [117] or arrayed waveguide

gratings [114], and occasionally by discrete filter arrays. In comparison to AWGs which have fixed filter bandwidth and filter profile, a WSS is based on LCoS technology, enabling flexibility in choosing filter shapes and bandwidth [117]. Nyquist optical filtering is especially attractive for high data rates, as optical filters with higher bandwidths can attain a near rectangular transfer function. Additionally, data shaping with digital filters at higher data rates is challenging from the electronics point of view. Sub-Nyquist channel spacing has been obtained by optical filtering of 28 GBaud PDM-RZ-QPSK signal spaced by 25 GHz [118]. Filed trial experiments of optically shaped Nyquist WDM systems have been reported for terrestrial and transoceanic systems [119, 120].

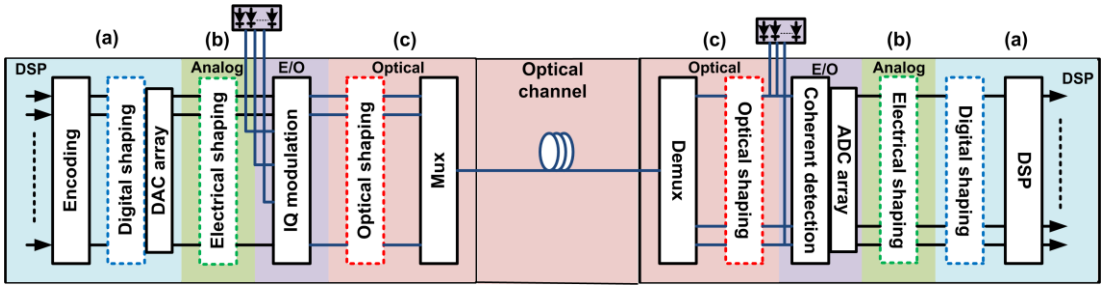

Figure 1.19. Generation of the Nyquist signal (a) using digital filter, (b) using analog electrical filter and (c) using optical filter.

Additionally, data can be shaped electrically by analog or digital filters. In the case when analog electrical filters are used, they shape the electrical driving signals at the output of the electrical transmitter. Therefore binary drivers suffice, which potentially reduces overall cost of the transmitter significantly [49]. Shaped data signals are then fed to the optical modulator as shown in Figure 1.19. Digital filtering is dominantly used for pulse shaping in optical communication systems, especially for lower symbol rates. Digital Nyquist pulse-shaping has achieved excellent performance in ultra-densely spaced WDM networks [121]. Digital pulse shaping is performed by convolving a data sequence with a digitally generated finite impulse response (FIR) filter which has the desired number of taps [49]. The spectrum evolves towards an ideal rectangle with a spectral width equal to the Nyquist bandwidth F_s with the increase in number of taps. In this case, the sub-channels can be placed very close to each other, to have guard band of a few percent signal bandwidth when employing high order m-QAM formats [122].

Figure 1.20 compares different pulse forms from digital (left, green), electrical (middle, red), and optical (right, blue) pulse-shapers [69]. As expected, the digital pulse-shaper approximates a sinc-shaped pulse most accurately. The electrical pulse-shaper still

produces sinc-typical side lobes, whereas the optical pulse-shaper matches a sinc-function the worst. However, recent advances in the area of optical filters show the possibility of obtaining sinc-like impulse response of optical filters, even for low filter bandwidths [123].

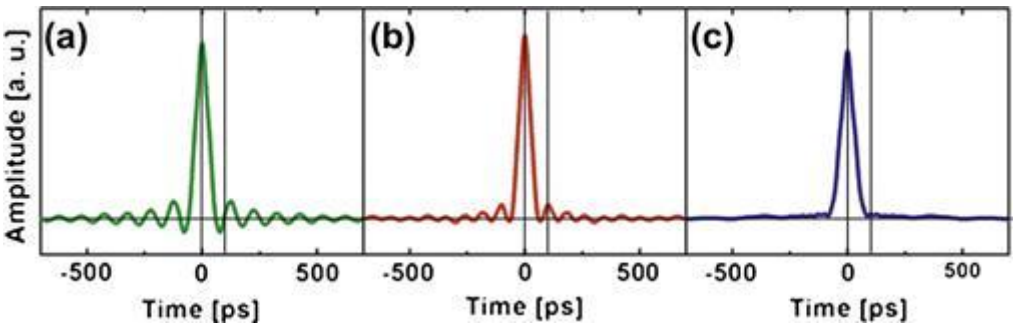

Figure 1.20. Comparison of Nyquist pulses generated (a) using digital filter, (b) using analog electrical filter and (c) using optical filter. After [69].

1.4 Key Components, Devices and Enabling Techniques

The advances in optical communication systems have been enabled by the evolution of the underlying technologies. The steady development of components and devices used in optical communications has laid the foundations for the increase of system capacity. As previously mentioned in the chapter about optical networks, the technology breakthroughs such as the invention of the optical amplifier led to the rapid development of the optical systems. Furthermore, the development of optical components will have a major influence on the upgrade and evolution of the current optical networks. While core networks are less cost sensitive and allow for the implementation of expensive components and devices, the upgrade of metro and access networks should take place in a cost effective manner.

1.4.1 Optical Transmitter

Encoding of an electrical signal (i.e. data) onto an optical carrier can be achieved using direct or external modulation. Direct modulation is the simplest technique for the modulation of an optical carrier which uses the property of the laser diode that the emitted light is linearly proportional to the drive current of a laser source. By modulating the laser drive current the electrical data can be encoded onto the optical

carrier, which is known as intensity modulation. Due to its simplicity and cost effectiveness, direct modulation has always been used in optical communications. It is still the prime choice in the current networks when low data rates (up to 2.5 Gb/s) and transmission over short distances (access networks and data centres) are required. However, the signal quality of the directly modulated lasers is affected by impairments such as frequency chirp [124], with the effects on system performance become more evident at higher data rates (10 Gb/s and beyond). The limited modulation bandwidth of the laser diodes further restricts the employment of direct modulation in high speed systems. NRZ-OOK modulation format has been dominantly used for direct modulation of laser diodes.

The bandwidth limitations of the directly modulated laser diodes can be overcome by the employment of the electro-optical external modulators, which use electro-absorption (electro-absorption modulator (EAM)) or Pockels effect (Mach-Zehnder modulator) to encode an electrical data signal onto an optical carrier. EAMs are suitable for dense integration with laser diodes due to their small dimension and laser-like structure [124]. However, EAMs support only intensity modulation and therefore they are typically used coupled with laser diodes to form a device called an externally modulated laser (EML) [125, 126]. EMLs provide higher bit rates and longer transmission distances, and have lower chirp compared to the directly modulated lasers. In order to enable chirp-free operation and provide full versatility in using various modulation formats at high bandwidths, MZMs are often employed to modulate the optical carrier.

1.4.2 Mach-Zehnder Modulator

The schematic of the Mach-Zehnder modulator structure is shown in Figure 1.21. The MZM is composed of two couplers and two electro-optic modulators placed in the modulator arms (some MZMs have only one electro-optic modulator). Incoming light from a laser diode operating in continuous wave mode is split into two paths each containing an electro-optic modulator.

By controlling the refractive index of the waveguide material by an external applied field, the phase of the electric field of the optical signal can be modulated. Therefore, such electro-optic modulators are sometimes referred to as phase modulators [127]. The operating principle of the phase modulators is based on the linear electro-optic

effect (Pockels effect). The induced phase shift is proportional to the applied voltage on the electrodes. This phase modulation can be converted to amplitude modulation using a Mach–Zehnder interferometer structure (see Figure 1.21). The interference between the two coherent signals varies from constructive to destructive depending on the relative phase shift between the two paths and the output signal can be modulated in terms of optical intensity.

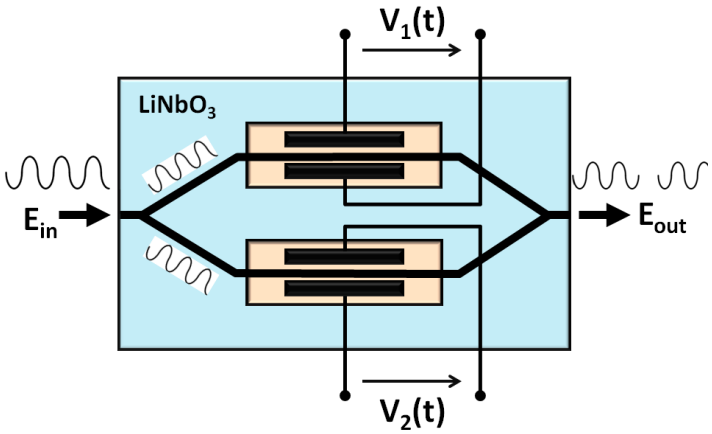

Figure 1.21. Illustration of the integrated dual-drive Mach-Zehnder optical intensity modulator.

The transfer function of the dual-drive MZM is given by [128, 129]:

$$\begin{aligned}\frac{E_{out}(t)}{E_{in}(t)} &= \frac{1}{2}\left(e^{j\varphi_1(t)} + e^{j\varphi_2(t)}\right) \\ &= \cos\left(\frac{\varphi_1(t)-\varphi_2(t)}{2}\right)e^{j\left(\frac{\varphi_1(t)+\varphi_2(t)}{2}\right)},\end{aligned} \tag{1.11}$$

where $\varphi_1(t)$ and $\varphi_2(t)$ are phase shifts in the upper and lower paths of the MZM and they are given as $\varphi_{1,2}(t) = \pi v_{1,2}(t)/V_\pi$. The voltage swing required to generate a relative phase difference between the two optical paths equal to π radians is known as V_π. The first term of Eq. 1.11 represents the amplitude modulation and the second term gives the phase modulation. One can notice that such a transfer characteristic allows all amplitude and phase states to be achieved depending on the values of $\varphi_1(t)$ and $\varphi_2(t)$ [129]. The operating mode when $\varphi_1(t) = \varphi_2(t)$ is known as push-push operation, whilst the mode when $\varphi_1(t) = -\varphi_2(t)$ is referred as push-pull operation. The later one enables chirp-free amplitude modulation [128]. The transfer function for field

and intensity of the MZM operating in push-pull mode is plotted in Figure 1.22. In the ideal case, a shift of V_π in the voltage difference between the two arms of the modulator is capable of changing the output optical intensity from minimum to maximum which is illustrated in Figure 1.22. In order to obtain intensity modulation, the operating point is set to be in the linear region between minimum and maximum transmission points (quadrature point). However, the phase modulation is achieved when the operating point is set to the minimum transmission point.

Various intensity and phase modulation formats can be generated using the dual-drive MZM. For example, NRZ-OOK and 50% RZ-OOK formats are generated when the MZM is biased at the quadrature point and is driven from minimum to maximum transmission with a voltage swing of V_π. For the generation of the duobinary, DPSK and CSRZ formats, the MZM should be biased at the minimum point and driven with a swing voltage of $2V_\pi$ [10].

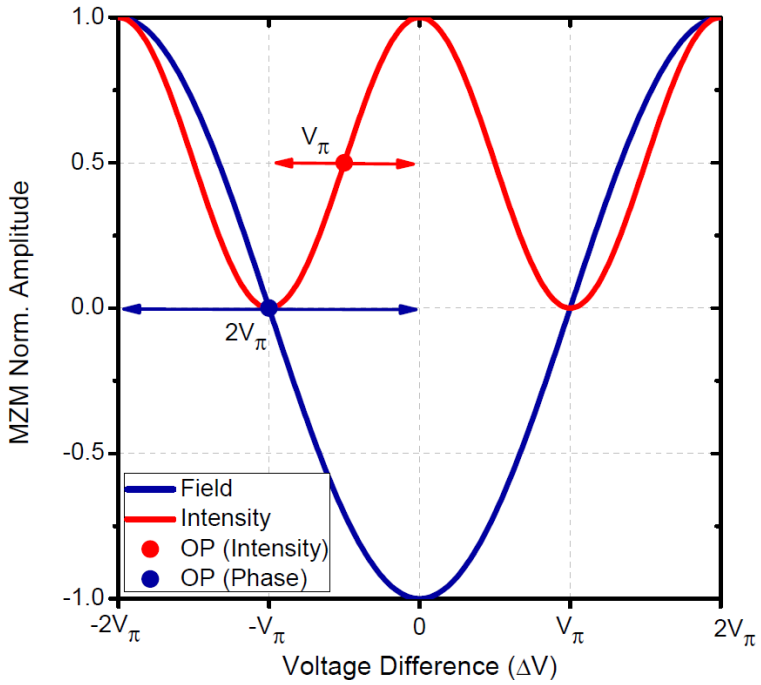

Figure 1.22. Normalised field (blue) and intensity (red) transfer functions of a dual-drive Mach-Zehnder modulator.

1.4.2.1 IQ Mach Zehnder Modulator

In order to generate advanced modulation formats, an optical complex field modulator (IQ modulator) is required. Optical IQ modulators consist of two MZMs with an

additional 90° phase shifter in one of the arms as shown in Figure 1.23 [10]. This way, any constellation point can be reached in the complex IQ-plane after recombination of the light from both paths (see Figure 1.23). The field transfer function of the IQ modulator is given as [128]:

$$\frac{E_{out}(t)}{E_{in}(t)} = \frac{1}{2}\cos\left(\frac{\varphi_I(t)}{2}\right) + j\frac{1}{2}\cos\left(\frac{\varphi_Q(t)}{2}\right), \tag{1.12}$$

where $\varphi_I(t)$ and $\varphi_Q(t)$ are given as $\varphi_{I,Q}(t) = \pi v_{I,Q}(t)/V_\pi$. For the generation of advanced modulation formats such as DQPSK, QPSK and *m*-QAM, the IQ MZM should be biased at the minimum point and driven with a swing voltage of $2V_\pi$ [10]. This way, real and imaginary parts of the electrical filed are modulated onto an optical carrier.

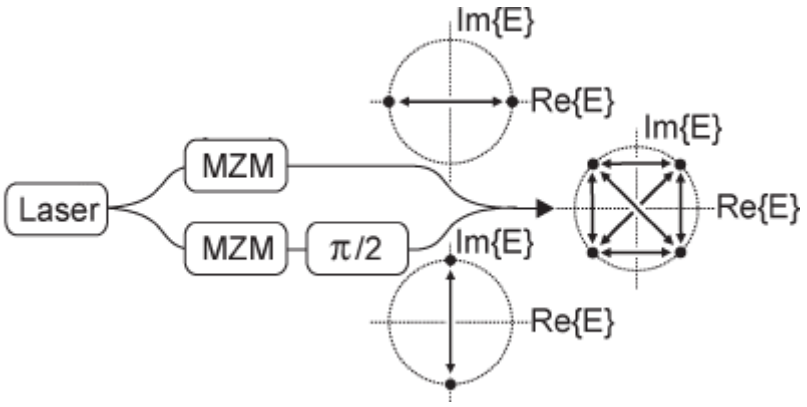

Figure 1.23. Illustration of the IQ Mach-Zehnder modulator. Also, QPSK constellation points are shown. After [10].

1.4.3 Optical Transmission Links

Nowadays, over 99% of all data is carried over optical fibres [47], due to their low loss and tremendous bandwidth. Depending on the application, several types of fibres can be used. ITU recommendations and standards for optical fibres are outlined in ITU.T G.652 – G.657 [130-134], where optical fibres are classified depending on their inherent characteristics and potential application. Optical fibres are mostly made of silicon, where the core has a higher refractive index compared to the cladding (which is the enabling condition for ensuring the optical wave is guided through the fibre. Besides SSMFs, some fibres are designed to guide multiple modes and they are called multimode fibres. Recently, few-mode fibres (a special case of MMF) and multi-

core fibres have been proposed [35]. No matter what type of fibre is employed, any optical signal propagating over an optical fibre link suffers from distortion due to the several linear and non-linear effects.

1.4.3.1 Fibre Dispersion and Nonlinearities

Dispersion is the linear effect which leads to a broadening of the signal in the temporal domain [1]. There are several types of dispersion:

Modal Dispersion occurs in MMFs and it is caused by multiple modes travelling at different speeds in MMF. Modal dispersion is the major effect that limits the maximum transmission distance in MMFs. It can be avoided by using SSMFs.

Polarisation Mode Dispersion occurs due to the polarisation dependent refractive index which means that different polarisations of the optical signal travel at different speeds. The polarisation dependent refractive index is a consequence of the imperfect structure of optical fibres [1]. PMD becomes a limiting factor for optical communication systems operating at high bit rates [10]. Degradation due to PMD can be effectively compensated by using DSP algorithms [47, 135].

Chromatic Dispersion is the limiting effect for the transmission of broadband optical signals over SSMF. Chromatic dispersion is caused by the wavelength dependent refractive index of the optical fibres. This causes different wavelengths of a signal spectrum to travel at different speeds, which leads to a temporal signal broadening. The effects of chromatic dispersion become more evident at higher data rates and for longer transmission distances [10]. The effects of dispersion can be compensated in the optical domain (using dispersion compensation modules (DCM)) [10] or electronic (using DSP) domain [47, 135].

Nonlinear effects in optical fibre occur due to the high confinement of the optical signal in a fibre core which can cause high optical intensity to be reached inside the fibre, inducing changes in the fibre's refractive index [10]. Consequently, nonlinear phase and amplitude distortions of the propagating signal could be induced [1]. The nonlinear effects within the optical fibre can be classified as intra-channel and inter-channel nonlinearities [10]. The first one includes interaction between pulses of the same channel and interaction between a signal and amplified spontaneous emission (ASE) noise within the single channel. The later one includes nonlinear interactions

between two or more channels, and between channels and noise within WDM systems.

Intra-channel signal-signal nonlinear distortions caused by the intensity dependence of the refractive index leads to chirping and spectral broadening of optical pulses [1, 10]. Self-phase modulation (SPM) is the dominant intra-channel nonlinear effect which can be further divided into isolated pulse SPM, intra-channel cross-phase modulation (IXPM) and intra-channel four-wave mixing (IFWM) [10]. Isolated pulse SPM refers to the interaction of a pulse with itself, while IXPM and IFWM relate to the interactions between pulses within the same channel.

Inter-channel signal-signal nonlinear distortions occur when two or more signals at different wavelengths propagate simultaneously inside an optical fibre, and they are caused by the intensity dependence of the refractive index. The phases of optical signals are then affected not only by SPM but also by cross-phase modulation (XPM) and four-wave mixing (FWM). Due to the XPM, the phase of each optical channel is affected by both the average power and the bit pattern of all other channels [1]. As a majority of WDM systems contains more than 3 channels, FWM becomes the dominant source of nonlinear crosstalk in WDM systems [1, 10]. Nonlinear interaction between 3 optical channels within the fibre leads to the generation of new optical carriers at corresponding frequencies [1]. The generated optical signals might have the same frequency as other channels in a WDM system, which can cause significant performance degradation.

Typically, inter-channel nonlinearities have higher impact at lower data rates, whilst intra-channel nonlinearities affect systems most strongly at higher data rates (above 10 Gb/s) [10]. However, the impact of fibre nonlinearities depends on many factors such as the employed modulation format, local fibre dispersion, channel spacing, etc. In general, lower dispersion fibres have stronger inter-channel effects than fibres with high local dispersion [10]. Signal-noise nonlinear interactions depend significantly on the noise level and become stronger for higher noise powers, i.e. lower OSNR values. Previously, dispersion mapping has been used for reduction of the impact of nonlinear effects. Recently, DSP based algorithms, such as digital backpropagation (DBP) have been proposed for effective compensation of nonlinear impairments [47, 136].

1.4.4 Optical Amplifiers

Besides fibres, optical links also comprise optical amplifiers. SSMFs typically have a loss of approximately 0.2 dB/km, and therefore amplification of the signal is usually required every few tens of kilometres depending on the system design. Furthermore, optical components e.g. optical modulators, introduce additional loss which needs to be compensated. Depending on the position in the optical system, amplifiers are referred as booster amplifiers (after transmitter), in-line amplifiers (between fibre spans) and pre-amplifiers (before receiver). There are three types of optical amplifiers which are dominantly used in current optical networks: semiconductor optical amplifier, Erbium doped fibre amplifier and Raman amplifier.

Semiconductor Optical Amplifier has a laser-like structure, but without the laser cavity. Such a structure allows SOAs to be integrated with lasers, modulators and detectors on the same chip creating an economical and size effective solution. However, SOAs typically have lower gain and saturation power, and higher noise figure (NF) compared to EDFAs and Raman amplifiers. The amplification of the optical signal which is passing through an SOA gain medium, which is electrically pumped, is achieved by stimulated emission [137]. SOAs are typically used as booster amplifiers or pre-amplifiers due to the ease of integration with other modules, but are rarely employed as in-line amplifiers.

Erbium Doped Fibre Amplifiers are dominantly used in current optical systems due to their inherent characteristics. When used as a preamplifier, an EDFA typically has high gain, and low NF, but low maximum output power as well. In-line and booster EDFAs have high saturation power at the expense of having higher NF. High gain and low NF EDFAs are typically optically pumped at 980 nm, whilst high saturation power EDFAs are pumped at 1480 nm [138, 139]. The disadvantage of EDFAs is their bulky structure, inability of integration and high cost. Due to the optical pumping of the gain medium EDFAs are less energy efficient than SOAs.

Raman Amplifier operation is based on energy transfer between the pump and signal. Raman gain arises from the transfer of power from one optical carrier to another that is downshifted in frequency by the energy of an optical phonon [9]. Raman amplifiers exhibit wide gain bandwidth, with approximately 100 nm around the central wavelength of 1500 nm [9]. Broadband amplification can be achieved with multiple pumps at different wavelengths. The advantages of Raman amplifiers are

that they use transmission fibres as a gain medium, the gain band shifts with the pump central wavelength, and the gain spectrum can be tailored by adjusting the pump frequency [9]. The main disadvantage of Raman amplifiers is their requirement for high power laser pumps, which often exceed the safety limits. The NF of Raman amplifiers can be lower than the NF of an EDFA [9], and Raman amplifiers are typically used as in-line amplifiers in core networks.

1.4.5 Optical Receivers

An optical receiver is the last part of an optical communication link. It converts an optical data signal into an electrical signal by means of direct or coherent reception. A direct detection receiver is a simple and economical solution. However, due to the square law detection it allows only intensity modulated formats to be detected, as the phase information carried in the optical signal is lost when applied to a conventional square law detector. The generated photocurrent is proportional to the responsivity of the receiver and intensity of optical signal, i.e. $i(t) = RP$.

In order to detect a phase modulated signal, the optical phase information has to be converted to an optical intensity which can then be detected using square law detectors. The phase to intensity conversion can be achieved using interferometric structures. For example, if two optical signals are coupled in a 3-dB coupler, they interfere constructively or destructively at the output, depending on the phase difference. One of optical signals serves as a reference, which is required for demodulation of phase modulated signals. Differentially precoded modulation formats such as DPSK and DQPSK use a delayed version of the received signal to serve as a phase reference, and this configuration is referred to as differential or self-coherent detection [10, 128]. If a second optical source, a local oscillator, is used as a phase reference than this configuration is called coherent detection. Depending on the frequency offset between an optical signal and LO, one can distinguish between homodyne, intradyne and heterodyne detection. In the case of homodyne reception an optical signal and LO have the same optical frequency, and therefore at the output an electrical baseband signal is generated. For intradyne reception, there is a small offset between an optical signal and LO. Most of practical and commercial solutions are based on intradyne reception, where the frequency offset is chosen to be as small as possible depending on the quality of optical sources employed. Finally, in the case

of heterodyne reception, the frequency offset is usually chosen to be higher than the signal bandwidth.

The extraction of all information from the optical signal (amplitude, frequency, phase and polarisation) is enabled by the 90° optical hybrids and balanced photodetectors. The phase diversity quadrature frontend composed of a 90° optical hybrid and a pair of balanced detectors is shown in Figure 1.24(a). The quadrature frontend is used for detection of in-phase and quadrature components of an optical signal. The in-phase and quadrature photocurrents at the output of the balanced detector pairs are given as [138]:

$$\begin{aligned} i_I(t) &\sim 2R|E_S||E_{LO}|\cos\left(\omega_{IF}t+\theta_S(t)-\theta_{LO}(t)\right) \\ i_Q(t) &\sim 2R|E_S||E_{LO}|\sin\left(\omega_{IF}t+\theta_S(t)-\theta_{LO}(t)\right) \end{aligned}, \tag{1.13}$$

where R is responsivity, E_S and E_{LO} are electrical fields of optical signal and local oscillator respectively, and ω_{IF} is the frequency difference between the signal frequency and LO frequency. Finally, θ_S and θ_{LO} are phases of the signal and LO, respectively. The in-phase and quadrature photocurrents are sufficient to recover a complex signal and extract phase information which is encoded on the optical carrier. The signal phase θ_S contains the phase of the optical carrier and the phase of the encoded data.

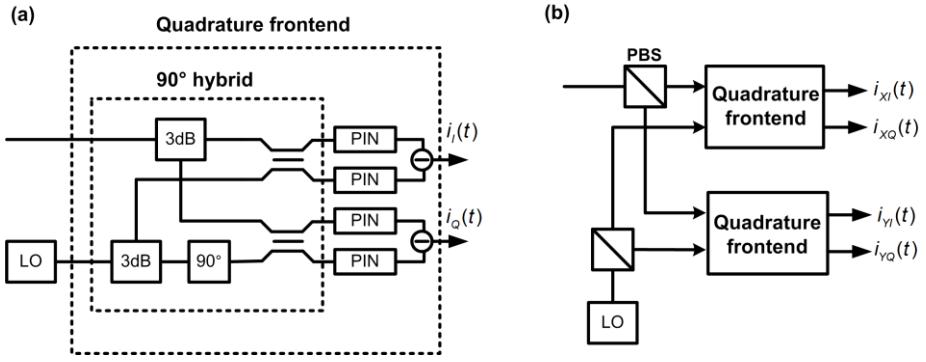

Figure 1.24. (a) Illustration of optical quadrature frontend comprised of 90° hybrid and two balanced detectors. (b) Polarisation diversity coherent detector.

After detection with the quadrature frontend the signal is quantized by means of an ADC and further digital signal processing is carried out in order to fully recover the received data [140, 141]. The typical DSP block at the receiver is shown in Figure 1.25. The first step in signal recovery is compensation of the accumulated chromatic dispersion, which is generally carried out by using FIR filters [47, 135]. The FIR filters for CD compensation can be realised in time or frequency domain. For the systems

which use polarisation multiplexing to double the spectral efficiency, polarisation demultiplexing is digitally performed to separate two polarisations with the minimum residual inter-polarisation interference. Generally, adaptive equalisers are used to compensate for PMD and for polarisation demultiplexing. Different algorithms have been proposed to update the filter taps to the changing channel conditions [47, 135, 138]. Constant modulus algorithms (CMA) are widely adopted for polarisation demultiplexing of phase shift keying (PSK) modulation formats (QPSK, 8-PSK), and have been modified for *m*-QAM formats as well [47, 135, 138]. Some DSP blocks include compensation (or at least mitigation) of nonlinear impairments as well [47, 136]. If the signal has been digitally shaped at the transmitter side, the corresponding digital matched filter is applied at the receiver to minimise inter-carrier interference. After the clock and timing recovery which synchronises the transmitter and receiver and thus minimises ISI, the frequency offset between received signal and LO is estimated [47, 141]. The digital phase estimation, required to recover the signal's carrier phase is performed prior to FEC and decision making.

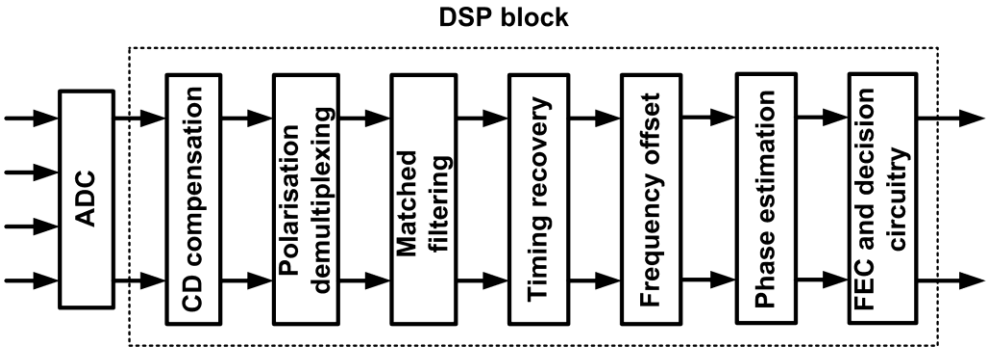

Figure 1.25. Schematic diagram of receiver DSP block

1.5 Conclusion

Demand for bandwidth, driven by media-rich applications, shows no sign of abating and is pushing service providers to deploy optical networks with increased capacity. The current trends predict that network traffic will grow 10 times faster than system capacity over the next decade. Therefore, various capacity scaling methods have been proposed recently to cope with bandwidth demands. The revival of coherent optical communications enabled the employment of higher-order modulation formats which led to the increase of throughput and effective compensation of transmission impairments. Simultaneously, versatile pulse shaping methods were investigated,

which enabled a significant reduction of guard bands between adjacent optical channels and the generation of highly spectrally efficient multicarrier systems and optical superchannels.

Along with the development of high capacity and spectrally efficient optical systems and interconnects, the requirement for compact optical sources with sufficiently good inherent properties, such as optical linewidth, RIN, OCNR, etc., has been created. Reduction of guard bands between optical channels created the need for exceptional frequency stability of optical sources. The constant frequency separation between channels cannot be provided by conventional WDM laser banks without additional control mechanisms. An attractive alternative is an optical multicarrier source, sometimes referred to as an optical frequency comb, which simultaneously generate multiple phase correlated optical carriers which provide constant and equidistant frequency separation between optical channels. A number of optical multicarrier sources have been proposed, such as mode-locked lasers, fibre lasers, electro-optic based multi-carrier sources, gain-switched comb sources, Kerr microresonator combs and parametric frequency comb sources. This thesis explores ways in which optical multicarrier sources can be employed in spectrally efficient optical systems to provide the data rates and performance required for next generation optical access and metro networks, and data centre interconnects.

References

[1] G. P. Agrawal, “Fiber-Optic Communication Systems, 4th Edition”, Wiley, 2010.

[2] R. J. Essiambre and R. W. Tkach, “Capacity Trends and Limits of Optical Communication Networks”, Proceedings of the IEEE, vol. 100, no. 5, pp. 1035-1055, May 2012.

[3] A. D. Ellis, J. Zhao, D. Cotter, “Approaching the Non-Linear Shannon Limit”, Journal of Lightwave Technology, vol. 28, no. 4, pp. 423-433, Feb. 2010.

[4] R. J. Mears, L. Reekie, I. M. Jauncey, and D. N. Payne, “High-gain rare-earth-doped fiber amplifier at 1.54 μm”, in Proc. OFC, Nevada, US, paper WI2, Jan. 1987.

[5] P. M. Becker, Anders A. Olsson, Jay R. Simpson, “Erbium-Doped Fiber Amplifiers: Fundamentals and Technology”, Academic Press, 1997.

[6] Cisco Systems, Available: http://en.wikipedia.org/wiki/Internet_traffic#cite_note-CSCO-15

[7] Cisco Systems, “Cisco Visual Networking Index: Forecast and Methodology 2013–2018”, White paper, Jun. 2014. Available: http://www.cisco.com/c/en/us/solutions/collateral/service-provider/ip-ngn-ip-next-generation-network/white_paper_c11-481360.pdf

[8] Cisco Systems, “The Zettabyte Era: Trends and Analysis”, White paper, Jun. 2014. Available: http://www.cisco.com/c/en/us/solutions/collateral/service-provider/visual-networking-index-vni/VNI_Hyperconnectivity_WP.pdf

[9] M. N. Islam, “Raman Amplifiers for Telecommunications”, Journal of Selected Topics in Quantum Electronics, vol. 8, no. 3, pp. 548-559, May/Jun. 2002.

[10] P. J. Winzer, R. J. Essiambre, "Advanced Modulation Formats for High-Capacity Optical Transport Networks", Journal of Lightwave Technology, vol. 24, no. 12, pp. 4711-4728, Dec. 2006.

[11] I. Djordjevic, W. Ryan, B. Vasic, “Coding for Optical Channels”, Springer, 2010.

[12] K. Roberts, S. H. Foo, M. Moyer, M. Hubbard, A. Sinclair, J. Gaudette, C. Laperle, “High Capacity Transport—100G and Beyond”, Journal of Lightwave Technology, vol. 33, no. 3, 563-578, Feb. 2015

[13] Available: https://www.vimp.com/en/web/hosting.html

[14] P. Littlewood, F. Masoud, E. Follis, “Optical Transport Networking”, Ciena Expert Series, White paper, 2014.

[15] A. A. M. Saleh, J. M. Simmons,“ All-Optical Networking – Evolution, Benefits, Challenges, and Future Vision”, Proceedings of the IEEE, vol. 100, no. 5, pp. 1105-1117, May 2012.

[16] P. J. Winzer, “High-Spectral-Efficiency Optical Modulation Formats”, Journal of Lightwave Technology, vol. 30, no. 24, pp. 3824-3835, Dec. 2012.

[17] International Telecommunications Union, “Recommendation G.709/y.1331 (02/12)”, Feb. 2012. Available: http://www.itu.int/rec/T-REC-G.709-201202-I/en

[18] S. Gringeri, B. Basch, V. Shukla, R. Egorov, T. J. Xia, “Flexible Architectures for Optical Transport Nodes and Networks”, IEEE Communications Magazine, vol. 46, no. 7, pp. 40-50, Jul. 2010

[19] T. A. Strasser, J. L. Wagener, “Wavelength-Selective Switches for ROADM Applications”, Journal of Selected Topics in Quantum Electronics, vol. 16, no. 5, pp. 1150-1157, Sep/Oct. 2010.

[20] ASE cable system, NEC, Available: http://www.nec.com, 2013.

[21] G. Bruno, “Evolutions of a pan-European Network over TrueWave-RS fiber enabled by flexible grid and coherent detection”, in Proc. OFC/NFOEC, Los Angeles, CA, USA, paper JW2A.5, Mar. 2012.

[22] Bell Labs, “Metro Network Traffic Growth: An Architecture Impact Study”, White Paper, 2013. Available: http://www.tmcnet.com/tmc/whitepapers/documents/whitepapers/2013/9378-bell-labs-metro-network-traffic-growth-an-architecture.pdf

[23] L. Eldada, “Optical add/drop multiplexing architecture for metro area networks”, SPIE Newsroom, DOI: 10.1117/2.1200801.0950, Jan. 2008.

[24] W. Idler, E. Lach, W. Kuebart, B. Junginger, K. Schuh, A. Klekamp, D. Werner, A. G. Steffan, A. Schippel, M. Schneiders, S. Vorbeck, R.-P. Braun, “16 x 112 Gb/s NRZ-DQPSK lab experiments and WDM field trial over ultimate metro distances including high PMD fibers”, Journal of Lightwave Technology, vol. 29, no. 15, pp. 2195-2203, Aug. 1, 2011.

[25] A. Gladisch, R.-P. Braun, D. Breuer, A. Ehrhardt, H.-M. Foisel, M. Jaeger, R. Leppla, M. Schneiders, S. Vorbeck, S. Weiershausen, F. Westphal, “Evolution of terrestrial optical system and core network architecture”, Proceedings of the IEEE, vol. 94, no. 5, pp. 869-891, May 2006.

[26] OECD, Jun. 2014. Available: http://www.oecd.org/sti/broadband/ oecdbroadbandportal.htm#Penetration

[27] L. G. Kazovsky, W.-T. Shaw, D. Gutierrez, N. Cheng, S.-W. Wong, “Next-Generation Optical Access Networks”, Journal of Lightwave Technology, vol. 25, no. 11, pp. 3428-3442, Nov. 2007.

[28] S. Gupta, “Residential broadband technologies for high-speed internet access”, in IET International Conference on Wireless, Mobile and Multimedia Networks, Beijing, China, pp. 279–282, Jan. 2008.

[29] L. Kazovsky, S.-W. Wong, T. Ayhan, K. M. Albeyoglu, M. RN Ribeiro, A. Shastri, “Hybrid optical–wireless access networks”, Proceedings of the IEEE, vol. 100, no. 5, pp. 1197-1225, May 2012.

[30] V. Vujicic, P. M. Anandarajah, C. Browning, R. Zhou, S. O’Duill, L. P. Barry, “Optical Multicarrier based IM/DD DWDM-SSB-OFDM Access Networks with SOAs for Power Budget Extension”, in Proc. ECOC, Cannes, France, paper We.1.6.6, Sep. 2014.

[31] N. Cvijetic, “OFDM for Next-Generation Optical Access Networks”, Journal of Lightwave Technology, vol. 30, no. 4, pp. 384-398, Feb. 2012.

[32] N. Cvijetic, M. Cvijetic, M.-F. Huang, E. Ip, Y.-K. Huang, T. Wang, “Terabit Optical Access Networks Based on WDM-OFDMA-PON”, Journal of Lightwave Technology, vol. 30, no. 4, pp. 493-503, Feb. 2012.

[33] C. Kachris, I. Tomkos, “A Survey on Optical Interconnects for Data Centers”, IEEE Communications and Tutorials, vol. 14, no. 4, pp. 1021-1036, Fourth Quarter, 2012.

[34] A. Biberman and K. Bergman, “Optical interconnection networks for high-performance computing systems,” Reports on Progress in Physics, vol. 75, no. 4, 046402, 2012.

[35] P. J. Winzer, R. Ryf, S. Randel, “Spatial Multiplexing Using Multiple-Input Multiple-Output Signal Processing” in Optical Fiber Telecommunications VIB, Academic Press, 2013.

[36] R. S. Tucker, G. I Eisenstein, S. K. Korotky, ”Optical Time-Division Multiplexing For Very High Bit-Rate Transmission”, Journal of Lightwave Technology, vol. 6, no. 11. pp. 1737-1749, Nov. 1988.

[37] S. Inao, T. Sato, S. Senstsui, T. Kuroha, Y. Nishimura, “Multicore optical fiber”, In Proc. Optical Fiber Communication Conf., Washington, DC, USA, paper WB1, 1979.

[38] S. Berdague, P. Facq, “Mode division multiplexing in optical fibers”, Applied Optics, vol. 21, no. 11, pp. 1950–1955, 1982.

[39] H. Takara, A. Sano, T. Kobayashi, H. Kubota, H. Kawakami, A. Matsuura, Y. Miyamoto, Y. Abe, H. Ono, K. Shikama, Y. Goto, K. Tsujikawa, Y. Sasaki, I. Ishida, K. Takenaga, S. Matsuo, K. Saitoh, M. Koshiba, T. Morioka , “1.01-Pb/s (12 SDM/222 WDM/456 Gb/s) crosstalk-managed transmission with 91.4-b/s/Hz aggregate spectral efficiency”, in Proc. ECOC, Amsterdam, Netherlands, paper Th.3.C.1, Sep. 2012.

[40] M. J. Chawki, E. Delevaque, V. Tholey, “Optical add-drop multiplexer using optical circulators and photoinduced Bragg gratings”, US patent US5726785 A, Mar. 1998.

[41] S. Yuan, N. Madamopoulos, R. Helkey, V. Kaman, J. Klingshirn, J. Bowers, “Fully Integrated NxN MEMS Wavelength Selective Switch with 100% Colorless Add-Drop Ports”, in Proc. OFC/NFOEC, San Diego, CA, USA, paper OWC2, 2008.

[42] S. Frisken, G. Baxter, D. Abakoumov, H. Zhou, I. Clarke, S. Poole, “Flexible and Grid-less Wavelength Selective Switch using LCOS Technology”, in Proc. OFC/NFOEC, Los Angeles, CA, USA, paper OTuM3, 2011.

[43] M. K. Smit, C. van Dam, “PHASAR-Based WDM-Devices: Principles, Design and Applications”, Journal of Selected Topics in Quantum Electronics, vol. 2, no. 2, pp. 236-250, Jun. 1996.

[44] K. Kikuchi, “Coherent Optical Communications: Historical Perspectives and Future Directions”, in High Spectral Density Optical Communication Technologies, Springer, 2010.

[45] S. Chandrasekhar, X. Liu, Fellow, “OFDM Based Superchannel Transmission Technology”, Journal of Lightwave Technology, vol. 30, no. 24, pp. 3816-3823, Dec. 2012.

[46] International Telecommunications Union, “G.694.1 spectral grids for WDM applications: DWDM frequency grid”, Series G: Transmission Systems and Media, Digital Systems and Networks, 2012

[47] P. Bayvel, C. Behrens, David S. Millar, “Digital Signal Processing (DSP) and Its Application in Optical Communication Systems” in Optical Fiber Telecommunications VIB, Academic Press, 2013.

[48] A. D. Ellis, F.C. Garcia Gunning, “Spectral density enhancement using coherent WDM”, IEEE Photonics Technology Letter, vol. 17, no. 2, pp. 504-506, Feb. 2005.

[49] R. Schmogrow, S. Ben-Ezra, P. C. Schindler, B. Nebendahl, C. Koos, W. Freude, J. Leuthold, “Pulse-Shaping With Digital, Electrical, and Optical Filters—A Comparison”, Journal of Lightwave Technology, vol. 31, no. 15, pp. 2570-2577, Aug. 2013.

[50] M. Birk, L. Raddatz, D. A. Fishman, P. Magill, S. Woodward, “Field Trial of End-to-End OC-768 Transmission Using 9 WDM Channels over 1000km of Installed Fiber”, in Proc. OFC, Atlanta, Georgia, USA, paper TuS4, 2003.

[51] T. Foggi, E. Forestieri, G. Colavolpe, G. Prati, “Maximum-Likelihood Sequence Detection With Closed-Form Metrics in OOK Optical Systems Impaired by GVD and PMD”, Journal of Lightwave Technology, vol. 24, no. 8, pp. 3073-3087, Aug. 2006.

[52] L. G. Kazovsky, “Phase and polarization-diversity coherent optical techniques”, Journal of Lightwave Technology, vol. 7, no. 2, pp. 279-292, Feb. 1989.

[53] A. H. Gnauck, G. Charlet, P. Tran, P. J. Winzer, C. R. Doerr, J. C. Centanni, E. C. Burrows, T. Kawanishi, T. Sakamoto, and K. Higuma, “25.6-Tb/s WDM Transmission of Polarization-Multiplexed RZ-DQPSK Signals”, Journal of Lightwave Technology, vol. 26, no. 1, pp. 79-84, Jan. 2008.

[54] P. J. Winzer, G. Raybon, H. Song, A. Adamiecki, S. Corteselli, A. H. Gnauck, D. A. Fishman, C. R. Doerr, S. Chandrasekhar, L. L. Buhl, T. J. Xia, G. Wellbrock, W. Lee, B. Basch, T. Kawanishi, K. Higuma, Y. Painchaud, “100-Gb/s DQPSK

Transmission: From Laboratory Experiments to Field Trials", Journal of Lightwave Technology, vol. 26, no. 20, pp. 3388-3402, Oct. 2008.

[55] C. R. Doerr, L. Chen, "Monolithic PDM-DQPSK receiver in silicon", in Proc. ECOC, Torino, pp. 1-3, Sep. 2010.

[56] C. R. Doerr, N. K. Fontaine, L. L. Buhl, "PDM-DQPSK silicon receiver with integrated monitor and minimum number of controls", IEEE Photonics Technology Letters, vol. 24, no. 8, pp. 697-699, Apr. 15, 2012.

[57] R. Nagarajan, J. Rahn, M. Kato, J. Pleumeekers, D. Lambert, V. Lal, H-S. Tsai, A. Nilsson, A. Dentai, M. Kuntz, R. Malendevich, J. Tang, J. Zhang, T. Butrie, M. Raburn, B. Little, W. Chen, G. Goldfarb, V. Dominic, B. Taylor, M. Reffle, F. Kish, D.Welch, "10 channel, 45.6 Gb/s per channel, polarization-multiplexed DQPSK, InP receiver photonic integrated circuit", Journal of Lightwave Technology, vol. 29, no. 4, pp. 386-395, Feb. 2011.

[58] J. Renaudier, G. Charlet, O. Bertran Pardo, H. Mardoyan, P. Tran, M. Salsi and S. Bigo, "Experimental Analysis of 100Gb/s Coherent PDM-QPSK Long-Haul Transmission under Constraints of Typical Terrestrial Networks", in Proc. ECOC, Brussels, Belgium, paper Th.2.A.3, Sep. 2008.

[59] P. J. Winzer, A. H. Gnauck, C. R. Doerr, M. Magarini, L. L. Buhl, "Spectrally efficient long-haul optical networking using 112-Gb/s polarization-multiplexed 16-QAM", Journal of Lightwave Technology, vol. 28, no. 4, pp. 547-556, Feb. 2010.

[60] P. J. Winzer, A. H. Gnauck, S. Chandrasekhar, S. Draving, J. Evangelista, B. Zhu, "Generation and 1,200-km Transmission of 448-Gb/s ETDM 56-Gbaud PDM 16-QAM using a Single I/Q Modulator", in Proc. ECOC, Torino, Italy, Sep. 2010.

[61] X. Zhou, L. E. Nelson, P. Magill, R. Isaac, B. Zhu, D. W. Peckham, P. I. Borel, K. Carlson, "PDM-Nyquist-32QAM for 450-Gb/s Per-Channel WDM Transmission on the 50 GHz ITU-T Grid", Journal of Lightwave Technology, vol. 30, no. 54, pp. 553-559, Feb. 2012.

[62] X. Zhou, and L. E. Nelson, "400G WDM Transmission on the 50 GHz Grid for Future Optical Networks", Journal of Lightwave Technology, vol. 30, no. 24, pp. 3779-3792, Dec. 2012.

[63] A. H. Gnauck, P. J. Winzer, A. Konczykowska, F. Jorge, J.-Y. Dupuy, M. Riet, G. Charlet, B. Zhu, D. W. Peckham, “Generation and Transmission of 21.4-Gbaud PDM 64-QAM Using a Novel High-Power DAC Driving a Single I/Q Modulator”, Journal of Lightwave Technology, vol. 30, no. 4, pp. 532-536, Feb. 2012.

[64] R.-J. Essiambre, G. Kramer, P. J. Winzer, G. J. Foschini, B. Goebel, “Capacity limits of optical fiber networks,” Journal of Lightwave Technology, vol. 28, no. 4, pp. 662–701, Feb. 2010.

[65] S. Okamoto, K. Toyoda, T. Omiya, K. Kasai, M. Yoshida, M. Nakazawa, “512 QAM (54 Gbit/s) Coherent Optical Transmission over 150 km with an Optical Bandwidth of 4.1 GHz”, in Proc. ECOC, Torino, Italy, Sep. 2010.

[66] P. J. Winzer, “Optical Network Scaling - Spatial and Spectral Superchannels”, Tutorial, Available: http://www.optics.rochester.edu/workgroups/knox/myweb/ISUPT2013/archive/Winzer.pdf

[67] G. Raybon, A. L. Adamiecki, S. Randel, C. Schmidt, P. J. Winzer, A. Konczykowska, F. Jorge, J-Y. Dupuy, L. L. Buhl, S. Chandrasekhar, X. Liu, A. H. Gnauck, C. Scholz, R. Delbue, “All-ETDM 80-Gbaud (640-Gb/s) PDM 16-QAM Generation and Coherent Detection”, IEEE Photonics Technology Letters, vol. 24, no. 15, pp. 1328-1330, Aug. 2012.

[68] J. Proakis, M. Salehi “Digital Communications, 5th Edition”, McGrow Hill, 2007.

[69] J. Leuthold, W. Freude, “Optical OFDM and Nyquist Multiplexing”, in Optical Fiber Telecommunications VIB, Academic Press, 2013.

[70] W. Shieh and I. Djordjevic, “OFDM for Optical Communications”, Elsevier/Academic Press, Oct. 2009.

[71] M. S. Erkılınc, S. Kilmurray, R. Maher, M. Paskov, R. Bouziane, S. Pachnicke, H. Griesser, B. C. Thomsen, P. Bayvel and R. I. Killey, “Nyquist-shaped dispersion-precompensated subcarrier modulation with direct detection for spectrally-efficient WDM transmission”, Optics Express, vol. 22, no. 8, pp. 9420-9431, Nov. 2013.

[72] R. W. Chang, “Synthesis of band-limited orthogonal signals for multichannel data transmission”, Bell Systems Technology Journal, 1966.

[73] S. B. Weinstein and P. M. Ebert, "Data Transmission by Frequency-Division Multiplexing Using the Discrete Fourier Transform", IEEE Transactions on Communication Technology, Vol. COM-19, No. 5, Oct. 1971.

[74] L. J. Cimini, Jr., “Analysis and simulation of a digital mobile channel using orthogonal frequency division multiplexing”, IEEE Transactions on Communications, vol. CM-33, pp. 665–675, 1985.

[75] R. Lassalle and M. Alard, “Principles of modulation and channel coding for digital broadcasting for mobile receivers”, EBU Technical Review, pp. 168–190, 1987.

[76] Q. Pan and R. Green, “Bit-Error-Rate performance of lightwave hybrid AM/OFDM systems with comparison with AM/QAM systems in the presence of clipping impulse noise,” IEEE Photonics Technology Letters, vol. 8, no. 2, pp. 278–280, 1996.

[77] B. Dixon, R. Pollard, and S. Iezekiel, “Orthogonal Frequency Division Multiplexing in wireless communication systems with Multimode Fiber feeds,” IEEE Transactions on Microwave Theory and Techniques, vol. 49, no. 8, pp. 1404–1409, 2001.

[78] W. Shieh, C. Athaudage, "Coherent optical orthogonal frequency division multiplexing," Electronics Letters , vol. 42, no.10, pp. 587-589, May 2006

[79] A. J. Lowery, et al., “Orthogonal frequency division multiplexing for adaptive dispersion compensation in long haul WDM systems,” in Proc. OFC/NFOEC, Anaheim, CA, USA, paper PDP39, Mar. 2006.

[80] S. L. Jansen, I. Morita, and H. Tanaka, “10x121.9-Gb/s PDM-OFDM Transmission With 2-b/s/Hz Spectral Efficiency Over 1,000km of SSMF,” in Proc. OFC/NFOEC, San Diego, CA, USA, paper PDP2, 2008.

[81] Y. Tang and W. Shieh, "Coherent Optical OFDM Transmission up to 1-Tb/s per Channel," Journal of Lightwave Technology, vol. 27, pp. 3511-3517, Aug. 2009.

[82] E. Yamada, A. Sano, H. Masuda, T. Kobayashi, E. Yoshida, Y. Miyamoto, Y. Hibino, K. Ishihara, Y. Takatori, K. Okada, K. Hagimoto, T. Yamada, and H. Yamazaki, “Novel No-Guard-Interval PDM CO-OFDM Transmission in 4.1 Tb/s (50x88.8-Gb/s) DWDM Link Over 800km SMF Including 50-GHz Spaced ROADM Nodes,” in Proc. OFC/NFOEC, San Diego, CA, USA, paper PDP8, 2008.

[83] K. Yonenaga, A. Sano, E. Yamazaki, F. Inuzuka, Y. Miyamoto, A. Takada, T. Yamada, "100 Gbit/s All-Optical OFDM Transmission Using 4x25 Gbit/s Optical

Duobinary Signals with Phase-Controlled Optical Sub-Carriers," in Proc. OFC/NFOEC, San Diego, CA, USA, paper JThA48, 2008.

[84] R. Schmogrow, M. Winter, M. Meyer, D. Hillerkuss, S. Wolf, B. Baeuerle, A. Ludwig, B. Nebendahl, S. Ben-Ezra, J. Meyer, M. Dreschmann, M. Huebner, J. Becker, C. Koos, W. Freude, J. Leuthold, “Real-time Nyquist pulse generation beyond 100 Gbit/s and its relation to OFDM”, Optics Express, vol. 20, no. 1, pp. 317-337, Jan. 2012.

[85] I. B. Djordjevic and B. Vasic, “Orthogonal Frequency Division Multiplexing for High-Speed Optical Transmission,” Optics Express, vol. 14, no. 9, pp. 3767–3775, Apr. 2006.

[86] J. Armstrong, “OFDM for Optical Communications”, Journal of Lightwave Technology, vol. 27. no. 3, pp. 189-2004, Feb. 2009.

[87] D. Hillerkuss, M. Winter, M. Teschke, A. Marculescu, J. Li, G. Sigurdsson, K. Worms, S. Ben Ezra, N. Narkiss, W. Freude, and J. Leuthold, “Simple all-optical FFT scheme enabling Tbit/s real-time signal processing”, Optics Express, vol. 18, no. 9, pp. 9324-9340, Apr. 2010.

[88] A. Peled and A. Ruiz, “Frequency domain data transmission using reduced computational complexity algorithms,” in Proc. ICASSP 80, Denver, CO, USA, vol. III, pp. 964–967, 1980.

[89] S. L. Jansen, I. Morita, T. C. W. Schenk, N. Takeda, H. Tanaka, “Coherent Optical 25.8-Gb/s OFDM Transmission Over 4160-km SSMF”, Journal of Lightwave Technology, vol. 26, no. 1, pp. 6-15, Jan. 2008.

[90] B. J. C. Schmidt, A. J. Lowery, J. Armstrong, “Experimental Demonstrations of Electronic Dispersion Compensation for Long-Haul Transmission Using Direct-Detection Optical OFDM”, Journal of Lightwave Technology, vol. 26, no. 1, pp. 196-203, Jan. 2008.

[91] Y. Ma, Qi Yang, Y. Tang, S. Chen, W. Shieh, “1-Tb/s single-channel coherent optical OFDM transmission over 600-km SSMF fiber with subwavelength bandwidth access”, Optics Express, vol. 17, no. 11, pp. 9421-9427, May 2009.

[92] X. Yi, N. K. Fontaine, R. P. Scott, S. J. Ben Yoo, “Tb/s Coherent Optical OFDM Systems Enabled by Optical Frequency Combs”, Journal of Lightwave Technology, vol. 28, no. 14, pp. 2054-2061, Jul. 2010.

[93] S. Chen, Y. Ma, and W. Shieh, “110-Gb/s Multi-band Real-time Coherent Optical OFDM Reception after 600-km Transmission over SSMF Fiber”, in Proc. OFC/NFOEC, San Diego, CA, USA, paper OMS2, Mar. 2010.

[94] R. Schmogrow, M. Winter, B. Nebendahl, D. Hillerkuss, J. Meyer, M. Dreschmann, M. Huebner, J. Becker, C. Koos, W. Freude, and J. Leuthold, “101.5 Gbit/s Real-Time OFDM Transmitter with 16-QAM Modulated Subcarriers”, in Proc. OFC/NFOEC, Los Angeles, CA, USA, paper OWE5, Mar. 2011.

[95] D-Z. Hsu, C-C.Wei, H-Y. Chen, J. Chen, M. C. Yuang, S-H. Lin, W-Y. Li, “21 Gb/s after 100 km OFDM long-reach PON transmission using a cost-effective electro-absorption modulator”, Optics Express, vol. 18, no. 26, pp. 27758- 27763, Dec. 2010.

[96] A. J. Lowery, L. Du, J. Armstrong, “Orthogonal Frequency Division Multiplexing for Adaptive Dispersion Compensation in Long Haul WDM Systems”, in Proc. OFC/NFOEC, Anaheim, CA, USA, paper PDP39, Mar. 2006.

[97] W. R. Peng, B. Zhang, X. Wu, K. M. Feng, A. E. Willner, and S. Chi, “Experimental demonstration of 1600 km SSMF transmission of a generalized direct detection optical virtual SSB-OFDM system,” in Proc. ECOC, Brussels, Belgium, Paper Mo 3.E.6, Sep. 2008.

[98] D. Qian, T. T-O. Kwok, N. Cvijetic, J. Hu, T. Wang, “41.25 Gb/s Real-Time OFDM Receiver for Variable Rate WDM-OFDMA-PON Transmission”, in Proc. OFC/NFOEC, San Diego, CA, USA, paper PDPD9, Mar. 2010.

[99] R. Giddings, “Real-time Digital Signal Processing for Optical OFDM-Based Future Optical Access Networks”, Journal of Lightwave Technology, vol. 32, no. 4. pp. 553-570, Feb. 2014.

[100] Y. Benlachtar, P. M. Watts, R. Bouziane, P. Milder, R. Koutsoyannis, J. C. Hoe, M. Püschel, M. Glick and R. I. Killey, “21.4 GS/s Real-Time DSP-Based Optical OFDM Signal Generation and Transmission Over 1600 km of Uncompensated Fibre”, in Proc. ECOC, Vienna, Austria, Sep. 2009.

[101] J-K. K. Rhee, N. Cvijetic, N. Wada, T. Wang, “Optical orthogonal frequency division multiplexed transmission using all-optical discrete Fourier transform”, Laser Photonics Review vol. 7, no. 4, pp. 539–553, Feb. 2013

[102] A. Sano, H. Masuda, E. Yoshida, T. Kobayashi, E. Yamada, Y. Miyamoto, F. Inuzuka, Y. Hibino, Y. Takatori, K. Hagimoto, T. Yamada, and Y. Sakamaki, “30x100 Gb/s all-optical OFDM transmission over 1300 km SMF with 10 ROADM nodes,” presented at the Eur. Conf. Optical Communication, Berlin, Germany, Paper PD1.7, 2007.

[103] A. Sano, E. Yamada, H. Masuda, E. Yamazaki, T. Kobayashi, E. Yoshida, Y. Miyamoto, R. Kudo, K. Ishihara, and Y. Takatori, “No-guard-interval coherent optical OFDM for 100 Gb/s long-haul WDM transmission”, Journal of Lightwave Technology, vol. 27, no. 16, pp. 3705–3713, Aug. 2009.

[104] S. Chandrasekhar and X. Liu, “Experimental investigation on the performance of closely spaced multi-carrier PDM-QPSK with digital coherent detection”, Optics Express, vol. 17, no. 24, pp. 21350–21361, Nov. 2009.

[105] X. Liu, S. Chandrasekhar, B. Zhu, and D. W. Peckham, “Efficient digital coherent detection of a 1.2 Tb/s 24-carrier no-guard-interval Co-OFDM signal by simultaneously detecting multiple carriers per sampling”, in Proc. OFC/NFOEC, San Diego, CA, USA, paper OWO2, 2010.

[106] J. Zhao, A. Ellis, “Electronic Impairment Mitigation in Optically Multiplexed Multicarrier Systems”, Journal of Lightwave Technology, vol. 29, no. 3, pp. 278-290, Feb. 2011.

[107] D. Hillerkuss, R. Schmogrow, T. Schellinger, M. Jordan, M. Winter, G. Huber, T. Vallaitis, R. Bonk, P. Kleinow, F. Frey, M. Roeger, S. Koenig, A. Ludwig, A. Marculescu, J. Li, M. Hoh, M. Dreschmann, J. Meyer, S. Ben Ezra, N. Narkiss, B. Nebendahl, F. Parmigiani, P. Petropoulos, B. Resan, A. Oehler, K. Weingarten, T. Ellermeyer, J. Lutz, M. Moeller, M. Huebner, J. Becker, C. Koos, W. Freude, J. Leuthold, “26 Tbit/s line-rate super-channel transmission utilizing all-optical fast Fourier transform processing”, Nature Photonics, vol. 5, no. 6, pp. 364-371, May 2011.

[108] A. K. Mishra, I. Nellas, I. Tomkos, C. Koos, W. Freude, J. Leuthold, “Comb Generator for 100 Gbit/s OFDM and Low-Loss Comb-Line Combiner Using the

Optical Inverse Fourier Transform (IFFT)", in Proc. ICTON, Stockholm, Sweden, paper We.A1.4, 2011.

[109] J. Schroder, L. Bangyuan Du, J. Carpenter, B. J. Eggleton, and A. J. Lowery, "All-Optical OFDM With Cyclic Prefix Insertion Using Flexible Wavelength Selective Switch Optical Processing", Journal of Lightwave Technology, vol. 32, no. 4, pp. 752-759, Feb. 2014.

[110] H. Nyquist, "Certain topics in telegraph transmission theory", Transactions of the American Institute of Electrical Engineers, pp. 617 – 644, Apr. 1928.

[111] Available: https://en.wikipedia.org/wiki/Raised-cosine_filter

[112] A. Carena, V. Curri, P. Poggiolini, G. Bosco, F. Forghieri, "Maximum Reach Versus Transmission Capacity for Terabit Superchannels Based on 27.75-GBaud PM-QPSK, PM-8QAM, or PM-16-QAM", IEEE Photonics Technology Letters, vol. 22, no. 11, pp. 829-831, Jun. 2010.

[113] G. Bosco, A. Carena, V. Curri, P. Poggiolini, F. Forghieri, "Performance Limits of Nyquist-WDM and CO-OFDM in High-Speed PM-QPSK Systems", IEEE Photonics Technology Letters, vol. 22, no. 15, pp. 1129-1131, Aug. 2010.

[114] G. Bosco, A. Carena, V. Curri, P. Poggiolini, E. Torrengo, F. Forghieri, "Investigation on the Robustness of a Nyquist-WDM Terabit Superchannel to Transmitter and Receiver Non-Idealities", in Proc. ECOC, Torino, Italy, paper Tu.3.A.4, Sep. 2010.

[115] G. Gavioli, E. Torrengo, G. Bosco, A. Carena, S. J. Savory, F. Forghieri, P. Poggiolini, "Ultra-Narrow-Spacing 10-Channel 1.12 Tb/s D-WDM Long-Haul Transmission Over Uncompensated SMF and NZDSF", IEEE Photonics Technology Letters, vol. 22, no. 19, pp. 1419-1421, Oct. 2010.

[116] S. Shimizu, G. Cincotti, N. Wada, "Demonstration and performance investigation of all-optical OFDM systems based on arrayed waveguide gratings", Optics Express, vol. 20, no. 26, pp. B525-B534, Dec. 2012.

[117] D. Sinefeld, S. Ben-Ezra, D. M. Marom, "Nyquist-WDM filter shaping with a high-resolution colorless photonic spectral processor", Optics Letters, vol. 38, no. 17, pp. 3268-3271, Sep. 2013.

[118] J-X. Cai, C. R. Davidson, A. Lucero, H. Zhang, D. G. Foursa, O. V. Sinkin, W. W. Patterson, A. N. Pilipetskii, G. Mohs, N. S. Bergano, “20 Tbit/s Transmission Over 6860 km With Sub-Nyquist Channel Spacing”, Journal of Lightwave Technology, vol. 30, no. 4 pp. 651-657, Feb. 2012.

[119] J. Yu, Ze Dong, H-C. Chien, Z. Jia, D. Huo, H. Yi, M. Li, Z. Ren, N. Lu, L. Xie, K. Liu, X. Zhang, Y. Xia, Y. Cai, M. Gunkel, P. Wagner, H. Mayer, A. Schippel, “Field Trial Nyquist-WDM Transmission of 8×216.4Gb/s PDM-CSRZ-QPSK Exceeding 4b/s/Hz Spectral Efficiency”, in Proc. OFC/OFOEC, Los Angeles, CA, USA, paper PDP5D.3, Mar. 2012.

[120] M-F. Huang, A. Tanaka, E. Ip, Y-K. Huang, D. Qian, Y. Zhang, S. Zhang, P. N. Ji, I. B. Djordjevic, T. Wang, Y. Aono, S. Murakami, T. Tajima, T. J. Xia, G. A. Wellbrock, “Terabit/s Nyquist Superchannels in High Capacity Fiber Field Trials Using DP-16-QAM and DP-8QAM Modulation Formats”, vol. 32,no. 4, pp. 776-782, Feb. 2014.

[121] Z. Dong, H-C. Chien, J. Yu, Z. Jia, J. Zhang, L. Cheng, G-K. Chang, “A Bandwidth-Efficient Coherent Ultra-Dense WDM-PON Based on Nyquist Independent-Sideband Modulation”, in Proc. ECOC, Cannes, France, paper Th.2.6.5, Sep. 2014.

[122] J. Pfeifle, V. Vujicic, R. T. Watts, P. C. Schindler, C. Weimann, R. Zhou, W. Freude, L. P. Barry, C. Koos, “Flexible terabit/s Nyquist-WDM super-channels using a gain-switched comb source”, Optics Express, vol. 23, no. 2, pp. 724-738, Jan. 2015.

[123] R. Rudnick, A. Tolmachev, D. Sinefeld, O. Golani, S. Ben-Ezra, M. Nazarathy, D. M. Marom, “Sub-Banded / Single-Sub-Carrier Drop-Demux and Flexible Spectral Shaping with a Fine Resolution Photonic Processor”, in Proc. ECOC, Canness, France, paper PD.4.1, Sep. 2014.

[124] K. Petermann, “Laser Diode Modulation and Noise”, Springer, 1988.

[125] L. A. Coldren, S. W. Corzine, M. L. Mashanovitch, “Diode Lasers and Photonic Integrated Circuits”, Wiley, 2012.

[126] W. Kobayashi, M. Arai, T. Yamanaka, N. Fujiwara, T. Fujisawa, M. Ishikawa, K. Tsuzuki, Y. Shibata, Y. Kondo, F. Kano, “Wide Temperature Range (25C–100C) Operation of a 10-Gb/s 1.55-μm Electroabsorption Modulator Integrated DFB Laser

for 80-km SMF Transmission", IEEE Photonics Technology Letters, vol. 21, no. 15, pp. 1054-1056, Aug. 2009.

[127] S. O. Kasap, "Optoelectronics and Photonics: Principles and Practices", Prentice Hall, 2001.

[128] M. Seimetz, "High-Order Modulationfor Optical Fiber Transmission", Springer, 2009.

[129] D. Hillerkuss, "Single-Laser Multi-Terabit/s Systems", KIT Scientific Publishing, 2012.

[130] ITU-T recomm. G.652. Available online: https://www.itu.int/rec/T-REC-G.652.

[131] ITU-T recomm. G.653. Available online: http://www.itu.int/rec/T-REC-G.653

[132] ITU-T recomm. G.654. Available online: http://www.itu.int/rec/T-REC-G.654

[133] ITU-T recomm. G.655. Available online: https://www.itu.int/rec/T-REC-G.655

[134] ITU-T recomm. G.656. Available online: http://www.itu.int/rec/T-REC-G.656

[135] S. J. Savory, "Digital filters for coherent optical receivers", Optics Express, vol. 16, no. 2, pp. 804-817, Jan. 2008.

[136] R. Maher, T. Xu, L. Galdino, M. Sato, A. Alvarado, K. Shi, S. J. Savory, B. C. Thomsen, R. I. Killey, P. Bayvel, "Spectrally Shaped DP-16-QAM Super-Channel Transmission with Multi-Channel Digital Back-Propagation", Scientific Reports 5, Article number: 8214, Feb. 2015.

[137] M. J. Connelly, "Semiconductor Optical Amplifiers", Springer, 2007.

[138] R. M. Schmogrow, "Real-time Digital Signal Processing for Software-defined Optical", KIT Scientific Publishing, 2013.

[139] P. M. Becker, A. A. Olsson, J. R. Simpson, "Erbium-Doped Fiber Amplifiers: Fundamentals and Technology", Academic Press, Mar. 1999.

[140] M. Cvijetic, I. Djordjevic, "Advanced Optical Communication Systems and Networks", Artech House, 2013

[141] M. Nakazawa, K. Kikuchi, T. Miyazaki, "High Spectral Density Optical Communication Technologies", Springer, 2010.

Chapter 2

2 Optical Multicarrier Sources

Further to the discussions in the previous chapter, superchannel enabling technologies such as OFDM and Nyquist WDM are promising architectures for the future evolution of optical networks. The generation of superchannels using these technologies require a multi-wavelength transmitter. In this chapter, several optical multicarrier sources have been presented, analysed and compared.

2.1 Introduction

A conventional approach for generation of an optical multicarrier signal is to incorporate a certain number of single mode lasers together, which can be constructed using discrete lasers or an integrated laser array. In the case of OFDM and Nyquist WDM based superchannels, where guard bands are omitted or very small, the wavelength drift of independent lasers can cause undesired crosstalk between adjacent channels. Conventional WDM laser banks struggle to provide a constant frequency separation between channels without additional control mechanisms [1]. Furthermore, the independent lasers are not phase correlated to each other, which is for instance the enabling condition for coherent WDM (Co-WDM) transmission technology [2].

An optical multicarrier source, also known as an optical frequency comb source (OFCS), provides a number of precisely spaced equidistant spectral carriers is an attractive alternative for multi-wavelength transmitters. Optical multicarrier sources have recently attracted much interest in the optical communications community due to wide ranging applications in directly and coherently detected OFDM and Nyquist WDM based systems [1-10]. OFCSs with good spectral flatness, stability, low linewidth and low RIN on each tone, and a tuneable FSR are highly desirable in multicarrier transmission systems. Furthermore, optical comb sources are expected to reduce component count and power consumption at the optical transmitters. Other

critical parameters are OCNR on each comb tone and power per line. These parameters of optical multicarrier sources define the quality of an optical comb and determine the modulation formats that can be employed.

The typical generation of an optical multicarrier signal assumes stabilising the optical multicarrier source (a single component (laser) or a set of subsystem devices) to an underlying clock signal (RF signal). A number of methods for the generation of optical multicarrier signals have been proposed which include, for example, mode locking, electro-optic modulation, gain switching, Kerr microresonators, and parametric processes.

2.2 Mode-Locked Laser

Traditionally, a mode-locked laser is a popular candidate for the generation of optical multicarrier signals [4, 5]. The term mode-locking describes the phase locking (correlation) between multiple longitudinal modes in a laser cavity [11]. When the correlation between the phases of different modes is accomplished, pulsed radiation can be produced, which in the frequency domain corresponds to an optical multicarrier signal with equidistant frequency separation between the carriers. Mode-locking occurs when the cavity modes are made to oscillate with comparable amplitudes and locked phases. If these modes have the same phase, they will constructively interfere at the same instant of the round-trip time and the output will consist of a series of pulses, i.e. laser is mode-locked. The idea of mode-locking and the first publications clearly identifying the mechanism were proposed in 1964 [11]. Mode-locking can be achieved using lasers with different designs and structures and mode-locking mechanisms can be classified into active, passive and hybrid mode-locking [11, 12].

Active mode-locking can be achieved through periodic external modulation of the optical signal in the cavity, causing the round trip phase changes being synchronised with resonator round trips [11-13]. The modulation can be realised with the use of a semiconductor electro-optic or acousto-optic modulator placed in the cavity and driven by an external signal. The frequency of the external RF modulating signal must be synchronised with the frequency spacing between modes (round trip time of the resonator) or a factor of a multiple integer of it, in order to achieve stable operation.

Passive mode locking exploits non-linear optical effects in the device to generate broadband optical multicarrier signal [14]. Passively mode locked lasers typically have a saturable absorber instead of an active component (as in the case of actively mode locked lasers) placed in the laser cavity [11], as shown in Figure 2.1(a). A saturable absorber is an optical intensity dependent component, having an absorption that decreases with increasing incident intensity of the optical signal until it saturates and becomes completely transparent to the signal inside the cavity. Therefore, when the simultaneous emission within the laser cavity reaches a certain level, the pulses with sufficient energy to saturate the absorber are generated which allows for the peak of the pulse to travel through. During this brief period of time, the gain is greater than the loss and a short duration pulse of light is amplified. As most of the modes within the gain region of the cavity are lasing at the same time, they start with the approximately same phase. The short duration pulses (i.e. broadband spectrum) are generated as the leading edge of the pulse experiences losses when saturating the absorber, while the peak experiences gain.

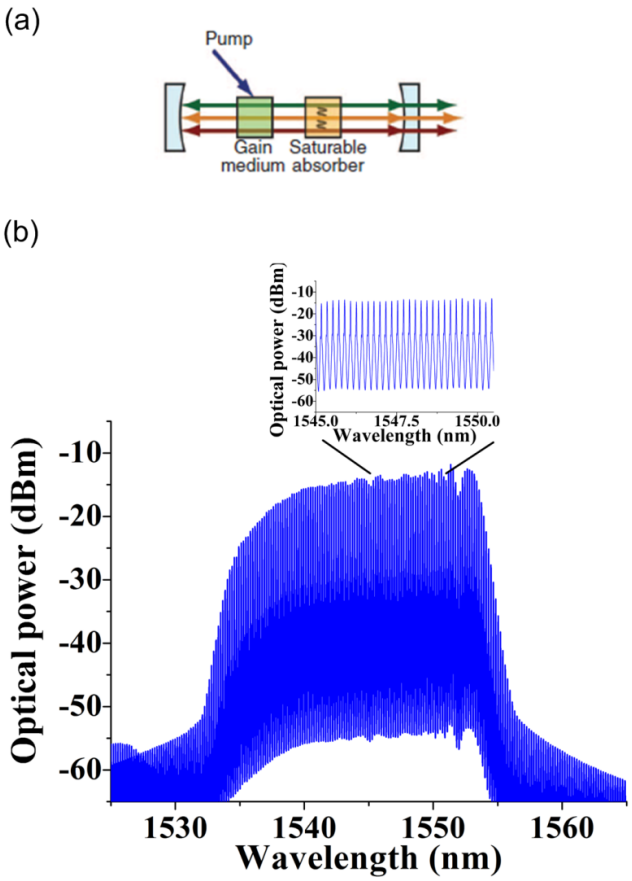

Figure 2.1. (a) Illustration of passively mode-locked laser; After [20]. (b) Optical spectrum obtained with the Q-Dash passive mode-locked laser; Inset: zoomed portion of the spectrum. Resolution Bandwidth (RBW) 0.02 nm.

Passive mode locking can be obtained using non-linear effects within laser cavity instead of a saturable absorber. The passive mode-locking can occur due to the nonlinear interactions between the longitudinal modes which can be greatly improved when the active region consists of a quantum structure (well, dash, dot) where the interactions between the optical modes in the active region are stronger because of the better confined optical field [16]. Four-wave mixing is marked as a dominant non-linear effect causing the passive mode-locking of the longitudinal modes. As illustrated in Figure 2.2, the beating between two longitudinal modes (E_1 and E_2 in this case) results in the generation of additional side modes (S_1,S_2,S_3,S_4) which are equidistantly spaced around parental longitudinal modes. Generated side mode (e.g. S_4), whose amplitude and phase are related to modes E_1 and E_2, pulls the nearest mode (e.g. E_3) from the Fabry-Perot (FP) resonant position and correlates the phase of mode E_3 with the two modes, E_1 and E_2. The similar process occurs when other pairs of longitudinal modes beat together. The side modes created through this FWM process acts as optical injection signals for modes leading to a mutual injection-locking phenomenon [14].

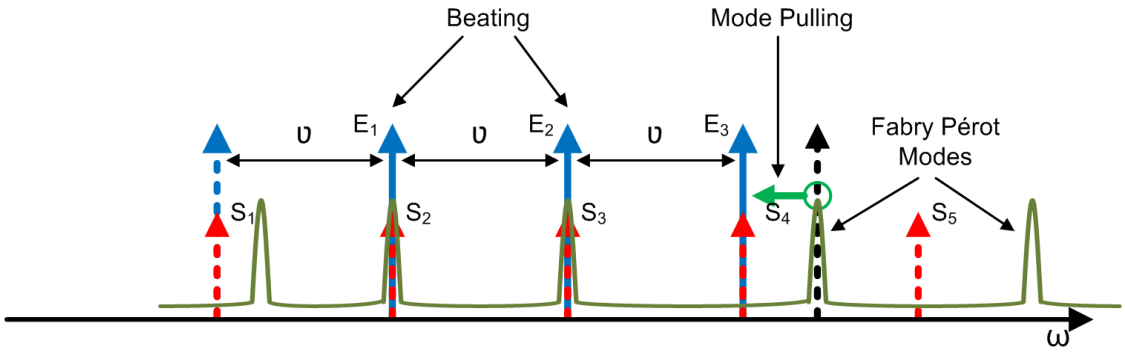

Figure 2.2. Mode-locking via FWM. E_1, E_2 and E_3 represent the lasing modes while S_1 to S_5 are the sidebands resulting from FWM.

Hybrid-mode locking occurs when the active and passive mode-locking are present simultaneously in the same laser. In a hybrid mode-locked laser, the generation of the optical pulses are in the same way as in a passively mode-locked laser, while the pulses are synchronised with an external RF signal like in the actively mode-locked lasers.

Mode-locked lasers can generate multicarrier signals over a wide bandwidth, but they suffer from cavity complexity, relatively large linewidth and RIN of individual comb lines, and usually do not offer FSR tunability. Due to the large linewidth on each comb

line, mode-locked lasers have been typically used in directly detected systems [4, 5]. However, if an appropriate phase noise reduction scheme is applied coherent detection is possible as well [17]. Low linewidth mode-locked lasers employed in coherently detected systems enabled transmission of 32.5 Tb/s signal over 227 km of SSMF [18]. Viewed from a practical perspective, the technology has control difficulties in starting and maintaining mode locking. This is because typical mode-locked lasers, consisting of multi–mode cavities, have multiple stabilities [19]. The optical spectrum generated using a Q-Dash passive mode-locked laser is shown in Figure 2.1(b).

2.3 Electro-Optic Modulation

The use of electro-optic modulators for the generation of optical multicarrier sources was introduced in 1972 [21]. However, the principle for pulse generation using the Fabry-Perot electro-optic modulator, which later was used for the optical multicarrier signal generation, was reported in 1962 by Bell Labs [22]. With the technical development of electro-optic modulators (bandwidth improvement, reduction of driving voltages and etc.) and high power optical amplifiers, the generation of electro-optic modulation based comb sources was enabled. Generally, the optical multicarrier signal is generated when the electro-optic modulator is nonlinearly driven with a large-amplitude sinusoidal signal (multiple V_π), as illustrated in Figure. 2.3(a). It is known that electro-optic modulation with a larger-amplitude signal promotes the generation of higher-order harmonics of the driving signal centred around the optical carrier (CW signal), conforming to Bessel functions [19].

A number of architectures utilising one or multiple phase modulators [23, 24], single or multiple intensity and field modulators [25-28], and variety of their combinations [29, 30] have been proposed to generate optical multicarrier signals. The spectrum of an optical multicarrier signal generated using a single phase modulator is shown in Figure 2.3(b). The frequency comb generated with a single phase modulator typically does not have good flatness. Better flatness of optical multicarrier signals generated with a single phase modulator can be achieved when it is driven with two sine waves at different amplitudes and frequencies [23]. Generating a greater number of carriers and fine tuning of the comb flatness can be achieved by cascading phase modulators [24]. Mach-Zehnder modulators offer more flexibility for an improvement of the spectral flatness of an optical multicarrier signal by employing certain drive conditions

on the two MZM arms [25-28]. By cascading several MZMs the flat spectral output with relatively high number of optical tones is generated, similar to the case when phase modulators are cascaded. Generally, the hybrid approach where phase and intensity modulators are combined represents a good compromise between system complexity and obtained spectral quality [29].

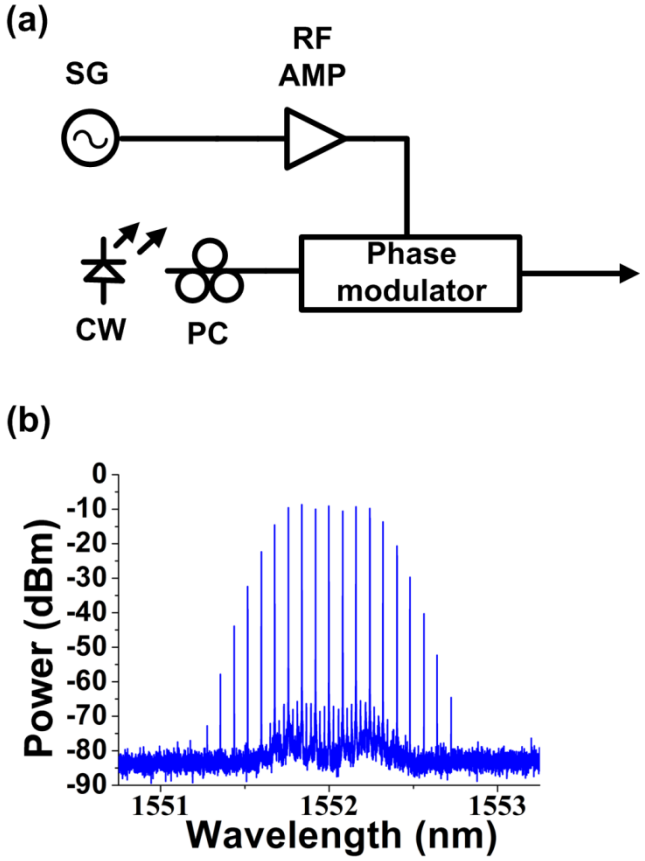

Figure 2.3. (a) Illustration of electro-optical source. (b) Optical spectrum obtained with a single electro-optical phase modulator. RBW=1.44pm.

The central wavelength, phase noise and linewidth, as well as relative intensity noise of electro-optic comb sources are determined by the external seeding CW laser. Typically, electro-optic comb sources have high OCNR and power per line. Tuneable FSR enables further flexibility and it is only limited by the bandwidth of the modulators and electrical amplifiers used to drive the modulators with a large-amplitude RF signal. However, the main disadvantages of electro-optic multicarrier sources are the high insertion loss and poor stability. Cascading two or more electro-optic modulators is required in order to generate a broad and flat multicarrier signal; unfortunately the typical insertion loss of $LiNbO_3$ based modulators is around 5-6 dB per device, cascading of several modulators can cause excessive total insertion losses that will limit the OCNR of the carriers after amplification. Recently, silicon and InP based

modulators, which are more suitable for photonic integration than $LiNbO_3$ based devices, have been proposed [31]. Silicon-organic hybrid (SOH) modulators have very low V_π, which significantly relaxes the requirements for driving electrical amplifiers and reduces the overall power consumption [32]. Additionally, SOH modulators provide very high bandwidth in excess of 100 GHz [33]. However to date, the insertion loss of SOH modulators are still higher than the insertion loss of $LiNbO_3$ based modulators, though the losses should reduce with better alignment and input/output fibre coupling. Electro-optic modulation multicarrier sources have been used in directly and coherently detected systems [34, 35].

2.4 Gain-Switched Laser

Gain switching is a technique for the generation of optical pulses using direct modulation of a semiconductor laser [36-39]. Gain switching is achieved by driving a laser diode with a large RF signal at the desired frequency (Figure 2.4(a)), in combination with a DC bias current, while the laser is temperature controlled. Furthermore, the laser is typically driven around relaxation oscillation frequency, which enables excitation of the first oscillation spike; the electrical pulse is terminated before the onset of the second spike. The electrical driving signal causes the increase of carrier density, which is maintained during a turn-on delay until there is large photon density build up and the carriers deplete [40]. While mode-locking can occur only in multimode laser cavities, gain switching can be achieved in single mode and multimode lasers. Furthermore, periodic external modulation of the optical signal in a laser cavity is required to achieve gain switching, whilst mode-locking can be achieved passively (see section 2.2). A modulating RF signal can have a variable frequency in the case of gain switching, whilst a frequency is predetermined by the cavity length in the case of actively mode-locked lasers.

The operating principle behind gain switching technique is illustrated in Figure 2.4(b). A large amplitude sinusoidal electrical signal is applied to the laser which is biased above the threshold as presented in Figure 2.4(b). With the increase of the driving sinusoidal signal (i.e. sinusoidal current), the carrier density within the cavity starts to rise rapidly. Simultaneously, the photon density inside the cavity increases and depletes the carriers. When the carrier density reaches the threshold, the lasing occurs. The optical pulses reach the peak level after the carrier density reaches the

maximum. As the sinusoidal driving current decreases below the threshold, the carrier and photon density within the cavity decrease consequently, which prevent the onset of second and subsequent optical spikes.

The pulses generated by direct modulation of the laser suffer from timing jitter. However, optical injection is often used together with gain switching to reduce the timing jitter and linewidth of the individual comb lines. The external light injection also reduces the RIN and phase noise associated with each of the individual comb tones [7, 41, 42]. The optical spectrum of a typical gain switched distributed feedback (DFB) laser is shown in Figure 2.5 whereby the frequency separation is determined by the repetition rate of the pulses. In this case, an electrical sinusoidal signal at a frequency of 18.1 GHz was applied to the DFB laser.

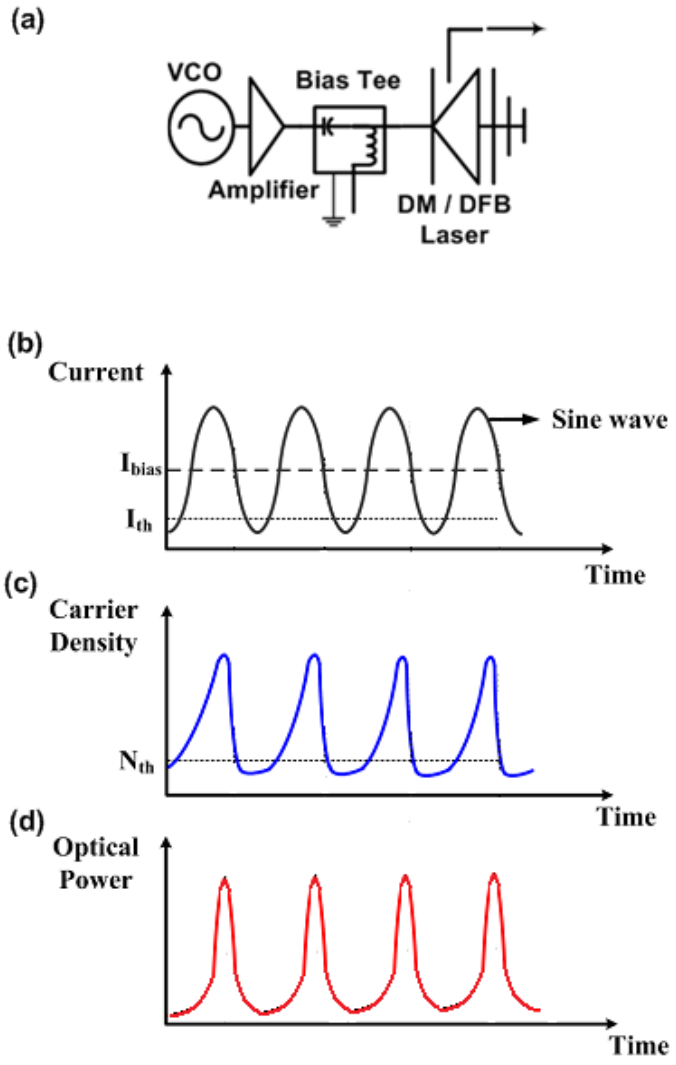

Figure 2.4. Gain switching: (a) gain switched source. Typical time evolution of (b) the applied driving current, (c) the carrier density and (d) the generated output pulses. After [41, 42].

Although the pulse generation by gain switching of semiconductor lasers have been reported in early 1980's, its utility as an optical multicarrier source have been proposed only in 2009 [42]. The main advantage of the gain switched comb source is its inherent stability without any bias control. With respect to the possible number and the power of lines, the GSCS competes with frequency combs generated with a single electro-optic modulator. Flexibility in tuning FSR is enabled by changing the frequency of the driving RF signal [7]. An externally injected GSCS adopts inherent characteristics of a master laser and therefore typically exhibits low linewidth and RIN. Data rates up to 2.1 Tb/s, with very high spectral efficiency (7.8 bit/s/Hz) have been achieved using externally injected gain switched comb sources as multicarrier sources in spectrally efficient WDM systems [7, 43].

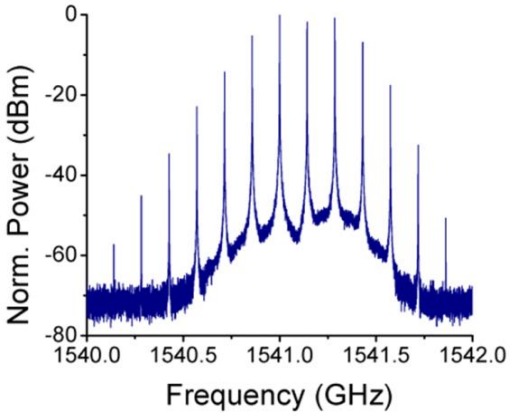

Figure 2.5. Optical spectrum obtained by gain switching of a DFB laser. RBW=100 MHz.

2.5 Microresonator Based Kerr Combs

In recent years a new frequency comb generation method which uses parametric frequency conversion in planar microresonators has emerged [20, 44-46]. The optical multicarrier signal is generated when an optical signal is trapped and confined in a microresonator, which is shown in Figure 2.6(a). As the signal is confined in a small area this results in an enhancement of the light intensity and consequently non-linear interactions. The quality of microresonators is determined by the quality factor (Q-factor) which defines threshold for non-linear interactions and interaction lengths [20]. The dominant non-linear effect responsible for the generation of optical multicarrier signals in such a structure is FWM. The intensity dependent refractive index, $n_0 + I \cdot n_2$, where n_2 is the Kerr coefficient, n_0 is the linear refractive index

and *I* denotes the optical signal intensity, enables the formation of new frequency components. If the signal and idler frequencies coincide with the optical microresonator modes, the parametric process is enhanced leading to the efficient generation of side modes [20]. The generated frequency components are phase correlated with the pump laser signal.

The optical spectrum of a microresonator based frequency comb is shown in Figure 2.6(b). With respect to the possible number of lines, the microresonator Kerr comb competes with frequency combs generated by mode-locked lasers. Recently, the microresonator Kerr comb covering full C and L band and enabling total capacity of 20 Tbit/s has been proposed [45]. Furthermore, Kerr combs exhibit good OCNR and power per line. The comb spectrum and its phase noise depend precisely on the pump conditions, i.e., on polarisation and power of the pump laser, and on its wavelength detuning with respect to the pumped resonance [46]. The main disadvantage of microresonator Kerr combs is the requisite for sophisticated pumping schemes and the line spacing is inherently tied to the free spectral range of the underlying resonator.

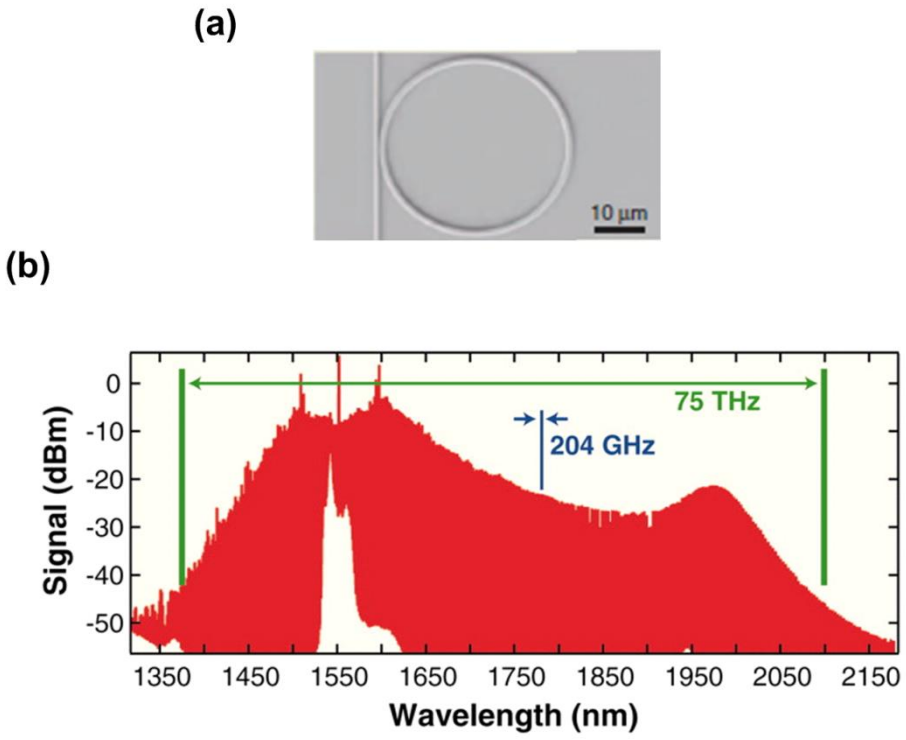

Figure 2.6. (a) Chip based SiN ring resonator. (b) Optical spectrum obtained by SiN microresonator based frequency comb. After [20]

2.6 Parametric Frequency Combs

The cavity and resonance based optical multicarrier frequency sources, such as mode-locked lasers and Kerr microresonator combs, provide a high number of carriers but typically do not offer FSR tunability, due to the inherent inability of the cavity and resonant conditions reconfiguration. The cavity-less approaches such as electro-optic modulation and gain-switching of semiconductor lasers, provide full FSR and central wavelength flexibility, but they are unable to generate a high number of carriers in comparison with cavity and resonance based combs. An alternative approach which offers central wavelength and FSR tunability, and high number of carriers is based on parametric mixing in highly non-linear fibre (HNLF). The operating principle of the parametric frequency comb is illustrated in Figure 2.7 [47, 48].

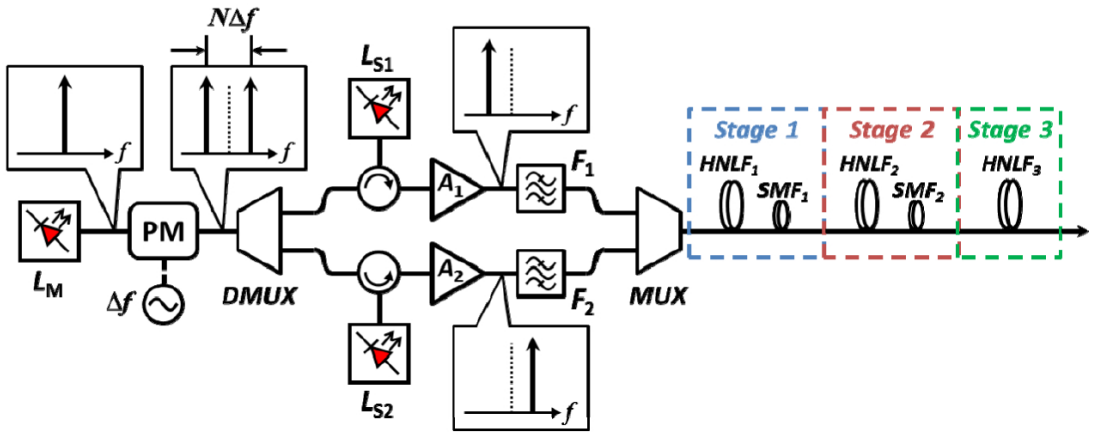

Figure 2.7. Illustration of parametric mixing comb generation. After [48]

A low linewidth CW laser, used to seed the comb generator, is used to drive a phase modulator to generate two optical carriers at a certain frequency. The generated tones are used to injection-lock high power slave lasers via circulators (LS_1 and LS_2). The optical signals from the slave lasers can be further amplified in order to generate wide and flat frequency comb and jointly coupled into the parametric mixer consisting of a few stages. The first stage was made of a highly-nonlinear fibre and subsequent standard single-mode fibre (SMF_1) to provide adequate anomalous dispersion to compress the output field of $HNLF_1$, thereby increasing its peak power [47, 48]. The comb is further expanded using a second stage of HNLF and SMF. A wide and flat optical comb is created by adding an additional mixing stage ($HNLF_3$). The optical spectrum of the parametric comb is shown in Figure 2.8. As can be seen from Figure

2.8, parametric combs have high power per line and good OCNR. Also, the low phase noise of the seeding laser is transferred to the comb lines [47, 48]. The disadvantage of parametric frequency combs is the high level of complexity, high number of components required for the comb generation and inability for the full chip scale integration. It requires sophisticated nonlinear fibre - dispersive fibre schemes to enable parametric processes. Recently, the transmission of 31.8 Tb/s signal over 50 km of SSMF incorporating 1520 channels from parametric frequency comb has been demonstrated [9].

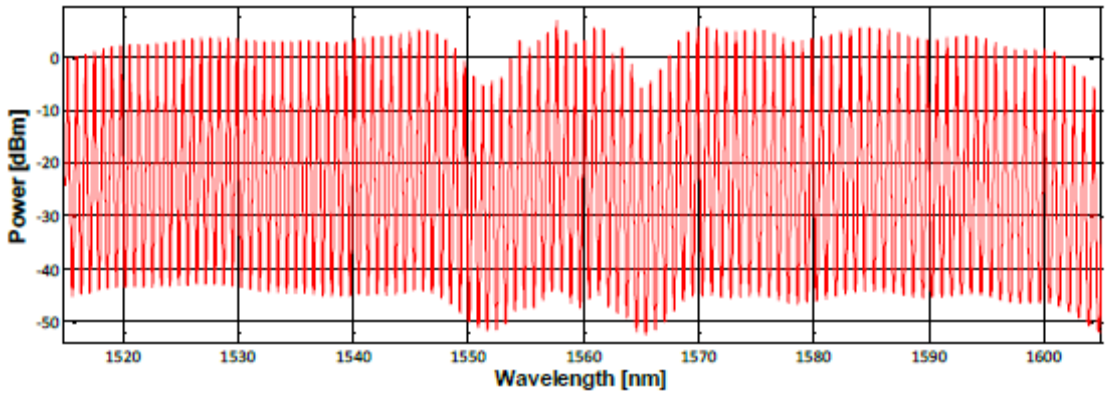

Figure 2.8. Optical spectrum of the parametric frequency comb. RBW= 0.1 nm. After [48].

2.7 Conclusion

Superchannel enabling technologies such as OFDM and Nyquist WDM require a multi-wavelength transmitter, and a conventional approach for generation of an optical multicarrier signal is to incorporate a certain number of single mode lasers together. However, due to the limitations of this approach (e.g. wavelength drift, high linewidth and phase noise), an attractive alternative in form of an optical multicarrier source has been proposed. In this chapter, several optical multicarrier sources have been presented, analysed and compared. Mode-locked lasers, mircoresonator ring Kerr combs and parametric combs typically generate large number of carriers with good power per carrier. However, semiconductor MLLs typically have a large linewidth and phase noise on each carrier, whilst microresonator Kerr combs and parametric combs require sophisticated pumping schemes and nonlinear fibre - dispersive fibre schemes, respectively. Electro-optic based combs and gain-switched combs, provide full FSR and central wavelength flexibility, and low phase noise on each carrier, but they are unable to generate a high number of carriers.

References

[1] K. Igarashi, T. Tsuritani, I. Morita, K. Katoh, K. Kikuchi, “Frequency stabilization of multiple semiconductor lasers for Nyquist-WDM transmission systems”, in Proc. OFC/NFOEC, Anaheim, CA, USA, paper OTu2I.6, Mar. 2013.

[2] A. D. Ellis, F. C. G. Gunning, B. Cuenot, T. C. Healy, E. Pincemin, “Towards 1 TbE using Coherent WDM”, in Proc. OECC/ACOFT, Sydney, Australia, paper WeA-1, 2008.

[3] Z. Wang, Y-K. Huang, E. Ip, P. R. Prucnal, T. Wang, “Performance investigation of polarization-multiplexed 16-QAM using all-optical OFDM transmission and digital coherent detection”, in Proc. OFC/NFOEC, Los Angeles, CA, USA, paper OMS5, 2011.

[4] V. Vujicic, P. M. Anandarajah, C. Browning, L. P. Barry, “WDM-OFDM-PON based on compatible SSB technique using a mode locked comb source,” IEEE Photonics Technology Letters, vol. 25, no. 21, pp. 2058-2061, Nov. 2013.

[5] Y. Ben M’Sallem, Q. T. Le, L. Bramerie, Q.-T. Nguyen, E. Borgne, P. Besnard, A. Shen, F. Lelarge, S. LaRochelle, L. A. Rusch, and J.-C. Simon, “Quantum-Dash Mode-Locked Laser as a Source for 56-Gb/s DQPSK Modulation in WDM Multicast Applications,” IEEE Photonics Technology Letters, vol. 23, no. 7, pp. 453–455, Mar. 2011.

[6] X. Yi, N. K. Fontaine, R. P. Scott, S. J. Ben Yoo, “Tb/s Coherent Optical OFDM Systems Enabled by Optical Frequency Combs”, Journal of Lightwave Technology, vol. 28, no. 14, pp. 2054-2061, Jul. 2010.

[7] J. Pfeifle, V. Vujicic, R. T. Watts, P. C. Schindler, C. Weimann, R. Zhou, W. Freude, L. P. Barry, C. Koos, “Flexible terabit/s Nyquist-WDM super-channels using a gain-switched comb source”, Optics Express, vol. 23, no. 2, pp. 724-738, Jan. 2015.

[8] J. Pfeifle, V. Brasch, M. Lauermann, Y. Yu, D. Wegner, T. Herr, K. Hartinger, P. Schindler, J. Li, D. Hillerkuss, R. Schmogrow, C. Weimann, R. Holzwarth, W. Freude, J. Leuthold, T. J. Kippenberg, C. Koos, “Coherent terabit communications with microresonator Kerr frequency combs”, Nature Photonics, vol. 8, pp. 375–380, Apr. 2014.

[9] V. Ataie, E. Temprana, L. Liu, E. Myslivets, B. P.-P. Kuo, N. Alic, and S. Radic, „Flex-grid Compatible Ultra Wide Frequency Comb Source for 31.8 Tb/s Coherent Transmission of 1520 UDWDM Channels“, in Proc. OFC/NFOEC, San Francisco, CA, USA, paper Th5B.7, Mar. 2014.

[10] C. Weimann, P. C. Schindler, R. Palmer, S. Wolf, D. Bekele, D. Korn, J. Pfeifle, S. Koeber, R. Schmogrow, L. Alloatti, D. Elder, H. Yu, W. Bogaerts, L. R. Dalton, W. Freude, J. Leuthold, and C. Koos, “Silicon-organic hybrid (SOH) frequency comb sources for terabit/s data transmission”, Optics Express, vol. 22, no. 3, pp. 3629-3637, Feb. 2014.

[11] H. A. Haus, “Mode-Locking of Lasers”, Journal on Selected Topics in Quantum Electronics, vol. 6, no. 6, pp. 1173-1185, Nov/Dec 2000.

[12] B. Saleh and M. Teich, “Fundamentals of Photonics”, John Wiley & Sons, Inc., USA, 1991.

[13] L. Hargrove, R. Fork, and M. Pollack, “Locking of he:ne laser modes induced by synchronous intracavity modulation,” Applied Physics Letters, vol. 5, no. 1, pp. 4–5, Jul 1964.

[14] J. Renaudier, G.-H. Duan, P. Landais, P. Gallion, “Phase Correlation and Linewidth Reduction of 40 GHz Self-Pulsation in Distributed Bragg Reflector Semiconductor Lasers”, IEEE Journal of Quantum Electronics, vol. 43, no. 2, pp. 147-156, Feb. 2007.

[15] R. Koumans, R. van Roijen, “Theory for passive mode-locking in semiconductor laser structures including the effects of self-phase modulation, dispersion, and pulse collisions”, Journal of Quantum Electronics, vol. 32, no. 3, pp. 478–492, Mar. 1996.

[16] F. Lelarge, B. Dagens, J. Renaudier, R. Brenot, A. Accard, F. van Dijk, D. Make, O. Le Gouezigou, J.-G. Provost, F. Poingt, J. Landreau, O. Drisse, E. Derouin, B. Rousseau, F. Pommereau, and G.-H. Duan, “Recent advances on InAs/InP Quantum Dash based semiconductor lasers and optical amplifiers operating at 1.55 μm,” IEEE Journal of Selected Topics in Quantum Electronics, vol. 13, no. 1, pp. 111–124 Jan/Feb, 2007.

[17] J. Pfeifle, R. Watts, I. Shkarban, S. Wolf, V. Vujicic, P. Landais, N. Chimot, S. Joshi, K. Merghem, C. Calò, M. Weber, A. Ramdane, F. Lelarge, L. P Barry, W. Freude, C. Koos, “Simultaneous Phase Noise Reduction of 30 Comb Lines from a

Quantum-Dash Mode-Locked Laser Diode Enabling Coherent Tbit/s Data Transmission", in Proc. OFC/NFOEC, Los Angeles, CA, USA, paper, Tu3I. 5, Mar. 2015.

[18] D. Hillerkuss, R. Schmogrow, M. Meyer, S. Wolf, M. Jordan, P. Kleinow, N. Lindenmann, P. C. Schindler, A. Melikyan, X. Yang, S. Ben-Ezra , B. Nebendahl, M. Dreschmann, J. Meyer, F. Parmigiani, P. Petropoulos, B. Resan, A. Oehler, K. Weingarten, L. Altenhain, T. Ellermeyer, M. Moeller, M. Huebner, J. Becker, C. Koos, W. Freude, J. Leuthold, "Single-laser 32.5 Tbit/s Nyquist WDM transmission", Journal of Optical Communications and Networking, vol. 4, no. 10, pp. 715-723, 2012.

[19] T. Sakamoto, T. Kawanishi, and M. Izutsu, "Optoelectronic oscillator using a LiNbO3 phase modulator for self-oscillating frequency comb generation", Optics Letters, vol. 31, no. 6, pp. 811-813, Mar. 2006.

[20] T. J. Kippenberg, R. Holzwarth, S. A. Diddams, "Microresonator-Based Optical Frequency Combs", Science, vol. 332, pp. 555-559, Apr. 2011.

[21] Sheng Liu, Trina T. Ng, David J. Richardson, Periklis Petropoulos, "An Optical Frequency Comb Generator as a Broadband Pulse Source", in Proc. OFC/NFOEC, San Diego, CA, USA, paper OThG7, Mar. 2009.

[22] E. I. Gordon and J. D. Rigden, "The Fabry-Perot Electrooptic modulator", The Bell System Technical Journal, Oct. 1962.

[23] S. Ozharar, F. Quinlan, I. Ozdur, S. Gee, and P. J. Delfyett, "Ultraflat optical comb generation by phase-only modulation of continuous-wave light", IEEE Photonics Technology Letters vol. 20, no. 36, pp. 36-38, Jan. 2008.

[24] J. Zhang, N. Chi, J. Yu, Y. Shao, J. Zhu, B. Huang, and L. Tao, "Generation of coherent and frequency-lock multi-carriers using cascaded phase modulators and recirculating frequency shifter for Tb/s optical communication", Optics Express, vol. 19, no. 11, pp. 12891-12902, Jun. 2011.

[25] T. Sakamoto, T. Kawanishi, and M. Izutsu, "Asymptotic formalism for ultraflat optical frequency comb generation using a Mach-Zehnder modulator", Optics Letters vol. 32, no. 11, 1515-1517, Jun. 2007.

[26] T. Sakamoto, T. Kawanishi, and M. Izutsu, “Widely wavelength-tunable ultra-flat frequency comb generation using conventional dual-drive Mach-Zehnder modulator”, Electronic Letters, vol. 43, no. 19, Sep. 2007.

[27] A. K. Mishra, R. Schmogrow, I. Tomkos, D. Hillerkuss, C. Koos, W. Freude, and J. Leuthold, “Flexible RF-based comb generator”, IEEE Photonics Technology Letters vol. 25, no. 7, pp. 701-704, Aug. 2013.

[28] T. Healy, F. C. G. Gunning, A. D. Ellis, “Multi-wavelength source using low drive-voltage amplitude modulators for optical communications”, Optics Express, vol. 15, no. 6, pp. 2981-2986, Mar. 2007.

[29] M. Fujiwara, M. Teshima, J. Kani, H. Suzuki, N. Takachio, and K. Iwatsuki, “Optical carrier supply module using flattened optical multicarrier generation based on sinusoidal amplitude and phase hybrid modulation”, Journal of Lightwave Technology, vol. 21, no. 11, pp. 2705-2714, Nov. 2003.

[30] C. Chen, C. He, D. Zhu, R. Guo, F. Zhang, and S. Pan, “Generation of a flat optical frequency comb based on a cascaded polarization modulator and phase modulator,” Optics Letters vol. 38, no. 16, 3137-3139, Aug. 2013.

[31] D. Petousi, L. Zimmermann, K. Voigt, J. Kreissl, K. Petermann, “Comparison of InP and Silicon Mach-Zehnder Modulators in Terms of Chirp”, in Proc. ECOC, London, UK, 2013.

[32] R. Palmer, S. Koeber, D. L. Elder, M. Woessner, W. Heni, D. Korn, M. Lauermann, W. Bogaerts, L. Dalton, W. Freude, J. Leuthold, C. Koos “High-Speed, Low Drive-Voltage Silicon-Organic Hybrid Modulator Based on a Binary-Chromophore Electro-Optic Material”, Journal of Lightwave Technology, vol. 32, no. 16, pp. 2726-2734, Aug. 2014.

[33] L. Alloatti, R. Palmer, S. Diebold, K. P. Pahl, B. Chen, R. Dinu, M. Fournier, J-M. Fedeli, T. Zwick, W. Freude, C. Koos, J. Leuthold, “100 GHz silicon–organic hybrid modulator”, Nature Photonics, Light: Science & Applications, vol. 3, e173, May 2014.

[34] V. Vujicic, P. M. Anandarajah, R. Zhou, C. Browning, L. P. Barry, “Performance Investigation of IM/DD Compatible SSB-OFDM Systems Based on Optical Multicarrier Sources”, IEEE Photonics Journal, vol. 6, no. 5, Oct. 2014.

[35] C. Weimann, P. C. Schindler, R. Palmer, S. Wolf, D. Bekele, D. Korn, J. Pfeifle, S. Koeber, R. Schmogrow, L. Alloatti, D. L. Elder, H. Yu, W. Bogaerts, L. R. Dalton, W. Freude, J. Leuthold, C. Koos, “Silicon-organic hybrid (SOH) frequency comb sources for terabit/s data transmission”, Optics Express, vol. 22, no. 3, pp. 3629—3637, Feb. 2014.

[36] H. Ito, H. Yokoyama, S. Murata, H. Inaba, “Picosecond optical pulse generation from an R.F. modulated AlGaAs D.H. diode laser”, Electronic Letters vol. 15, no. 23, pp. 738-740, Nov. 1979.

[37] P. Torphammar and S. T. Eng, “Picosecond pulse generation in semiconductor lasers using resonance oscillation”, Electronic Letters, vol. 16, no. 15, pp. 587-589, Jul. 1980.

[38] S. Tarucha and K. Otsuka, “Response of semiconductor laser to deep sinusoidal injection current modulation”, Journal of Quantum Electronics, vol. 17, no. 5, pp. 810-816, May 1981.

[39] D. Pataca, P. Gunning, M. Rocha, J. Lucek, R. Kashyap, K. Smith, D. Moodie, R. Davey, R. Souza, and A. Siddiqui, “Gain-switched dfb lasers”, Journal of Microwaves and Optoelectronics, vol. 1, no. 1, pp. 46-63, May 1997.

[40] P. M. Anandarajah, R. Maher, Y. Q. Xu, S. Latkowski, J. O’Carroll, S. G. Murdoch, R. Phelan, J. O’Gorman, L. P. Barry, “Generation of Coherent Multicarrier Signals by Gain Switching of Discrete Mode Lasers”, IEEE Photonics Journal, vol. 3, no. 1, pp. 112-122, Feb. 2011.

[41] R. Zhou, “Optical Frequency Comb Source for Next Generation Access Networks”, Ph.D. dissertation, Dublin City University.

[42] P. M. Anandarajah, K. Shi, J. O’Carroll, A. Kaszubowska, R. Phelan, L. P. Barry, A. D. Ellis, P. Perry, D. Reid, B. Kelly, and J. O’Gorman, “Phase shift keyed systems based on a gain switched laser transmitter”, Optics Express vol. 17, no. 15, pp. 12668-12677, Jul 2009.

[43] V. Vujicic, J. Pfeifle, R. Watts, P. C Schindler, C. Weimann, R. Zhou, W. Freude, C. G. Koos, L. P. Barry, “Flexible Terabit/s Nyquist-WDM superchannels with net SE> 7bit/s/Hz using a gain-switched comb source”, in Proc. CLEO: Science and Innovations, San Jose, CA, USA, paper SW1J. 3, Jun. 2014.

[44] P. Del'Haye, A. Schliesser, O. Arcizet, T. Wilken, R. Holzwarth, T. J. Kippenberg, "Optical frequency comb generation from a monolithic microresonator", Nature, vol. 450, no. 7173, pp. 1214-1217, Dec. 2007.

[45] J. Pfeifle, A. Kordts, P. Marin, M. Karpov, M. Pfeiffer, V. Brasch, R. Rosenberger, J. Kemal, S. Wolf, W. Freude, T. Kippenberg, C. Koos, "Full C and L-Band Transmission at 20 Tbit/s Using Cavity-Soliton Kerr Frequency Combs", in Proc. CLEO, San Jose, CA, USA, paper JTh5C.8, May 2015.

[46] J. Pfeifle, M. Lauermann, D. Wegner, J. Li, K. Hartinger, V. Brasch, T. Herr, D. Hillerkuss, R. Schmogrow, T. Schimmel, R. Holzwarth, T. J. Kippenberg, J. Leuthold, W. Freude, C. Koos, "Microresonator-Based Frequency Comb Generator as Optical Source for Coherent WDM Transmission", in Proc. OFC/NFOEC, Anaheim, CA, USA, paper OW3C.2, Mar. 2013.

[47] B. P.-P. Kuo, E. Myslivets, V. Ataie, E. G. Temprana, N. Alic, S. Radic, "Wideband Parametric Frequency Comb as Coherent Optical Carrier", Journal of Lightwave Technology, vol. 31, no. 21, pp. 3414-3419, Nov. 2013.

[48] E. Temprana, V. Ataie, B. P.-P. Kuo, E. Myslivets, N. Alic, S. Radic, "Low-noise parametric frequency comb for continuous C-plus-L-band 16-QAM channels generation", Optics Express, vol. 22, no. 6, pp. 6822-6828, Mar. 2014.

Chapter 3

3 Performance Characterisation of Optical Multicarrier Sources for IM/DD OFDM systems

Further to the discussions in the previous chapter, where several types of optical multicarrier sources have been presented and compared, the three optical comb sources have been selected, characterised and implemented in the intensity modulated and directly detected OFDM system. The semiconductor MLL, electro-optical modulation based comb source and externally injected GSCS have been characterised in terms of RIN and OCNR which have been recognised as limiting parameters for the performance of back-to-back intensity modulated and directly detected OFDM systems. The influence of RIN and OCNR on the system performance has been investigated experimentally and by simulations.

3.1 Introduction

The significant growth of traffic in long–haul, metropolitan and access networks translates to the on–going increase in demand for bandwidth. WDM technology has been successfully used to increase the aggregate capacity of optical transmission systems, and thereby meet increasing bandwidth demands. The effective use of available bandwidth is further increased by using advanced modulation formats and modulation techniques such as OFDM and Nyquist WDM.

OFDM has been proposed for optical transmission systems due to its advantages in overcoming transmission impairments such as chromatic and polarisation mode dispersion, and also due to its high spectral efficiency [1, 2]. Based on the structure of the optical receiver, the OFDM system can be categorised either as a direct–detected (DD) or a coherent receiver based system [1, 2]. Compared to DD systems, coherent OFDM has better sensitivity and spectral efficiency, but the complexity of coherent

receivers increases the cost of the system which limits their usage in access and metropolitan networks. An attractive alternative are low cost OFDM systems, which employ intensity modulation and direct detection. The use of directly detected WDM OFDM systems, for both access [3-7] and metropolitan networks [7, 8], has been extensively investigated in recent years. Several methods can be used for the generation of IM/DD OFDM signals, which can be double side-band (DSB) or single side-band [1]. DSB OFDM [1, 5] suffers from chromatic dispersion induced power fading [1, 5, 9] and occupies larger bandwidth when used in a WDM scenario. SSB OFDM signals can have a spectral gap between the optical carrier and sideband providing sufficient frequency separation for unwanted photodetection products [10], or have no spectral gap to provide very efficient usage of available bandwidth [1, 11-13]. The gapless (gap of a few hundred MHz) SSB OFDM [11-13] is used in the experiments and simulations presented in this thesis.

Compared to coherently detected optical WDM OFDM systems which often employ various multicarrier optical sources [14, 15], WDM OFDM systems based on intensity modulation and direct detection usually incorporate laser arrays at the transmitter side [4]. The characterisation of the RIN and the OCNR of the multicarrier source used in DD OFDM systems is of significant importance. The high carrier-to-signal ratio (CSR), which is a property of gapless intensity modulated OFDM signals [12], is determined by the peak-to-average power ratio (PAPR) of the OFDM signal [11]. The linear operation of an intensity modulator can be assured with a small modulation index of the input signal, which will cause the signal sidebands to have much lower power than that of the carrier. Hence, such systems will be vulnerable to optical noise [13], and therefore be sensitive to the RIN and the OCNR of the multicarrier source used. In addition, a baseband OFDM signal in an IM/DD system is usually up-converted to a desired RF frequency prior to modulation onto an optical carrier [10-13], resulting in essentially an analog modulation of the optical carrier [16], thereby making the system more sensitive to intensity noise. The influence of the RIN in a single channel directly detected OFDM system with a frequency gap between optical carrier and sideband was investigated in [17].

3.2 Experimental Setup

The experimental setup used for the WDM-SSB-OFDM system is shown in Figure 3.1. The optical multi-tone source at the transmitter consists of an optical frequency comb source, a tunable optical filter to select the desired number of comb lines i.e.

channels and an EDFA. A detailed description of the optical frequency comb sources employed in this work are given in the subsection 3.2.1.

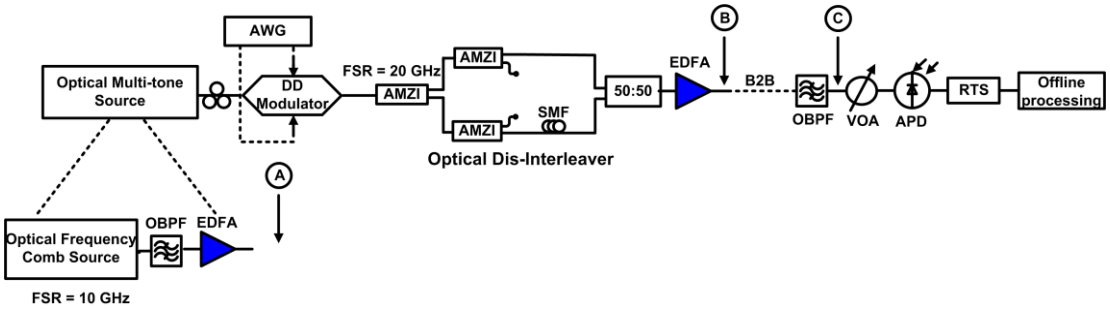

Figure 3.1. Schematic of the experimental and simulation setup; Optical Band-Pass Filter (OBPF); Polarisation Controller (PC); Arbitrary Waveform Generator (AWG); Asymmetric Mach-Zehnder Interferometer (AMZI); Erbium Doped Fibre Amplifier (EDFA); Variable Optical Attenuator (VOA); Avalanche Photodetector (APD); Real Time Scope (RTS).

The spectral output from the optical multi-tone source consists of 8-10 tones (based on the multicarrier source used) spaced by 10 GHz, which exhibit spectral ripple of 3 dB. In field installations, the generated comb lines would be separated by a de-multiplexer and each individual channel would be modulated independently. Due to the lack of an appropriate de-multiplexer with a FSR of 20 GHz, in this experiment all the comb tones are modulated by a single dual-drive Mach-Zehnder modulator (DD-MZM). The DD-MZM is biased at the quadrature point and then modulated with a SSB OFDM signal waveform [18] derived from an arbitrary waveform generator operating at 10 GSa/s. The analytical derivation of the implemented SSB OFDM signal waveform is given bellow. In this case, the electrical OFDM signal is applied on the amplitude of the optical filed, as first proposed by Schuster *et al.* [11].

A real signal *x(t)* can be extended by its Hilbert transform in order to generate so-called analytic signal:

$$s(t) = x(t) + jH\left[x(t)\right] \tag{3.1}$$

where H denotes the Hilbert transform [18, 19]. It is known from telecommunication theory that analytic signal can be used for generation of SSB signal [19-22]. The amplitude of a generated SSB signal should contains only the information part of the signal and the phase should be used only to remove one of the sidebands of the signal in order to enable detection using square law detectors [19]. The procedure to generate such SSB signal is shown below.

In this case, *x(t)* is the OFDM signal, $x_{OFDM}(t)$. Therefore, the electrical field of the optical SSB signal has a form:

$$E(t) = A(t)e^{j\Phi(t)} = e^{x(t)}e^{jH[x(t)]} = e^{x(t)+jH[x(t)]}. \quad (3.2)$$

where $A(t) = e^{x(t)}$ and $\Phi(t) = H(x(t))$. As the direct detection is used, the data is recovered from the amplitude term. This means that a natural logarithm must be applied digitally after detection to retrieve the OFDM signal. This leads to the higher PAPR due to the exponential term and can contribute to increased quantisation noise of the received signal at the ADC [18]. Therefore, in order to avoid additional signal processing at the receiver, by choosing the signal at the transmitter to be $x=\ln(x_{OFDM}(t))$, the OFDM signal itself can be retrieved using direct detection, i.e. amplitude term becomes $A(t) = e^{\ln(x(t))} = x(t)$.

The SSB modulation with a DD-MZM is achieved when signal waveforms used to drive the DD-MZM are tailored to provide the necessary phase changes on the modulator arms. The transfer function of a DD-MZM given by Eq. 1.11 can be rewritten as [23]:

$$E(t) = E_{in}(t)e^{j\phi_0(t)}\sin(\Delta\phi(t)), \quad (3.3)$$

where $\phi_0(t) = (\phi_1(t) + \phi_2(t))/2$ and $\Delta\phi(t) = (\phi_1(t) - \phi_2(t))/2$, and $\phi_1(t)$ and $\phi_2(t)$ are the phases on the two arms. Under small signal approximation, Eq. 3.3 can be rewritten as:

$$E(t) = E_{in}(t)e^{j\phi_0(t)}\Delta\phi(t). \quad (3.4)$$

In order to satisfy the SSB condition, Eq. 3.4 should represent Eq. 3.2, that is:

$$A(t)e^{j\Phi(t)} = e^{j\phi_0(t)}\Delta\phi(t) \quad (3.5)$$

Therefore, $A(t) = \Delta\phi(t)$ and $e^{j\phi_0(t)} = e^{j\Phi(t)}$. From the last expressions, after substitutions for $A(t)$ and $\Phi(t)$, we have SSB enabling signal waveforms used to drive two DD-MZM arms:

$$\phi_1(t) = e^{x_{OFDM}(t)} + H[x_{OFDM}(t)], \qquad \phi_2(t) = H[x_{OFDM}(t)] - e^{x_{OFDM}(t)}. \quad (3.6)$$

The 12.5 Gb/s SSB OFDM signal is composed of 80 subcarriers with 16-QAM modulation format on each subcarrier, and an OFDM symbol rate of 39.06 MHz. The incorporation of the 7% FEC overhead together with a cyclic prefix length of 6.25% of the IFFT size (which has 256 inputs) gives a net data rate of 11.2 Gb/s. The total bandwidth of the signal is about 3 GHz. Clipping was used, which reduced the PAPR of the signal from 14 dB to 12 dB.

The use of gapless Hilbert transform based SSB-OFDM was motivated by the fact that high spectral efficiency can be achieved using this approach. Although Hermitian based OFDM signal generation is more cost effective approach, due to the fact that direct modulation of a laser is possible and only one DAC is required, the total data rate is halved compared to the upper case [1, 10]. This is due to the requirements that the half of an IFFT data inputs are complex conjugates of original data in order to enable Hermitian symmetry and real signal generation at the output of an IFFT [1, 10]. Furthermore, a sufficient guard band between an optical carrier and an OFDM signal should be provided. Finally, the generated optical signal is a DSB. If the full utilisation of an IFFT is enabled (i.e. no complex conjugated inputs) then the aggregate data rate is equal to the Hilbert transform based SSB-OFDM. However, a sufficient guard band is required between an optical carrier and an OFDM signal. Furthermore, in order to generate a SSB signal, an optical filtering of one sideband after intensity modulator is required [1, 10]. A SSB-OFDM generation at full data rate can be enabled using optical complex modulator, but sufficient guard band between an OFDM signal and optical carrier is still required [1, 10].

The signal de-correlation is performed by splitting the channels into odd and even sub-channels with tunable cascaded dis-interleavers based on asymmetric Mach-Zehnder interferometers (AMZI), with a FSR of 20 GHz. The even channels are subsequently passed through a de-correlation fibre patchcord, and then passively combined with the odd channels. The combined signals are then optically amplified with an EDFA which operates in constant power mode. At the receiver the desired channel is filtered with a narrow optical band-pass filter (OBPF). In field installations, an appropriate de-multiplexer would be used instead of a single optical filter. The filtered channel is detected by using a 10 GHz receiver that consists of an avalanche photodetector (APD) and an integrated trans-impedance amplifier (TIA). An APD based receiver provides better sensitivity compared to a PIN receiver, which can reduce the number of required optical amplifiers in the system, especially when transmission over optical fibre is performed. The received signal is captured with a

real time oscilloscope operating at 50 GSa/s. Digital processing of the received signal, and bit error rate (BER) calculations as a function of the received optical power, are performed offline using Matlab.

3.2.1 Optical Frequency Comb Sources

The optical multicarrier sources used in this work are shown in Figure 3.2. The optical frequency comb generated with an electro-optic phase modulator is obtained when the modulator is nonlinearly driven with a large-amplitude sinusoidal signal (~$3V_{\pi}$), as depicted in Figure 3.2(a). A phase shifter is used to improve the flatness of the comb. As already stated in Chapter 2, the electro-optic modulation with a larger-amplitude RF signal promotes the generation of higher-order harmonics of the driving signal, conforming to Bessel functions [24]. The optical spectrum of the 10 GHz FSR comb generated by using a phase modulator (EO space, V_{π}=5 V) is shown in Figure 3.2(d). A relatively flat optical comb with 7-8 comb lines within 3 dB flatness, and excellent OCNR (~68 dB) was obtained.

An attractive alternative method for generating an optical frequency comb entails the gain switching of an externally injected DFB laser [25, 26]. Figure 3.2(b) shows the experimental setup of the externally injected GSCS. Gain switching is achieved by driving a slave laser diode (NEL DFB laser, I_{th} ~ 12.5mA) with a large sinusoidal signal (24 dBm) at the desired frequency (10 GHz in this case), in combination with a DC bias current (~$4I_{th}$), while the laser is temperature controlled at 25°C. Additionally, a master laser (Furukawa integrated tunable DFB array) injects light into the slave laser via a polarisation controller and an optical circulator, and thereby transfers its characteristic optical linewidth to the individual modes of the comb [25]. The external light injection also reduces the RIN associated with each of the individual comb tones [27]. A polarisation controller is used to align the polarisation state of the injected light with the optical waveguide of the slave laser. The wavelength of the master laser is tuned to match the slave laser, and the injection power is set to approximately 4 dBm (measured at the output of the polarisation controller). The output of the externally injected gain switched DFB laser is subsequently analysed with the aid of a high resolution bandwidth (20 MHz) optical spectrum analyser, which is shown in Figure 3.2(e). An optical comb with good flatness and higher number of comb tones (10-11

lines within 3 dB flatness), but with lower OCNR (~50dB) compared to the comb generated using the electro-optic modulation based comb, was obtained.

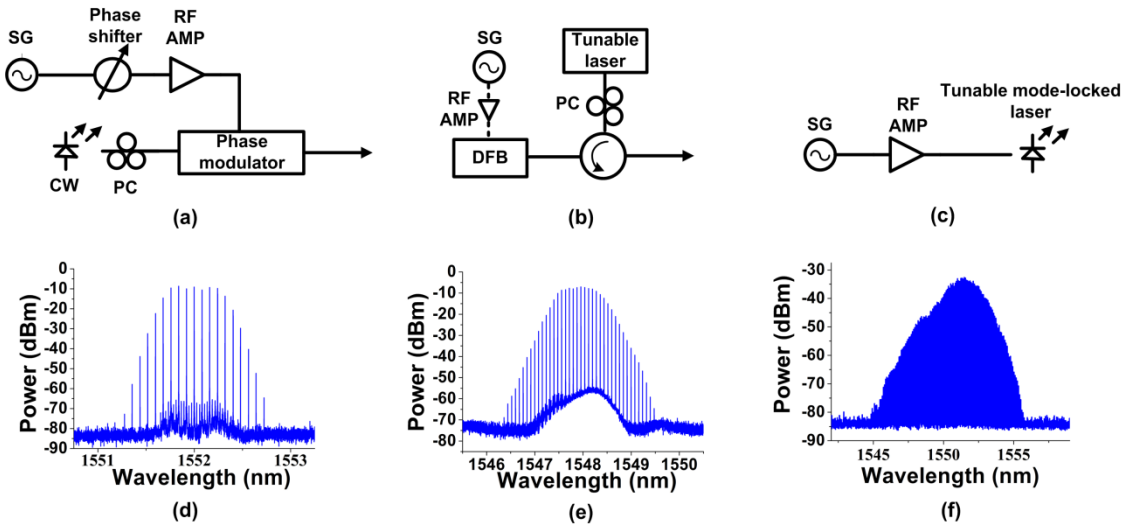

Figure 3.2. (a) Electro-optic modulation based comb source; (b) Externally injected gain switched comb source; (c) Tunable mode-locked laser comb source; (d) Optical spectrum of electro-optic modulation based comb (20 MHz resolution bandwidth (RBW)); (e) Optical spectrum of GSCS (20 MHz RBW); (f) Optical spectrum of MLL (20 MHz RBW); SG: signal generator; CW: continues wave laser; DFB: distributed feedback laser; PC; polarisation controller.

Conventionally, a semiconductor mode-locked laser is a popular candidate for such optical frequency comb generation [28]. A typical setup for optical comb generation by using a hybrid mode-locked laser is depicted in Figure 3.2(c), and it is achieved by applying a large amplified sinusoidal signal (about 23 dBm) at the predetermined frequency (10 GHz in this case) to the mode-locked laser which has a saturable absorber inside the cavity (u^2t semiconductor MLL). The spectrum of the generated optical comb is shown in Figure 3.2(f). Compared to the electro-optical modulation based comb, and externally injected GSCS based comb, a significantly higher number of lines (~25 lines within 3 dB flatness) were generated, with an OCNR of ~50 dB, but with a higher RIN on each comb line, as will be shown in the following section.

3.3 Experimental Results and Discussion

The optical spectra for the three comb sources mentioned above, at different stages, are shown in Figure 3.3. The filtered comb tones from the electro-optical modulation based comb, externally injected GSCS and semiconductor MLL comb source are

shown in Figure 3.3(a)-(c) (measured at point A in Figure 3.1), whilst the signal after modulation (at point B in Figure 3.1) is presented in Figure 3.3(d)-(f). Figure 3.3(g)-(k) depicts one filtered channel at the receiver prior to detection (point C on Figure 3.1).

The generated optical comb sources exhibit different levels of OCNR as can be observed from Figure 3.3(a), (b) and (c). Table 3.1 summarises the OCNRs for different channels of the three different optical comb sources (measured at the output of the optical comb source). The highest OCNR was obtained with the electro-optical modulation based comb, whilst the externally injected GSCS had marginally better OCNR than semiconductor MLL. The RIN of the optical comb sources employed is an important parameter as intensity noise is one of the limiting factors in IM/DD systems, such as SSB OFDM. Hence, RIN measurements of individually filtered comb lines were carried out as shown in Figure 3.4 and described in [29, 30]. The optical output of the device under test is passed through isolator and amplified using an EDFA. The individual lines are filtered and then coupled into high bandwidth photodetector (50 GHz u^2t photodiode). The received optical power during the measurement was ~ 1 dBm. The voltage proportional to the generated photocurrent is measured via bias-tee and used for the estimation of the photodiode shot noise power. The electrical signal is then amplified and characterised with the aid of an electrical spectrum analyser (ESA). It is important to note that the same setup was used for the RIN measurements of single-mode laser diodes.

The average linewidth values of each comb source are shown in Table 3.2. The optical linewidth is not a limiting parameter in short and medium reach directly detected OFDM systems operating at moderate data rates [31]. However, optical sources which have high linewidth usually possess significant RIN, and therefore optical linewidth can be used as an indicator of a RIN level.

	EO modulator comb (dB)	Externally injected GSCS (dB)	Semiconductor MLL (dB)
Ch1	66	53	49.5
Ch4	69	51	50.5
Ch6	67	49	50.5
Ch7/Ch9	67	48.5	52

Table 3.1. Measured OCNR for different channels of the three different optical comb sources.

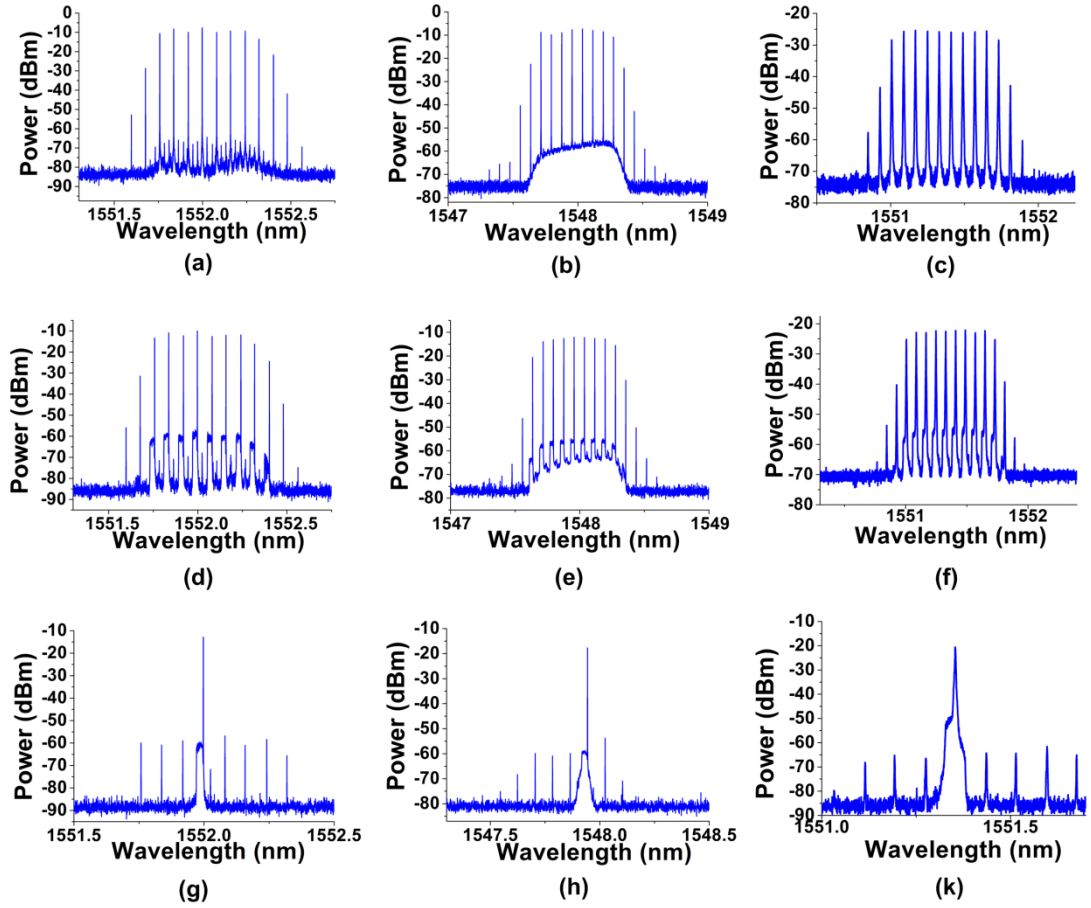

Figure 3.3. Filtered optical spectra of (a) electro-optical modulation based comb source, (b) externally injected GSCS and (c) semiconductor MLL comb source. Optical spectra of the modulated (d) electro-optical modulation based comb source, (e) externally injected GSCS and (f) MLL comb source. Optical spectra of a filtered channel at the receiver prior to detection for (g) electro-optical modulation based comb source, (h) externally injected GSCS and (k) MLL comb source. The resolution bandwidth for the captured optical spectra is 20 MHz.

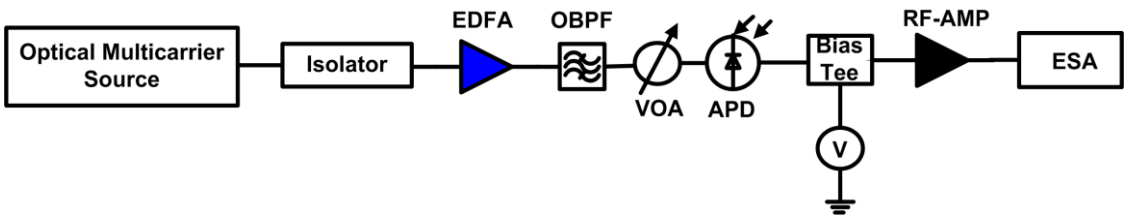

Figure 3.4. Experimental setup used for RIN measurements of optical multicarrier sources.

The achieved results are shown in Figure 3.5, and the averaged RIN (DC – 3.5 GHz) for different channels of the different three comb sources is given in Table 3.2. Electro-optical modulation based comb has the lowest averaged RIN, followed by

externally injected GSCS. The effect of mode partition noise, which is a characteristic of semiconductor mode-locked lasers [32], causes the averaged RIN for individually filtered lines of the semiconductor MLL to have higher values compared to the other two optical comb sources. Each of the four filtered channels has a RIN of ~ – 116 dB/Hz, whilst the averaged RIN (DC – 3.5GHz) for the all channels is ~ – 132 dB/Hz.

	EO modulator comb (dB/Hz)	Externally injected GSCS (dB/Hz)	Semiconductor MLL (dB/Hz)
Ch1	–129	–127	– 116
Ch4	–135	–123	– 116
Ch6	–129	–123	– 116
Ch7/Ch9	–129	–127	– 116
Linewidth	<100 kHz	<100 kHz	>60 MHz

Table 3.2. Measured average RIN (DC - 3.5GHz) for different channels of the three different optical comb sources. Measured average linewidth of each comb source.

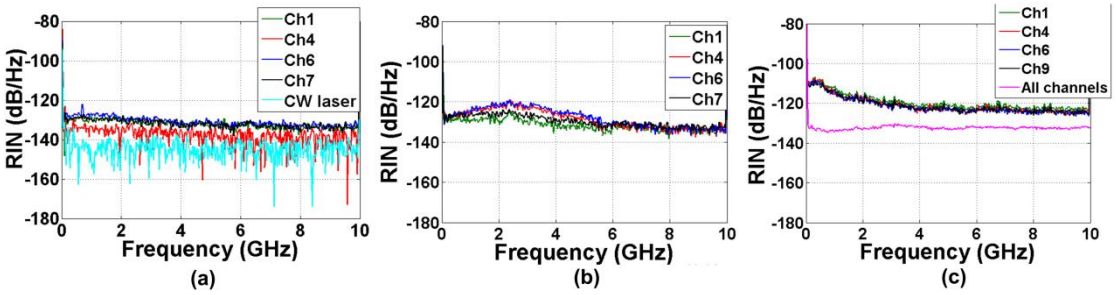

Figure 3.5. Measured RIN versus frequency for (a) electro-optical modulation based comb; (b) externally injected gain switched comb; (c) semiconductor mode locked laser.

The experimentally measured performances of the IM/DD SSB OFDM system, employing all three optical comb sources, are shown in Figure 3.6. The BER was measured by varying the received optical power with the aid of a variable optical attenuator (VOA). Results obtained show that the best performance in the IM/DD SSB OFDM system was achieved by using the electro-optical modulation based comb. This was followed by externally injected GSCS and semiconductor MLL respectively. The difference in performance can be explained by the different values of RIN and OCNRs for the comb sources under investigation. All three combs sources have the same sensitivity at the 7% FEC limit ($4.4 \cdot 10^{-3}$ [33, 34]), as system performance for low levels of received power was dominated by thermal and shot noise at the APD receiver. However, at the higher power levels, system performance was limited by the RIN and OCNR of the employed comb sources. The performance of the CW laser, which has averaged (DC - 3.5GHz) RIN=-141.5 dB/Hz and OCNR=76 dB (measured

at 20 MHz resolution bandwidth), is shown in Figure 3.6(a). The best performance and the lowest error floors, among optical comb sources, were obtained by using the electro-optical modulation based comb (Figure 3.6(a)). Channel 4 (Ch4) of the electro-optical modulation based comb, which has the lowest level of RIN (–135 dB/Hz) and the highest OCNR (69 dB), has better performance compared to the other three channels. Ch6 and Ch7 have slightly better performance than Ch1 as they have a 1 dB higher OCNR, while the average RIN values are the same for all three channels.

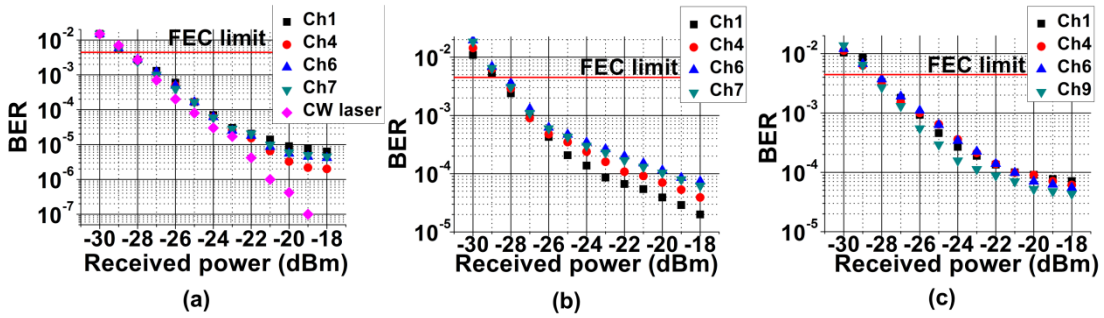

Figure 3.6. BER versus received optical power for (a) electro-optical modulation based comb; (b) externally injected gain switched comb; (c) semiconductor mode locked laser.

The performance of the externally injected GSCS is shown in Figure 3.6(b). The results obtained show that Ch1, which has the highest OCNR (53 dB) and the lowest RIN (~ –127 dB/Hz), has the best performance. Although Ch7 has lower OCNR than Ch6, it has slightly better performance due to the lower RIN. In the case of the semiconductor MLL (Figure 3.6(c)), the measured penalty in performance (at the BER=$7 \cdot 10^{-5}$) between different channels is determined by the difference in OCNR between the channels, as all channels have approximately the same RIN. The best performing channel of the GSCS has a 1 dB higher OCNR than the best performing channel of the semiconductor MLL, but the penalty in performance of the MLL channel (at the BER=$4.5 \cdot 10^{-5}$) was around 3 dB due to the significantly lower RIN of the filtered GSCS carriers compared to the semiconductor MLL filtered carriers.

The characterisation of carrier-to-signal ratio is performed to ensure that system is operating at the optimum point. The optimum CSR for employed gapless SSB-OFDM with PAPR ~12 dB was found to be around 11 dB, as shown in Figure 3.7 which presents BER values for different CSR levels for one filtered channel of semiconductor MLL. The measured optimum CSR level has good matching with the previously reported values [12]. The characterisation of the CSR was performed by changing the bandwidth and central wavelength of the narrow band optical filter used

to select the desired signal prior to photodetection. Therefore, the power of the carrier relative to the power of the signal was modified. IM/DD OFDM systems which incorporate guard band in between signal and carrier (Figure 3.8) to separate carrier-signal (wanted products) and the signal-signal (unwanted products) beating products, have the optimum CSR of ~0 dB, i.e. same power of carrier and signal [35]. However, this condition is changed when the desired carrier-signal beating products overlap with the signal-signal beating products after photodetection, which is the case with gapless OFDM [35]. In this case carrier-signal beating products are larger than signal-signal beating products due to the higher power of carrier compared to the signal, i.e. the high CSR provides that carrier-signal beating products are sufficiently larger than signal-signal beating products enabling gapless detection.

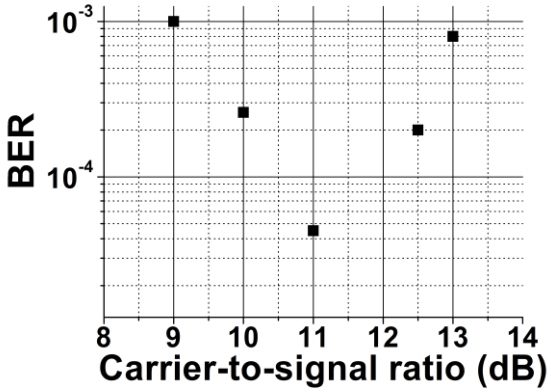

Figure 3.7. BER versus carrier-to-noise ratio for one of the filtered channels of semiconductor MLL.

Further investigation on the influence of the OCNR on the performance of the system was performed by loading white noise at the output of the semiconductor MLL source prior to the modulation (point A in Figure 3.1). Accordingly, the values of the OCNR were varied and the system performance was measured.

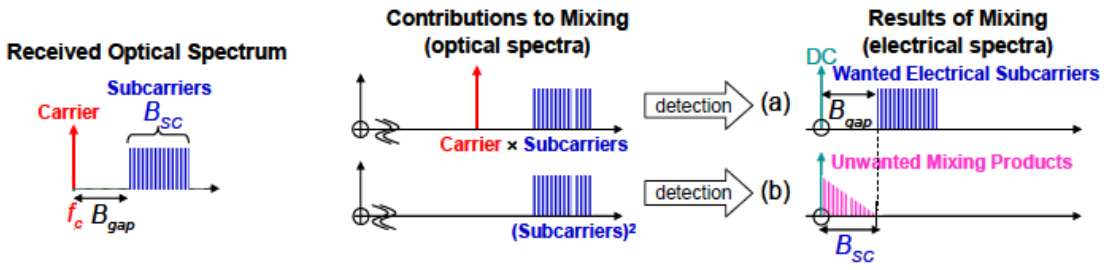

Figure 3.8. Received optical spectrum (left) of IM/DD OFDM, its components (middle) and the results (right) of photodetection in the electrical domain. After [36].

The obtained measurement results are given in Figure 3.9. Figure 3.9(a) shows the performance of one channel filtered from the semiconductor MLL comb for a range of received optical power and different values of OCNR, whilst Figure 3.9(b) shows the measured penalty (at the maximum received power of -18 dBm) for four MLL channels for different values of OCNR, relative to the performance achieved with the maximum OCNR on each channel. Depending on the initial OCNR, the channels exhibit different penalties when OCNR is changed from initial level to OCNR=45 dB. Further changes in OCNR cause approximately the same penalties for all channels.

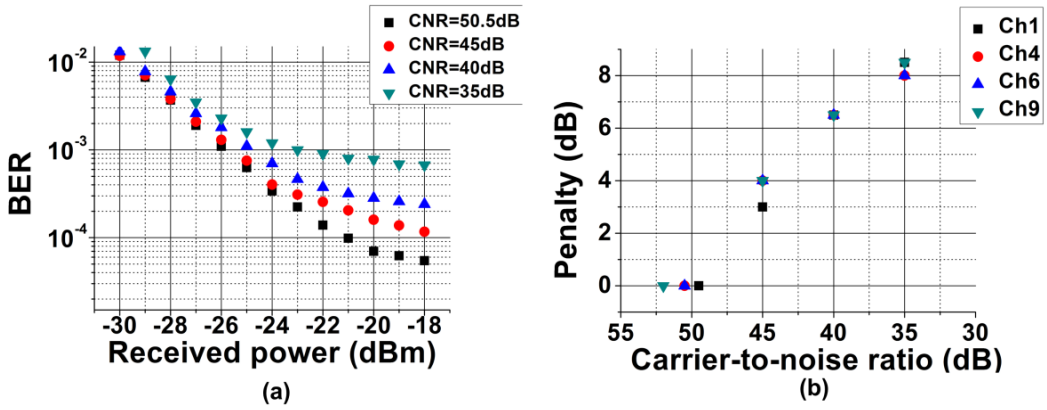

Figure 3.9. (a) Measured BER versus received power for different values of OCNR of semiconductor MLL for Ch 6; (b) Measured penalty (at the maximum received power of -18 dBm) for different values of OCNR relative to the maximum OCNR for each channel.

3.4 Simulations

The influence of RIN on the system performance was further investigated through simulations. The system setup shown in Figure 3.1 was simulated by using co-simulations of Matlab and Virtual Photonics Incorporated Transmission Maker (VPI TM 9.0). The 12.5 Gb/s SSB OFDM signal was generated in Matlab and applied to VPI-TM by using a co-simulation interface. An optical multicarrier signal was generated (as in Figure 3.2(a)), modulated, de-correlated and detected in VPI-TM. After detection the signal was linked and analysed with Matlab. Optical spectra of the generated optical comb and the modulated optical signal (point B in Figure 3.1) are shown in Figure 3.10(a) and (b) respectively, whilst the obtained simulation results are illustrated in Figure 3.10(c). The BER was measured as a function of the received optical power and for different values of RIN of the one filtered channel from the optical multicarrier signal.

By setting the RIN to a specific value, the corresponding OCNR was obtained. The OCNR of the channel under investigation was ~ 51.5 dB for the case when the RIN was -110 dB/Hz, and gradually increased with a reduction in the RIN. For the case when the RIN was -150 dB/Hz, the OCNR was measured to be ~ 53.5 dB. However, the penalty in performance between the case with the lowest and highest RIN was around 7 dB (at the BER=$1 \cdot 10^{-4}$). Comparison of the experimental and simulation system performance results yielded excellent agreement between the two and is depicted in Figure 3.10(d). For instance, comparing the experimental result for Ch1 of the externally injected GSCS, which has a OCNR of 53 dB and a RIN = -127 dB/Hz, with the simulation result for the case when the OCNR ~ 53 dB and RIN = -130 dB/Hz, shows that the performances are very similar (Figure 3.10(d) denoted by a square and a circle respectively)). Also, comparison of Ch9 of the semiconductor MLL experimental result (OCNR=52 dB, RIN= -116 dB/Hz) with the simulation result (OCNR=52 dB, RIN= -115 dB/Hz) also show that there is good agreement (denoted by a triangle and a diamond respectively). A comparison between certain simulation results obtained for the electro-optical modulation based comb source (Figure 3.2(a)) and experimental results for the GSCS and semiconductor MLL is relevant, as the simulation is performed for specified values of the parameters which determine the system performance, such as RIN and OCNR.

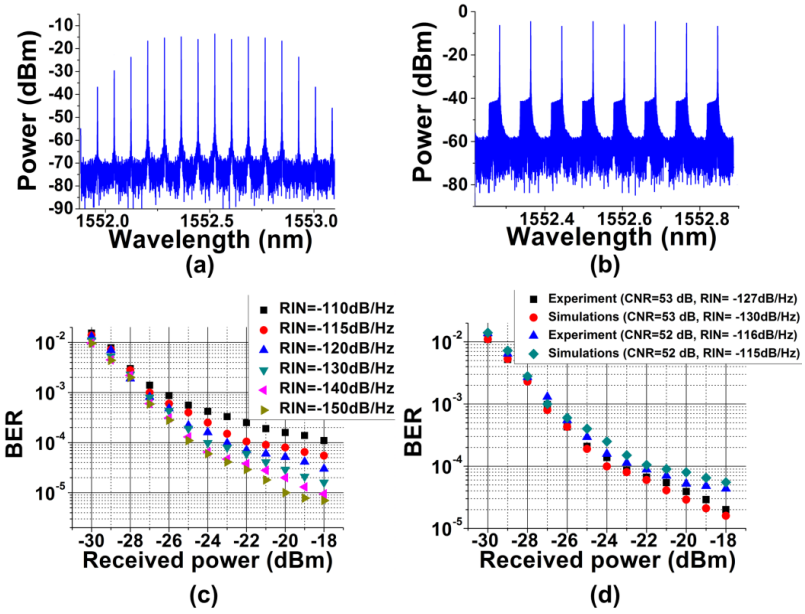

Figure 3.10. Simulation results: (a) Optical spectra of the generated optical comb and (b) modulated optical signal; (c) BER versus received optical power for different values of RIN; (d) Comparison between experimental (black squares (CNR=53 dB, RIN ~-127 dB/Hz); blue triangles (CNR=52 dB, RIN~ -116 dB/Hz)) and simulation results (red circles (CNR=53 dB, RIN~ -130 dB/Hz); green diamonds (CNR=52 dB, RIN~ -115 dB/Hz)).

It can be observed from Figure 3.5 that the RIN has the highest values within the range from DC to 5 GHz. Therefore, if a spectral gap between the carrier and the OFDM signal is provided, such in the case of the offset OFDM [37], reduced penalty caused by the RIN can be expected. However, the occupied spectral bandwidth would be larger, and this could cause problems when filtering out one channel from the WDM signal, as the spectral separation between channels will be reduced.

3.5 Conclusion

Intensity modulated OFDM has recently been considered as a promising candidate for future access/regional networks due to advantages such as overcoming transmission impairments (such as chromatic and polarisation mode dispersion), high spectral efficiency, and relatively low cost. The analog optical systems, such as gapless IM/DD SSB-OFDM, are vulnerable to optical noise. Therefore, such systems are sensitive to relative intensity noise and carrier-to-noise ratio of the optical source used, which significantly impacts the possibility of employing optical multicarrier sources. In this work, the performances of three different multicarrier optical sources in an IM/DD SSB OFDM system are investigated and compared. The RIN and OCNR of the electro-optical modulation based comb, externally injected GSCS and semiconductor MLL have been characterised, and their influence on the performance of IM/DD SSB OFDM system investigated. The results obtained show significant performance dependence of the investigated system on RIN and OCNR levels of the multicarrier optical source employed. Furthermore, through experimentation and simulations we determine the values of RIN and OCNR sufficient for satisfactory system operation, and it is also shown that optical multicarrier sources with low relative intensity noise and high carrier-to-noise ratio levels can assure very good performance of the system.

This work is further expanded in the next chapter, where the MLL source has been employed in an optical access network as an optical multicarrier transmitter. Also, a comparison in performance of SOA and EDFA amplified IM/DD SSB-OFDM systems is presented.

References

[1] W. Shieh and I. Djordjevic, “OFDM for Optical Communications”, Elsevier/Academic Press, Oct. 2009.

[2] J. Armstrong, “OFDM for optical communications”, Journal of Lightwave Technology, vol. 27, no. 3, pp. 189–204, Feb. 2009.

[3] N. Cvijetic, “OFDM for next-generation optical access networks”, Journal of Lightwave Technology. vol. 30, no. 4, pp. 384-398, Jan. 2012.

[4] N. Cvijetic, M. Cvijetic, M-F. Huang, E. Ip, Y-K. Huang, and T. Wang, “Terabit optical access networks based on WDM-OFDMA-PON”, Journal of Lightwave Technology, vol. 30, no. 4, pp. 493-503, Feb. 2012.

[5] C. Browning, K. Shi, S. Latkowski, P. M. Anandarajah, F. Smyth, B. Cardiff, R. Phelan, and L. P. Barry, “Performance improvement of 10Gb/s direct modulation OFDM by optical injection using monolithically integrated discrete mode lasers”, Optics Express, vol.19, no. 26, pp. B289-294, Nov. 2011.

[6] R. P. Giddings, E. Hugues-Salas, X. Q. Jin, J. L. Wei, and J. M. Tang, “Experimental demonstration of real-time optical OFDM transmission at 7.5 Gb/s over 25-km SSMF using a 1-GHz RSOA”, IEEE Photonics Technology Letters, vol. 22, no. 11, Jun 2010.

[7] D. Qian, N. Cvijetic, J. Hu, T. Wang, “Optical OFDM transmission in metro/access networks”, in Proc. OFC/NFOES, San Diego, CA, USA, paper OMV1, Mar. 2009.

[8] E. Giacoumidis, I. Tomkos, and J. M. Tang, “Adaptive modulation-induced reduction in filter concatenation impairment for optical OFDM metro/regional systems”, Journal of Optical Communications and Networking, vol. 3, no. 7, pp. 587-593, Sep. 2011.

[9] G. H. Smith, D. Novak, Z. Ahmed, “Novel technique for generation of optical SSB with carrier using a single MZM to overcome fiber chromatic dispersion”, in Proc. Microwave Photonics, Kyoto, Japan, pp. 5-8, Dec. 1996.

[10] B. J. C. Schmidt, A. J. Lowery, and J. Armstrong, “Experimental demonstrations of electronic dispersion compensation for long-haul transmission using direct-

detection optical OFDM", Journal of Lightwave Technology, vol. 26, no. 1, pp. 196-203, Jan. 2008.

[11] M. Schuster, S, Randel, C. A. Bunge, S. C. J. Lee, F. Breyer, B. Spinnler, K. Petermann, "Spectrally efficient compatible single-sideband modulation for OFDM transmission with direct detection", IEEE Photonics Technology Letters, vol. 20, no. 9, pp. 670-672, May 2008.

[12] Z. Xu, M. O'Sullivan, and R. Hui, "OFDM system implementation using compatible SSB modulation with a dual-electrode MZM", Optics Letters, vol. 35, no. 8, pp. 1221-1223, 2010.

[13] Y. Zhang, M. O'Sullivan, R. Hui, "Theoretical and experimental investigation of compatible SSB modulation for single channel long-distance optical OFDM transmission", Optics Express, vol. 18, no. 16, pp. 16751-16764, Jul 2010.

[14] S. Chandrasekhar, and Xiang Liu, "OFDM based superchannel transmission technology", Journal of Lightwave Technology, vol. 30, no. 24, pp. 3816-3823, Dec. 2012.

[15] W. Shieh, Q. Yang, and Y. Ma, "107 Gb/s coherent optical OFDM transmission over 1000-km SSMF fiber using orthogonal band multiplexing", Optics Express, vol. 16, no. 9, pp. 6378-6386, Apr. 2008.

[16] J. L. Prince, E. I. Ackerman, and C. H. Cox, "Analog Fiber-optic Link Technology", LEOS Summer Topical Meetings, TuB2.1, Jun. 2004.

[17] Z. Zan, M. Premaratne and A. J. Lowery, "Laser RIN and linewidth requirements for direct detection optical OFDM", in Proc. CLEO, San Jose, CA, USA, paper CWN2, May 2008.

[18] C. Browning, K. Shi, A. D. Ellis, L. P. Barry, "Optical burst-switched SSB-OFDM using a fast switching SG-DBR laser", Journal of Optical Communications and Networking, vol. 5, no. 9, pp. 994-1000, Sep. 2013.

[19] R. J. Davies, "Optical Single Sideband for Broadband and Subcarrier Systems", Doctoral Distertation, University of Alberta, Canada, 1999.

[20] H. Voelcker "Toward A Unified Theory Of Modulation - Part 1 : Phase-Envelope Relationships"', Proceedings of the IEEE, vol. 54, no. 3, pp. 340-353, Mar. 1966.

[21] H. Voelcker "Demodulation of single-sideband signals via envelope detection", IEEE Transactions on Communication Technology, vol. COM-14, pp. 22-30, Feb. 1966.

[22] L. R. Kahn, "Compatible Single Sideband", Proceedings of the IRE, pp. 1503-1527, Oct. 1961

[23] R. M. Schmogrow, “Real-time Digital Signal Processing for Software-defined Optical”, KIT Scientific Publishing, 2013.

[24] T. Sakamoto, T. Kawanishi, and M. Izutsu, “Optoelectronic oscillator using a LiNbO3 phase modulator for self-oscillating frequency comb generation”, Optics Letters, vol. 31, no. 6, pp. 811-813, Mar. 2006.

[25] P. M. Anandarajah, R. Maher, Y. Q. Xu, S. Latkowski, J. O’Carroll, S. G. Murdoch R. Phelan, J. O’Gorman, L. P. Barry, “Generation of coherent multicarrier signals by gain switching of discrete mode lasers”, IEEE Photonics Journal, vol. 3, no. 1, pp. 112-122, Jan. 2011.

[26] V. Vujicic, R. Zhou, P. M. Anandarajah, J. O’Carroll, and Liam P. Barry, “Performance of a semi-Nyquist NRZ-DQPSK system employing a flexible gain-switched multi-carrier transmitter”, Journal of Optical Communications and Networking. vol. 6, no. 3, pp.282-290, Feb. 2014.

[27] G. Yabre, H. de Waardt, H. P. A. Van den Boom, and G.-D. Khoe, “Noise characteristics of single-mode semiconductor lasers under external light injection”, IEEE Journal of Quantum Electronics, vol. 36, no. 3, pp. 385–393, Mar. 2000.

[28] Y. Ben M’Sallem, Q. T. Le, L. Bramerie, Q.-T. Nguyen, E. Borgne, P. Besnard, A. Shen, F. Lelarge, S. LaRochelle, L. A. Rusch, and J.-C. Simon, “Quantum-Dash Mode-Locked Laser as a Source for 56-Gb/s DQPSK Modulation in WDM Multicast Applications”, IEEE Photonics Technology Letters, vol. 23, no. 7, pp. 453–455, Mar. 2011.

[29] (2014, Aug.). Relative Intensity Noise of Distributed Feedback Lasers [Online], Available: http://www.eagleyard.com

[30] P. M. Anandarajah,, S. Latkowski, C. Browning, R. Zhou, J. O’Carroll, R. Phelan, B. Kelly, J. O’Gorman, L. P. Barry, “Integrated two-section discrete mode laser”, IEEE Photonics Journal, vol. 4, no. 6, pp. 2085-2094, Nov. 2012.

[31] W.-R. Peng, “Analysis of Laser Phase Noise Effect in Direct-Detection Optical OFDM Transmission”, Journal of Lightwave Technology, vol. 28, no. 17, pp. 2526-2536, Sep. 2010.

[32] F. X. Kartner, U. Morgner, T. Schibli, R. Ell, H. A. Haus, J. G. Fujimoto, E. P. Ippen, “Few-cycle pulses directly from a laser”, Topics in Applied Physics, 95, 73-136, 2004.

[33] (2014, Apr.). 100G CI-BCH-3™ eFEC Encoder/Decoder Core and Design Package [Online]. Available: http://www.vitesse.com

[34] I. B. Djordjevic, M. Arabaci, L. L. Minkov, “Next Generation FEC for High-Capacity Communication in Optical Transport Networks”, Journal of Lightwave Technology, vol. 27, no. 16, pp. 3518-3530, Aug. 2009.

[35] W-R. Peng, B. Zhang, K-M. Feng, X. Wu, A. E. Willner, S. Chi, “Spectrally efficient direct-detected OFDM transmission incorporating a tunable frequency gap and an iterative detection techniques”, Journal of Lightwave Technology, vol. 27, no. 24, pp. 5723-5735, Dec. 2009.

[36] A. J. Lowery, “Improving Sensitivity and Spectral Efficiency in Direct-Detection Optical OFDM Systems“, in Proc. OFC/NFOEC, San Diego, CA, USA, paper OMM4, Feb. 2008.

[37] A. J. Lowery and J. Armstrong, “Orthogonal-frequency-division multiplexing for dispersion compensation of long-haul optical systems”, Optics Express, vol. 14, no. 6, pp. 2079-2084, Mar. 2006.

Chapter 4

4 Optical Multicarrier based IM/DD DWDM-SSB-OFDM Access Networks with SOAs for Power Budget Extension

Multicarrier optical sources offer a number of advantages over laser arrays such as constant frequency separation between optical carriers, tuneable FSR and central wavelength (not provided by all comb sources) and the possibility to reduce component count and power consumption at the optical transmitters. However, the critical parameter of optical multicarrier sources is power per line. Therefore, an amplification of optical multicarrier signals is required at the transmitter side to enable sufficient power per line. The amplification of optical multicarrier signals is typically performed by EDFAs. However, the use of SOAs in such systems can be an attractive alternative primarily due to the possibilities for significant cost, power consumption and footprint reduction via integration.

In this chapter, an experimental demonstration of the use of SOAs in spectrally-efficient, intensity modulated and directly detected DWDM-SSB-OFDM passive optical network, for the simultaneous amplification of optical multicarrier OFDM signals using a single SOA is presented. Furthermore, the system performance is compared to a scenario when an EDFA is used instead of a SOA as an optical power budget extender. The performance comparison with an EDFA shows that a ~4 dB penalty is incurred when the SOA is used, at the maximum received power though there is negligible extra penalty when operating at the FEC limit.

4.1 Introduction

Although OFDM modulation has been used in commercially available solutions for wireless (WiFi, WiMax) [1] and wired (DSL) [2] communications for more than a decade, it became part of research in optical communications around 2006 [2-5].

However, OFDM gained significant interest amongst the research community and in a few years a number of proposals and field trials proved that OFDM can be considered as an attractive solution in optical access networks [6-10]. Operator demands for increased data rate per user and simple upgradability has further accelerated research on the deployment of OFDM systems for passive optical networks. As previously mentioned in Chapter 1, PONs consist of optical line terminal (OLT) (i.e. central office), remote node and optical network units connected by optical fibre. The traffic in direction from OLT towards ONUs is denoted as downstream (DS), whilst the traffic in the opposite direction (from ONUs towards OLT) is known as upstream (US) traffic. Various solutions incorporating OFDM for both DS and/or US signals have been proposed based on the user requirements, such as using a single OFDM subcarrier per user to assigning a specific wavelength to each user [6]. Figure 4.1 illustrates a single wavelength optical access OFDM PON architecture which uses OFDM subcarriers for delivery of arbitrary signals, and therefore enables heterogeneous service [6].

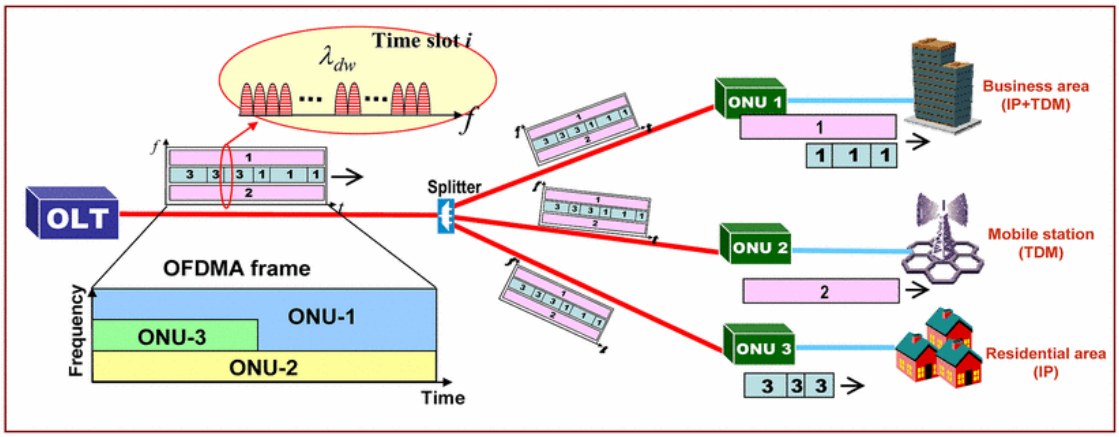

Figure 4.1. Single-wavelength optical OFDMA-PON architecture for delivery of arbitrary signals. After [6]

Additionally, reduction of the development cost of access networks is an important factor, and it has been shown that an increase in the optical budget dedicated to the splitting ratio and/or the reach, would enable the evolution of future access and metropolitan networks with an optimum number of central offices for any aggregated access traffic [11]. In recent works, optical amplification based on EDFAs and/or SOAs has been reported as a solution to increase the optical budget of optical access networks [12]. EDFAs are predominantly used in WDM-PONs for the simultaneous amplification of multiple OFDM signals. However, the use of SOAs in such systems can be an attractive alternative primarily due to the possibilities for significant cost

and footprint reduction via integration. Due, in part, to the high PAPR of OFDM signals, transmission performance can be degraded by the nonlinear properties of SOAs [13]. Hence, a detailed characterisation of an SOA and its impact on system performance is paramount. Recent experimental works on employment of SOAs in both directly and coherently detected OFDM systems have been limited to single channel systems [12, 13]. However, a numerical study on the employment of SOAs for simultaneous amplification of multiple OFDM channels was recently proposed [14], where an optical multicarrier signal was generated by using a bank of lasers at the transmitter. The simulation results indicated that DS transmission of OFDM signals with QPSK modulation format on each subcarrier, and power budget for a 64 split was feasible, but with significant penalty in performance compared to the case when an EDFA is used [14].

In this chapter, an experimental demonstration of the use of SOAs in spectrally efficient intensity modulated and directly detected DWDM-SSB-OFDM-PONs for the simultaneous amplification of multiple OFDM channels using a single SOA, is presented. The characterisation of the SOA used and full system performance analysis is presented. The DS signal consists of 10×12.5 Gb/s SSB-OFDM, with 16 QAM format on each OFDM subcarrier, whilst the US consists of 10×2.5 Gb/s NRZ-OOK signals. The attained power budget enables a 128 split per wavelength after the remote node and the potential to transmit over 100 km of standard single mode fibre. Furthermore, the system performance is compared to a scenario when an EDFA is used instead of a SOA as an optical power budget extender. The aspect of spectral efficiency is considered, as the DS signal is SSB-OFDM, and additionally, the US signals are interleaved in-between DS signals.

4.2 Experimental Setup

The schematic of the proposed architecture is shown in Figure 4.2. The downstream part of the central office consists of an optical multi-tone source, which consists of an optical frequency comb source, a tunable optical filter (to filter enough optical carriers for the desired number of channels) and an EDFA to overcome the loss of the filter. The OFCS is based on a mode-locked laser whose spectral output consists of about 40 tones spaced by 10 GHz, which exhibit a spectral flatness of 10 dB. The spectral output of the optical multi-tone source consists of 10 tones spaced by 10 GHz with a

spectral flatness of 3 dB. In field installations, the generated comb lines would be separated by an arrayed waveguide grating and each individual channel would be modulated independently, as shown in Figure 4.2. However, due to the unavailability of densely spaced AWGs, in this experiment all 10 comb tones are modulated by a single dual-drive Mach-Zehnder modulator. The DD-MZM is biased at the quadrature point and then modulated with a SSB OFDM signal waveform derived from an arbitrary waveform generator. The detailed analytical derivation of the SSB OFDM signal waveform is presented in the previous chapter, Section 3.2. The 12.5 Gb/s SSB OFDM signal is composed of 80 subcarriers with 16-QAM modulation format imposed on each subcarrier at an OFDM symbol rate of 39.06 MHz. The total bandwidth of the OFDM signal is about 3 GHz. Signal decorrelation is performed by splitting channels into odd and even sub-channels with the aid of asymmetric Mach Zehnder interferometers, with a FSR of 20 GHz. The 5 even channels are subsequently passed through a de-correlation fibre patchcord, and then passively re-combined with the 5 odd channels. The decorrelated DS channels are then optically amplified with an EDFA (~10 dBm average optical power), prior to being launched into a 50 km reel of SSMF.

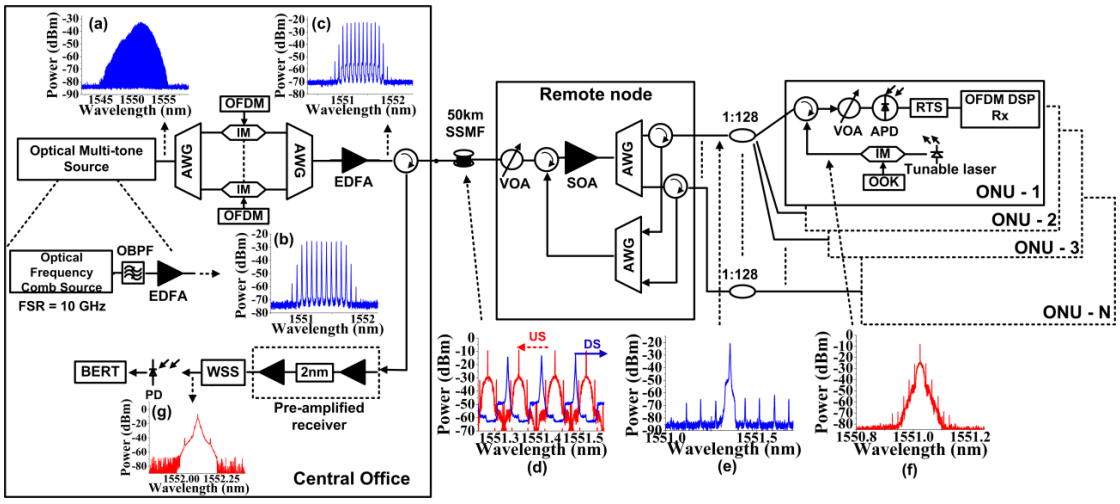

Figure 4.2. Schematic of the proposed WDM-SSB-OFDM-PON system with an optical multicarrier transmitter and a SOA amplification at the remote node. IM - intensity modulator; AWG - arrayed waveguide grating; OBPF - optical band-pass filter; VOA – variable optical attenuator; APD - avalanche photodetector; OOK – On-off Keying; BERT - bit error rate tester.

At the remote node the DS signal is first amplified by the SOA (Kamelian), and then the desired channel is filtered with a narrow optical band-pass filter. In a practical scenario (Figure 4.2), an appropriate AWG would be used to send the required channel to a specific ONU, instead of tunable optical filters. Depending on system

requirements, a single wavelength can be dedicated per user, or further divided among users [6]. The filtered channel is detected within the optical network unit using a 10 GHz receiver that consists of an avalanche photodetector and an integrated trans-impedance amplifier. The received signal is captured with a real time oscilloscope operating at 50 GSa/s. Digital processing of the received signal and BER calculations are performed offline using Matlab.

For the US signal, a 2.5 Gb/s NRZ-OOK signal is generated within each ONU by modulating a tunable laser output with an intensity modulator driven by a 2^{15}-1 pseudo-random binary sequence (PRBS) from the pulse pattern generator (PPG). In field installations, US signals would be combined at the remote node by an AWG and launched back towards the CO. A TDM protocol may be implemented to handle the US data from all the users at the same wavelength [15]. The US signal is separated from the DS signal at the CO with the aid of an optical circulator and then amplified by a two stage optical pre-amplifier. The desired channel is filtered by a wavelength selective switch and detected by using a 10 GHz PIN receiver with an integrated TIA. The performance of the DS and US channels are evaluated by measuring the BER as a function of received optical power.

4.3 Results and Discussion

The SOA used was initially characterised in terms of system performance as a function of bias current and input optical power, as shown in Figure 4.3. For the fixed input optical power of -15 dBm, the results obtained show slight dependence of the system performance on bias current (see Figure 4.3(a)). The best performance was obtained for bias currents higher than 200 mA, due to the better OCNR (more power in the signal) due to the larger SOA gain for higher bias currents. Investigation on dependence of the system performance on input optical power show that the best performance was obtained for the input optical power of -15 dBm, at a bias current of 240 mA, for the SSB-OFDM signal with PAPR ~ 12 dB. Furthermore, the bias current of 240 mA provides the highest output optical power ~10 dBm, and therefore the biggest power budget. The system performance was limited by SOA nonlinearities for higher input optical powers and by amplified spontaneous emission noise for lower input powers [13] (see Figure 4.3(b)). It is important to emphasise that the optimum value for input optical power was selected after detailed investigation of the influence

of input optical power and bias current on the system performance (two parameters that simultaneously determine the system performance).

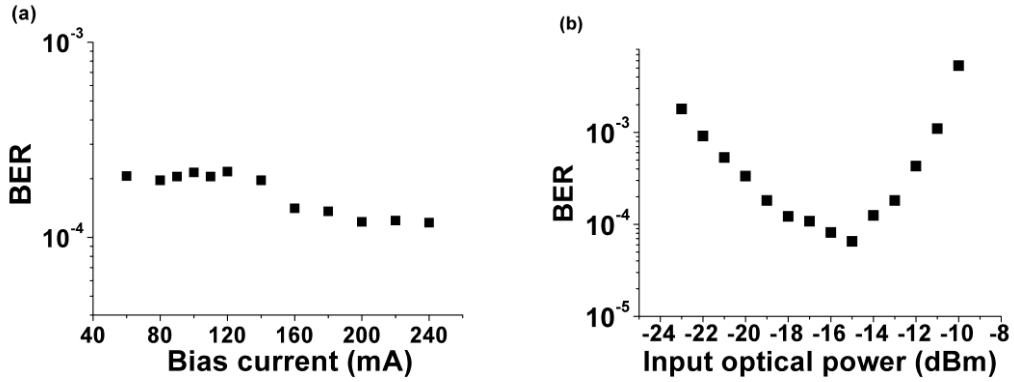

Figure 4.3. SOA characterization as a function of (a) bias current for fixed input optical power of -15 dBm and (b) input optical power for fixed bias current of 240 mA.

The performance of the DS signal in B2B case and after 50 km of SSMF and SOA amplification at the RN is shown in Figure 4.4. The penalty after transmission over 50 km SSMF compared to the B2B case is less than 1 dB power penalty at a 7% FEC limit (BER=$4.4 \cdot 10^{-3}$), for all channels. Evidently, effects of transmission impairments on the proposed system are very low. This is partially due to the fact that dispersive fading is negligible for SSB OFDM signals. Furthermore, the optical launch power (12 dBm) into the fibre is controlled in order to avoid significant non-linear distortions. Slight differences in performance between DS channels can be associated to the difference in the OCNR of the optical multicarrier source lines. As shown in the previous chapter, all MLL optical carriers exhibit very similar RIN. Optical spectra of the DS signal at different stages are shown as insets in Figure 4.2. Insets in Figure 4.4 show the obtained constellation diagrams for one of the DS channels in B2B and after 50 km transmission scenarios. The obtained power budget (between the AWG at the RN and a VOA at the ONU) dedicated for splitting and “last mile” transmission was 26 dB, enabling a 128 split per wavelength at the FEC limit (Figure 4.4(b)). As the optimum input power into the SOA was -15 dBm, the launched optical power into the fibre (10 dBm) would suffice to extend the transmission reach up to 100 km, as dispersion will not degrade performance. The DS transmission over ~90 km of SSMF without in-line amplification was successfully demonstrated as well [16], as shown in Figure 4.5. Note that the obtained performance after 90 km of SSMF is measured at the received power of -28 dBm [16].

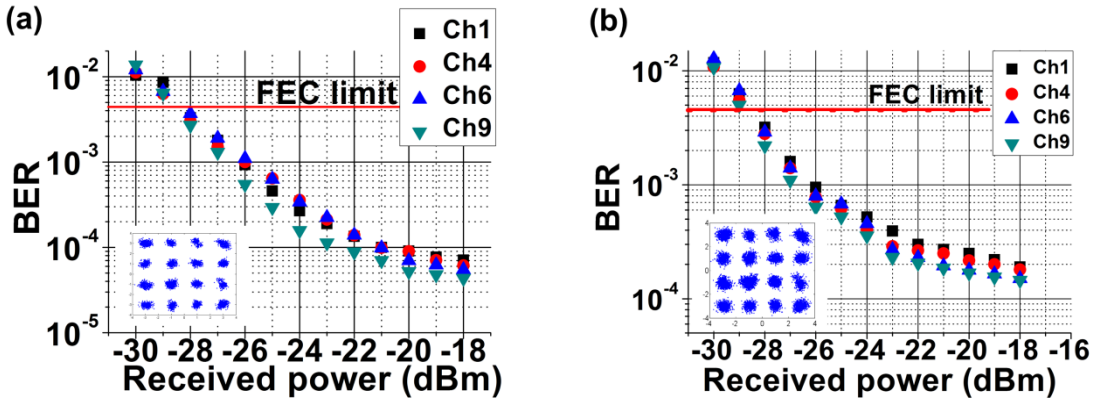

Figure 4.4. Measured bit error rate for (a) back-to-back and (b) after 50 km transmission.

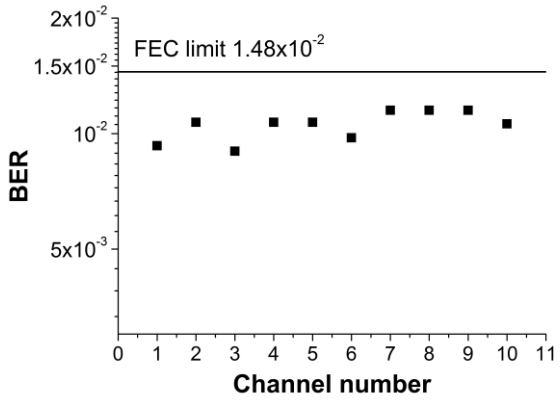

Figure 4.5. Measured bit error rate for all 10 channels after 87 km transmission.

The performance of the selected US channels are given in Figure 4.6. All US channels have similar performance. Inset in Figure 4.6 show the obtained eye diagram of the received US signal. Good sensitivity for the US signal is enabled by optically pre-amplified receiver. Also, for the data rate of 2.5 Gb/s, dispersion is not a limiting factor which allows transmission over 100 km of SSMF without CD compensation. Furthermore, the launched power of the US signal was around -2.5 dBm per channel which was not sufficient to excite non-linear effects in the fibre. Optical spectra of US signal at different stages are shown as insets in Figure 4.2.

The spectral efficiency of the system is also optimised, as the US data is placed in the spectral gap between DS channels which can be seen on the inset (d) in Figure 4.2. Even though the frequency separation between DS and US signals is very low and the signals almost “overlap”, the effect of back scattering is negligible. The measured penalty in performance of selected channels is less than 0.5 dB at the FEC limit, relative to the case when the DS signal is not transmitted.

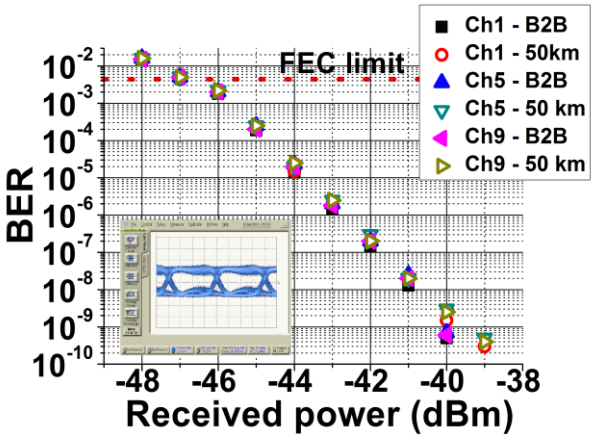

Figure 4.6. BER versus received optical power for upstream 2.5 Gb/s NRZ OOK channels.

Figure 4.7 shows the performance comparison of the EDFA and the SOA in the DWDM-SSB-OFDM-PON system, in a B2B scenario, when they are used at the RN. Results obtained show a ~4 dB improvement in performance when the EDFA is used instead of the SOA, at the maximum received power. The noise figure of EDFA was ~ 4.5 dB, whilst the noise figure of the SOA was ~ 6 dB. The additional penalty in performance is due to the higher nonlinear interactions in a SOA compared to an EDFA. Also, the EDFA used enables a 6 dB increase in the power budget as the maximum output power was 16 dBm, compared to 10 dBm in the case of SOA. However, at the 7% FEC limit, the penalty in performance when using the SOA is negligible. Even though the EDFA provides better system performance and a higher power budget, the SOA reduces the complexity and cost of the overall system, with the potential for integration. The results obtained show the possibility to use an SOA as a power budget extender at the RN and/or booster amplifier at the CO.

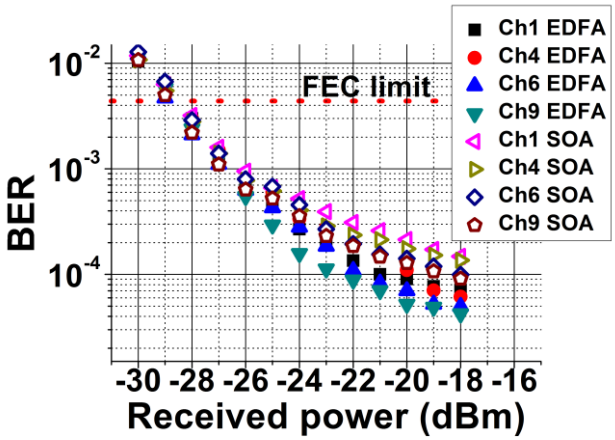

Figure 4.7. BER versus received optical power B2B performance comparison between the EDFA and SOA.

4.4 Conclusion

The use of a single SOA for simultaneous amplification of optical multicarrier OFDM signals in a DWDM PON was proposed with experimental demonstration of 10×12.5 Gb/s SSB-OFDM DS signals and 10×2.5 Gb/s NRZ-OOK US signals. Furthermore, the performance comparison with an EDFA shows that a ~4 dB penalty is incurred when the SOA is used, at the maximum received power though there is negligible extra penalty when operating at the 7% FEC limit. However, as a simple and cost effective solution, with the potential for integration, the use of an SOA as a power budget extender at the RN and/or booster amplifier at the CO in IM/DD WDM-SSB-OFDM-PONs is an attractive solution. Additionally, the proposed system, incorporating an SOA at the RN, enables a 128 passive split. The spectrally efficiency of the system is also optimised, and the effect of back scattering is avoided, as the US data is placed in the spectral gap between DS channels.

The use of semiconductor MLLs (Quantum Dash lasers) and IM/DD SSB-OFDM modulation scheme for data centre interconnects is covered in the next chapter. High capacity interconnects (400 Gb/s, 1 Tb/s, 2 Tb/s and 4 Tb/s) have been enabled by using certain Q-Dash MLLs. The results presented in Chapter 3 on the influence of RIN on the performance of IM/DD SSB-OFDM systems have been confirmed in the next chapter after detailed investigation on the influence of RIN on OFDM subcarriers.

References

[1] R. Prasad, “OFDM for Wireless Communications Systems”, Electronic books, Artech House, Jan, 2004.

[2] W. Shieh and I. Djordjevic, “OFDM for Optical Communications”, Elsevier/Academic Press, Oct. 2009.

[3] I. B. Djordjevic, B. Vasic, “Orthogonal frequency division multiplexing for high-speed optical transmission”, Optics Express, vol. 14, no. 9, pp. 3767-3775, May 2006.

[4] W Shieh, C Athaudage, “Coherent optical orthogonal frequency division multiplexing”, Electronics Letters, vol. 42, no. 10, pp. 587-589, May 2006

[5] A. Lowery, J. Armstrong, “Orthogonal-frequency-division multiplexing for dispersion compensation of long-haul optical systems”, Optics Express, vol. 14, no.6, pp. 2079-2084, Mar. 2006.

[6] N. Cvijetic, “OFDM for next-generation optical access networks,” Journal of Lightwave Technology, vol. 30, no. 4, pp. 384-398, Feb. 2012.

[7] N. Cvijetic, M. Cvijetic, M-F. Huang, E. Ip, Y-K. Huang, T. Wang, “Terabit Optical Access Networks Based on WDM-OFDMA-PON”, Journal of Lightwave Technology, vol. 30, no. 4, pp. 493-503, Feb. 2012.

[8] R. Giddings, „Real-time Digital Signal Processing for Optical OFDM-Based Future Optical Access Networks“, Journal of Lightwave Technology, vol. 32, no. 4, pp. 553-570, Feb. 15, 2014.

[9] Y. Luo, X. Zhou, F. Effenberger, X. Yan, G. Peng, Y. Qian, Y. Ma, “Time- and wavelength-division multiplexed passive optical network (TWDM-PON) for next-generation PON stage 2 (NG-PON2)”, Journal of Lightwave Technology, vol. 31, no. 4, pp. 587–593, Feb. 2013.

[10] C. Ruprecht, Y. Chen, D. Fritzsche, J. von Hoyningen-Huene, N. Hanik, E. Weis, D. Breuer, W. Rosenkranz, “37.5 km Urban Field Trial of OFDMA-PON Using Colorless ONUs With Dynamic Bandwidth Allocation and TCM”, Journal of Optical Communications and Networking, vol. 7, no. 1, pp. A153-A161, Jan. 2015.

[11] P. Chanclou, J.-P. Lanquetin, S. Durel, F. Saliou, B. Landousies, N. Genay, Z. Belfqih, “Investigation into optical technologies for access evolution”, in Proc. OFC/NFOEC, San Diego, CA, USA, paper. OWH1, Mar. 2009.

[12] F. Saliou, P. Chanclou, B. Charbonnier, T. N. Duong, N. Genay, A. Gharba, J. Le Masson, C. Milion, M. Ouzzif, “SOA or EDFA Amplifying 10Gbit/s OFDM Signals for Access Networks”, in Proc. ECOC, Vienna, Austria, paper. P6.21, Sep. 2009.

[13] H. Khaleghi, P. Morel, A. Sharaiha, T. Rampone, “Experimental Validation of Numerical Simulations and Performance Analysis of a Coherent Optical-OFDM Transmission System Employing a Semiconductor Optical Amplifier", Journal of Lightwave Technology, vol. 31, no. 1, pp. 161-170, Dec. 2013.

[14] A. Emsia, M. Malekizandi, T. Q. Le, I. B. Djordjevic, F. Kuppers, “1 Tb/s WDM-OFDM-PON Power Budget Extension Techniques”, in Proc. Photonics Conference (IPC), Bellevue, WA , USA, paper WG3.3, Sep. 2013.

[15] F-T. An, D. Gutierrez, K. Soo Kim, J. Woo Lee, L. G. Kazovsky, “SUCCESS-HPON: A Next-Generation Optical Access Architecture for Smoth Migration from TDM-PON to WDM-PON”, IEEE Optical Communications, pp. S40-S47, Nov. 2005.

[16] V. Vujicic, P. M. Anandarajah, C. Browning, L. P. Barry, “WDM-OFDM-PON based on compatible SSB technique using a mode locked comb source”, IEEE Photonics Technology Letters, vol. 25, no. 21, pp. 2058-2061, Nov. 2013.

Chapter 5

5 Quantum Dash Mode-Locked Lasers for Data Centre Applications

The last decade has witnessed the rise of social networks, video-on demand and mobile based services and many more trends all leading to the building of hundreds of data centres around the world. The global scale of data centre databases and networks have created the need for large amounts of data to be transported between the various geographic sites. As data centres have continued to grow in size and number, the requirement for solutions which will enable economical and sustainable scaling of the data centres has arisen. The main drawbacks of the current data centres are high power consumption of switches and routers, and mismatch in bandwidth performance between the core and edge network which introduces significant latency. Integrated optical interconnects are considered as a potential solution to enable high throughput, reduce the size of modules, overall power consumption and latency.

In this chapter, high capacity data centre interconnects based on a single laser source, are investigated. An experimental demonstration of high capacity WDM transmission (400 Gb/s, 1 Tb/s, 2 Tb/s and 4 Tb/s) for interconnect applications within and between data centres based on Quantum Dash passively mode-locked lasers is presented. Inherent characteristics of Q-Dash passively mode-locked lasers, such as RIN and OCNR, have been analysed in detail. Furthermore, the effect of the RIN spectrum on the system performance by examining the error-vector magnitude of OFDM subcarriers over the desired frequency range is investigated.

5.1 Introduction

An exponential increase in the amount of network traffic due to cloud computing and other emerging web applications has created the need for more powerful data centres [1, 2]. WDM optical interconnects employing arrays of independent oscillators as

optical sources are gaining significant attention as a promising solution offering high throughput, reduced latency and power consumption [1-4]. Integrated interconnect solutions which often incorporate strong confinement microphotonic devices are typically polarisation sensitive [5], and the simplest solution is to encode data on only a single polarisation of light. Furthermore, transmission links within data centres are anticipated to be no longer than 2 km and therefore performance specifications for the optical transceivers within the data centre are significantly relaxed, compared to long-haul transceivers, allowing for a lower cost per module. For example, shorter transmission distances will reduce the penalty due to RIN, and transmitter lasers used in data centre interconnects will potentially adopt the IEEE standards which tolerate higher values of RIN (e.g. 802.3 GBase standard which tolerates -125 dB/Hz of RIN) [6]. Slightly more stringent RIN requirements can be expected for interconnect applications between data centres, where optical links are typically no longer than 80 km [6-8]. The requirements for reduced network complexity and a cost-effective approach cannot be fulfilled by simple scaling based on current optical technology within the data centres. Data centre operators will require much higher density optical interfaces that offer scalability from tens or hundreds of gigabits per second, to terabits per second [4, 9]. Integrated laser arrays, e.g. vertical cavity surface emitting laser (VCSEL) arrays, are typically used to meet data centre operators' requirements regarding scaling network capacity [10, 11]. Nevertheless, several limitations due to the practical implementation of parallel VCSEL arrays occur, such as imperfect alignment with embedded lensed arrays, e.g. smile error, when increasing the number of oscillators. An attractive alternative in developing WDM data centre interconnect solutions is based on a single multi-channel laser source [4, 9].

In this work, the WDM transmission with capacities higher than 400 Gb/s, 1 Tb/s and 2 Tb/s, have been demonstrated. Also, the possibility of obtaining a capacity greater than 4 Tb/s for interconnect applications within and between data centres based on a single laser source is considered. The Quantum Dash passively mode-locked lasers [12], grown on an S-doped (001) InP substrate with an active region composed of nine layers of InAs Q-Dashes separated by InGaAsP barriers, were used for the generation of a large number of carriers, enabling high data rate transmission. The lasers exhibit the characteristic square-shaped emission spectra [12-14], with a spectral bandwidth in excess of 1.7 THz, and free spectral ranges of 82.8, 44.7, 22.7 and 10.2 GHz. The system performance was investigated for propagation distances of 3 km and 50 km of SSMF indicating its potential for data centre applications. The RIN of all devices was studied extensively, and was found to be sufficiently low for the

desired application. In reaching interconnect capacities in excess of 2 Tb/s, and showing the possibility of further increasing to more than 4 Tb/s, this work represents a considerable improvement in transmission capacity for Q-Dash based comb sources, with previous work achieving a capacity of 504 Gb/s (9 channels × 56 Gb/s) [15]. The effect of the RIN spectrum on the system performance by examining the EVM of OFDM subcarriers over the desired frequency range is investigated as well.

5.2 Envisioned Fully Integrated Solution

The vision of a future chip-scale terabit-per-second optical interconnect transceiver incorporating the mode-locked lasers used in this work is illustrated in Figure 5.1. The envisaged transmitters and receivers consist of a multi-chip assembly, with single-mode photonic wire bonds connecting the individual chips, for example described in [16]. In contrast to monolithic integration, this hybrid approach allows for the combination of different photonic integration platforms: a Q-Dash laser can be realised using III–V semiconductors [12], and ring resonator filters, used for separation of optical carriers, could be made in silicon [9, 17].

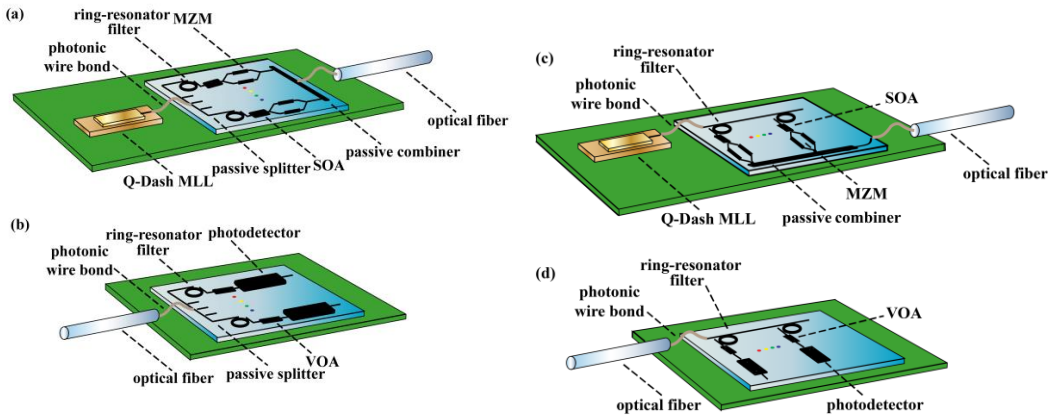

Figure 5.1. Illustration of chip-scale terabit-per-second interconnect transmitters and receivers. (a) A transmitter based on passive splitting and parallel ring-resonator structure for filtering of optical carriers. The filtered carriers are individually modulated and passively combined. (b) A receiver based on passive splitting and parallel ring-resonator structure for demultiplexing of optical carriers. Demultiplexed carriers are detected using direct detection receiver, for example an APD (c) A transmitter based on serial ring-resonator structure. (d) A receiver based on serial ring-resonator structure for demultiplexing of optical carriers.

The use of advanced modulation formats can increase the achievable channel bit rate from a given transmitter bandwidth beyond that of a directly modulated laser using

OOK signalling, but requires the use of external modulators. Here suitable external modulator structures could be fabricated with a silicon-on-insulator process [18].

The optical carriers generated by the Q-Dash PMLL are demultiplexed using ring-resonator filters, which can be assorted in a parallel or serial manner, as shown in Figure 5.1(a) and Figure 5.1(c) respectively. A feedback loop might be used to ensure the alignment of tunable ring-resonator filters and emission wavelength of the Q-Dash PMLL. Due to the size constraints, EDFAs are not used within current data centres, and therefore integrated SOAs can be used to compensate for losses within the hybrid photonic integrated chip. The SOAs could be fabricated on the same III-V platform that is used for the Q-Dash source [12, 19]. Filtered and amplified carriers are individually modulated on a transmitter chip. At the receiver side optical carriers are demultiplexed using a similar ring-resonator filter structure, which can be arranged in a parallel or serial manner (Figure 5.1(b), and Figure 1.5(d)), like at the transmitter, detected using a direct detection receiver, for example an APD.

5.3 Q-Dash Devices and Characterisation

The devices used in these transmission experiments were single-section Q-Dash based lasers. The devices were grown by a gas source molecular beam epitaxy (GSMBE) on an S-doped (001) InP substrate. The active region consists of nine layers of InAs Q-Dashes separated by InGaAsP barriers. This design provides a low optical confinement factor, resulting in a reduced impact of spontaneous emission on the amplitude and phase noise of the laser longitudinal modes [12]. Because of the lower coupling of amplified spontaneous emission to the lasing modes in Q-Dash structures, the intensity noise at frequencies around that of the carrier may be lower compared to Quantum Well (Q-Well) structures. These buried-ridge stripe waveguide devices were processed with a ridge width of 1.5 μm. The as-cleaved lasers used here have a total length of 550, 950, 1870 and 4000 μm, corresponding to repetition frequencies, hence channel mode spacings, of 82.8 GHz, 44.7 GHz, 22.7 GHz and 10.2 GHz, respectively. All lasers were temperature controlled throughout the measurements at 25°C using a thermoelectric cooler module, which had an accuracy of ±0.1°C. When biased with a single current source (here, 300 mA for the 82.8 GHz Q-Dash laser, 380 mA for the 44.7 GHz Q-Dash laser, 350 mA for the 22.7 GHz Q-Dash laser and 500 mA for the 10.2 GHz Q-Dash laser), all lasers exhibited square-

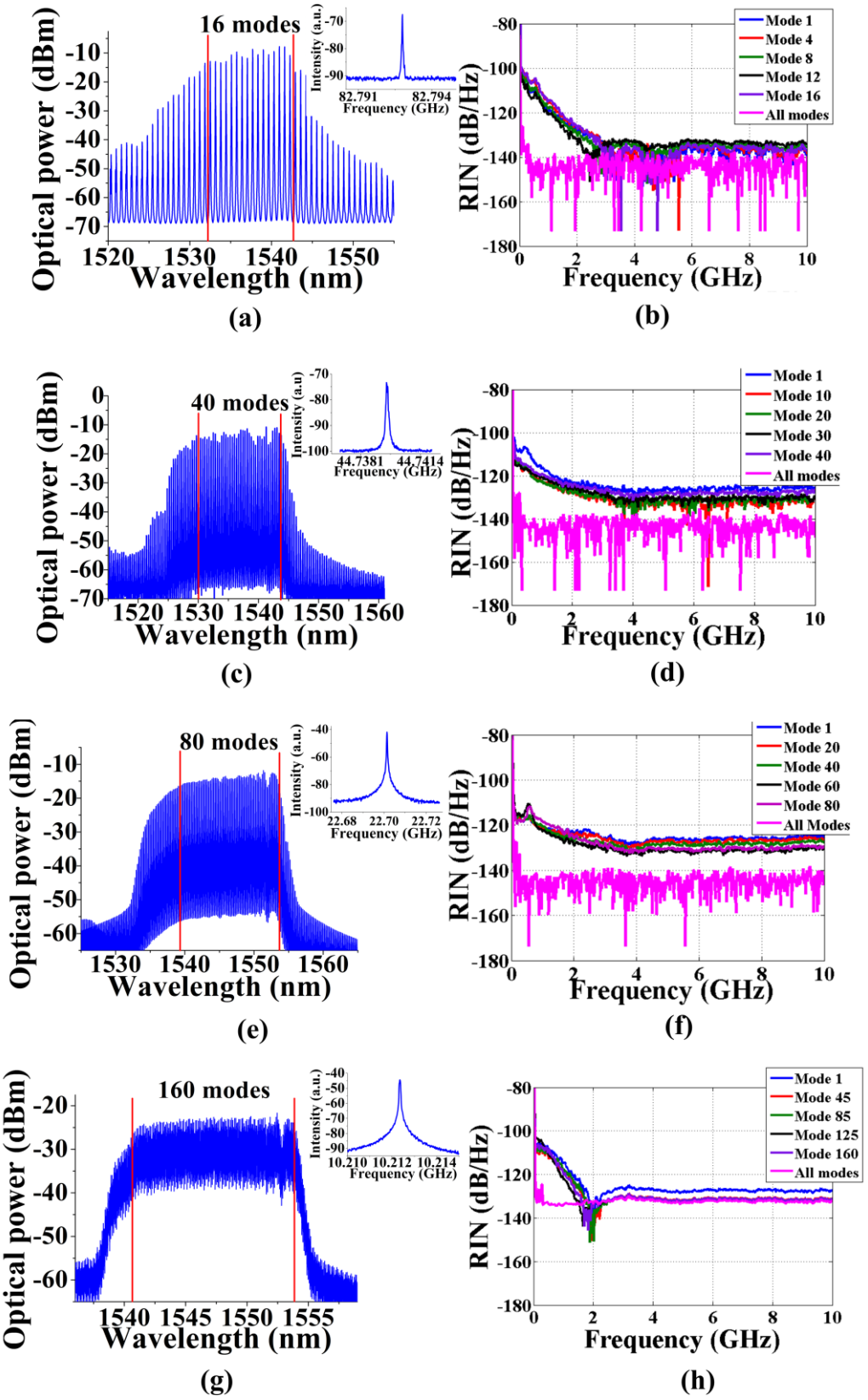

Figure 5.2. (a) Optical spectrum of 82.2 GHz Q-Dash PMLL (Resolution bandwidth (RBW) was 0.02nm), and detected RF linewidth (inset), (b) RIN for selected filtered modes and all modes. Figure 5.2 (c-d), (e-f) and (g-h) show the same results as (a-b), but for the Q-Dash PMLL with 44.7, 22.7 and 10.2 GHz mode spacing, respectively.

shaped emission spectra with a spectral bandwidth in excess of 1.7 THz, as shown in Figure 5.2(a), (c), (e) and (g). The applied bias currents provided an average power in fibre of 6-8 dBm. The detected RF spectra for the three devices are shown as insets in Figure 2(a), (c), (e) and (g). The measured RF linewidths for the 82.8, 44.7, 22.7 and 10.2 GHz Q-Dash lasers have values of 20 kHz, 90 kHz, 200 kHz and 60 kHz, respectively, indicating strong passive mode-locking [20]. The optical linewidth for each wavelength channel, measured for all devices using the delayed self-heterodyne technique, was found to be on the order of 10 to 20 MHz.

Characterisation of the amplitude noise is critically important as semiconductor mode-locked lasers can exhibit significant mode-partition noise (MPN) [21], which could impair system performance [22]. The RIN of the 82.8, 44.7 and 22.7 GHz Q-Dash devices was determined for each individual spectral mode (16 selected modes for the 82.8 GHz laser; 40 modes for the 44.7 GHz laser; 80 modes for the 22.7 GHz laser) and also for the entire emission spectrum. Additionally, the RIN of the 10.2 GHz laser was determined for several selected modes, and also for the entire emission spectrum. Measured RIN spectra are shown in Figure 5.2(b), (d), (f) and (h), and in all cases the individual spectral modes possess considerable intensity noise at frequencies below 2 GHz, but lower intensity noise at higher frequencies. However, the measured RIN of the entire emission spectrum is very low over the entire frequency range. This disparity indicates the presence of MPN in these devices. A decrease in OCNR is observed for the devices with lower free-spectral ranges because for the same spectrum full width at half maximum (FWHM), and for the same power coupled in the fibre (6-8 dBm), a larger number of modes were generated by longer devices. However, OCNR values of the comb lines used for data transmission experiments (in excess of 38 dB for the 10.2 GHz laser, 43 dB for the 22.7 GHz laser, 45 dB for the 44.7 GHz laser and 50 dB for 82.8 GHz laser) have been measured using a high-resolution (resolution bandwidth (RBW) = 1.44 pm) optical spectrum analyser, indicating suitable performance for IM/DD OFDM transmission [22].

5.4 Experimental Setup

The experimental setup for the IM/DD SSB OFDM system is shown in Figure 5.3. The optical multi-tone source at the transmitter consisted of a Q-Dash PMLL, an EDFA and a programmable optical filter (Waveshaper (WS)) to select the desired number of

channels. The spectral output from the optical multicarrier source consisted of between 16-160 tones (based on the Q-Dash PMLL used). In field installations, the generated comb lines would be separated by a de-multiplexer and each individual channel would be modulated independently. In this experiment all filtered comb lines were modulated by a single dual-drive Mach-Zehnder modulator. The DD-MZM was biased at the quadrature point and then used to modulate the selected comb lines with an amplified SSB OFDM signal waveform generated from an arbitrary waveform generator (Tektronix AWG70002A) operating at 25 GSa/s. The detailed analytical derivation of the implemented SSB OFDM signal waveforms is given in Chapter 3. Depending on the assumed FEC with 7 or 20% overheads, SSB OFDM signals with raw data rates of either 28.2 Gb/s or 33.6 Gb/s were used, respectively. The 28.2 Gb/s SSB OFDM signal was composed of 72 subcarriers, whilst the 33.6 Gb/s SSB OFDM signal consisted of 86 subcarriers. 16-QAM modulation was applied on each subcarrier, and the OFDM symbol rate was 97.65 MHz. The cyclic prefix occupied 6.25% of the IFFT size (which had 256 inputs), and the peak-to-average power ratios of the signals were about 11.5 dB. The total bandwidth of the 28.2 Gb/s signal was about 7 GHz, whilst the 33.6 Gb/s signal had a bandwidth of 8.3 GHz. An additional frequency offset of 800 MHz from the carrier frequency was applied, so the highest frequency component of the modulated signal was 7.8 GHz for the 28.2 Gb/s signal and 9.1 GHz for the 33.6 Gb/s signal. The offset was incorporated to avoid the strongest components of harmful signal-signal beating, characteristic for IM/DD OFDM systems [23, 24].

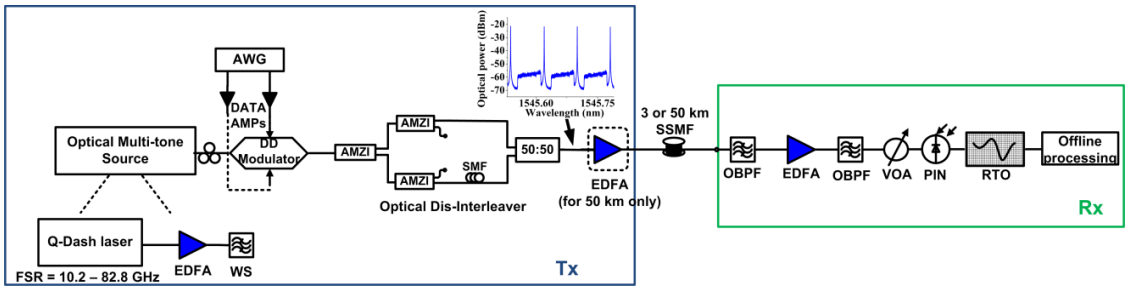

Figure 5.3. Schematic of the Q-Dash Terabit/s transmitter (Tx) which employs IM, and DD based receiver (Rx). Inset depicts part of the optical spectrum of the transmitted signal, showing SSB-OFDM modulation. Waveshaper (WS); Optical Band-Pass Filter (OBPF); Polarisation Controller (PC); Arbitrary Waveform Generator (AWG); Asymmetric Mach Zehnder Interferometer (AMZI); Data Amplifiers (DATA AMPs) (JDS Uniphase H301-1210); Erbium Doped Fibre Amplifier (EDFA); Variable Optical Attenuator (VOA); Real Time Oscilloscope (RTO).

The WDM signal was de-correlated using an odd and even configuration with tunable cascaded dis-interleavers based on asymmetric Mach Zehnder interferometers. This

is a fair method of de-correlation as channel separations are larger than the bandwidth of the signals, thereby eliminating any performance penalty due to linear crosstalk [25]. The even channels were subsequently passed through a de-correlation fibre patchcord, and then passively combined with the odd channels. The de-correlated signals were then transmitted over 3 and 50 km of SSMF. For the case when the signal was transmitted over 50 km of SSMF, an additional EDFA was used to amplify the combined signals prior to launching the signal into the fibre. At the receiver side, the selected channels were filtered with the first tunable optical band-pass filter prior to being amplified by the receiver EDFA. After amplification, the desired channel was filtered with a narrow tunable OBPF. The filtered channel was detected using a 10 GHz receiver that consists of a PIN photodetector and an integrated trans-impedance amplifier. An avalanche photodetector based receiver provides significantly better sensitivity compared to a PIN receiver. Therefore, if an APD were used instead of the PIN, the EDFA at the receiver side would not be required. However, due to the bandwidth limitation of our APD, a PIN receiver is used in this experiment. The received signal was captured with a real time oscilloscope operating at 50 GSa/s. Digital processing of the received signal, and BER calculations, were performed offline using Matlab.

5.5 Results

The obtained experimental results are shown in Figure 5.4. Figure 5.4(a)-(c) show the results for the Q-Dash PMLL with 82.8 GHz FSR, whilst Figure 5.4(d)-(f) show results for the Q-Dash PMLL with 44.7 GHz FSR. Next, Figure 5.4(g)-(i) show results for the Q-Dash PMLL with 22.7 GHz FSR, and finally, Figure 5.4 (j)-(l) present the results for the Q-Dash PMLL with 10.2 GHz FSR.

The filtered 16 channels from the 82.8 GHz Q-Dash PMLL, which exhibit flatness of ~ 4 dB, are shown in Figure 5.4(a). The corresponding OCNR, measured prior to amplification at the optical multi-tone source (see Figure 5.3), for all comb lines that were used for the data transmission experiments is found to be greater than 50 dB (RBW=1.44 pm) - owing to the relatively high output power distributed among the small number of modes. Channel performance was determined using BER measurements (for the received optical power of ~0 dBm), and results obtained for the 82.8 GHz Q-Dash PMLL are given in Figure 5.4(b).

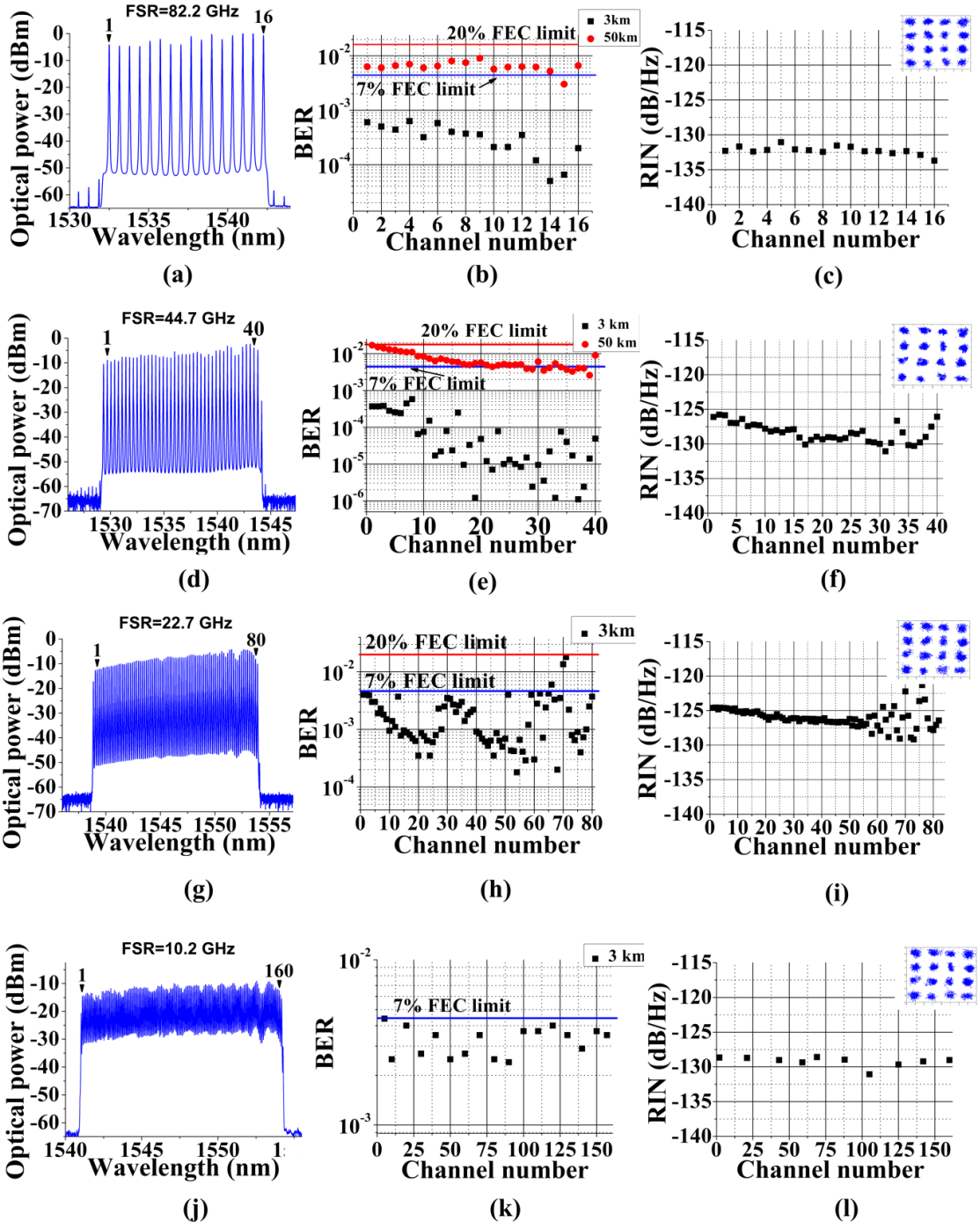

Figure 5.4. a) Optical spectrum of filtered Q-Dash PMLL with 82.8 GHz channel spacing (RBW=0.02 nm), (b) measured BER for each channel, after transmission over 3 and 50 km of SSMF, (c) the measured average RIN (DC-10 GHz) for all modes; Inset: measured constellation diagram for the middle channel after 3 km of SSMF. Figure 5.4 (d-f) and (g-i) show the same results as (a-c), but for the Q-Dash PMLL with 44.7 GHz and 22.7 GHz channel spacing. i) Optical spectrum of filtered Q-Dash PMLL with 10.2 GHz channel spacing (RBW=0.02 nm), (b) measured BER for selected channels, after transmission over 3 km of SSMF, (c) the measured average RIN (DC-10 GHz) for selected modes; Inset: measured constellation diagram for the middle channel after 3 km of SSMF.

After transmission over 3 km of SSMF, all channels exhibit performance below the 7% FEC limit (BER=4×10^{-3}), whilst after transmission over 50 km all channels had performance better than the 20% FEC limit (BER=1.6×10^{-2}). The performance after transmission over 50 km exhibits degradation, compared to the case when the signal was transmitted over 3 km of SSMF, which can be attributed to the significant nonlinear phase shifts among OFDM subcarriers, introduced by the data amplifiers used after the AWG to drive the DD-MZM [26, 27]. This, coupled with a large amount of dispersion, causes penalties as the linear equaliser cannot properly compensate for this effect. The best achievable performance for the test bed, obtained using the external cavity laser (ECL, Emcore ITLA module), gives BER=1×10^{-6} after 3 km, and BER=1.5×10^{-3} after transmission over 50 km of SSMF. The wavelength of the ECL used was 1545 nm and its OCNR was around 70 dB (RBW=1.44 pm). Figure 5.4(c) shows the measured average RIN (DC-10 GHz) for all 16 channels. RIN measurements of individually filtered comb lines were carried out as described in Chapter 3, and the received optical power during the measurements was ~ 1 dBm. The measured average RIN values for 82.8 GHz PMLL were in the range from -131 dB/Hz to -134 dB/Hz. The total measured average RIN (DC-10 GHz) for all channels was -144.2 dB/Hz. The measured constellation diagram (of all OFDM subcarriers) for channel 8 after 3 km of SSMF is shown as inset in Figure 5.4(c). Degradation in performance can be observed when moving from higher wavelength channels towards the lower wavelength channels, and the degradation is due to the reduction of the OCNR and increase of the RIN [22]. The aggregate raw capacities achieved with the 82.8 GHz Q-Dash PMLL were 451.2 Gb/s (16×28.2 Gb/s IM/DD SSB OFDM) after transmission over 3 km (7% FEC), and 537.6 Gb/s (16×33.6 Gb/s IM/DD SSB OFDM) after transmission over 50 km (20% FEC).

The 40 filtered channels from the 44.7 GHz Q-Dash PMLL, which exhibit a flatness of ~ 6 dB, are shown in Figure 5.4(d). The OCNR measured prior to amplification for all comb lines that were used for the data transmission experiments is found to be greater than 45 dB (RBW=1.44 pm). The BER values obtained for the 44.7 GHz Q-Dash PMLL are given in Figure 5.4(e). All channels exhibit performance far below the 7% FEC limit after transmission over 3 km of SSMF. Furthermore, all channels have performance below the 20% FEC limit after transmission over 50 km. Similar to the case where the 82.8 GHz Q-Dash PMLL was used, the trend of reduced OCNR and increased RIN, when moving from higher wavelength channels towards lower ones, caused a degradation in performance. Figure 5.4(f) shows the measured average RIN

(DC-10 GHz) for all 40 channels. The measured average RIN values for the 44.7 GHz PMLL were in the range from -125 dB/Hz to -132 dB/Hz, and the total measured average RIN (DC-10 GHz) for all channels was -143.6 dB/Hz. The measured constellation diagram for channel 20 after 3 km of SSMF is shown as inset in Figure 5.4(f). The aggregate raw capacity achieved with the 44.7 GHz Q-Dash PMLL was 1.128 Tb/s (40×28.2 Gb/s IM/DD SSB OFDM) after transmission over 3 km of SSMF (7% FEC), and 1.344 Tb/s (40×33.6 Gb/s) after transmission over 50 km (20% FEC).

The filtered 80 channels from the 22.7 GHz Q-Dash PMLL, which exhibit flatness of ~8 dB, are shown in Figure 5.4(g). Only 3 channels had performance worse than 7% FEC limit (Figure 5.4(h)) after transmission over 3 km of SSMF, but better than 20% FEC limit. Those channels correspond to the wavelengths which exhibit higher RIN and lower OCNR [22]. The measured average RIN (DC-10 GHz) values for 22.7 GHz PMLL were in range from -122 dB/Hz to -129 dB/Hz, Figure 5.4(i). The plot of the measured constellation diagram for channel 40 is shown as inset in Figure 5.4(i). The performance fluctuation of the system can be observed in the region of higher wavelengths, which is due to the fluctuations in RIN values and OCNRs. The aggregate capacity achieved with 22.7 GHz Q-Dash PMLL was 2.256 Tb/s (80×28.2 Gb/s IM/DD SSB OFDM), which corresponds to a SE of 1.25 bit/s/Hz. Given the small bandwidth of the SSB OFDM signal (~7 GHz), Q-Dash devices with narrower FSR can be used to get better SEs.

The filtered optical spectrum from the 10.2 GHz Q-Dash PMLL, which contains 160 channels within ~ 7 dB flatness, is shown in Figure 5.4(j). All filtered modes exhibit OCNR higher than 38 dB (RBW=1.44 pm). The performances of the selected channels after transmission over 3 km of SSMF are given in Figure 5.4(k). The measured average RIN (DC-10 GHz) for the selected channels is shown in Figure 5.4(l), and the values obtained, for the 10.2 GHz PMLL, were in the range from -128 dB/Hz to -131 dB/Hz. The total measured average RIN (DC-10 GHz) for all channels was -132.5 dB/Hz. The measured constellation diagram for channel 80 is shown as inset in Figure 5.4(l). The selected channels, which uniformly cover the entire emission spectrum of the 10.2 GHz Q-Dash PMLL, all exhibit performance below 7% FEC limit, indicating the possibility of a further increase in aggregate data rate up to 4.5 Tb/s (160×28.2 Gb/s IM/DD SSB OFDM). The spectral efficiency achieved with the 10.2 GHz PMLL was 2.76 bit/s/Hz, and the optical spectrum of one filtered channel prior to photodetection is shown in Figure 5.5 (measured with resolution bandwidth of 1.44 pm). Narrow optical filtering was used here to isolate one

of the wavelength channels (3-dB bandwidth of the filter was ~ 8 GHz). Filtering caused minor signal degradation due to spectral roll-off, as the data spectrum has slightly deviated from the ideal OFDM spectral profile. Additionally, system performance was affected by in-band interference from non-ideally suppressed adjacent channels (see Figure 5.5).

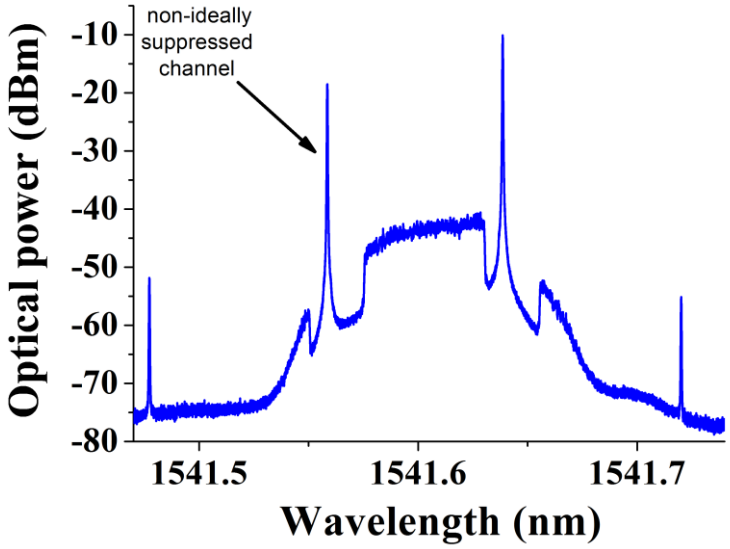

Figure 5.5. Optical spectrum of one filtered channel prior to photodetection for 10.2 GHz Q-Dash PMLL (RBW=1.44 pm). Achieved spectral efficiency was 2.76 bit/s/Hz.

The effect of RIN on the system performance is made clear when the EVM of the 16-QAM SSB ODFM signal is examined more closely. The EVM values of 72 OFDM subcarriers for channel 14 (after transmission over 3 km of SSMF) of the 82.8 GHz Q-Dash PMLL (blue circles), and the ECL (dashed red squares), are shown in Figure 5.6(a). The RIN for channel 14 of the 82.8 GHz Q-Dash PMLL (blue line), and the ECL (dashed red line), over a frequency range of DC-10 GHz, is given in Figure 5.6(b). The best performance was achieved using the ECL (red squares) and these results show that the EVM degraded with increasing frequency (increasing subcarrier number). This is due to a non-linear phase shift introduced by the data amplifiers used after the AWG to drive the DD-MZM, significantly impairing the ability to correctly reconstruct the OFDM signal at higher frequencies. Figure 5.7 shows difference of the amplitude and phase response of the two data amplifiers used in the setup. It can be seen that the difference of the magnitude response of the two amplifiers is relatively small. However there is a significant difference of the phase response of the two data amplifiers which can cause non-linear phase shift. This could be deterministically corrected in the AWG or eliminated by using electrical data

drivers which have linear phase characteristic [27]. At frequencies above 3 GHz, the performance of channel 14 from the 82.8 GHz Q-Dash PMLL closely resembled the performance of the ECL, albeit with a slight penalty. However, below 3 GHz the EVM of the filtered channel from the Q-Dash laser was significantly worse than that achieved with the ECL, and increased with decreasing frequency (or decreasing OFDM subcarrier number). The RIN spectra shown in Figure 5.6(b) clearly indicate that the intensity noise of the filtered line from the Q-Dash laser increases at the lower frequencies, and the EVM increases accordingly. In comparison, the ECL exhibited a flat power spectrum and average RIN (DC-10 GHz) of -142.5 dB/Hz. This indicates that low-frequency intensity fluctuations are the main cause of performance degradation when using Q-Dash PMLLs as comb sources for IM/DD SSB OFDM transmission.

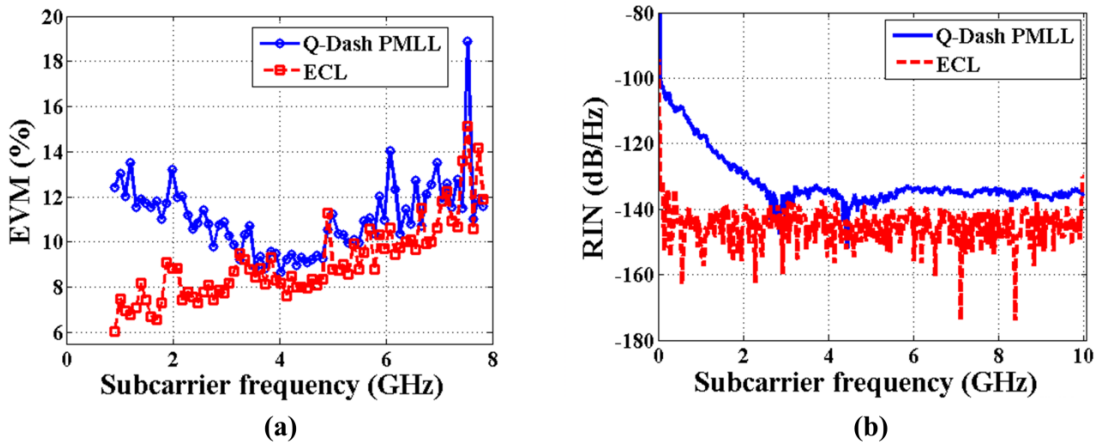

Figure 5.6. (a) Comparison of the EVM of 72 OFDM subcarriers for channel 14 (after transmission over 3 km of SSMF) from the 82.8 GHz Q-Dash PMLL (blue circles) and ECL (dashed red squares). (b) RIN for channel 14 from the 82.8 GHz Q-Dash PMLL (blue line) and ECL (dashed red line) over frequency range DC-10 GHz.

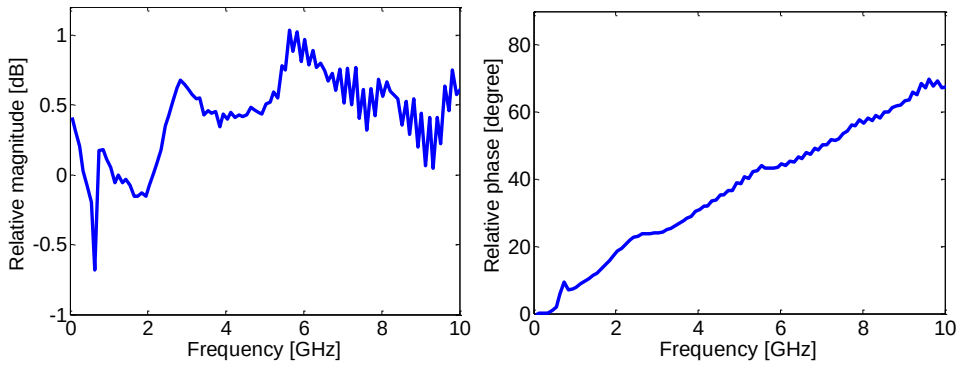

Figure 5.7. Difference of the frequency response of the two data amplifiers, (left) magnitude (right) phase. After [27].

5.6 Conclusion

The exponential increase of internet traffic, and the continued growth of cloud based services, has created the requirement for higher data throughputs within, and between, data centres. Industry surveys predict threefold growth of global data centre traffic until 2017. WDM based optical interconnects have been considered as a promising solution to meet increased data centres traffic demands offering high throughput and interface density, reduced latency and power consumption. Recently, interest in developing WDM data centre interconnect solutions based on a single multi-channel laser source has been expressed. This approach enables a more compact interface design, when compared to an equivalent design with multiple discrete lasers and components. Furthermore, hybrid integration platforms may enable designs which combine Q-Dash laser sources with silicon photonics-based components, which can greatly reduce the overall footprint and module size within the data centre optical interconnects.

In this chapter, single-polarisation WDM transmission with capacities higher than 400 Gb/s, 1 Tb/s, 2 Tb/s is demonstrated and the possibility of obtaining capacity greater than 4 Tb/s for interconnect applications within and between data centres based on a single laser source is shown. The Q-Dash passively mode-locked lasers used in this work exhibit the square-shaped emission spectra with a spectral bandwidth in excess of 1.7 THz, with FSRs of 82.8, 44.7, 22.7 and 10.2 GHz, and provide a large number of carriers. Aggregate capacities of 451.2 Gb/s (16×28.2 Gb/s) and 537.6 Gb/s (16×33.6 Gb/s), using single-polarisation IM/DD SSB OFDM signals, were achieved with an 82.8 GHz Q-Dash PMLL. The aggregate capacities obtained with a 44.7 GHz Q-Dash PMLL, using IM/DD SSB OFDM signals, were 1.128 Tb/s (40×28.2 Gb/s) and 1.344 Tb/s (40×33.6 Gb/s). Furthermore, the aggregate capacity obtained with a 22.7 GHz Q-Dash PMLL, using IM/DD SSB OFDM signals, was 2.256 Tb/s (80×28.2 Gb/s). Finally, by investigating the performance of a selected number of channels from a 10.2 GHz Q-Dash PMLL, we show the possibility to further increase capacity up to 4.5 Tb/s (160×28.2 Gb/s). The spectral efficiency achieved with the 10.2 GHz PMLL was 2.76 bit/s/Hz. Additionally, the RIN of the Q-Dash devices employed was determined for individual spectral modes, and for the entire emission spectrum. The results obtained show that tolerable levels of RIN were achieved for the desired application. Finally, the effect of RIN on the system performance was demonstrated by examining the error-vector magnitude values of OFDM subcarriers over the

desired frequency range and by comparing the performance of OFDM subcarriers obtained with the external cavity laser and the filtered channel from 82.2 GHz Q-Dash PMLL.

The previous chapters have presented results on the investigation of inherent properties of various optical multicarrier sources and their performance in IM/DD optical systems. OFDM modulation with 16-QAM modulation format has been used to enable efficient utilisation of available spectral bandwidth. In the following chapter, employment of Nyquist WDM modulation technique and *m*-QAM modulation formats in coherently detected system has been considered to enable high throughput and spectral efficiency in short and medium reach optical systems. Externally injected gain-switched comb sources and passive mode-locked lasers are used as optical multicarrier sources in these systems.

References

[1] C. Kachris and I. Tomkos., “A survey on optical interconnects for data centers,” IEEE Communications Surveys and Tutorials, vol. 14, no. 4, pp. 1021-1036, Fourth Quarter, 2012.

[2] M. Cvijetic, “Datacenters: New Challenges and Opportunities for Optical Technologies,” in Proc. OECC/CLEO Conf, Kyoto, Japan, paper TuP1-5, Jun 2013.

[3] L. Schares, J. A. Kash, F. E. Doany, C. L. Schow, C. Schuster, D.M. Kuchta, P. K. Pepeljugoski, J. M. Trewhella, C. W. Baks, R. A. John, L. Shan, Y. H. Kwark, R. A. Budd, P. Chiniwalla, F. R. Libsch, J. Rosner, C. K. Tsang, C. S. Patel, J. D. Schaub, R. Dangel, F. Horst, B. J. Offrein, D. Kucharski, D. Guckenberger, S. Hegde, H. Nyikal, C.-K. Lin, A. Tandon, G. R. Trott, M. Nystrom, D. P. Bour, M. R. T. Tan, and D. W. Dolf, “Terabus: Terabit/Second-Class card-level optical interconnect technologies,” IEEE Journal of Selected Topics in Quantum Electronics, vol. 12, no. 5, pp. 1032-1044, Sep/Oct., 2006.

[4] M. J. R. Heck, H.-W. Chen, A. W. Fang, B. R. Koch, D. Liang, H. Park, M. N. Sysak, and J. E. Bowers, “Hybrid Silicon Photonics for Optical Interconnects,” IEEE Journal of Selected Topics in Quantum Electronics, vol. 17, no. 2, pp. 333-346, Mar/Apr., 2011.

[5] T. Barwicz, M. R. Watts, M. A. Popovic, P. T. Rakich, L. Socci, F. X. Kartner, E. P. Ippen and H. I. Smith, “Polarization-transparent microphotonic devices in the strong confinement limit,” Nature Photonics, vol. 1, pp. 57-60, Jan. 2007.

[6] D. Minoli, “Telecommunications technology handbook,” Artech House, 2003.

[7] IEEE 802.3™-2012 – IEEE Standard for Ethernet, Available online: http://standards.ieee.org/about/get/802/802.3.html, Oct. 2014.

[8] B. Mason, “Use of Higher Order Modulation to Achieve Single Wavelength 100Gbit/s Links For Data Center Applications,” OIDA 100GbE per Lambda for Data Center Workshop, San Jose, CA, USA, Jun. 2014.

[9] “Quantum dot lasers and silicon photonics advance data-center connectivity,” Available online: www.lightwaveonline.com, Oct. 2014.

[10] A. Vahdat, H. Liu, X. Zhao and C. Johnson, “The Emerging Optical Data Center,” in Proc. OFC/NFOEC, Los Angeles, CA, USA, paper OTuH2, 2011.

[11] F. E. Doany, C. L. Schow, B. G. Lee, R. Budd, C. Baks, R. Dangel, R. John, F. Libsch, J. A. Kash, B. Chan, H. Lin, C. Carver, J. Huang, J. Berry, D. Bajkowski, “Terabit/sec-Class Board-Level Optical Interconnects Through Polymer Waveguides Using 24-Channel Bidirectional Transceiver Modules,” in Proc. ECTC, Lake Buena Vista, FL, USA, pp. 790 – 797, 2011.

[12] F. Lelarge, B. Dagens, J. Renaudier, R. Brenot, A. Accard, F. van Dijk, D. Make, O. Le Gouezigou, J.-G. Provost, F. Poingt, J. Landreau, O. Drisse, E. Derouin, B. Rousseau, F. Pommereau, and G.-H. Duan, “Recent advances on InAs/InP Quantum Dash based semiconductor lasers and optical amplifiers operating at 1.55 μm,” IEEE Journal of Selected Topics in Quantum Electronics, vol. 13, no. 1, pp. 111–124 Jan/Feb, 2007.

[13] R. Rosales, R. T. Watts, K. Merghem, C. Calò, A. Martinez, A. Accard, F. Lelarge, L. P. Barry, A Ramdane, “Quantum Dash Mode Locked Lasers as optical comb sources for OFDM superchannels,” in Proc. ECOC, Amsterdam, Mo.1.E.5, Sep. 2012.

[14] K. Merghem, C. Calò, R. Rosales, X. Lafosse, G. Aubin, A. Martinez, F. Lelarge, and A. Ramdane, “Stability of optical frequency comb generated with InAs/InP Quantum-Dash-Based Passive Mode-Locked Lasers,” IEEE Journal of Quantum Electronics, vol. 50, no. 4, pp. 275-280, Apr. 2014.

[15] Y. B. M’Sallem, Q. T. Le, L. Bramerie, Q.-T. Nguyen, E. Borgne, P. Besnard, A.Shen, F. Lelarge, S. LaRochelle, L. A. Rusch, and J.-C. Simon, “Quantum-Dash Mode-Locked Laser as a source for 56-Gb/s DQPSK modulation in WDM multicast applications,” IEEE Photonics Technology Letters, vol. 23, no. 7, pp. 453-455, Apr. 2011.

[16] N. Lindenmann, G. Balthasar, D. Hillerkuss, R. Schmogrow, M. Jordan, J. Leuthold, W. Freude, and C. Koos, “Photonic wire bonding: a novel concept for chip-scale interconnects,” Optics Express, vol. 20, no. 16, pp. 17667-17677, Jul. 2012.

[17] A. Biberman and K. Bergman, “Optical interconnection networks for high-performance computing systems,” Reports on Progress in Physics, 75, 046402 (15pp), 2012.

[18] L. Liao, D. Samara-Rubio, M.l Morse, A. Liu, D. Hodge, “High speed silicon Mach-Zehnder modulator,” Optics Express, vol. 13, no. 8, pp. 3129-3135, Apr. 2005.

[19] F. van Dijk, G. Kervella, M. Lamponi, M. Chtioui, F. Lelarge, E. Vinet, Y. Robert, M. J. Fice, C. C. Renaud, A. Jimenez, and G.Carpintero, “Integrated InP Heterodyne Millimeter Wave Transmitter,” IEEE Photonics Technology Letters, vol. 26, no. 10, pp. 965-968, May. 2014.

[20] Kartner, F. X., Morgner, U., Schibli, T., Ell, R., Haus, H. A., Fujimoto, J. G., and Ippen, E. P., “Few-cycle pulses directly from a laser”, Topics in Applied Physics, 95, 73-136, 2004.

[21] K. Sato and H. Toba, ”Reduction of mode partition noise by using semiconductor optical amplifiers,” IEEE Journal of Selected Topics in Quantum Electronics, vol. 7, no. 2, pp. 328-333, Mar/Apr 2001.

[22] V. Vujicic, P. M. Anandarajah, R. Zhou, C. Browning, and L. P. Barry, “Performance investigation of IM/DD Compatible SSB-OFDM systems based on optical multicarrier sources,” IEEE Photonics Journal, vol. 6, no. 5, 7903110, Oct. 2014.

[23] M. Schuster, S, Randel, C. A. Bunge, S. C. J. Lee, F. Breyer, B. Spinnler, K. Petermann, “Spectrally efficient compatible single-sideband modulation for OFDM transmission with direct detection”, IEEE Photonics Technology Letters, vol. 20, no. 9, pp. 670-672, May 1, 2008.

[24] W-R. Peng, B. Zhang, K-M. Feng, X. Wu, A. E. Willner, S. Chi, “Spectrally efficient direct-detected OFDM transmission incorporating a tunable frequency gap and an iterative detection techniques”, Journal of Lightwave Technology, vol. 27, no. 24, pp. 5723-5735, Dec. 15, 2009.

[25] L. B. Du and A. J. Lowery, “Experimental investigation of the effect of using ‘Odd and Even’ channels in all-optical OFDM and Nyquist WDM system comparisons,” in Proc. ECOC, Amsterdam, Netherlands, Tu.4.C.5, 2012.

[26] M. Martone, “On the necessity of high performance RF front-ends in broadband wireless access employing multicarrier modulations (OFDM),”in Proc. Global Telecommunications Conference, GLOBECOM, San Franciso, CA, USA, Dec. 2000.

[27] T. Shao, R. Zhou, M. D. G. Pascual, P. M. Anandarajah, L. P. Barry, “Integrated Gain Switched Comb Source for 100 Gb/s WDM-SSB-DD-OFDM System”, Journal of Lightwave Technology, vol. 33, no. 7, pp. 3525-3532, Sep. 2015.

Chapter 6

6 Nyquist-WDM Terabit/s Transmission Using a Gain-Switched Comb Sources and Quantum Dash Mode-Locked Lasers

The directly detected systems based on OFDM and Nyquist WDM modulation schemes provide a noticeable increase in spectral efficiency compared to the conventional optical systems. However, the full utilisation of the available spectrum is only possible when using coherent detection. The requirement to have spectral guard bands between optical channels due to the imperfect optical channel filtering at the receiver is eliminated by employing a local oscillator to carry out the signal selection. Furthermore, advanced modulation schemes in coherently detected systems do not require an optical carrier to be transmitted together with the signal, and therefore guard bands between carrier and signal are eliminated as well. Coherent detection also enables efficient compensation of various system impairments allowing for further increase in spectral efficiency.

The increase in spectral efficiency puts more stringent requirements on frequency stability of optical sources. Optical multicarrier sources have been recognised as promising candidates to provide constant frequency separation between optical channels. Optical frequency comb sources such as electro-optic based combs, Kerr microresonator combs and parametric frequency combs have been previously used for generation of optical superchannels. In this chapter, gain-switched comb sources are used as an alternative approach to generate Tb/s superchannels, with high spectral efficiency. Furthermore, a feed-forward heterodyne phase noise reduction scheme is used to simultaneously reduce the linewidth of 30 lines from a Q-Dash mode-locked laser, enabling coherent WDM data transmission at Tb/s data rates using Q-Dash PMLL as a comb source.

6.1 Introduction

Interfaces operating at 400 Gb/s or 1 Tb/s are foreseen as the next standards after 100 Gb/s Ethernet [1-3]. In this context, optical superchannels are promising candidates, combining a multitude of sub-channels in a WDM scheme, while each sub-channel operates at a moderate symbol rate that complies with currently available CMOS driver circuitry. Typically the superchannels use spectrally efficient advanced modulation formats such as QPSK or 16-QAM in combination with advanced multiplexing schemes such as OFDM [4-6] or Nyquist-WDM [7-10]. The performance of these transmission schemes depends heavily on the properties of the optical source, in particular on the number of lines, the power per line, the optical carrier-to-noise ratio, the optical linewidth (phase noise), and on the relative intensity noise. In addition, tunability of emission wavelength and line spacing are important features providing flexibility of the transmission scheme. Tb/s superchannel transmission has been demonstrated before, using different approaches for realising the optical source. These approaches include ensembles of independent lasers [11, 12], single-laser concepts with sidebands generated by external modulation [13, 14] or by Kerr comb generation in optically nonlinear high-Q microresonators [15], and fibre-based spectral broadening [5, 9, 16-18]. Arrays of independent lasers offer flexibility and do not require filters for spectrally separating the comb lines at a transmitter before modulation. However, the achievable spectral efficiency is limited by the relative drift of the individual emission wavelengths and the associated required spectral guard bands. For modulator-based comb sources, the number of comb lines is generally limited by the achievable modulation depth [13] unless complex arrangements of cascaded modulators with synchronised driving signals are used [14, 19]. Moreover, if large numbers of lines are to be generated, the power of the comb lines is limited by the power handling capacity and by the insertion loss of the modulator. Kerr comb sources can provide a large numbers of lines, but require sophisticated pumping schemes and the line spacing is inherently tied to the free spectral range of the underlying resonator. Broadband frequency combs for Tb/s superchannels can also be generated by solid-state mode-locked lasers in combination with highly nonlinear fibres [5, 9, 20], or multi-stage parametric mixers [16-18]. However, both approaches require strong optical pumps and large interaction lengths in delicately arranged sequences of specialised optical fibres. Therefore, integration density is limited. While this might be acceptable when considering the ultra-high data rates achieved with these sources — several tens of terabit/s — the

associated higher power consumption is not very well suited for point-to-point links that require only a limited number of comb lines (order of 10) to form a terabit/s superchannel.

An alternative technique to generate broadband frequency combs for Tb/s superchannels is by using semiconductor mode-locked lasers, which are a compact, low-cost, energy-efficient optical multicarrier sources. As shown in Chapter 5, single-section Q-Dash passive mode-locked lasers are able to deliver several tens of comb lines each with decent optical power while being driven simply by a constant current of the order of 100 mA [21]. However, the spectral modes of Q-Dash PMLL generally exhibit strong phase noise and broad optical linewidths, typically of the order of 10-20 MHz [22, 23]. As a consequence, WDM data transmission using these combs has been restricted to direct detection schemes [24] and DQPSK with high symbol rates and aggregate data rates of up to 504 Gb/s [25], whereas fully coherent transmission has been impeded by excessive phase noise up to now. Reduction the optical linewidth of Q-Dash PMLL can be achieved by optical injection using a narrow-linewidth master laser, but it also changes the internal dynamics of the slave that distorts the comb envelope and reduces the usable number of lines [26], thereby limiting its utility within broadband WDM systems. Digital approaches, using feed-forward schemes, have been proposed to reduce the influence of excessive phase noise in either the transmitter laser or local oscillator laser in coherent receivers [27, 28]. Therefore, these digital schemes could be employed to permit the use of Q-Dash PMLL in coherent systems. An analogue equivalent has recently been shown to reduce the phase noise for multiple comb lines simultaneously by using a feed-forward heterodyne scheme [29]. However, the viability of this concept for high-speed coherent data transmission has not been shown before.

In this chapter, it is demonstrated that gain-switched comb sources can be used as an alternative approach to generate Tb/s superchannels. These devices exploit injection locking of a gain-switched laser diode and feature an electrically tuneable free spectral range [30], an electrically tuneable centre wavelength [31], good spectral flatness, high OCNR, low RIN and low optical linewidth. A coherent detection employing such a comb source has been reported in [32, 33], where it is used to transmit several channels operating at 10 Gb/s and 40 Gb/s, respectively, in a passive optical network. The spectral efficiency in these experiments amounted to 1 bit/s/Hz and 2 bit/s/Hz, respectively. Here, six distinct Tb/s superchannel experiments using PDM QPSK and 16-QAM in combination with Nyquist pulse

shaping for efficient use of the available bandwidth are presented. Transmission over various distances of SSMF has been tested. An aggregate data rate (net data rate) of 1.296 Tb/s (1.074 Tb/s) after transmission over 150 km of SSMF in a spectral bandwidth of 166.5 GHz is achieved. This corresponds to a (net) spectral efficiency of 7.8 bit/s/Hz (6.5 bit/s/Hz). When combining 16-QAM on strong carriers and QPSK modulation on the weaker carriers, the aggregate data rate (net data rate) can be boosted to 2.112 Tb/s (1.839 Tb/s) and transmitted over 300 km using a bandwidth of 300 GHz.

Furthermore, in a separate experiment, the analogue FFH scheme [29] is used to simultaneously reduce the linewidth of 30 lines from a Q-Dash PMLL with 42 GHz FSR. The resulting lines are used for coherent WDM data transmission at Tb/s data rates. This approach has permitted the use of coherent detection with a semiconductor Q-Dash PMLL.

6.2 Gain Switched Comb Source

Figure 6.1(a) shows the experimental setup of the GSCS. Gain switching is achieved by driving a DFB slave laser diode with a large sinusoidal signal (24 dBm) at a frequency that corresponds to the desired line spacing, in combination with a DC bias current of approximately four times the threshold current ($I_{th} \approx 12.5$ mA).

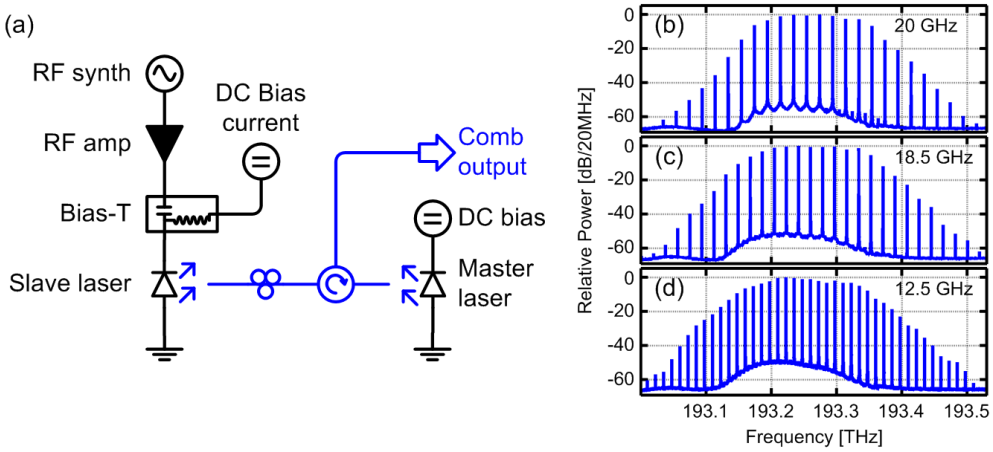

Figure 6.1. (a) Setup schematic of the GSCS. A frequency comb is generated by gain switching of the DFB slave laser. The line spacing is determined by the frequency of the RF drive signal. By injecting light from the master laser to the slave laser via a circulator, the low linewidth and RIN of the master laser are transferred to the comb lines. (b-d) Comb spectra with a line spacing of (b) 20 GHz, (c) 18.5 GHz, and (d) 12.5 GHz (RBW 20 MHz).

Additionally, a master laser (Agilent N7711A) injects continuous-wave light into the slave laser via a polarisation controller and an optical circulator. The master laser establishes coherence between subsequent pulses and transfers its characteristically low optical linewidth (80 kHz) to the individual modes of the comb [33, 34], and reduces the RIN of the comb modes [35]. The comb's centre wavelength can be tuned by simultaneously adjusting the emission wavelength of the master laser and the temperature of the DFB slave. The polarisation controller is used to align the polarisation state of the injected light with that of the slave laser mode. By carefully selecting the wavelength detuning and the injected power, long-term (during several days) operational stability of the GSCS can be achieved. The GSCS operates without automated feedback control, and without need for manual adjustment of detuning and polarisation. In those experiments, the injection power is set to approximately 7 dBm, and the slave laser is temperature-controlled at 25 °C.

The GSCS with three different line spacings, 20 GHz, 18.5 GHz and 12.5 GHz is investigated, by appropriately changing the frequency of the RF synthesizer. The respective GSCS spectra are depicted in Figure 6.1(b)–(d). The power levels correspond to the actual power of the comb measured at position "Comb output" in Figure 6.1(a). The total power in all three cases amounts to +3.5 dBm. The origin of the noise floor in the GSCS spectra is discussed in [36], where the trade-off between flatness and high-frequency FM noise was elaborated. The injected gain switched comb generation depends highly on the injection conditions, namely the optical injection power and the wavelength detuning between the master and slave laser. By carefully choosing these conditions, optical combs with different noise properties can be generated due to the various interactions between the injecting signal and the photons generated in the slave cavity. Two sets of conditions were chosen in [36], which enabled generation of "low noise" and "flat" combs. Here, "flat combs" are considered [36], accepting the noise penalty in favour of a higher number of sub-channels and hence higher aggregate data rates.

Note that the optical bandwidth of all three combs in Figure 6.1(b)–(d) is the same. The bandwidth is dictated by the intrinsic dynamics of photons and electrons within the slave laser. Choosing a smaller line spacing will yield a larger number of lines. With respect to the possible number and the power of carriers, the GSCS competes with frequency combs generated with a single electro-optic modulator. The main advantage of the GSCS is its inherent stability without any bias control. Even the polarisation of the master laser is uncritical once it is set, because a slight polarisation

change results in a minor reduction of the locking range only. The temperature control of the master laser would be required anyway for the laser in a modulator-based comb generator. Note that the current setup for comb generation comprises discrete components. Further cost and complexity reduction as well as a stability improvement can be obtained by a monolithic integration of master and slave lasers [37].

6.2.1 Superchannel Generation and Characterisation

For a given line spacing, superchannel capacity is dictated by two parameters: First, the number of carriers that can be derived from the comb source, which defines the number of sub-channels, and second, the power levels and OCNR of the respective carriers that determine the modulation formats to be used on each sub-channel provided that the carrier linewidth is sufficiently low. As can be seen in Figure 6.1, the comb line power is highest in the centre of the GSCS spectrum and decreases towards the periphery. In practical transmission systems, however, equal power distribution among all involved sub-channels is desired. This requires attenuation of the centre comb lines relative to the power of the outer ones, and subsequent amplification to overcome insertion and modulation losses of the transmitter. The associated ASE noise limits the performance of the entire superchannel and is hence a crucial parameter when designing comb-based transmission systems. In the following experiments, the goal is to maximise superchannel performance for a given transmission system, and to investigate the trade-off between spectral efficiency and transmission reach for the case of the GSCS.

The experimental setup to emulate a superchannel transmitter and receiver is depicted in Figure 6.2. A programmable filter (Finisar WS) is used to equalise the power in the comb lines and to reject outer comb lines that feature too little power for sufficient modulation. The comb lines are then dis-interleaved into two sets of sub-carriers (odd and even). For the 20 GHz and 18.5 GHz line spacing, the dis-interleaving can be directly performed by the programmable filter, while for the 12.5 GHz comb, a commercially available interleaver (Optoplex) is used. The two sets of sub-carriers are amplified by two nominally identical EDFA operated in constant output power mode set to 16 dBm. Note that the equalisation of the comb results in a reduction of the input power to these amplifiers. This limits the flattening of the comb lines as stronger equalisation requires higher amplification afterwards, and hence

more ASE noise is added to the comb lines. While this has a negative effect on the OCNR of the carriers, it helps to ensure comparable input power levels for the transmission EDFA and at the receiver input, so that the various transmission experiments can be compared.

The two sub-carrier sets are then independently modulated using an IQ modulator driven by band-limited Nyquist pulses that are generated by a proprietary multi-format transmitter (Nyquist-Tx) [8, 38]. Polarisation division multiplexing is emulated by splitting the combined outputs of the two Nyquist-Tx into two paths, which are recombined after different delays to form two orthogonal polarisation states in a SSMF. The insets show exemplary optical spectra, RBW=0.01 nm, of the separate sub-carrier sets and the combined Tb/s data stream for the case of the 20 GHz comb and 18 GBd QPSK modulation. When using the waveshaper for dis-interleaving and flattening, the crosstalk, i. e., the ratio of the power of a comb line at its allocated waveshaper output port and the residual power of the same comb line at the other output port is actually a function of the attenuation supplied to this particular comb line. A correlation between crosstalk attenuation and the performance of the sub-channels have not been observed, and hence the results are not limited by crosstalk effects. This finding is in accordance to the one reported in [39], where a SNR penalty of less than 1 dB is predicted for observed levels of crosstalk.

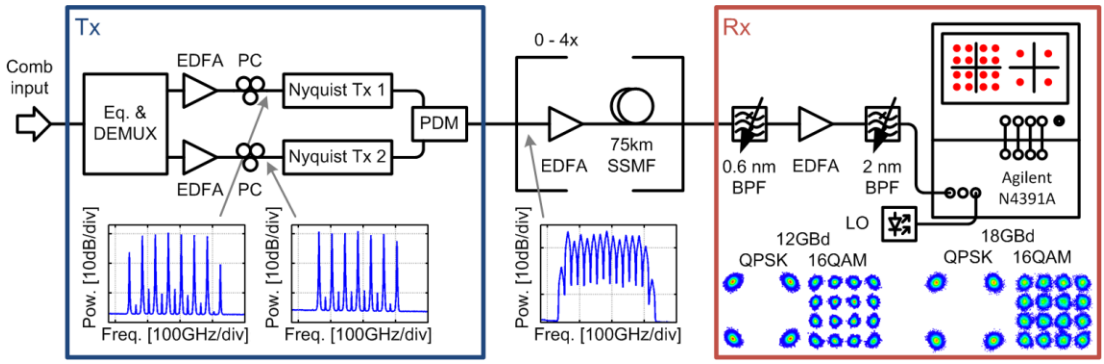

Figure 6.2. Schematic of the GSCS Tb/s super-channel transmitter and coherent receiver. Insets show the optical spectra measured using a 0.01 nm resolution bandwidth. The presented constellation diagrams are obtained using an ECL as a carrier, and serve as reference measurements.

The superchannels were either sent directly to the receiver for back-to-back characterisation, or transmitted over up to four spans of 75 km SSMF with an EDFA before each span. The launch power into the transmission fibres has been set to approximately –3 dBm per sub-channel, providing a good compromise between nonlinear signal impairments and noise. An ECL specified with a linewidth less than

100 kHz is a local oscillator. The signals were analysed using an optical modulation analyser (Agilent N4391A) and with offline processing. Digital signal processing at the receiver include digital brick-wall filtering, polarisation demultiplexing, dispersion compensation, and adaptive equalisation before evaluating the BER and the error vector magnitude (EVMm) of each sub-channel individually. The EVM subscript “m” indicates the normalisation of the EVM to the maximum power of the longest ideal constellation vector [40] (see Appendix B).

As a performance measure of the system, both modulation paths are tested individually with a narrow-linewidth ECL that is comparable to the ECL used as local oscillator. With 18 GBd modulation an average EVMm of 10.5 % and 9.8 % for QPSK and 16-QAM is achieved, respectively, while an average EVMm of 8.5 % and 7.5 % is obtained for 12 GBd modulation, respectively. The dependence of the performance on symbol rate is attributed to the limited bandwidth of the anti-aliasing filters after digital-to-analog conversion.

Assuming that the signal is impaired by additive white Gaussian noise only, a direct relation from the EVMm to the BER can be established [40, 41]. Here, this assumption is not perfectly fulfilled as the constellations show a small signature of phase noise. This behaviour is also observed for the reference measurements with an ECL (see insets in Figure 6.2), and this can be attributed to the transmitter hardware rather than to the linewidth of the optical source. Nevertheless, the results are presented using the EVMm metric, since for the QPSK experiments a high-enough number of errors within the length of one recording have not been accumulated. For the 16-QAM experiments both the EVMm and the BER are presented. One can see that the EVMm slightly overestimates the signal quality, which is attributed to the small phase error introduced by the transmitter hardware as well as the fact that the EVMm measurement is non-data-aided while the relation in [41] assumes a data-aided measurement of the EVMm.

6.2.2 Experimental results

6.2.2.1 Experimental Parameters and Comparison of Superchannels

The six different superchannel architectures investigated are based on three different line spacings, 20 GHz, 18.5 GHz and 12.5 GHz, and two different modulation formats,

QPSK and 16-QAM. The results of all six experiments are summarised in Table 6.1. For each superchannel the maximum number of comb lines is taken, each carrying a Nyquist-WDM sub-channel. Comb lines that were too weak for the respective modulation format are suppressed by the equalisation filter (equaliser "Eq." in Figure 6.2) prior to recording the data presented here. For the superchannels that were derived from the 20 GHz and the 18.5 GHz comb, a symbol rate of 18 GBd is used and hence have a sub-channel line rate of 72 Gb/s for PDM-QPSK modulation and 144 Gb/s for PDM-16-QAM. A symbol rate of 12 GBd was used for the superchannels based on the 12.5 GHz comb leading to a sub-channel line rate of 48 Gb/s and 96 Gb/s for the two modulation formats employed. For all symbol rates, the clock rate of the digital-to-analog converters of the Nyquist-Tx was kept constant at 24 GHz, while the oversampling factor q for generating the sinc-shaped output pulses was adapted to q = 4/3 for 18 GBd and q = 2 for 12 GBd.

Line spac. [GHz]	Modulation format	No. of sub-ch.	Sub-ch. line rate [Gb/s]	Aggr. data rate [Tb/s]	Occupied bandwidth [GHz]	Net aggr. data rate [Tb/s]	Net SE [bit/s/Hz] (transm. dist.)
20	PDM-QPSK	13	72	0.936	260	0.870	3.3 (300 km)
	PDM-16-QAM	8	144	1.152	160	1.034	6.5 (150 km)
18.5	PDM-QPSK	15	72	1.080	277.5	1.004	3.6 (300 km)
	PDM-16-QAM	9	144	1.296	166.5	1.074	6.5 (150 km)
12.5	PDM-QPSK	24	48	1.152	300	1.071	3.6 (300 km)
	PDM-QPSK /PDM-16-QAM	4 / 20	48 / 96	2.112	300	1.839	6.1 (300 km)

Table 6.1. Summary of all superchannels

In Table 6.1, the aggregate data rate is obtained by multiplication of the number of sub-channels with the sub-channel line rate, and the bandwidth of the superchannel is given by the product of sub-channel number with the comb line spacing. For calculating the net aggregate data rate one needs to take into account the overhead for forward error correction. FEC schemes with 7% overhead can cope with BER of up to 4.5×10^{-3} [42], a requirement which was fulfilled for all B2B experiments. For some transmission experiments, this BER threshold is exceeded as discussed in the subsequent sections. In these cases, some of the sub-channels require more advanced FEC codes with a larger overhead of, e.g. 20%, having a higher BER limit of, e.g., 1.5×10^{-2} [43]. The net aggregate data rate for each superchannel after the longest tested transmission distance is calculated by taking into account the respective overhead for each sub-channel individually. The net SE is then calculated from the ratio of the net aggregate data rate and the occupied bandwidth. In the

parenthesis, the actual fibre transmission distance over which this spectral efficiency has been achieved is indicated.

6.2.2.2 Terabit/s Superchannels with an 18.5 GHz Comb

For the highest spectral efficiency the Nyquist-Tx is operated at a symbol rate of 18 GBd and comb line spacing is 18.5 GHz (see spectrum of Figure 6.1(c)). A total of 15 lines are selected using the equalisation filter and the spectrum is flattened to the level of the weakest carrier. Figure 6.3(a) shows the spectrum of the superchannel using PDM-QPSK modulation with a total aggregate data rate of 1.08 Tb/s, measured in a resolution bandwidth of 0.01 nm. For each sub-channel the measured EVMm, averaged over both polarisations, is presented in Figure 6.3(b) for the B2B case and for transmission distances of 75 km, 150 km, 225 km, and 300 km. The transmission lengths are distinguished by different symbols, colours, and by an offset in the horizontal direction. Note that an insufficient number of errors was accumulated in the recorded number of 4,500,000 bits for evaluating the BER reliably. Therefore it can be concluded that the BER of all sub-channels are clearly below the threshold for FEC with 7% overhead, given by a BER of 4.5×10^{-3}, which corresponds to an EVMm of 38.3% [40, 41]. Hence, the net superchannel capacity of 1.004 Tb/s in a bandwidth of 278 GHz is obtained, corresponding to a net spectral efficiency of 3.6 bit/s/Hz. Selected constellations diagrams of the B2B-experiments are displayed in Figure 6.3(c). Two sub-channels are compared, one at the edge and one at the centre of the superchannel spectrum, and similar performance is obtained for both polarisations.

The bandwidth requirement can be reduced by a factor of two when upgrading the system from QPSK to 16-QAM signalling. This doubles the data rate per channel but requires a higher OSNR. To satisfy this requirement, the equalisation power level for flattening the comb is increased, i.e., the average attenuation is decreased, which leads to carriers with a higher power. However, fewer comb lines contain the required power, hence the number of sub-channels is reduced from 15 to 9. Because a higher power level is input to the EDFA, the amplification and the ASE contribution is lower, leading to a larger OCNR. Additionally, the smaller attenuation results in a reduced crosstalk of the waveshaper (see Section 6.3). Spectrum, EVMm and measured BER are presented in Figure 6.3(d)–(f). For B2B and short transmission distances, the BER stays below the standard FEC limit for 7% overhead. For a transmission distance of 150 km, seven of the nine sub-channels exceed the BER mark for

standard FEC, and implementations with larger overhead, i.e., 20% overhead, become necessary. The remaining two sub-channels fall below the FEC threshold with 7% overhead even after transmission over 150 km. The aggregate data rate of this superchannel amounts to 1.296 Tb/s, corresponding to a (net) spectral efficiency of 7.8 bit/s/Hz (6.5 bit/s/Hz).

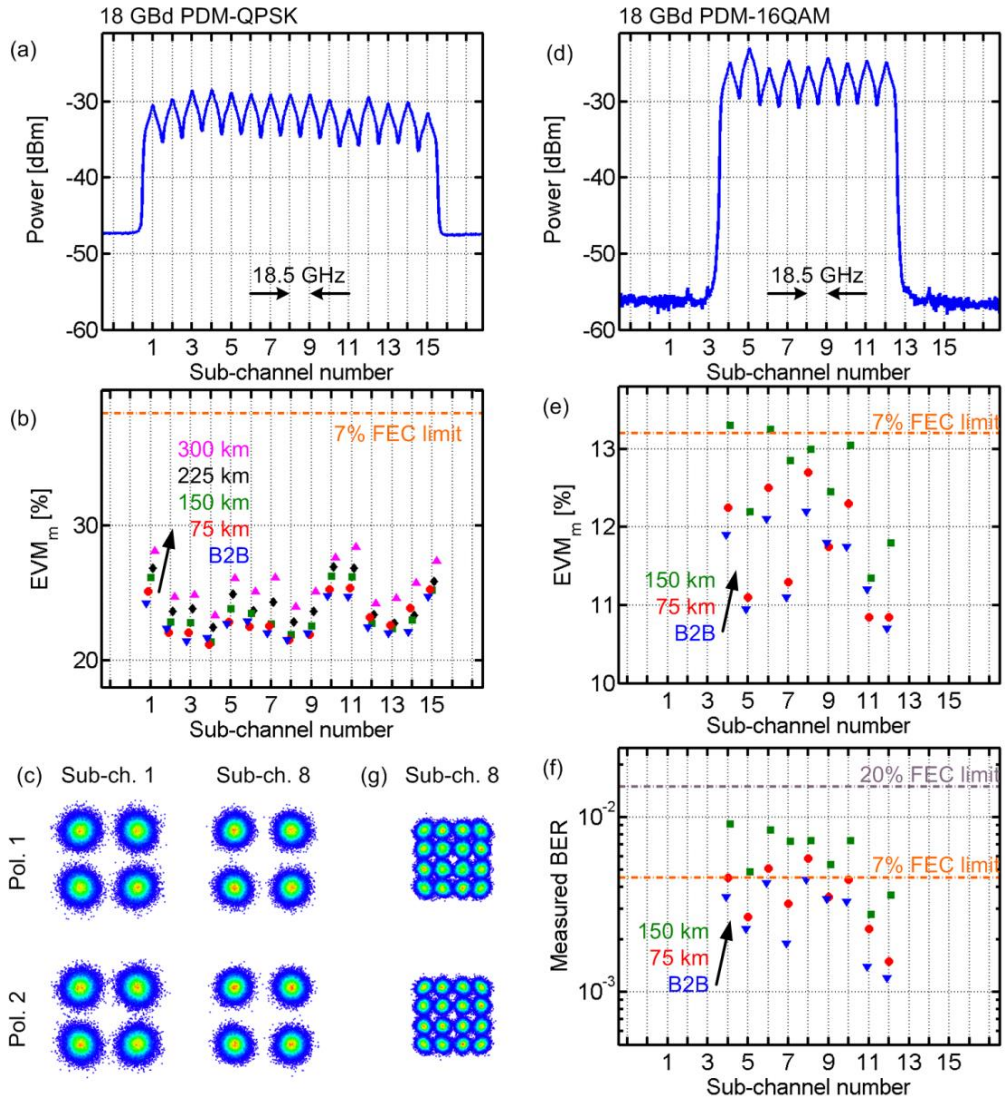

Figure 6.3. Spectra, signal quality and constellations for superchannel transmission with an 18.5 GHz comb. Left column for QPSK, right column for 16-QAM. (a) Spectrum of the superchannel derived from a 18.5 GHz comb with 18 GBd PDM-QPSK modulation (RBW 0.01 nm). The sub-channel number increases with carrier frequency. (b) Measured EVMm for each sub-channel and transmission over different distances. (c) Measured constellation diagrams for sub-channels 1 and 8 of the PDM-QPSK experiment. (d) Spectrum of the superchannel derived from a 18.5 GHz comb with 18 GBd PDM-16-QAM (RBW 0.01 nm). (e-f) Measured EVMm and BER for each sub-channel and transmission over different distances. (g) Measured constellation diagrams for sub-channel 8 of the PDM-16-QAM experiment.

This is among the highest values achieved for 16-QAM in terabit/s superchannels. In Figure 6.3(g) the constellation diagram of the central sub-channel 8 in two polarisations is shown. Note that the smaller noise clouds as compared to Figure 6.3(c) (QPSK) for the same sub-channel is a direct consequence of the higher power level of the flattened comb lines in the 16-QAM case, which yields a higher OSNR of all sub-channels.

6.2.2.3 Terabit/s Superchannels with a 20 GHz Comb

A more robust superchannel can be generated by increasing the guard band. Therefore, the line spacing of the comb is increased to 20 GHz (see spectrum in Figure 6.1(b)), while keeping the same symbol rate at the Nyquist-Tx. Again, 15 comb lines are selected, 13 of which are flattened to the same power level as in the 18.5 GHz experiment for better comparison. The outermost carriers do not reach this power level and hence their performance drops below that of the inner 13 carriers. This can be seen in the spectrum as well as in the EVMm results for QPSK modulation shown in Figure 6.4(a) and (b). Taking into account the inner 13 sub-channels, the superchannel aggregate data rate amounts to 0.936 Tb/s, with a (net) spectral efficiency of 3.6 bit/s/Hz (3.3 bit/s/Hz).

Selected constellations diagrams of the B2B experiments are displayed in Figure 6.4(c). Two sub-channels are compared, one at the edge of the comb (sub-channel 1, also representative for sub-channel 15), and the central sub-channel 8 (representative for sub-channels 2 to 14). Sub-channels 1 and 15 suffer from low carrier power and therefore from a small OCNR. However, the central sub-channels 2 to 14 have an EVMm which is slightly better than that of the corresponding sub-channels of the 18.5 GHz experiment. This can be attributed to the larger guard band that reduces inter-channel interference originating from imperfect Nyquist pulse shaping.

This fact becomes even more evident when comparing the 16-QAM 20 GHz comb experiment (Figure 6.4(d)–(f)) with the 18.5 GHz comb experiment in Figure 6.3(d)–(f). In this case, 6 (2) sub-channels are better than the 7% (20%) FEC limit after 150 km of fibre transmission. The aggregate data rate amounts to 1.152 Tb/s. The (net) spectral efficiency amounts to 7.2 bit/s/Hz (6.5 bit/s/Hz). These results must be compared to the case of the 18.5 GHz comb and illustrate the trade-off between

superchannel capacity and reach: For a comparable capacity, 9 sub-channels are used, but only 2 (7) were better than the 7% (20%) FEC limit after transmission over 150 km. Therefore, it can be concluded that transmission with the 20 GHz comb has the larger capacity for a reach.

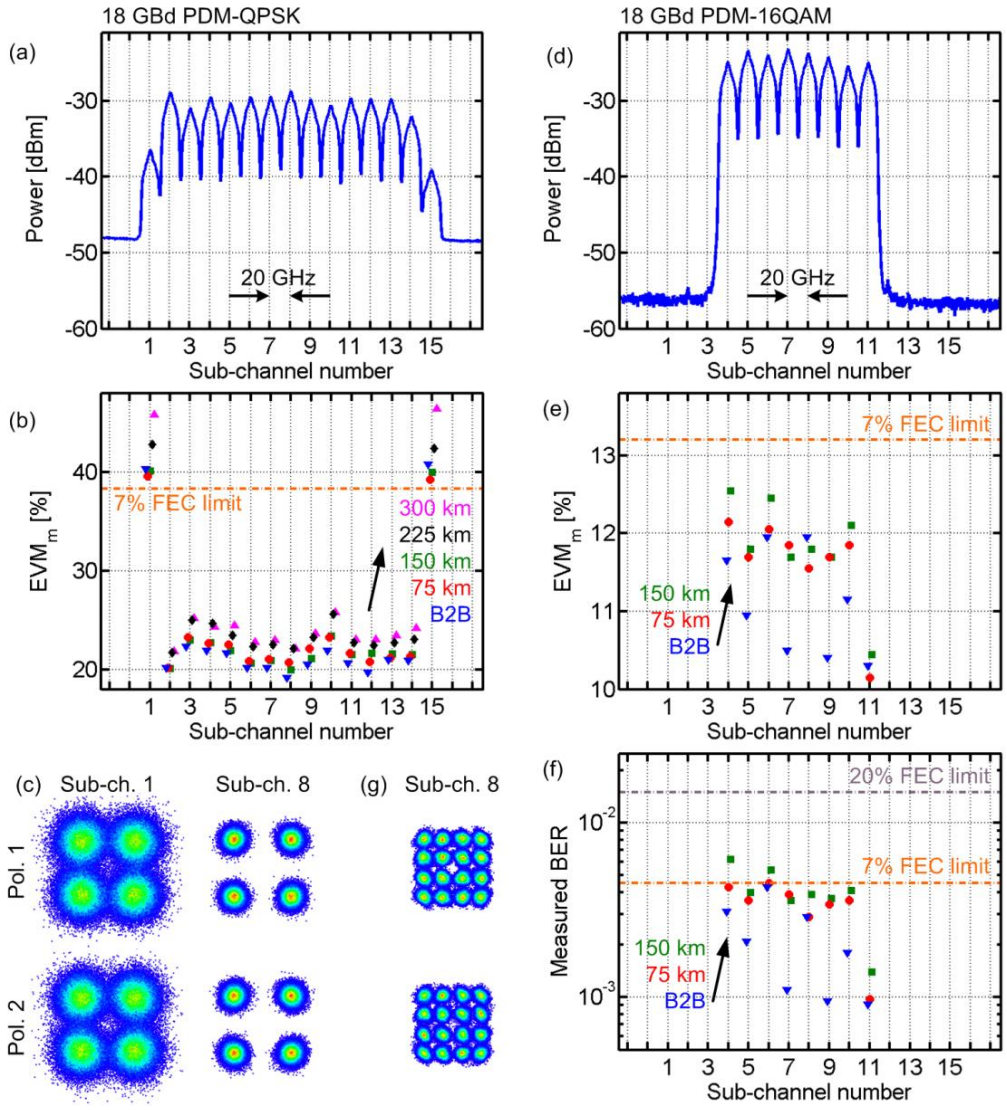

Figure 6.4. Spectra, signal quality and constellations for superchannel transmission with a 20 GHz comb. Left column for QPSK, right column for 16-QAM. (a) Spectrum of the superchannel derived from a 20 GHz comb with 18 GBd PDM-QPSK modulation (RBW 0.01 nm). The sub-channel number increases with carrier frequency. (b) Measured EVMm for each sub-channel and transmission over different distances. (c) Measured constellation diagrams for sub-channels 1 and 8 of the PDM-QPSK experiment. (d) Spectrum of the superchannel derived from a 20 GHz comb with 18 GBd PDM-16-QAM (RBW 0.01 nm). (e-f) Measured EVMm and BER for each sub-channel and transmission over different distances. (g) Measured constellation diagrams for sub-channel 8 of the PDM-16-QAM experiment.

In Figure 6.4(g), the constellation diagram of the central sub-channel 8 in two polarisations is showed. The smaller noise clouds as compared to Figure 6.4(c)

(QPSK) for the same sub-channel follow from the higher power level of the flattened comb (see Figure 6.3(c) and (g)).

6.2.2.4 Terabit/s Superchannels with a 12.5 GHz Comb

In a last set of experiments, the tuneability of the GSCS is utilised by adapting the line spacing and centre frequency to the 12.5 GHz ITU-grid (see spectrum in Figure 6.1(d)). This enables the use of a commercial fixed interleaver to separate odd and even sub-carriers. The interleaver exhibits an excellent extinction of the odd carriers in the path of the even carriers, and vice versa. The programmable filter is then used for equalisation only.

For the QPSK experiments, the same equalisation level as for the 18.5 GHz and the 20 GHz comb is used, while reducing the symbol rate to 12 GBd. This leads to 24 sub-channels with EVMm values well below the 7% FEC limit (see Figure 6.5(a) for the superchannel spectrum and Figure 6.5(b) for the EVMm results). The four outermost channels do not reach the power level which was used for flattening, and hence show performance degradation. The aggregate capacity of this superchannel is 1.152 Tb/s, and the (net) spectral efficiency amounts to 3.8 bit/s/Hz (3.6 bit/s/Hz). Figure 6.5(c) shows selected constellation diagrams for the QPSK experiment in the B2B case. The constellation diagrams represent peripheral (example: sub-channel 1) and central sub-channels (example: sub-channel 12), respectively.

Finally, the superchannel aggregate line rate is boosted to 2.112 Tb/s by increasing the equalisation level and by admitting the weak outer comb lines, too. This enables 16-QAM modulation on 20 sub-channels in the centre, while 4 of the outer sub-channels still enable QPSK operation below the 7% FEC threshold, see Figure 5(d)–(f). The aggregate net data rate amounts to 1.839 Tb/s with a net spectral efficiency of 6.1 bit/s/Hz for transmission over 300 km. Figure 6.5(g) shows the PDM-16-QAM constellation diagram of a central 16-QAM sub-channel.

Comparing the performance of the individual sub-channels for both superchannels with the 12.5 GHz GSCS it is possible to observe a slight reduction of the EVMm and the BER with increasing sub-channel number. This performance dependence on the sub-channel number seems to be correlated with the variations of the OCNR of the comb lines as shown in Figure 6.1(d). Note that, also the 18.5 GHz GSCS exhibits strong variations of the OCNR, but they do not seem to be correlated with the

respective EVMm. In contrast to operation at a symbol rate of 12 GBd, the cut-off frequency of the anti-aliasing filters becomes effective at the present symbol rate of 18 GBd (as explained in Section 6.3), and this dominates the OCNR-related performance degradation.

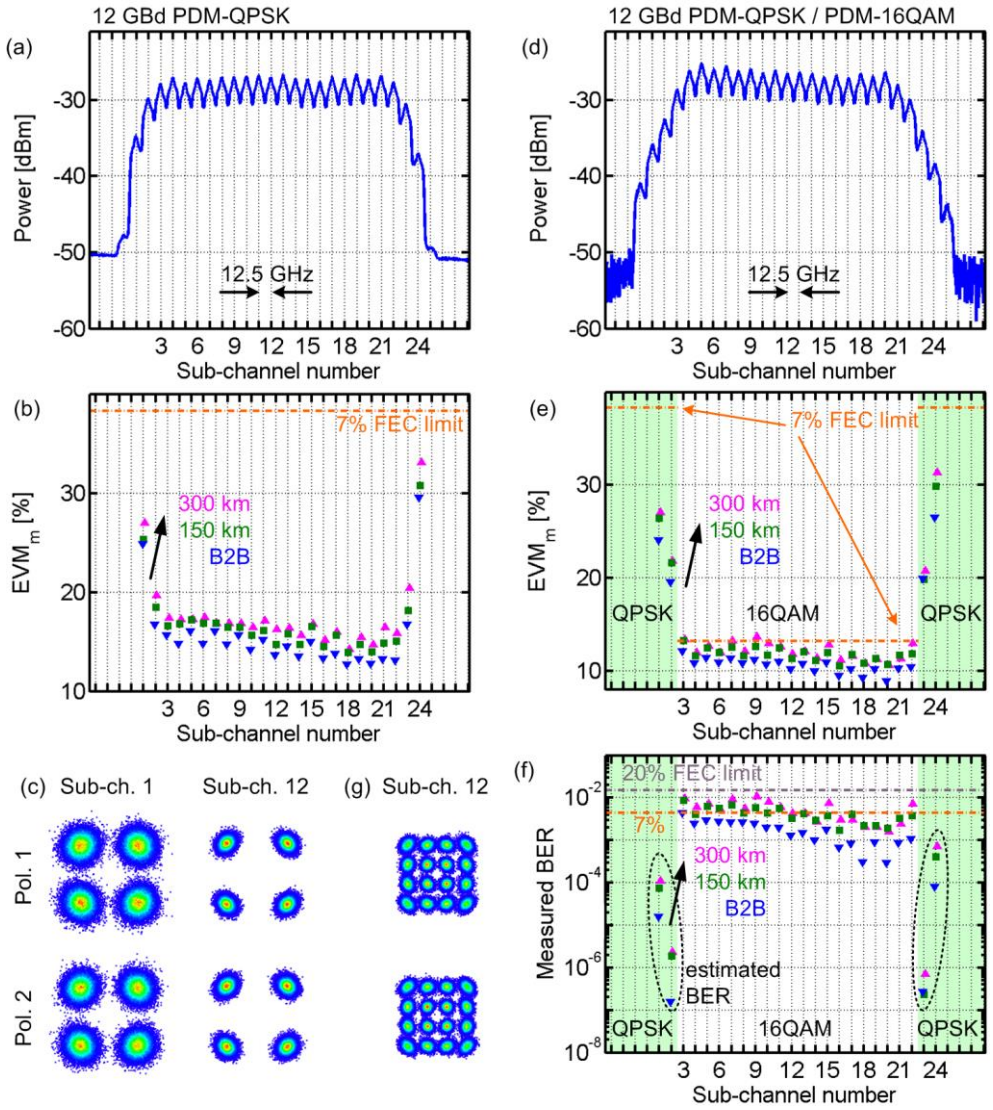

Figure 6.5. Spectra, signal quality and constellations for superchannel transmission with a 12.5 GHz comb. Left column for QPSK, right column for mixed QPSK / 16-QAM. (a) Spectrum of the superchannel derived from a 12.5 GHz comb with 12 GBd PDM-QPSK modulation (RBW 0.01 nm). The sub-channel number increases with carrier frequency. (b) Measured EVMm for each sub-channel and transmission over different distances. (c) Constellation diagrams for the sub-channels 1 and 12. (d) Spectrum of the superchannel derived from a 12.5 GHz comb with 12 GBd PDM-16-QAM (RBW 0.01 nm). (e-f) Measured EVMm and BER for 12 GBd PDM-16-QAM on the inner comb lines (white background) and PDM-QPSK on the outer lines (green background), again for different propagation distances. (g) Measured constellation diagrams for sub-channel 12 of the PDM-QPSK / PDM-16-QAM experiment.

6.2.3 Comparison with Previous Tb/s Experiments using Chip-Scale Comb Sources

For chip-scale integration of a Tb/s transmitter module using an optical frequency comb source it is desirable to co-integrate the comb source together with filters and modulators. In this section a comparison of comb generation concepts that have the potential for chip-scale integration, and were already used for Tb/s superchannel transmission, is presented.

Besides the GSCS, several coherent terabit/s data transmission schemes employing other frequency comb generator were previously demonstrated. Some demonstrations use electro-optic modulators that can, for example, be integrated on a silicon-on-insulator chip [13]. Other techniques employ Kerr frequency comb generation in a nonlinear high-Q silicon nitride microresonator [15]. Table 6.2 summarises key parameters of these experiments, and compares them with the GSCS data. In lines 1 – 6 of the table, the results obtained from the same setup as shown in Figure 6.2 are summarised, using the same pulse shape and an identical symbol rate, namely Nyquist-WDM with a symbol rate of 18 GBd. In all these experiments, aggregate data rates of 1 Tb/s or more were achieved, using up to 20 spectral lines. The specified data relate only to those comb lines that were actually used for Tb/s transmission.

For all these comb sources, a line spacing of the order of 20 GHz was used, which allows both an easy dis-interleaving and a high spectral efficiency. For a data rate in the terabit range, either a PDM-QPSK format was used with 13 to 20 comb lines, or a PDM-16-QAM format with 8 or 9 lines. The GSCS shows very good comb uniformity at an acceptable average power level. With respect to the OCNR, the GSCS shows the good uniformity, but its average value is smaller than for the other two approaches. It has to be noted that all three comb sources listed in Table 6.2, lines 1 to 6, are not yet fully optimised. Further steps towards a hybrid or even a monolithic integration are currently being investigated, and performance improvements are to be expected for all comb generation concepts. For the case of the GSCS it is possible to monolithically integrate two lasers, where the master laser synchronises the slave laser by injecting light at the back facet of the slave, while the comb is collected from its front facet. This removes the need for a circulator and a polarisation controller as in Figure 6.1.

	Comb generator type	FSR [GHz]	Number of carriers	Aggregate data rate [Tb/s]	Ref.
1	GSCS	20	13	0.936	This work
2	GSCS	20	8	1.152	
3	GSCS	18.5	15	1.080	
4	GSCS	18.5	9	1.296	
5	Kerr comb	25	20	1.440	[15]
6	SOH modulator	25	9	1.152	[13]
7	Casc. $LiNbO_3$ Mod	6.48	20	1.2	[14]
8	2 PM in RFS	25	112	11.2	[6]
9	Parametric comb	6.25	1520	31.8	[18]
10	MLL+HNLF	12.5	325	32.5	[9]

Table 6.2. Comparison of frequency comb generators for Tb/s data transmission

The SOH comb generator is a promising approach, since it also allows for easy adjustment of centre frequency and line spacing of the comb. Moreover, the underlying modulators feature very low V_π and can thus generate a reasonably large number of comb lines with moderate RF driving powers. It has been shown in [13] that a dual-drive SOH modulator can be used to generate a flat comb with seven lines within 2 dB, whereas the data transmission results listed here still stem from a single-drive modulator. As with any modulator-based approach it is possible to achieve a higher number of lines either by cascading multiple modulators [14] or by placing the modulator(s) into a loop [6]. Lines 7 and 8 of Table 6.2 show the results obtained for frequency comb generation based on cascaded modulators. The former experiment relies on a multi-core transmission fibre and demonstrates net data rates of 1.12 Tb/s per core by using orthogonal frequency division multiplexing. The latter experiment used two cascaded phase modulators in a recirculating frequency shifter and shows transmission of an OFDM data stream over 640 km SSMF with a net capacity of 10 Tb/s.

The Kerr frequency comb listed in Table 6.2 suffers from large line-to-line power variations, which limit the number of available channels and hence the achievable data rate. In the future, this limitation can be overcome by generating so-called soliton combs. Soliton combs have recently been demonstrated with crystalline resonators [44], and evidence of soliton combs has been also found in silicon-nitride resonators [45]. Further advances in fabrication processes will also help in reducing the pump power.

The GSCS as well as the silicon-organic hybrid modulator-based comb generators present tuneable line spacing, which is fixed for Kerr frequency combs by design. On

the other hand, Kerr frequency combs can be very broad, and spectral line spacings can be in the order of hundreds of GHz, a range that is not easily accessible with other approaches.

For comparison, lines 8 to 10 of Table 6.2 give reference data on experiments that achieved multi-Tb/s data transmission. For the cases of lines 9 and 10, the experiments were conducted using parametric comb generators that exploit Kerr nonlinearities in optical fibres, as shown in [18] and [9] respectively. Using two interleaved 12.5 GHz combs generated by multi-stage parametric mixing, data transmission on 77 carriers was demonstrated. Extrapolating the performance of these carriers to the ensemble of 1520 carriers, a total data rate of 31.8 Tb/s was estimated. Previously, transmission of 32.5 Tb/s was demonstrated using 325 carriers generated by a solid state mode-locked laser along with spectral broadening in a highly nonlinear fibre. These experiments demonstrate the immense potential of parametric frequency comb generation in conventional systems consisting of discrete elements. Transferring this performance to chip-scale systems could, e.g., be achieved by using soliton Kerr frequency combs [45, 46].

6.3 Q-Dash Passive Mode-Locked Laser Source

6.3.1 FFH phase noise reduction for a 42 GHz Q-Dash PMLL

As shown in the previous section, a variety of optical comb sources can be used to provide Tb/s transmission. All above mentioned optical multicarrier sources exhibit low phase noise and linewidth, which is the enabling criterion for their utilisation in coherent systems. Although semiconductor mode-locked lasers provide several tens of comb lines with decent optical power per line, which potentially can be utilised for Tb/s superchannel generation, up to now WDM data transmission using these combs has been restricted to direct detection schemes. This is because the spectral modes of semiconductor MLL generally exhibit strong phase noise and broad optical linewidths, typically of the order of tens of MHz.

The coherent detection using Q-Dash PMLL is enabled with feed-forward heterodyne phase noise reduction scheme. The as-cleaved Q-Dash PMLL used in this work has a total length of 980 µm, corresponding to repetition frequencies, hence channel mode spacings, of 42 GHz. The active region consists of six layers of InAs quantum

dashes emitting at 1550 nm, separated by InGaAsP barriers in a dash-in-a-barrier design [47]. A buried ridge waveguide of 1.25 µm width confines the optical mode. Feedback is provided by the cleaved end facets of the Q-Dash PMLL. The Q-Dash PMLL is biased at a constant current of 338 mA, which is optimised for a narrow RF beatnote, i.e., 16 kHz, with minimal side peaks. The combination of large optical linewidth and a narrowband RF beatnote indicates a high correlation of the comb line's phases [48-51]. The output spectrum is depicted in Figure 6.6(a). Optical spectrum of the 42 GHz comb features a 3-dB bandwidth close to 1.4 THz and an average output power of 10 dBm. The FFH phase noise reduction scheme is illustrated in Figure 6.6(b). A small percentage of the power of the comb is tapped, and a single line is filtered out with field strength $E_S(t) = E_{S0}\exp\left(j\omega_S t + j\varphi_S(t)\right)$, frequency $f_S = \omega_S / 2\pi$ and phase noise $\varphi_S(t)$. The filtered signal is amplified and mixed with a narrow-linewidth local oscillator laser (Koheras) $E_{LO}(t) = E_{LO0}\exp\left(j\omega_{LO}t + j\varphi_{LO}(t)\right)$, with frequency $f_{LO} = \omega_{LO} / 2\pi$, that is tuned to an offset of $f_S - f_{LO} = -8$ GHz from the comb line. The electrical signal at the output of the band-pass filter is given as:

$$i(t) = RE_{S0}E_{LO0}\cos\left(\left(\omega_S - \omega_{LO}\right)t + \varphi_S(t) - \varphi_{LO}(t)\right). \tag{6.1}$$

where R is the responsivity of the balanced photodetector. The beat signal is fed to a Mach-Zehnder modulator that is biased at zero transmission point. If the field strength of Q-Dash PMLL is given as $E(t) = \sum_{n=-N}^{N} E_{n0}(t)\cos\left(\omega_n t + \varphi_n\right)$, where index n represents mode number from the Q-Dash PMLL, the output signal of the MZM is given as:

$$\begin{aligned}
E_{MZM}(t) &= \sum_{n=-N}^{N} E_{n0}(t)\cos\left(\omega_n t + \varphi_n\right)\times \\
&\times RE_{S0}(t)E_{LO0}(t)\cos\left(\left(\omega_S - \omega_{LO}\right)t + \varphi_S(t) - \varphi_{LO}(t)\right) \\
&= \sum_{n=-N}^{N}\frac{1}{2}RE_{n0}(t)E_{S0}(t)E_{LO0}(t)\cos\left[\left(\omega_n - \left(\omega_S - \omega_{LO}\right)\right)t + \varphi_n - \varphi_S(t) + \varphi_{LO}(t)\right] \\
&+ \sum_{n=-N}^{N}\frac{1}{2}RE_{n0}(t)E_{S0}(t)E_{LO0}(t)\cos\left[\left(\omega_n + \left(\omega_S - \omega_{LO}\right)\right)t + \varphi_n + \varphi_S(t) - \varphi_{LO}(t)\right]
\end{aligned} \tag{6.2}$$

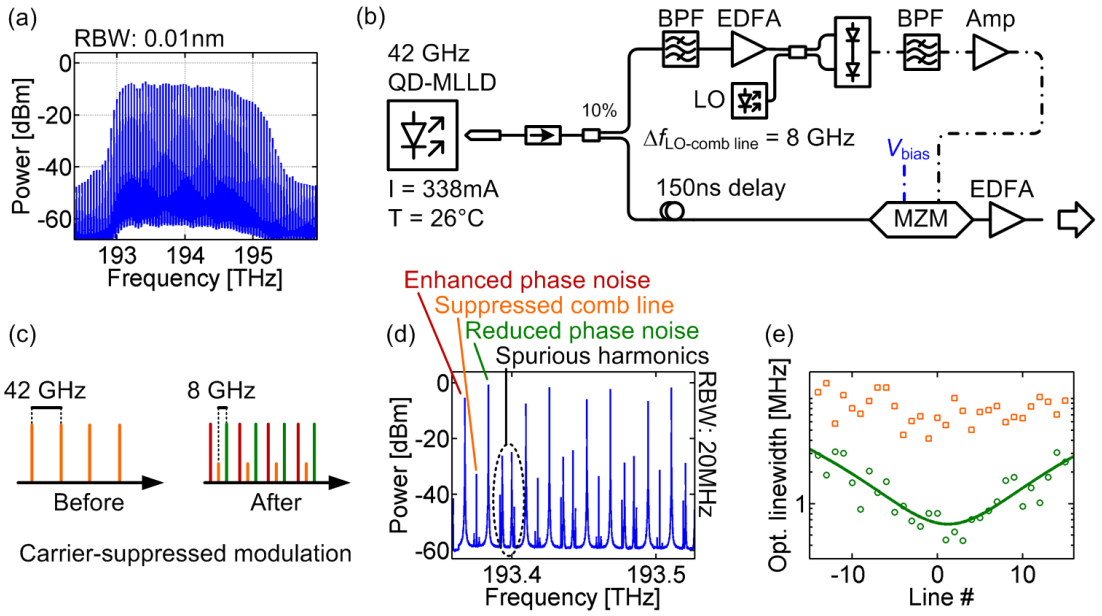

Figure 6.6. Setup for feed-forward heterodyne phase noise reduction. (a) Optical spectrum of the 42 GHz comb. (b) Experimental setup. (c) The upper sidemode (green line) exhibits reduced phase noise while the lower sidemode (red line) features enhanced phase noise. (d) Optical spectrum of the output from the FFH-scheme showing pairs of lines surrounding the suppressed comb line. (e) Result of the heterodyne optical linewidth measurement for the original comb lines (orange) and the lines with reduced phase noise at the output of the FFH-scheme (green). Line # 0 corresponds to the comb line that is mixed with the offset LO and is used to generate the MZM drive signal.

From Eq. 6.2, it can be seen that the signal from the output of the MZM contains two sidemodes at ±8 GHz while suppressing the original comb line, which is illustrated in Figure 6.6(c). Furthermore, it is shown in Eq. 6.2 that the upper sidemode (green lines in Figure 6.6(c) and (d)) exhibits reduced phase noise, whilst the lower sidemode (red lines in Figure 6.6(c) and (d)) exhibits increased phase noise [29]. Note that other offset frequencies could be chosen, too. In this setup 8 GHz represented the best trade-off between a high offset to allow separating the two sidebands and a low offset to not run into bandwidth limitations of the equipment. The optical linewidth reduction is confirmed through a direct measurement (see Figure 6.6(e)). The measurement was performed by beating each line with a narrow-linewidth laser and evaluating the width of the beat signal with a RF spectrum analyser, after the optical signal was detected by fast photodiode [52]. The FFH scheme reduces the optical linewidth for all 30 modes that have been tested. For the centre modes, the resulting linewidth is below 1 MHz, which is sufficiently low for applications in coherent data transmission with current digital signal processing. Typical linewidth requirements for a QPSK signal, considering a symbol rate of 18

GBd, are 3.8 MHz [53] or 7.4 MHz [54], depending on the complexity of the receiver implementation.

6.3.2 Coherent Terabit Data Transmission Employing FFH Phase-Noise Reduction

After FFH phase noise reduction, the frequency comb exhibits pairs of lines that correspond to the upper and lower modulation sidemode, as shown in Figure 6.6(c). For data transmission the upper sidemodes (green lines) which feature the reduced phase noise are used. Figure 6.7(a) shows an experimental setup of the WDM data transmission testbed used. The upper sidemodes are filtered and dis-interleaved into odd and even carriers using a Finisar WS while the lower sidemodes are suppressed. After dis-interleaving, the even and odd carriers are modulated with 18 GBd sinc-shaped QPSK signals using a pseudo-random bit sequence of length 2^{11}-1. The signals are combined and either tested in a B2B configuration, or amplified and sent through a 75 km of SSMF. The receiver comprises filters, a pre-amplifier and an optical modulation analyser (OMA, Keysight N4391A) that uses a coherent detection scheme with an ECL as LO. The quality of the received signal is evaluated using the signal offline processing which includes digital brick-wall filtering, dispersion compensation, and adaptive equalisation before evaluating the BER. Figure 6.7(b) shows constellation diagrams with and without using the FFH scheme for the case of line # 0. The reduction of the phase error can be seen clearly.

Figure 6.7(c) shows the dis-interleaved comb spectra. The suppression of the lower, unwanted sidemode was achieved by narrowing the bandwidth of the programmed filters, which unfortunately also leads to an additional attenuation for some of the carriers due to the inherent interpolation of the filter shape in the WS, where each pixel covers a frequency range of about 5 GHz. By replacing the MZM in the FFH scheme with an IQ modulator driven as a frequency shifter, only a single sidemode would be generated. The spectrum of the modulated comb is depicted in Figure 6.7(d) for the B2B case. It comprises 30 channels, which corresponds to a data rate of 1.08 Tb/s. The average OSNR of the channels at the receiver (input to the 0.6nm filter) is 26.4 dB for the B2B case and 25.0 dB after 75 km fibre transmission. BER results for B2B and 75 km are depicted in Figure 6.7(e). For B2B, all 30 channels are below the BER threshold for a standard 7% FEC, corresponding to a net data rate of

1 Tb/s. After transmission, the channel 14 exceeds the FEC limit, resulting in 29 channels within the 7% FEC limit. This corresponds to a net data rate of 0.971 Tb/s after transmission. The data rate could be doubled with polarisation multiplexing, which could not be tested in these experiments due to limited availability of hardware. Nevertheless, these results demonstrate that FFH phase-noise reduction can be used to simultaneously reduce the optical linewidth of a multitude of optical lines that are derived from one semiconductor Q-Dash PMLL, thereby enabling coherent data transmission experiment using a frequency comb from a Q-Dash PMLL.

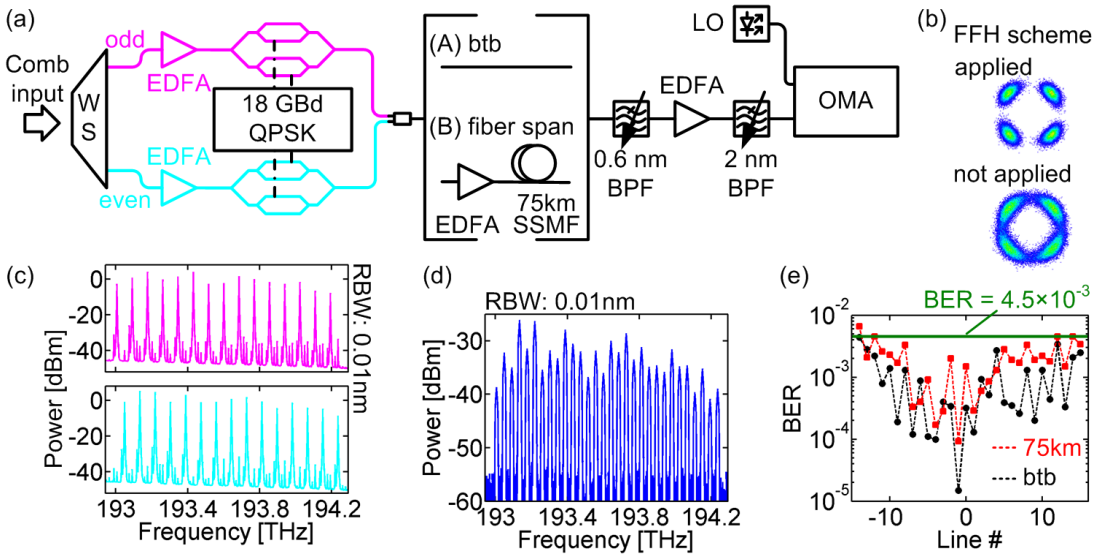

Figure 6.7. Setup for WDM data transmission and measured results. (a) Experimental setup. (b) Constellation diagrams obtained with and without the FFH-scheme. (c) Spectra of odd (top) and even (bottom) comb lines after dis-interleaving. (d) Optical spectrum of the 30 data channels. (e) BER results for 30 channels when applying the FFH-scheme.

6.4 Conclusion

In summary, it is shown that GSCSs are well suited for Tb/s superchannel generation. Six different superchannel architectures with different carrier spacings and modulation formats are investigated, and their performance for transmission over different distances is evaluated. The highest (net) spectral efficiency of 7.8 bit/s/Hz (6.5 bit/s/Hz) is obtained for a GSCS with a carrier spacing of 18.5 GHz using 18 GBd PDM-16-QAM, transmitted over 150 km. The data capacity transmitted over 300 km of SSMF can be increased to 2.112 Tb/s (1.839 Tb/s) by reducing the line spacing along with the symbol rate and by adapting the modulation format to the OSNR performance of the respective sub-channel. Finally, a comparison between optical

frequency comb sources that are suitable for terabit/s superchannel systems, and could be hybridly or monolithically integrated into a chip-scale transmitter module, is presented.

Furthermore, a FFH scheme that enables simultaneous optical linewidth reduction of a multitude of comb lines derived from a Q-Dash PMLL is presented. The scheme enables the coherent transmission experiment using Q-Dash PMLL as an optical source, even though this optical multicarrier source exhibit linewidth higher than 10 MHz. Net data rates of nearly 1 Tb/s could be achieved within the limits of standard FEC.

References

[1] P. Winzer, “Beyond 100G Ethernet”, IEEE Communication Magazine vol. 48, no. 7, pp. 26–30, Jul. 2010.

[2] C. R. Cole, “100-Gb/s and beyond transceiver technologies”, Optical Fiber Technology, vol. 17, no. 5, pp. 472 – 479, Sep. 2011.

[3] S. Gringeri, E. Basch, T. Xia, “Technical considerations for supporting data rates beyond 100 Gb/s”, IEEE Communations Magazine, vol. 50, no. 2, s21–s30, Feb. 2012.

[4] W. Shieh, I. Djordjevic, “OFDM for Optical Communications”, Elsevier Academic Press, Sep. 2009.

[5] D. Hillerkuss, R. Schmogrow, T. Schellinger, M. Jordan, M. Winter, G. Huber, T. Vallaitis, R. Bonk, P. Kleinow, F. Frey, M. Roeger, S. Koenig, A. Ludwig, A. Marculescu, J. Li, M. Hoh, M. Dreschmann, J. Meyer, B. Ezra, S., N. Narkiss, B. Nebendahl, F. Parmigiani, P. Petropoulos, B. Resan, A. Oehler, K. Weingarten, T. Ellermeyer, J. Lutz, M. Moeller, M. Huebner, J. Becker, C. Koos, W. Freude, J. Leuthold, “26 $Tbits^{-1}$ line-rate super-channel transmission utilizing all-optical fast Fourier transform processing”, Nature Photonics, vol 5, pp. 364–371, May 2011.

[6] J. Yu, Z. Dong, J. Zhang, X. Xiao, H.-C. Chien, N. Chi, “Generation of coherent and frequency-locked multi-carriers using cascaded phase modulators for 10 Tb/s optical transmission system”, Journal of Lightwave Technology, vol. 30, no. 4, pp. 458–465, Feb. 2012.

[7] H.-C. Chien, J. Yu, Z. Jia, Z. Dong, X. Xiao, “Performance assessment of noise-suppressed Nyquist-WDM for terabit superchannel transmission”, Journal of Lightwave Technology, vol. 30, no. 24, pp. 3965–3971, Dec. 2012.

[8] R. Schmogrow, M. Winter, M. Meyer, D. Hillerkuss, S. Wolf, B. Baeuerle, A. Ludwig, B. Nebendahl, S. Ben-Ezra, J. Meyer, M. Dreschmann, M. Huebner, J. Becker, C. Koos, W. Freude, J. Leuthold, “Real-time Nyquist pulse generation beyond 100 Gbit/s and its relation to OFDM”, Optics Express, vol. 20, no. 1, pp. 317–337, Jan. 2012.

[9] D. Hillerkuss, R. Schmogrow, M. Meyer, S. Wolf, M. Jordan, P. Kleinow, N. Lindenmann, P. Schindler, A. Melikyan, X. Yang, S. Ben-Ezra, B. Nebendahl,

M. Dreschmann, J. Meyer, F. Parmigiani, P. Petropoulos, B. Resan, A. Oehler, K. Weingarten, L. Altenhain, T. Ellermeyer, M. Moeller, M. Huebner, J. Becker, C. Koos, W. Freude, J. Leuthold, “Single-Laser 32.5 Tbit/s Nyquist WDM Transmission”, Journal of Optical Communications and Networking, vol. 4, no.10, pp. 715–723, Oct. 2012.

[10] G. Bosco, V. Curri, A. Carena, P. Poggiolini, F. Forghieri, “On the performance of Nyquist-WDM terabit superchannels based on PM-BPSK, PM-QPSK, PM-8QAM or PM-16QAM subcarriers”, Journal of Lightwave Technology, vol. 29, no. 1, pp. 53–61, Dec. 2011.

[11] Y.-K. Huang, E. Mateo, M. Sato, D. Qian, F. Yaman, T. Inoue, Y. Inada, S. Zhang, Y. Aono, T. Tajima, T. Ogata, Y. Aoki, “Real-time transoceanic transmission of 1-Tb/s Nyquist superchannel at 2.86-b/s/Hz spectral efficiency”, in Proc. Asia Communications and Photonics Conference, Guangzhou, China, paper PAF4C.2, Nov. 2012.

[12] X. Liu, D. Gill, S. Chandrasekhar, L. Buhl, M. Earnshaw, M. Cappuzzo, L. Gomez, Y. Chen, F. Klemens, E. Burrows, Y.-K. Chen, R. Tkach, “Multi-carrier coherent receiver based on a shared optical hybrid and a cyclic AWG array for terabit/s optical transmission”, IEEE Photonics Journal, vol. 2, no. 3, pp. 330–337, Jun. 2010.

[13] C. Weimann, P. C. Schindler, R. Palmer, S. Wolf, D. Bekele, D. Korn, J. Pfeifle, S. Koeber, R. Schmogrow, L. Alloatti, D. Elder, H. Yu, W. Bogaerts, L. R. Dalton, W. Freude, J. Leuthold, C. Koos, “Silicon-organic hybrid (SOH) frequency comb sources for terabit/s data transmission”, Optis Express, vol. 22, no. 3, pp. 3629–3637, Feb. 2014.

[14] X. Liu, S. Chandrasekhar, X. Chen, P. J. Winzer, Y. Pan, T. F. Taunay, B. Zhu, M. Fishteyn, M. F. Yan, J. M. Fini, E. Monberg, F. Dimarcello, “1.12-Tb/s 32-QAM-OFDM superchannel with 8.6-b/s/Hz intrachannel spectral efficiency and space-division multiplexed transmission with 60-b/s/Hz aggregate spectral efficiency”, Optics Express vol. 19, no. 26, pp. B958–B964, Dec. 2011.

[15] J. Pfeifle, V. Brasch, M. Lauermann, Y. Yu, D. Wegner, T. Herr, K. Hartinger, P. Schindler, J. Li, D. Hillerkuss, R. Schmogrow, C. Weimann, R. Holzwarth, W. Freude, J. Leuthold, T. J. Kippenberg, C. Koos, “Coherent terabit communications

with microresonator Kerr frequency combs", Nature Photonics, vol. 8, pp. 375–380, Apr. 2014.

[16] A. Gnauck, B. Kuo, E. Myslivets, R. Jopson, M. Dinu, J. Simsarian, P. Winzer, S. Radic, "Comb-based 16-QAM transmitter spanning the C and L bands", IEEE Photonics Technology Letters, vol. 26, no. 8, pp. 821–824, Apr. 2014.

[17] E. Temprana, V. Ataie, B. P.-P. Kuo, E. Myslivets, N. Alic, S. Radic, "Low-noise parametric frequency comb for continuous C-plus-L-band 16-QAM channels generation", Optics Express, vol. 22, no. 6, pp. 6822–6828, Mar. 2014.

[18] V. Ataie, E. Temprana, L. Liu, Y. Myslivets, P. P. Kuo, N. Alic, S. Radic, "Flex-grid compatible ultra wide frequency comb source for 31.8 Tb/s coherent transmission of 1520 UDWDM channels", in Proc. OFC/NFOEC, San Francisco, CA, USA, paper Th5B.7, Mar. 2014.

[19] A. Mishra, R. Schmogrow, I. Tomkos, D. Hillerkuss, C. Koos, W. Freude, and J. Leuthold, "Flexible RF-based comb generator", IEEE Photonics Technology Letters, vol. 25, no. 7, pp 701–704, Apr. 2013.

[20] D. Hillerkuss, T. Schellinger, M. Jordan, C. Weimann, F. Parmigiani, B. Resan, K. Weingarten, S. Ben-Ezra, B. Nebendahl, C. Koos, W. Freude, J. Leuthold, "High-quality optical frequency comb by spectral slicing of spectra broadened by SPM", IEEE Photonics Journal, vol. 5, no. 5, pp. 7201011–7201011, Oct. 2013.

[21] R. Rosales, S. G. Murdoch, R.T. Watts, K. Merghem, A. Martinez, F. Lelarge, A. Accard, L. P. Barry, Abderrahim Ramdane, "High performance mode locking characteristics of single section quantum dash lasers", Optics Express, vol. 20, no. 8, pp. 8649-8657, Apr. 2012.

[22] R. Watts, R. Rosales, F. Lelarge, A. Ramdane, L. Barry, "Mode coherence measurements across a 1.5 THz spectral bandwidth of a passively mode-locked quantum dash laser", Optics Letters, vol. 37, no. 9, pp. 1499-1501, May 2012.

[23] T. Habruseva, S. O'Donoghue, N. Rebrova, F. Kéfélian, S. P. Hegarty, G. Huyet, "Optical linewidth of a passively mode-locked semiconductor laser", Optics Letters, vol. 34, no. 21, pp. 3307-3309, Nov. 2009.

[24] A. Akrout, A. Shen, R. Brenot, F. Van Dijk, O. Legouezigou, F. Pommereau, F. Lelarge, A. Ramdane, D. Guang-Hua, "Separate error-free transmission of eight

channels at 10 Gb/s using comb generation in a quantum-dash-based mode-locked laser", Photonics Technology Letters, vol. 21, no. 23, pp. 1746-1748, Dec. 2009.

[25] Y. B. M'Sallem, L. Quang Trung, L. Bramerie, N. Quoc-Thai, E. Borgne, P. Besnard, A. Shen, F. Lelarge, S. LaRochelle, L. A. Rusch, J.-C. Simon, "Quantum-dash mode-locked laser as a source for 56-Gb/s DQPSK modulation in WDM multicast applications", Photonics Technology Letters, vol. 23, no. 7, pp. 453-455, Apr. 2011.

[26] E. Sooudi, G. Huyet, J. G. McInerney, F. Lelarge, K. Merghem, R. Rosales, A. Martinez, A. Ramdane, S. P. Hegarty, "Injection-Locking Properties of InAs/InP-Based Mode-Locked Quantum-Dash Lasers at 21GHz", Photonics Technology Letters, vol. 23, no. 20, pp. 1544-1546, Oct. 2011.

[27] T. Pfau, R. Peveling, J. Hauden, N. Grossard, H. Porte, Y. Achiam, S. Hoffmann, S. K. Ibrahim, Member, O. Adamczyk, S. Bhandare, D. Sandel, M. Porrmann, R. Noé, "Coherent digital polarisation diversity receiver for real-time polarisation-multiplexed QPSK transmission at 2.8Gb/s", Photonics Technology Letters, vol. 19, no. 24, pp. 1988-1990, Dec. 2007.

[28] D. Lavery, R. Maher, M. Paskov, B. C. Thomsen, P. Bayvel, S. J. Savory, "Digital Coherence Enhancement Enabling 6GBd DP-64QAM Using a 1.4MHz Linewidth Laser", Photonics Technology Letters, vol. 25, no. 22, 2213-2216, Nov. 2013.

[29] R. Watts, S. G. Murdoch, L. Barry, "Spectral linewidth reduction of single-mode and mode-locked lasers using a feed-forward heterodyne detection scheme", in Proc. CLEO, San Jose, CA, USA, paper, STh3O.8, Jun. 2014.

[30] P. M. Anandarajah, R. Zhou, R. Maher, D. M. G. Pascual, F. Smyth, V. Vujicic, L. Barry, "Flexible optical comb source for super channel systems", in Proc. OFC/NFOEC, LA, CA, USA, paper OTh3I.8, Mar. 2013.

[31] R. Zhou, S. Latkowski, J. O'Carroll, R. Phelan, L. P. Barry, and P. Anandarajah, "40nm wavelength tunable gain-switched optical comb source", Optics Express, vol. 19, no. 26, B415–B420, Dec. 2011.

[32] P. M. Anandarajah, R. Zhou, R. Maher, D. Lavery, M. Paskov, B. Thomsen, S. Savory, L. P. Barry, "Gain-switched multicarrier transmitter in a long-reach UDWDM PON with a digital coherent receiver", Optics Letters, vol. 38, no. 22, pp. 4797–4800, Nov. 2013.

[33] R. Zhou, P. Anandarajah, R. Maher, M. Paskov, D. Lavery, B. Thomsen, S. Savory, L. Barry, “80-km coherent DWDM-PON on 20-GHz grid with injected gain switched comb source”, Photonics Technology Letters, vol. 26, no. 4, pp. 364–367, Feb. 2014.

[34] P. M. Anandarajah, R. Maher, Y. Xu, S. Latkowski, J. O’Carroll, S. G. Murdoch, R. Phelan, J. O’Gorman, L. Barry, “Generation of coherent multicarrier signals by gain switching of discrete mode lasers”, IEEE Photonics Journal, vol. 3, no. 1, pp. 112–122, Feb. 2011.

[35] G. Yabre, H. de Waardt, H. P. A. Van den Boom, and G.-D. Khoe, “Noise characteristics of single-mode semiconductor lasers under external light injection”, IEEE Journal of Quantum Electronics, vol. 36, no. 3, pp. 385–393, Mar. 2000.

[36] R. Zhou, T. N. Huynh, V. Vujicic, P. M. Anandarajah, L. P. Barry, “Phase noise analysis of injected gain switched comb source for coherent communications”, Optics Express, vol. 22, no. 7, pp. 8120–8125, Apr. 2014.

[37] R. Zhou, P. M. Anandarajah, D. G. Pascual, J. O’Carroll, R. Phelan, B. Kelly, and L. P. Barry, “Monolithically integrated 2-section lasers for injection locked gain switched comb generation”, in Proc. OFC/NFOEC, San Francisco, CA, USA, paper Th3A.3, Mar. 2014.

[38] R. Schmogrow, D. Hillerkuss, M. Dreschmann, M. Huebner, M. Winter, J. Meyer, B. Nebendahl, C. Koos, J. Becker, W. Freude, J. Leuthold, “Real-time software-defined multiformat transmitter generating 64QAM at 28 GBd”, Photonics Technology Letters, vol. 22, no. 21, pp. 1601–1603, Nov. 2010.

[39] P. Winzer, A. Gnauck, A. Konczykowska, F. Jorge, J.-Y. Dupuy, “Penalties from in-band crosstalk for advanced optical modulation formats,” in Proc. ECOC, Geneva, Switzerland, paper Tu.5.B.7, Sep. 2011.

[40] R. M. Schmogrow, “Real-time Digital Signal Processing for Software-defined Optical Transmitters and Receivers”, KIT Scientific Publishing, 2013.

[41] R. Schmogrow, B. Nebendahl, M. Winter, A. Josten, D. Hillerkuss, S. Koenig, J. Meyer, M. Dreschmann, M. Huebner, C. Koos, J. Becker, W. Freude, J. Leuthold, “Error vector magnitude as a performance measure for advanced modulation formats”, Photonics Technology Letters, vol. 24, no. 1, pp. 61 –63, Jan. 2012. Correction: vol. 24, 2198 (2012).

[42] F. Chang, K. Onohara, T. Mizuochi, “Forward error correction for 100 G transport networks”, IEEE Communications Magazine, vol. 48, no. 3, pp. S48–S55, Mar. 2010.

[43] B. Li, K. J. Larsen, D. Zibar, I. T. Monroy, “Over 10 dB net coding gain based on 20% overhead hard decision forward error correction in 100G optical communication systems,” in Proc. ECOC, Geneva, Switzerland, paper Tu.6.A.3, Sep. 2011.

[44] T. Herr, V. Brasch, J. D. Jost, C. Y. Wang, N. M. Kondratiev, M. L. Gorodetsky, T. J. Kippenberg, “Temporal solitons in optical microresonators”, Nature Photonics vol. 8, pp. 145–152, 2014.

[45] V. Brasch, T. Herr, M. Pfeiffer, J. Jost, T. Kippenberg, “Temporal soliton generation in chip-based silicon nitride microresonators,” in Proc. CLEO, San Jose, CA, USA, paper FTh1D.1, Jun 2014.

[46] J. Pfeifle, A. Kordts, P. Marin, M. Karpov, M. Pfeiffer, V. Brasch, R. Rosenberger, J. Kemal, S. Wolf, W. Freude, T. Kippenberg, C. Koos, “Full C and L-Band Transmission at 20 Tbit/s Using Cavity-Soliton Kerr Frequency Combs”, in Proc. CLEO, San Jose, CA, USA, paper JTh5C.8, May 2015.

[47] F. Lelarge, B. Dagens, J. Renaudier, R. Brenot, A. Accard, F. van Dijk, D. Make, O. Le Gouezigou, J.-G. Provost, F. Poingt, J. Landreau, O. Drisse, E. Derouin, B. Rousseau, F. Pommereau, G.-H. Duan, “Recent advances on InAs/InP quantum dash based semiconductor lasers and optical amplifiers operating at 1.55 μm”, Journal of Selected Topics on Quantum Electronics, vol. 13, no. 1, pp. 111-124, Jan/Feb2007.

[48] R. Maldonado-Basilio, S. Latkowski, F. Surre, P. Landais, “Linewidth analysis of 40-GHz passively mode-locked multi-mode semiconductor lasers”, Optics Communications, vol. 283, no. 2, pp. 299-303, Jan. 2010.

[49] R. Maldonado-Basilio, J. Parra-Cetina, S. Latkowski, P. Landais, “Timing-jitter, optical, and mode-beating linewidths analysis on subpicosecond optical pulses generated by a quantum-dash passively mode-locked semiconductor laser”, Optics Letters, vol. 35, no. 8, pp. 1184-1186, Apr. 2010.

[50] R. Maldonado-Basilio, S. Latkowski, S. Philippe, P. Landais, “40 GHz mode-beating with 8 Hz linewidth and 64 fs timing jitter from a synchronized mode-locked quantum-dash laser diode”, Optics Letters, vol. 36, no. 16, pp. 3142-3144, Aug. 2011.

[51] K. Merghem, C. Calò, R. Rosales, X. Lafosse, G. Aubin, A. Martinez, F. Lelarge, A. Ramdane “Stability of Optical Frequency Comb Generated With InAs/InP Quantum-Dash-Based Passive Mode-Locked Lasers,” IEEE Journal of Quantum Electronics, vol. 50, no. 4, pp. 275-280, Apr. 2014.

[52] D. Derickson, “Fiber optic test and measurement,” Upper Saddle River, NJ: Prentice Hall, Vol. 1. 1998.

[53] E. Ip, J. M. Kahn, “Feedforward Carrier Recovery for Coherent Optical Communications”, Journal of Lightwave Technology, vol. 25, no. 9, pp. 2675 – 2692, Sep. 2007.

[54] T. Pfau, S. Hoffmann, R. Noé, “Hardware-Efficient Coherent Digital Receiver Concept with Feedforward Carrier Recovery for M-QAM Constellations”, Journal of Lightwave Technology, vol. 27, no. 8, pp. 989-999, Apr. 2009.

Chapter 7

7 Conclusions and Future Work

7.1 Conclusion

The increasing number of broadband connections causes continuous growth of total IP traffic. Starting from the 1980's, the capacity of commercial optical systems has increased more than five orders of magnitude. For more than three decades the capacities of installed optical systems exceeded the network traffic requirements, mainly due to the extraordinary scalability of WDM technology that has been successfully used to expand capacity in optical systems and meet increasing bandwidth requirements since the early 1990's. Nevertheless, the rapid growth of network traffic driven by media-rich applications such as on–demand HDTV, Voice over IP, video conferencing, social networking and online gaming, inverted this situation and current trends show faster growing network traffic than system capacity.

To cope with this problem and enable faster growing system capacity, optical coherent communications were revived, which triggered the employment of advanced modulation formats. Very efficient utilisation of the available spectral bandwidth was enabled with the introduction of OFDM and Nyquist WDM modulation techniques in optical communication systems. Since guard bands in highly spectrally efficient systems are minimised, a strict requirements on the performance of optical sources, especially frequency stability, has been created. Promising solutions are optical multicarrier sources which simultaneously generate multiple phase correlated optical carriers.

In this thesis, a number of optical multicarrier sources have been presented and analysed, with special focus on semiconductor mode-locked lasers and gain-switched comb sources. High capacity and spectrally efficient optical systems for short and medium reach applications (from 3 km up to 300 km), based on optical frequency combs as optical sources, advanced modulation formats (*m*-QAM) and modulation techniques (OFDM and Nyquist WDM) have been proposed and presented. Also,

certain optoelectronic devices (i.e. SOA) and techniques (FFH linewidth reduction scheme) have been utilised to enable the desired system performance.

Optical Multicarrier based Access Optical Networks and Data Centre Interconnects

The characterisation of the semiconductor MLL, the electro-optical modulation based comb source and the externally injected GSCS is given in Chapter 3. Also, their performance in B2B IM/DD OFDM systems is analysed experimentally and verified by simulations. RIN and OCNR have been recognised as limiting parameters for the system performance. Optical multicarrier sources should have RIN lower that -110 dB/Hz and OCNR higher than 35 dB to assure decent system performance.

In Chapter 4, an optical access network employing semiconductor MLL as an optical source and SSB-OFDM modulation is proposed. Furthermore, an SOA is characterised and used to simultaneously amplify ten OFDM channels. Furthermore, the performance comparison with an EDFA shows that a ~4 dB penalty is incurred when the SOA is used at the maximum received power, though there is negligible extra penalty when operating at the 7% FEC limit.

Chapter 5 demonstrates Tb/s optical interconnect solutions based on Q-Dash PMLL sources and SSB-OFDM modulation. High capacity WDM optical links for interconnect applications within and between data centres are presented. Along with detailed characterisation of Q-Dash passively mode-locked lasers, the effect of RIN on the system performance is investigated. The maximum spectral efficiency achieved was 2.76 bit/s/Hz (single polarisation).

Optical Multicarrier Based Tb/s Coherently Detected Medium Reach Systems

Finally, a demonstration of Tb/s superchannel architectures using gain-switched comb sources in a coherently detected system is presented in Chapter 6. Six different superchannel architectures with different carrier spacings and modulation formats are investigated, and their performance for transmission over different distances is evaluated. Spectral efficiencies up to 7.8 bit/s/Hz are obtained using polarisation division multiplexed 16-QAM format. Capacities up to 2.112 Tb/s and transmission up to 300 km of SSMF have been reported.

Furthermore, a feed-forward heterodyne phase noise reduction scheme that enables simultaneous optical linewidth reduction of 30 comb lines derived from a Q-Dash PMLL is proposed. The scheme enables high capacity transmission experiments with coherent detection using Q-Dash PMLL as an optical source, even though this optical multicarrier source exhibits linewidth higher than 10 MHz. Tb/s data rates have been achieved within the limits of standard FEC scheme.

7.2 Future work

Potential future work would be focused on the further investigation of single laser based data centre optical interconnects. The first goal of future work would be to increase the data rate per channel (wavelength) up to 50 Gb/s. This can be achieved, for example, using 25 GBaud 4 pulse-amplitude modulation (4-PAM) modulation format with IM/DD modulation-detection scheme using the Q-Dash PMLL as an optical multicarrier source. The system performance would need to be characterised in terms of RIN and OCNR, and compared to the case when OOK NRZ and OFDM modulation formats are used instead.

Furthermore, prototypes of fully integrated optical interconnect transmitters and receivers (as depicted in Chapter 5) could be manufactured, characterised and implemented in IM/DD and coherent systems. The fully integrated solution would be realised on silicon substrate, with flip-chip optical source made from III-V materials. Ring resonators could be used either to filter a desired channel or to perform filtering and modulation simultaneously. That will depend on the intended modulation formats to be used. At the receiver side, which also could be realised using silicon technology, commercially available flip-chip photodiodes would probably be used due to their reliable performance, as these components are previously tested and verified. The projected bandwidth of the chip is ~ 30 GHz.

Also, field programmable gate arrays (FPGA) implementation of transmitter and receiver hardware for the generation of various modulation formats could form part of the plans for future work. FPGA based hardware solution allows transmitter design flexibility and real-time information about the energy consumption of the electronic circuitry. Efficient power consumption management is the one of the major requirements for data centre interconnects. Therefore, the power consumption reduction enabled by the full integration of transmitter and receiver should be followed

by power efficient design of electronics for the signal generation and detection, and DSP algorithms.

Finally, photonic integration of the gain-switched comb source with demultiplexer is currently in the process. Further characterisation of the integrated optical frequency comb and its implementation in coherently detected systems is currently being planned.

Appendix A

List of Publications Arising From This Work

A.1 Referred Journal Papers

V. Vujicic, P. M. Anandarajah, C. Browning, and L. P. Barry, "WDM-OFDM-PON Based on Compatible SSB Technique Using a Mode Locked Comb Source", IEEE Photonics Technology Letters, vol. 25, no. 21, pp. 2058-2061, Nov. 1, 2013.

R. Zhou, T. N. Huynh, **V. Vujicic**, P. M. Anandarajah, and L. P. Barry, "Phase noise analysis of injected gain switched comb source for coherent communications", Optics Express, vol. 22, no. 7, pp. 8120-8125, Mar. 2014.

V. Vujicic, P. M. Anandarajah, R. Zhou, C. Browning, and L. P. Barry, “Performance investigation of IM/DD SSB-OFDM systems based on optical multicarrier sources“, IEEE Photonics Journal, vol. 6, no. 5, 7903110, Oct. 2014.

J. Pfeifle, **V. Vujicic**, R. T. Watts, P. C. Schindler, C. Weimann, R. Zhou, W. Freude, L. P. Barry, C. Koos, “Flexible Terabit/s Nyquist-WDM Super-Channels using a Gain-Switched Comb Source“, Optics Express, vol. 23, no. 2, pp. 724-728, Jan. 2015.

C. Calò, **V. Vujicic**, R. Watts, C. Browning, K. Merghem, V. Panapakkam, F. Lelarge, A. Martinez, B-E. Benkelfat, A. Ramdane, L. P. Barry, “Single-section quantum well mode-locked laser for 400 Gb/s SSB-OFDM transmission“, Optics Express, vol. 23, no. 20, pp. 26442-26449, Oct. 2015.

V. Vujicic, C. Calò, R. Watts, F. Lelarge, C. Browning, K. Merghem, A. Martinez, A. Ramdane, L. P. Barry, “Quantum Dash Mode-Locked Lasers for Data Center Applications“, IEEE Journal of Selected Topics in Quantum Electronics, vol. 21, no. 6, pp. 1101508, Nov/Dec. 2015.

A.2 Referred Conference Papers

P. Anandarajah, R. Zhou, R. Maher, D. M. Gutierrez Pascual, F. Smyth, **V. Vujicic**, L. Barry, “Flexible optical comb source for super channel systems”, in Proc. Optical

Fiber Communication Conference (OFC/NFOEC), Anaheim, USA, paper, OTh3I. 8, Mar. 2013.

R. Zhou, **V. Vujicic**, T. N. Huynh, P. M. Anandarajah, and L. P. Barry, "Effective Phase Noise Suppression in Externally Injected Gain Switched Comb Source for Coherent Optical Communications", in Proc. European Conference on Optical Communication (ECOC), London, Sep. 2013.

V. Vujicic, P. M. Anandarajah, C. Browning, and L. P. Barry, "WDM-OFDMA Based on Compatible SSB Employing an Optical Multi-Carrier Transmitter", in Proc. Photonics Ireland, Belfast, Sep. 2013.

V. Vujicic, J. Pfeifle, R. Watts, P. C. Schindler, C. Weimann, R. Zhou, W. Freude, C. Koos, and L. P. Barry, "Flexible Terabit/s Nyquist-WDM Superchannels with net SE > 7 bit/s/Hz using a Gain-Switched Comb Source", in Proc. Conference on Lasers and Electro-Optics (CLEO USA), San Jose, paper SW1J.3, June 2014.

V. Vujicic, P. M. Anandarajah, C. Browning, R. Zhou, S. O'Duill, and L. P. Barry, "Optical Multicarrier based IM/DD DWDM-SSB-OFDM Access Networks with SOAs for Power Budget Extension", in Proc. ECOC, Cannes, France, paper We.1.6.6, Sep. 2014.

J. Pfeifle, R. Watts, I. Shkarban, S. Wolf, **V. Vujicic**, P. Landais, N. Chimot, S. Joshi, K. Merghem, C. Calò, M. Weber, A. Ramdane, F. Lelarge, L. Barry, W. Freude, C. Koos, "Simultaneous Phase Noise Reduction of 30 Comb Lines from a Quantum-Dash Mode-Locked Laser Diode Enabling Coherent Tbit/s Data Transmission", in Proc. OFC/NFOEC, Los Angeles, CA, USA, paper Tu3I.5, Mar. 2015

V. Vujicic, C. Calò, R. Watts, F. Lelarge, C. Browning, K. Merghem, A. Martinez, A. Ramdane, L. P. Barry, "Quantum Dash Passively Mode-Locked Lasers for Tbit/s Data Interconnects", in Proc. OFC/NFOEC, Los Angeles, CA, USA, paper Tu3I.4, Mar. 2015

C. Calò, **V. Vujicic**, R. Watts, F. Lelarge, C. Browning, K. Merghem, V. Panapakkam, A. Martinez, A. Ramdane, L. P. Barry, "Single-Section Quantum Well Mode-Locked Laser for 400 Gbit/s Single-Polarization IM/DD SSB-OFDM Transmission", in Proc. CLEO/Europe-EQEC, Munich, Germany, paper CI_2_5, June 2015.

W. Freude, J. Pfeifle, R. Watts, I. Shkarban, S. Wolf, **V. Vujicic**, P. Landais, N. Chimot, S. Joshi, K. Merghem, C. Calò, M. Weber, A. Ramdane, F. Lelarge, L. Barry,

C. Koos, „Phase-noise Compensated Carriers from an Optical Frequency Comb Allowing Terabit Transmission“, **Invited Talk,** in International Conference on Transparent Optical Networks (ICTON), Budapest, Hungry, paper Tu.B5.1, Jul. 2015

V. Vujicic, C. Calò, R. Watts, F. Lelarge, C. Browning, K. Merghem, A. Martinez, A. Ramdane, L. P. Barry, “Tbit/s transmission based on mode locked laser frequency comb sources“, **Invited Talk,** in Proc. IEEE Photonics Conference, Virginia, USA, Oct. 2015.

Other Publications Arisen from the PhD Research

A.3. Journal Papers

T. N. Huynh, L. Nguyen, **V. Vujicic**, L. P. Barry, “Pilot-Tone-Aided Transmission of High-Order QAM for Optical Packet Switched Networks”, Journal of Optical Communications and Networking, vol. 6, no 2, pp.152-158, Feb. 2014.

V. Vujicic, R. Zhou, P. M. Anandarajah, J. O’Carroll, L. P. Barry, “Performance of a Semi-Nyquist NRZ-DQPSK System Employing a Flexible Gain-Switched Multi-Carrier Transmitter”, Journal of Optical Communications and Networking, vol. 6, no. 3, pp. 282-290, Mar. 2014.

T. Shao, E. Martin, P. M. Anandarajah, C. Browning, **V. Vujicic**, R. Llorente, L. P. Barry, “Chromatic Dispersion Induced Optical Phase Decorrelation in a 60 GHz OFDM-RoF System”, IEEE Photonics Technology Letters, vol. 26, no. 20, pp. 2016-2019, Oct. 2014.

E. P. Martin, T. Shao, **V. Vujicic**, P. M. Anandarajah, C. Browning, R. Llorente, L. P. Barry, “25 Gb/s OFDM 60 GHz Radio over Fibre System Based on a Gain Switched Laser“, Journal of Lightwave Technology, vol. 33, no. 8, pp. 1635-1643, Apr. 2015.

A.4. Conference Papers

T. N. Huynh, **V. Vujicic**, L. P. Barry, "Baudrate-Pilot-Aided Transmission for High Order QAM Modulation Format in Optical Communications", in Proc. Photonics Ireland, Belfast, Sep. 2013.

P. M. Anandarajah, R. Zhou, **V. Vujicic**, M. D. Gutierrez Pascual, E. Martin, L. P. Barry, “Long Reach UDWDM PON with SCM-QPSK Modulation and Direct Detection”, in Proc. OFC/NFOEC, San Francisco, CA, USA, paper W2A.42, Mar. 2014.

J. O’Carroll, **V. Vujicic**, N. Brochier, L. Bramerie, L. P. Barry, "Performance investigation of 112 Gb/s PDM-QPSK long-haul systems employing Discrete Mode Lasers", in Proc. Photonics Europe, Brussels, Belgium, Apr. 2014.

P. M. Anandarajah , R. Zhou, **V. Vujicic**, M. D. Gutierrez Pascual, R. Maher, D. Lavery, M. Paskov, B. Thomsen, S. Savory, L. P. Barry, “Long Reach UDWDM PON with Direct and Coherent Detection”, in Proc. ICTON, Graz, Austria, Jul. 2014.

E. Martin, T. Shao, **V. Vujicic**, P. Anandarajah, C. Browning, R. Llorente, L. Barry, „25 Gb/s OFDM 60 GHz Radio over Fibre System Using an Externally Injected Gain Switched Distributed Feedback Laser“, in Proc. ECOC, Cannes, France, paper. Tu.4.2.4, Sep. 2014.

E. Martin, T. Shao, P. Anandrajah, **V. Vujicic**, C. Browning, Roberto Llorente, L. Barry, “Impact and Reduction of Fibre Nonlinearities in a 25 Gb/s OFDM 60 GHz Radio over Fibre System”, MWP/APMP Conference, Sapporo, Japan, Nov. 2014

P. M. Anandarajah, T. Huynh, **V. Vujicic**, R. Zhou, and L. P. Barry, “UDWDM PON with 6×2.5GBaud 16-QAM Multicarrier Transmitter and Phase Noise Tolerant Direct Detection”, in Proc. OFC/NFOEC, Los Angeles, CA, USA, paper Th2A.58, Mar. 2015.

T. N. Huynh, **V. Vujicic**, M. D. G. Pascual, P. M. Anandarajah, L. P. Barry, “Digital coherent communications with a 1550 nm VCSEL”, in Proc. OFC/NFOEC, Los Angeles, CA, USA, paper M2D.7, Mar. 2015.

P. M. Anandarajah, M. D. G. Pascual, T. Shao, R. Zhou, **V. Vujicic**, F. Smyth, L. P. Barry, “Reconfigurable Optical Frequency Comb and its Applications“, **Invited Talk** at ICTON, Budapest, Hungry, Jul. 2015.

Appendix B

B.1. Error Vector Magnitude

Advanced modulation formats such as PSK and QAM which use the phase of the optical carrier to encode the data, require a quality metric that is different than for OOK signals. Firstly, BER and Q-factor calculations which are often used for the performance characterisation of the OOK based systems, do not offer the information about the phase error but only total error of the received signal. Secondly, in the laboratory experiments most receivers employ offline digital signal processing at much reduced clock rates [1, 2]. For reliable estimation of BER, a certain number of bits is required. For example, it is clear that a system that specifies a BER better than 10^{-9} must be tested by transmitting significantly more than 10^{9} bits in order to get an accurate and repeatable measurement [3]. Therefore, reliable BER estimation using offline DSP is a very time consuming process. Hence a faster and reliable quality metric is needed, in particular when characterising multicarrier systems [1, 2].

It is well known that the complex field of a QAM signal can be represented using a constellation diagram, and an ideal constellation for square 16-QAM modulation format is shown in Figure B.1.1. The constellation of the received signal usually deviates from the ideal constellation. The level of deviation can be characterised using the error vector magnitude. The deviation between received signal vector E_R and transmitted (ideal) signal vector E_I is denoted as an error vector E_{err}. Two definitions of EVM can be found in the literature. The first one uses the longest ideal constellation vector $E_{I,\max}$ for the normalisation. Another definition uses average power $\left|E_{I,avg}\right|^2$ of all symbol vectors within the constellation for the normalisation. When $E_{I,\max}$ is used for the normalisation, then the $EVM_{\max}$ is defined by a root mean square of E_{err} for a number N of randomly transmitted data [1, 2]:

$$EVM_{\max} = \frac{\sigma_{err}}{E_{I,\max}} \tag{B.1.1}$$

where $\sigma_{err}^2 = \frac{1}{N}\sum_{i=1}^{N}\left|E_{err,i}\right|^2$, and $E_{err,i} = E_{R,i} - E_{I,i}$.

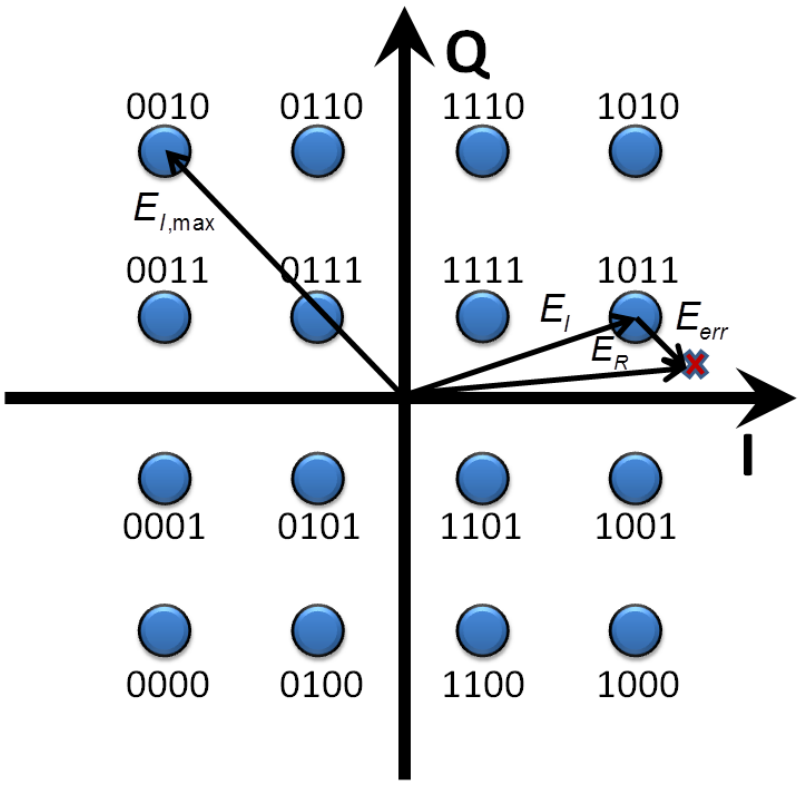

Figure B.1.1. Constellation diagram and error vector for 16-QAM signal.

The definition based on the normalisation using the average power of all symbol vectors within the constellation is related to the later one by the modulation format dependent factor *k*:

$$EVM_{avg} = k \cdot EVM_{\max} \tag{B.1.2}$$

where $k^2 = \frac{|E_{I,\max}|^2}{|E_{I,avg}|^2}$ and $|E_{I,avg}|^2 = \frac{1}{M}\sum_{i=1}^{N}|E_{I,i}|^2$.

The values of factor *k* for certain modulation formats are given in Table B.1.1 [1, 2]:

Modulation format	BPSK	QPSK	8PSK	16-QAM	32QAM	64QAM
k^2	1	1	1	9/5	17/10	7/3

Table B.1.1. Values of factor *k* for certain modulation formats.

In this thesis, EVM_{avg} is used for the system performance characterisation in Chapter 5, whilst $EVM_{\max}$ is used in Chapter 6.

BER and Q-factor can be estimated using EVM as outlined in [1, 2].

References

[1] R. Schmogrow, B. Nebendahl, M. Winter, A. Josten, D. Hillerkuss, S. Koenig, J. Meyer, M. Dreschmann, M. Huebner, C. Koos, J. Becker, W. Freude, J. Leuthold, “Error Vector Magnitude as a Performance Measure for Advanced Modulation Formats”, IEEE Photonics technology Letters, vol. 24, no. 1, pp. 61-63, Jan. 2012.

[2] R. Schmogrow, “Real-time Digital Signal Processing for Software-defined Optical Transmitters and Receivers”, KIT Scientific Publishing, Nov. 2014

[3] HFTA-010.0: Physical Layer Performance: Testing the Bit Error Ratio (BER). Available: http://pdfserv.maximintegrated.com/en/an/3419.pdf, Oct. 2015.